

Laser-assisted intradermal application of  
mRNA-loaded nanocarriers for  
minimally invasive ("needle free")  
vaccination via the skin

Dissertation  
zur Erlangung des Grades  
des Doktors der Naturwissenschaften  
der Naturwissenschaftlich-Technischen Fakultät  
der Universität des Saarlandes

von

**Lena Kliesch**

Saarbrücken

2024

Tag des Kolloquiums:	28. Juni 2024
Dekan:	Prof. Dr.-Ing. M. Vielhaber
Berichterstatter:	Prof. Dr. C.-M. Lehr
	Prof. Dr. A. Kiemer
Vorsitz:	Prof. Dr. T. Kraus
Akademischer Mitarbeiter:	Dr. S. Boettcher

Die vorliegende Arbeit wurde von Oktober 2018 bis Juni 2022 unter der Leitung von Herrn Prof. Dr. Claus-Michael Lehr am Institut für Pharmazeutische Technologie der Universität des Saarlandes und Helmholtz-Institut für Pharmazeutische Forschung Saarland (HIPS) in der Abteilung für Wirkstofftransport angefertigt.

“Wisdom comes from making mistakes, having the courage to face them and make adjustments moving forward based upon the knowledge acquired through those experiences.”

- *Ken Poirot*

# Table of Contents

I.	Short Summary.....	I
II.	Kurze Zusammenfassung.....	II
III.	List of Abbreviations.....	III
1	General Introduction.....	1
1.1	Vaccination as Promising Strategy to Combat Infectious Diseases.....	1
1.2	Application Techniques of Vaccines.....	4
1.3	Vaccination Technologies and Their Limitations.....	8
1.4	Nanoparticles as Delivery System for mRNA.....	12
1.5	Aim of This Thesis.....	16
2	Materials and Methods.....	17
2.1	Nanoparticle Preparation and mRNA Loading Procedure.....	17
2.2	Nanoparticle Characterization Without Cells.....	19
2.3	<i>In vitro</i> Characterization.....	22
2.4	Primary Bone Marrow Derived Dendritic Cells.....	25
2.5	<i>In vivo</i> studies with Mice.....	26
2.6	<i>Ex vivo</i> Skin Model.....	30
2.7	Statistical Analysis.....	32
3	Optimization of Nanocarriers.....	33
3.1	Influence of Adding DOPE to the Lipid Layer of Lipid-polymer Hybrid Nanoparticles.....	33
3.2	Evaluation of mRNA-loaded LPNs.....	41
4	Testing Nanoparticle Performance Under Stress Conditions.....	46
4.1	Uptake.....	46
4.2	Transfection Efficacy.....	48
4.3	RNase Stability.....	55
4.4	Performance in Primary Immune Cells.....	62
5	Minimally Invasive Application of LPNs to the Skin.....	65
5.1	Evaluation of P.L.E.A.S.E.® Laser Device.....	65
5.2	Pegylation of LPN.....	74
5.3	Development of <i>Ex vivo</i> Human Skin Model.....	80
5.4	Results <i>Ex vivo</i> Skin Model.....	89
6	Discussion.....	97
6.1	Lipid-polymer Hybrid Nanoparticles as Delivery System for mRNA.....	97
6.2	<i>Ex vivo</i> Human Skin Model to Test mRNA delivery.....	108
6.3	The P.L.E.A.S.E.® Laser as Minimally Invasive Application Strategy for Nanoparticles.....	118
7	Conclusion and Outlook.....	125

IV. References.....	V
V. Supplementary Figures.....	XXI
VI. Scientific Output.....	XXXI
7.1 Articles Published in Peer Reviewed Journals .....	XXXI
7.2 Oral Presentations.....	XXXI
7.3 Poster Presentations .....	XXXII
VII. Acknowledgements .....	XXXIII

## I. Short Summary

Vaccination is still the most promising way to combat infectious diseases. Despite tremendous progresses in delivery systems with the first approved mRNA vaccines, the application by intramuscular injection is suboptimal. Representing a natural biological barrier, the skin is equipped with a plethora of immune cells that can be targeted even by minimally invasive techniques. The main aim of this work was to evaluate the potential of transiently disrupting the skin barrier by laser microporation to enable the penetration of mRNA-loaded nanocarriers for skin vaccination.

Lipid-polymer hybrid nanoparticles (LPNs) that profit from high transfection rates of lipids and the stability of polymers were selected to complex mRNA. The impact of replacing the cationic lipid DOTMA by the phospholipid DOPE in the lipid layer was investigated concerning hydrodynamic parameters, stability, uptake, mRNA binding and protection and most important transfection efficacy. LPN(70/30) made of 70 mol% DOPE and 30 mol% DOTMA showed most stable transfection rates independent of medium additives and was further modified by pegylation.

Findings were complemented by the optimization of the P.L.E.A.S.E.<sup>®</sup> microporation parameters in mouse models and a newly developed *ex vivo* human skin model. Despite lower exposure compared to injection, laser-mediated application of 2.5 mol% PEG in LPN(70/30) showed most promising results with live transfected cells in tissue and stimulated immune cells in the supernatant.

## II. Kurze Zusammenfassung

Impfen bleibt der effektivste Weg, Infektionskrankheiten zu bekämpfen. Trotz des Durchbruchs mit den ersten zugelassenen mRNA-Impfstoffen ist deren intramuskuläre Injektion suboptimal. Als natürliche Barriere beherbergt die Haut viele Immunzellen, die sogar mittels minimal-invasiven Techniken erreicht werden können. Diese Arbeit zielt darauf ab, das Potenzial einer vorübergehenden Störung der Hautbarriere mittels P.L.E.A.S.E.<sup>®</sup>-Laser-Mikroporation für die Impfung mit mRNA-beladenen Nanoträgern zu bewerten.

Für die Komplexierung von mRNA wurden Lipid-Polymer-Hybrid-Nanopartikel (LPNs) gewählt, die von den hohen Transfektionsraten der Lipide und der Stabilität der Polymere profitieren. Der Effekt des Austauschs des kationischen Lipids DOTMA durch das Phospholipid DOPE in der Lipidschicht wurde hinsichtlich hydrodynamischer Parameter, Stabilität, Aufnahme, mRNA-Bindung und -Schutz sowie der relevantesten Transfektionseffizienz untersucht. LPN(70/30) aus 70 mol% DOPE und 30 mol% DOTMA zeigte unabhängig von Mediumzusätzen die stabilsten Transfektionsraten und wurde durch Pegylierung weiter modifiziert.

Ergänzt wurden die Erkenntnisse durch die Optimierung der Laserparameter in der Maus und in einem neu entwickelten *Ex-vivo*-Modell aus menschlicher Haut. Trotz geringerer Exposition im Vergleich zur Injektion zeigte die laserbasierte Applikation von 2,5 mol% PEG in LPN(70/30) die besten Ergebnisse mit lebenden transfizierten Zellen im Gewebe und stimulierten Immunzellen im Überstand.

### III. List of Abbreviations

AIF	artificial interstitial fluid
AIFa	artificial interstitial fluid including albumin
AIFb	artificial interstitial fluid - buffer only
APC	antigen presenting cell
BE	binding efficacy
BMDC	bone marrow derived dendritic cells
CDA	cyclic di-AMP (adenosine monophosphate)
CD	cluster of differentiation, surface marker on immune cells
CFSE	carboxyfluorescein succinimidyl ester
CLSM	confocal laser scanning microscope
CTL	cytotoxic T cell
DAPI	4',6-diamidino-2-phenylindole
DC	dendritic cell
DC2.4	murine dendritic cell line
DiD	1,1-dioctadecyl-3,3,3,3-tetramethylindodicarbocyanine
DLS	Dynamic Light Scattering
DMG-PEG2000	1,2-dimyristoyl-sn-glycero-3-methoxypolyethylene glycol
DNA	deoxyribonucleic acid
DOPE	1,2-dioleoyl-sn-glycero-3-phosphoethanolamine
DOTMA	1,2-di-O-octadecenyl-3-trimethylammonium propane
EDTA	ethylenediaminetetraacetic acid
FACS	Fluorescence Activated Cell Sorting
FCS	fetal calf serum
FDA	fluorescein diacetate
FITC	fluorescein isothiocyanate
HBSS	Hank's Balanced Salt Solution
HEPES buffer	4-(2-hydroxyethyl)piperazine-1-ethanesulfonic acid
HZI	Helmholtz Centre for Infection Research
JM	jetMESSENGER®
KC	keratinocyte
LC	Langerhans cell
LPN	lipid-polymer hybrid nanoparticle
MFI	measured fluorescence intensity
MHC	major histocompatibility complex

MHCI	major histocompatibility complex, class I
MHCII	major histocompatibility complex, class II
MQ	Milli-Q <sup>®</sup> ultra-purified water
MTT	3-(4, 5-dimethylthiazol-2-yl)-2, 5-diphenyltetrazolium bromide
MW	molecular weight
NFW	nuclease-free water
OECD	Organization for Economic Co-operation and Development
OT	OVA-specific T cells
OVA	ovalbumin, model antigen
p(I:C)	polyinosinic-polycytidylic acid
P.L.E.A.S.E <sup>®</sup>	precise laser epidermal system
PBAE	poly( $\beta$ -amino ester)
PBS	phosphate-buffered saline
PDI	polydispersity index
PEG	polyethylene glycol
PEIPEI	polyethyleneimine
PFA	paraformaldehyde
PLGA	poly(lactid-co-glycolid) or poly(lactic-co-glycolic acid)
PVA	polyvinyl alcohol
RNA	ribonucleic acid
RPMI	Roswell Park Memorial Institute, cell cultivation medium
RT	room temperature
SLN	solid lipid nanoparticle
TE	tris-EDTA-buffer
TEM	transmission electron microscopy

# 1 General Introduction

## 1.1 Vaccination as Promising Strategy to Combat Infectious Diseases

### 1.1.1 Threat of Infectious Diseases

It is a rather philosophic question if the human body consists mainly of the 40 trillion ( $4 \cdot 10^{13}$ ) eukaryotic cells or the naturally occurring 39 trillion microbiota that colonize all parts of the human body [1, 2]. In any case, these numbers emphasize the importance to control and to simultaneously tolerate the direct environment which is realized by the immune system.

If the defense mechanisms are impaired maybe due to stress or an injury of outer barriers, there is the chance for a pathogen to invade the body and cause an infection. When the exposure to a very potent pathogen is high enough, they can even overcome intact biological barriers and cause symptoms of illness. Another common cause of this switch to pathogenicity is the evolution of the pathogen itself acquiring survival benefits such as higher infectability or a resistance to established active compounds. Depending on the resulting advantage this new property has, the immune system needs more time to adapt and to control it while the modified pathogen can freely amplify and spread causing even more work for the immune system and thus probably more symptoms for the patient. Such an evolutionary process was impressively shown by the appearance of the Covid-19 virus that led to a fast developing pandemic influencing everyone's life worldwide [3]. Again, the fittest humans with the most potent immune systems suffered the least and survived an infection starting the cycle of evolution again.

As human beings and especially as scientists, we have more tools in hand than our body to fight this combat. Among them are easy to apply procedures like disinfection or wearing masks to reduce the burden of pathogens that the body is exposed to, but also sophisticated measures to help the immune system by either weakening the pathogen or enhancing the power of the immune response. On the side of the pathogens, there are many strategies one could think of depending on the pathogen type such as blocking surface proteins to reduce infectivity, specifically inhibiting production of components for growth and amplification or increasing sensitivity to other drugs by reducing resistance mechanism. In most cases, small molecules represent the active compound. To support the immune system in the second approach, mostly macromolecules are needed with high demands for application and delivery methods. Specific labeling of the infectious particles for instance with an antibody could enable an easier detection and elimination by the immune cells or simply block their cellular internalization. A more general and thus more potent method is the exposure to surrogates of the pathogen prior to the actual infection as preventive measure. The body has the chance to react to this less harmful variant and prepare for an infection with the real pathogen. This training is the basic principle behind vaccination.

In general, there are different vaccine types available but they all follow the same principles. The more the surrogate deviates from the original pathogen concerning route of invasion and size, the lower the immune reaction reducing side effects and increasing the safety. On the other hand, a very small surrogate like a protein requires a delivery system and an adjuvant to enhance the immune response to reach a protective level. Details on how to balance vaccine safety and sufficient protection in the different vaccine types and application methods will be discussed in the following chapters.

A trained immune system can react faster and more effectively to an invaded pathogen. Vaccines are mostly applied to healthy volunteers with an immune system in the best possible condition leading to the best possible reaction. When necessary in the case of an infection with the specific pathogen the immune system was trained for, the immune cells will need less time until the pathogen is under

control. The pathogen load will be reduced, the patient is less contagious and the transmission to other individuals is less likely. With high vaccination percentages, herd immunity can be achieved that also protects individuals that cannot be vaccinated [4, 5]. If the individual notices the infection at all, the symptoms will be drastically reduced maybe even making the difference between death and recovery. This is of special relevance in elderly or people with immune disorders.

Despite the direct costs for the vaccines, immunization in the long-term saves money otherwise spent for health care [6, 7]. At the individual level, the benefits of vaccination such as the mentioned reduction of symptoms strongly depends on the likelihood of an infection. If the person will never be exposed to the pathogen, the vaccine will not show an effect. For the same reason, it is important to vaccinate as early as possible to have the highest chance of protection. This administration in healthy young children raised the amount of safety data needed for the approval of new vaccines which increases for example the size of study cohorts and makes the development expensive.

Vaccination is still the most potent and fastest way to prevent the outbreak of a disease with a positive influence on everyone's lives. With a consequent vaccination campaign, it was even possible to reach a worldwide eradication of smallpox [8]. Even though that was not and will not be reached for Covid-19, vaccination mostly replaced acute measures like social distancing and enable the restart of all regular activities of daily life. With upcoming antibiotic resistances, it will gain even more relevance in the future.

### **1.1.2 Our Defense Mechanisms: The Immune System and How to Train it**

The immune system basically maintains the integrity of the body. It recognizes and eliminates pathogens or mutated cells but also tolerates for example the microbiome. As diverse cell types in all organs participate, their function and activity need to be balanced and continuously controlled. If the complex regulation mechanisms fail, patients suffer from chronic infections, cancer or autoimmune diseases. There is lots of research being conducted to understand every detail and new aspects are continuously being discovered that could be potentially exploited for the treatment of such a disease. In the sake of relevance, only a short overview will follow highlighting the parts most important for vaccination and this work.

When for example a bacterium enters the body, there is a first line of defense represented by the local innate immune system. Mainly phagocytotic cells like macrophages or dendritic cells (DCs) nonspecifically take them up and digest them. The intracellular presence of foreign antigens activates the cell, initiates its maturation resulting in the presentation of pathogenic epitopes on their surface via the major histocompatibility complex (MHC). Cytokines are secreted to attract more immune cells [9]. Next to this cellular component of the innate system, there are the soluble factors of the complement system. They can bind to surface structures of the invader and thus enable for example a faster uptake by macrophages.

The mentioned macrophages are derived from monocytes and have a high mobility to scan as much tissue as possible. They belong to the same group of professional antigen presenting cells (APCs) like dendritic cells that reside at all biological barriers and are in that function of particular relevance for the vaccination via the skin. DCs can bind 30–200 times more antigen than macrophages and are therefore the most efficient inducers of immune responses against extracellular proteins [10, 11]. When DCs are activated after the antigen contact, they migrate to lymphatic organs where they stimulate cells of the adaptive immune system eliciting humoral and cellular immune responses [12–14]. This is how they connect innate and adaptive immune responses. [15]

This second line of defense, the adaptive immune system, is based on B- and T cells. In contrast to the APCs, which can react to any pathogen, the activation of B- and T cells is dependent on specific stimulation. Every B- or T cells has a surface receptor specific for only one epitope, a small piece of

## 1 General Introduction

the antigen. The high amount of B- and T cells results in a large variety of recognizable antigens. When antigen parts are presented on the cell surface via MHC I or II, only immune cells with a receptor that fits to the epitope can bind. These cells are stimulated and selectively expanded. This process is a crucial mechanism of the adaptive immune system and called clonal expansion [16]. Activated antigen specific T cells coordinate the consecutive adaptive immune response, again by direct cell-to-cell contact and excreted stimulatory molecules.

This adaptive immune reaction can be further divided in two parts – the humoral and cellular response. Extracellular pathogens like bacteria will be presented mainly via MHCII on APCs and therefore preferentially stimulate T cells with a CD4<sup>+</sup> co-receptor. The expansion of CD4<sup>+</sup> T cells will stimulate specific B cells that mature into large plasma cells. Upon antigen contact, these cells will release specific antibodies that can neutralize toxins or label the pathogen for phagocytosis by binding the extracellular antigens. Titers of these high affinity antibodies will still be elevated in the blood for some time after the infection.

In contrast, intracellular pathogens like viruses probably infect somatic cells that do not have the MHCII receptor like the APCs but the MHC class I. All nucleated cells of the body have this MHC class I receptor and thus the chance to present material of foreign origin on its surface. T cells with the CD8<sup>+</sup> co-receptor will be stimulated by this presentation which will at the end lead to the expansion of antigen specific cytotoxic T cells (CTLs). These cells will recognize infected cells by antigen presentation via MHCI receptor and specifically kill them to stop the amplification of viral particles [17]. This cell-based reaction is most effective when complemented by co-stimulation of a CD4<sup>+</sup>-mediated response that is elicited by viral components in the extracellular space after the lysis of infected cells.

The expansion of antigen-specific T cells not only leads to different effector cells but also to the creation of memory cells. Their initial number depends on the intensity, location and duration of the stimulating signal. These memory cells are still in place long after the pathogen is eliminated. In case of a new infection with a pathogen with similar epitopes, these memory cells can be reactivated. The immune reaction starts with several of these effector memory cells instead of only a few specific T cells in the lymphatic organ. The time until enough specific T cells are available for a sufficient immune reaction is much shorter. After every new antigen contact, more memory cells are generated, and the immune reaction is accelerated. The immune system can be considered as trained.

There are many processes happening in parallel and several options how the immune system can react. As mentioned before, the reaction of the components is carefully orchestrated also in their order and time of appearance. The innate factors react first until the adaptive reaction reinforces the defense. For example, 5 h after application of a DNA-based vaccine by a gene gun in a mouse, antibodies titers raised, while T cell response started after 1 d [18].

Using this knowledge for vaccination, a balanced humoral and cellular response is advantageous after the first dose for a long-term protection. As for the targeted pathogen, it depends on the type of vaccine which one is the most stimulated. Every booster vaccine is then supposed to increase the number of memory cells and circulating antibodies.

All mentioned aspects apply especially to active vaccination where the immune system of the patients reacts to the administered vaccines. In case of an emergency, it is also possible to transfer serum with specific antibodies to the infected patient. This process is called passive immunization and has only a transient effect. In a life-threatening situation, this measure can bridge the time until the immune system generates its own antibodies. Immune sera can be collected from animals or other human beings that have been successfully exposed to the pathogen. Aiming for a more sustainable effect of the immunization, the focus of this work is on active vaccines. The next chapter

will be about application techniques of these active vaccines followed by explanations of the types of vaccines.

### **1.2 Application Techniques of Vaccines**

#### **1.2.1 State of the Art: Intramuscular Injection**

Active vaccination requires the direct contact of the immune system with the administered antigens. In case of a natural infection, the pathogen would most likely invade via the skin or the mucosae of the nose, mouth or gut. Even though following these paths to overcome the biological barriers of the human body would be reasonable, to date almost all approved vaccines are injected into the muscle.

This intramuscular injection is the established method with broadest experience, also in animal models. Needle type and orientation, as well as injection speed and type of fluid have an influence [19]. In adults, the deltoid muscle of the upper arm is used as site of injection while small children are usually injected into the thighs. Worldwide, health care personal is trained well, and patients know what to expect also when it comes to most common adverse effects. Among them are pain and heat at injection site [20]. For patients suffering from needle phobia, this procedure is very problematic and results in a lower numbers of fulfilled vaccination protocols [21].

The muscle does not present a natural entry port of the body and the number of tissue resident immune cells is low [22, 23]. After the injection of high doses of naked mRNA or DNA, it is therefore the muscle cells that take up and express the nucleic acids [19, 24]. The applied doses are higher – to reach the immune cells and to form a depot that compensates for the low immune cell density. This depot slowly releases the antigen and thereby stimulates the immune system over an extended period resulting in a protective immune response.

There are very few exceptions from this application method. The vaccines against cholera and rota viruses are swallowed which also represents the natural way of infection [25, 26]. Additionally, the former smallpox vaccine was applied to the skin of the upper arm by a scarification technique which enabled the eradication of the pathogen in 1980 [27]. Many patients still have visible scars on the site of application. Motivating patient to take such a new vaccine that is applied to the skin will probably be difficult but there are good reasons for it. This is the topic of the next chapter 1.2.2.

#### **1.2.2 The Skin as Target Tissue for Vaccination**

The skin is next to the gut and the lung one of the body's largest organ with a size of approximately 2 m<sup>2</sup> for adults [28]. It represents the main barrier of the human body and is therefore equipped with many immune cells that can directly react to environmental threats and prevent persistent infections and neoplasms [29–31]. The immune cells and all other components of the different skin layers are adapted to their function. The outermost layer is the stratum corneum that is made of dead cells and lipids. This mixture already impedes the penetration of most molecules or particles. Underneath, there is the viable skin tissue with the thin epidermis, the basal membrane separating both parts and the dermis with appendices and blood vessels. Lacking direct connection to the circulation, the nutrient supply for the epidermis happens only by diffusion. The subcutaneous fat is the slipping plane and buffering zone to the muscles but usually not counted as part of the skin.

The immune cells of the skin are distributed in the tissue according to their probability of antigen contact. In total, about 7% of the entire cells are immune cells [32]. The epidermis is exposed to many environmental influences and has therefore a generally high turnover of cells [33]. Langerhans cells (LCs) that are a subset of dendritic cells and as such professional antigen presenting cells. They reside in the epidermis and make up 3-5% of the entire population which is a high percentage compared to the maximum percentage of 1.6% for DCs in spleen cell suspensions [34–37]. LCs play a

key role in mediating immune responses in the skin [38]. After acquisition of the antigens in the tissue, the LCs migrate to the draining lymph node where they activate antigen-specific T cells via antigen presentation via MHCII [10, 39, 40]. The keratinocytes (KCs), the skin cells, can influence the immune reaction as well, for example by attracting neutrophils or monocytes as part of early inflammation [41].

In the dermis, there are resident dermal dendritic cells, too, but the ratio to skin cells is lower. Exceptions are for example hair follicles that reach down to the dermis. As a potential entry port, there are immune privileged parts in the deeper parts of the follicles as well [42].

Using the skin with its natural distribution of immune cells for vaccination purposes has many advantages. In general, the skin is large and has many possible application sites. One could treat either an area that is usually not visible or instead select one that is easily accessible.

When more immune cells are hit directly, the required dose to elicit a protective immune response will be lower or alternatively the immune response will be stronger, if the same amount of antigenic material is applied. This second effect was for example shown for naked DNA, that elicited 4fold higher antibody titers after intradermal than intramuscular injection [22]. With the same amount of antigen, more patients can be vaccinated which might be an advantage especially when a situation like a pandemic leads to a high demand of vaccines.

To reach the skin – independent of epidermis or dermis – less invasive methods could be used compared to the muscle. A more superficial application technique may cause less destroyed cells with benefits for the patients such as reduced pain. In this context, targeting the immune cells of the epidermis will be the most promising strategy as presentation via both MHC receptors by dendritic cells is the most efficient way to induce a protective immune responses against proteins [10, 12, 17]. In the following, the skin application methods clustered according to their invasiveness will be described.

It should be clarified that all mentioned application routes target the skin to exhibit a local effect that will later lead to an immune response and systemic protection. This aim differs from transcutaneous and subcutaneous applications where applied formulations should reach the circulation to show a systemic effect. For transcutaneous application protocols, the formulation has to cross the skin by itself while it is injected into the subcutaneous fat underneath the skin in the second method [43]. Nanoparticles are too large for the route across the skin and even for proteins it was shown that a factor of 1000 in the applied transcutaneous amount is not enough to compensate for the lost material of antigen when antibody titers are compared to intradermal injection [44, 45].

### 1.2.3 Invasive Skin Application Techniques

To overcome the stratum corneum as main skin barrier, it is possible to use a syringe with a needle. In contrast to intramuscular injection where a 90° angle is favorable, a thinner needle is injected in a 10–15° angle to the skin to reach the dermis. The aim is a superficial application of the dose which creates a visible bleb. This technique needs practice, and the volume is very limited. The epidermis itself is too thin to reproducibly hit it with a needle.

Targeting the skin by such an injection, was successfully applied for experimental vaccines and outperformed the muscle. For instance, the antibodies found after intradermal injection of high doses of naked DNA or protein had a higher affinity and higher titers when compared to intramuscular application and the onset of a cytotoxic T cell (CTL) response was faster [35, 46].

Next to this injection method, there are methods available that target the epidermis, for example skin scarification techniques where skin is abraded in a controlled way. This stimulates an immune reaction that is higher than after intramuscular, subcutaneous or even intradermal injection [47] but leads to the creation of a scar as the defect is usually too large. Such an application will lead to

compliance problems as other options are available. Compared to scarification, tape stripping is less invasive and could be counted even as minimally invasive because only the most superficial layers are removed with a sticky tape while the viable skin is not influenced. This reduces the barrier function transiently and enables the particle penetration [48, 49].

In experimental setups in animal models, there are more application techniques described mostly based on technical devices. Immunologic benefits were shown for electroporation, tattooing machines and gene guns [17, 18, 50]. After DNA tattooing, the T cell responses were up to 100times better than after intramuscular injection [51]. An epidermal application of DNA-loaded gold beads with a gene gun, required the lowest dose for a sufficient immune response when compared to intravenous, intramuscular and mucosal administration [52]. Elicited immune response were even higher than after dermal delivery [53]. Gene gun-based application of mRNA resulted in a humoral immune response as well [54].

### **1.2.4 Non-invasive Application: Transfollicular Route**

In contrast to these invasive skin application techniques, there are the non-invasive methods which would be the optimum as skin remains intact increasing safety, no devices are required and patients could even apply it by themselves enhancing compliance and decreasing costs [43]. As small antigens and nanoparticles cannot overcome the stratum corneum, the most promising option is the route via the hair follicle. Despite many improvements, to date no vaccine candidate made it to the clinic. One problem for the application in humans, is for example the low hair follicle density at possible administration sites such as the upper arm and the smaller size of vellus hair follicles there [55]. At the baseline, the main limitation seems to be the amount of delivered antigen [56, 57]. An adjuvant is needed in any case [58].

### **1.2.5 Minimally Invasive Strategies**

A compromise between invasive and non-invasive methods could be a minimally invasive strategy. The most advanced option is the application of microneedles. When applied to the skin, these needles reach down to the dermis up to 2000  $\mu\text{m}$  but not far enough to stimulate nociceptors [59]. The application is therefore painless [60]. There are different experimental technologies available, among them are adapters for regular syringes that can be combined with any liquid vaccine [61, 62]. Microneedles can be prepared of dissolvable material releasing the antigen or they can be covered with the vaccine [59]. Microneedles represent a one-step application procedure and could also be applied by the patients at home. Such a minimally invasive procedure outperformed the application of a DNA-based smallpox vaccine by skin scarification and underlines the benefits for the patient [63].

An alternative are laser-mediated application procedures. Lasers are widely used to treat all kinds of skin defects and are available in many different types. Based on the available experience in the vaccination context, it makes sense to divide them into non-ablative and ablative. For both kinds, it was shown, that the controlled destruction of cells stimulates the immune system like an injury. With non-ablative lasers the barrier remains intact which does not solve the problem of antigen application. There is a published protocol of a stimulation with the non-ablative laser followed by an intradermal injection of the vaccine, but this protocol does not fulfil the aim of minimally invasive application [58].

For this work, the P.L.E.A.S.E<sup>®</sup> system by Pantec biosolutions was selected instead. The abbreviation stands for **precise laser epidermal system** [64]. It is an ablative laser which means that cells are destroyed by the immediate evaporation of the water which disrupts the barrier of the skin. The tissue defect is only small with a pore diameter around 150  $\mu\text{m}$  that can fast be re-epithelized. For

## 1 General Introduction

the application of vaccines, the main advantage is the user friendliness and easy adaptation onto the customer's demands. The number and the depth of pores can be easily changed. It is possible to target only the epidermis or to cross this layer reaching down to the dermis. This method can be counted as minimally invasive, too, as barrier disruption is only transient, the application is painless or even not noticeable for the patient and tissue completely recovers from the treatment [65]. In any case, the vaccination protocol would have two steps – first microporation and second the application of the vaccine.

When applied with commercially available protein vaccines, antibody titers were comparable to intramuscular injection [64]. The application of peptide-loaded patches together with an adjuvant successfully elicited a CTL response [66]. These studies confirmed the suitability of the laser for cutaneous delivery and to elicit an immune response. It was furthermore shown that the laser microporation is already enough to stimulate the immune system and that an additional adjuvant is not needed [67, 68]. Such an adjuvant-free vaccination potentially reduces the risk for side effects and holds great promise for the application also with other antigen than proteins. It has been already published that the P.L.E.A.S.E.<sup>®</sup> microporation enables the intradermal delivery not only of macromolecules but also of nanocarriers of 500 nm [69, 70]. Though, to date, there is no study available that combines this laser treatment with a nanoparticle-based vaccine opening the door for this work. As the application route is only the vehicle and will never work without the vaccine itself, the next chapter will focus on available vaccine types.

## 1.3 Vaccination Technologies and Their Limitations

### 1.3.1 Traditional Vaccines/Pathogen-based Vaccines

Having described the mechanisms behind active vaccination and the application techniques, this section is about strategies how the immune reaction is elicited. In general, the highest immune response is stimulated when the body is exposed to the pathogen itself. This of course, would lead to all unwanted effects and symptoms that shall be avoided with the vaccination. The development of a new vaccine is therefore always a search for the best compromise between immunogenicity and patient safety.

The closest surrogate for natural pathogens is achieved by destroying their ability to proliferate for example by formaldehyde or heating the sample [71]. All surface structures are maintained, and the immune system can react as normal. The risk of this approach is in an insufficient killing and the reacquisition of the pathogenicity resulting in a regular infection with all consequences.

For viral particles the attenuation to another species is a common method to create an injectable vaccine. Viruses are able to adapt to their host very fast. When cultivated in hen eggs for several generations, only the viral particles with the optimal mutations in their components survive due to the evolutionary pressure. Transferring these modified viruses to humans again, the suboptimal adaptation to the host probably leads to prolonged replication times giving the immune system enough time to react. This method is suitable especially for fast adapting viruses to control the production time in the other hosts. After administration of the live but attenuated virus particles, they can of course re-adapt to human cells and cause unwanted strong responses. This is also the reason why such attenuated vaccines are not approved for immunocompromised patients [72]. This limitation also applies for engineered viral particles as delivery system for proteins or nucleic acids. Such viral vectors have the additional problem that immune stimulation by the carrier lead to a fast elimination [46].

### 1.3.2 Protein and Subunit Vaccines

The next vaccine type in the row with increasing distance to the original pathogen are the protein and subunit vaccines. As described in 1.1.2, the immune system reacts only to small sections of the pathogen, so called epitopes. Every pathogen has many of these epitopes the immune cells could possibly recognize. During the development, the epitopes on proteins and other structures first need to be identified and selected. It should be considered how likely a mutation of this epitope is because it will jeopardize the success of the vaccine when pathogens can evade the immune response. Good candidates are for example surface structures that the virus needs for the contact with the host cell because these are essential for its survival and therefore rather conserved than often mutated [73]. This increases the chance that the vaccine is also effective against new variants that may have modified properties for instance for protein translation but still with the same surface structure. A general drawback of this approach is the time and cost consuming, complex production, isolation and purification of the proteins from large bioreactors [74].

An advantage of subunit vaccines is that the thorough selection of the antigenic regions reduces the risk to unwanted adverse effects to a minimum but on the same time, the small size of particles also reduced the immunogenicity. The elicited immune response will not be sufficient to reach a protection of the patient. One option is to combine different epitopes which also reduces the risk of immune escape after mutation. The more common way is the addition of adjuvants, which can be combined with the first approach. Long-known adjuvants like alum (aluminum salts) that increases the size by precipitation and adsorption [75], agonist of the toll-like receptors like polyinosinic-polycytidylic acid, a double stranded RNA analog (p(I:C)), or oil-in-water emulsions generate a danger

signal stimulating an immune reaction [76]. These adjuvants are approved only for intramuscular vaccination where they compensate for the low immune cell density in the muscle. An application to the skin would cause severe and persistent inflammation with skin lesions, erythema, local reactogenicity and ulceration [58]. Nevertheless, the addition of any kind of adjuvant has a certain risk of adverse side effect.

There are also approved vaccines where the antigen is covalently linked or adsorbed to immunogenic subunits of other species which increases the size and immunogenicity [77]. New approaches that use extracellular vesicles mimicking pathogens with all their surface structures are currently investigated on a preclinical level [78].

In theory, all these kinds of antigens independent of their modification could be delivered with nanocarriers as well which increases the size, the immunogenicity and potentially the amount of delivered antigen. As mentioned before, viral particles were engineered to carry the antigen but also a variety of non-viral vectors are in focus of research and have been recently approved for the SARS Cov2 vaccine. The different nanoparticle technologies will be discussed later (see chapter 1.4). Compared to the other vaccine types described before, there is no pathogen applied and is therefore considered as safer without any potential to regain virulence. Thus, vaccines of this type are approved for elderly and immunocompromised patients, too. For these patient populations, there is not anymore the risk to cause severe symptoms but instead the chance of insufficient protection due to a suboptimal immune response.

### 1.3.3 Nucleic Acid-based Vaccines

The next generation of vaccines are based on nucleic acids encoding for the antigen instead of delivering the protein itself. This eliminates the main drawback of the protein-based vaccines – the production and purification of the antigen. When delivering nucleic acids, the host cell takes over this job and produces the antigen by itself resulting in the presentation towards the immune system. As for proteins, the epitopes need to be investigated and selected but with less restrictions. Nucleic acids delivery for instance enables the selection of large transmembrane proteins, post-translationally processed proteins and adds the flexibility that the protein product could be secreted or remain intracellular which is not possible with delivering the protein [79].

Having chosen the sequence of nucleobases encoding for the antigen epitope, the amplification is possible *in vitro* from the scratch using automated protocols generating huge amounts of a good purity in a short time [46]. Having large amounts of the material available already early in the development, accelerates the acquisition of needed data for the application of approval and thus the entire process. These progresses in standard production procedures further led to commercially available nucleic acids encoding for fluorescent proteins or model antigens. The high price per microgram still limits the broad access, but nevertheless more researchers can work with nucleic acids to test their hypothesis and thus improve general knowledge.

Another important advantage lies in the interchangeability of encoded information. When results indicate that the epitope is suboptimal and should be exchanged, a change of the sequence of nucleobases only minimally affects the properties of the molecule. All established production steps can be continuously used. Most findings of process optimization assessments can be for instance transferred independent of the application of the nucleic acid molecule. In that sense, the developer of the first mRNA-based vaccine profited a lot from earlier research on cancer vaccines, especially when it came to the carrier system [80]. This transferability even applies for results with different types of nucleic acids such as siRNA, DNA or mRNA but differences in length, stability and charge density must be considered. It should be tested in every case if findings are also valid in the selected setup, especially concerning the transfection potential [81].

## 1 General Introduction

Nucleic acids have an inherent immunostimulatory effect that is especially interesting for vaccination. As viruses use nucleic acids to encode for their genetic material as well, the intracellular presence of foreign nucleic acids is an indicator for an infection and stimulates innate pattern recognition receptors like toll like receptors [82]. The activated cascade leads to presentation of the nucleic acids via MHC I to finally elicit the eradication of the cell and thus the virus. For vaccination purposes, it is important that the transfected cell is not attacked before the antigen can be produced for a certain time. It was therefore necessary to reduce the immune stimulating potential of the applied nucleic acids. A modification of single nucleobases by replacing uridine by pseudouridine [83] or methylating uracil reduces the interaction with intracellular sensors and thus the immunogenicity [84]. Another approach is the engineering of the base sequence while maintaining the translatable information [85]. These modifications also improve the stability of the nucleic acids which is a welcomed side effect. A balance between stimulation and escape of cellular sensing mechanisms needs to be found.

This additional effect of immune stimulation by nucleic acids was for example proofed for DNA vaccines. The direct comparison of DNA with the corresponding protein, showed similar IgG titers but a 100fold higher interaction strength (avidity) with DNA after intramuscular and even 1000fold improvement after intradermal injection of both candidates. Estimating the amount of produced protein after DNA administration to be in the nanogram range, the amount of protein that was needed for similar responses was hundreds fold higher [46]. It's worth to mention that there is also the next development step under investigation with self-amplifying mRNA that has the potential to further decrease the required dose [32].

The delivery of nucleic acid-based vaccines mimics the infection with an intracellular pathogen like a virus. The elicited immune response is therefore concentrated mainly on cellular effector cells like CTL that destroy the transfected or later the infected cells [19]. The humoral response is weaker than for protein-based vaccines, where the balance is more on the side of antibody-based defense mechanisms [86]. For the protection of the individual against infection or severe symptoms, a broad antigen expression is needed to trigger both parts [87].

The described advantages apply for all kinds of nucleic acids. For vaccination purposes, information has to be added to the cells which excludes for example siRNA from the list of candidates. In theory, vaccination with both, DNA and mRNA are thinkable and great successes have been realized but to date there are only mRNA-based vaccines approved for human use and there are clear reasons for it. All eucaryotic cells use DNA as genetic material to transfer the information for all peptides and proteins to the next generation. The integrity of the nucleic acid molecule is crucial for the survival of the organism. Several mechanisms to protect the DNA from potentially harmful influences or modifications have been implemented by evolutionary processes such as the enclosure in the nucleus. Furthermore, the translation of the encoded information works only in one direction and even happens in two different cellular compartments. DNA is transcribed into mRNA that is then translocated to the cytoplasm and there translated into peptides.

When delivering DNA to a cell, the nucleic acids have to reach the nucleus. The delivered plasmid needs to enclose all needed sequences for the successful transcription and later – after the translocation of the corresponding mRNA to the cytosol – also for the translation. These aspects render the design of plasmids more complex and enlarge their size. In contrast, the construction of a deliverable mRNA molecule is more straight forward. On the other side, the extra step of transcription is a possibility of amplification. Out of one delivered plasmid, several mRNAs can be generated resulting probably in more antigen molecules at the end. Favoring mRNA, one could also argue that the smaller size of the corresponding mRNA enables a delivery of more than one molecule on the same carrier which might compensate to the lack of this amplification step. But this rather a property of the carrier that will be discussed in the following.

## 1 General Introduction

Another considerable aspect of the inherent biological functions of the nucleic acids is their half-life. DNA is more durable and meant to persist many generations of cells. For skin vaccination, there are reports about device-based techniques that work with naked DNA, too, but require high doses. Even though protein production was only observed 1 and 7 d post application, foreign DNA was still detectable in the muscle after 6 months [88].

On the other side, mRNA is only transiently needed to produce a protein for example in reaction to a changed nutrient supply. After 5 h, mRNAs will be degraded which would also apply for the delivered antigen mRNA unless modification increase stability [89, 90]. The protein antigen will endure the mRNA for some time finally leading to a resolution of the antigen signal. This transient nature of mRNA delivered signal is rather beneficial as it increases the safety of the vaccine.

In contrast, with foreign DNA in the nucleus there is the chance that parts are integrated into the host DNA. This process of insertional mutagenesis cannot be reversed intentionally and the modifications will be even transferred to the next generation [91]. The consequences strongly depend on the site of insertion with unpredictable effects. Among them is the risk of malignancy. This represents the main safety concern of DNA application to human and is probably the reason for the lack of an approved DNA vaccine despite the uncountable reports of successful stimulation of immune responses in preclinical animal models in the last three decades [92].

These tremendous benefits of using nucleic acids can only elicit an effect when inside the cell. There are many reports available that proof that naked mRNA only elicits an immune response when delivered with a vehicle [93–95]. The delivery is essential but remains a challenge due to the nucleic acid properties such as large size, hydrophilicity and high negative charge. This is the topic of the next chapter.

## 1.4 Nanoparticles as Delivery System for mRNA

Depending on the cargo and the selected application route, the delivery system must fulfil different demands. At the baseline, it must carry the cargo in its intact form in sufficient amounts to the site of action. While the amount is often the limiting factor for encapsulated proteins, the main challenge for nucleic acids is their protection.

As part of cellular resource saving and regulation mechanisms, there are nucleases in every cell to digest nucleic acids that are not anymore needed. Especially in the endo- and lysosomes, nucleases protect cells from foreign genetic material that could potentially harm the host. For this reason, nucleases are also excreted to the extracellular space. Being a non-specific defense method, nucleases are found for example on the skin surface, too. This ubiquitous presence of nuclease everywhere in the human body limits the application of naked nucleic acids. In the blood, the half-life of naked DNA is for example less than 5 min, nothing of the injected dose is left after one hour [88]. mRNA is even more sensitive as added molecules cannot be amplified anymore after 15 s in plasma [96].

Independent of the human body, nucleases are also detectable abundant in our environment, for instance on the surface of lab benches, vials or in liquids. Nuclease-free material is therefore a prerequisite for any handling procedure of nucleic acids in the lab.

Next to their omnipresent nature, these enzymes are fast and effective in deleting the information that is encoded in the sequence. When the nucleic acid molecule is cut at only one position, the message is lost. This accounts also for vaccines as the intact antigen first needs to be produced by the cells. For proteins instead, a partly degraded antigen could still elicit an immune reaction if not all epitopes are destroyed.

This crucial demand for protection can be realized by many different strategies. Most of these delivery technologies have in common that complexation to the carrier generates a steric barrier for the enzymes and that delivery systems are in the nanometer range (1–1000 nm) [97]. Taking the first hurdle to protect the nucleic acids by complexation, the next step is the application route. Very large particles may be immunogenic themselves and above 200 nm, they cause embolization when injected intravenously for instance [98]. A small size is also beneficial to profit from the EPR (enhanced permeation and retention) effect. Through the endothelial gaps and pores in liver, tumors or infected tissues nanoparticles leave the circulation and selectively accumulate representing a passive targeting mechanism [99, 100]. Reducing the size of the particles also increases the surface that is available for complexation.

When the nanocarrier then gets in contact with the cell, it needs to be uptaken. This will probably happen by endocytosis [101]. A direct transfer through the membrane is unlikely. The escape from the endosome prior to digestion finally releases the nucleic acid to the cytosol. This process of disruption after swelling of the endosomes can be initiated by the buffering capacity of nanoparticles that activates proton pumps which raises osmotic pressure [102–104]. An alternative hypothetical mechanism is the electrostatic interaction of cationic particles with the anionic endosomal membrane with destabilizes the latter [102].

The key parameter that is influenced by all these described properties, and additionally by the characteristics of the nucleic acid and cellular process that are independent of the other factors is the transfection efficacy. It summarizes all these components and is therefore suitable to compare different systems as the establishment of structure activity relations remains difficult [105]. In an experimental setup, the amount of produced protein can be quantified. The onset and interval of protein production may be complementing parameters. For vaccination, it is furthermore important

## 1 General Introduction

if the delivered antigen elicits an immune reaction. That feature strongly depends on the application route and has therefore already been discussed in chapter 1.1.2.

All these criteria apply for all kinds of nucleic acids. For DNA, there would be an additional step for the delivery to the nucleus. As mentioned earlier, engineered viruses like particles are generally an option for nucleic acid delivery but their high immunogenicity bears the risk of side effects, and their production is challenging. Non-viral vectors can be in contrast prepared by chemical synthesis that enables larger scales. They theoretically have a lower toxicity and a higher delivery capacity also for larger nucleic acids which is beneficial for the application [106, 107]. In the following, it will be illustrated what kind of nanocarriers fulfill these specifications. As the aim of this work is the delivery of mRNA by non-viral vectors, only those carrier systems will be described in more detail now.

First delivery systems were based on lipids that form liposomes with lipid bilayers. It is possible to encapsulate the nucleic acid in the core or after preparation of the lipid nanoparticle on the outside. Results proved that both ways protect the nucleic acids from degradation enzymes [108, 109]. The systemic application is limited by opsonization of serum proteins and toxicity associated with complement activation [110]. In the context of mRNA vaccination, the first publication by Martinon et al. in 1993 showed that it was possible to trigger a CTL response after subcutaneous and intravenous application [93]. These results were later complemented by successfully eliciting both, cellular and humoral responses with mRNA-loaded liposomes [111].

As an alternative to the rather soft liposomes, a variety of polymers was investigated for mRNA delivery. As with lipids, there is the option to complex the nucleic acid in the core or on the outside. Polymers should be biodegradable or at least well eliminated from the body. Their origin can be either synthetic or based on naturally occurring polymers that are modified to meet the requirements. The interaction can be reversible or covalent. There are long known polymers such as the cationic PEI (polyethyleneimine) or newly synthesized polymers with tunable properties [112–114]. Mixing mRNA with the natural occurring cationic peptide protamine already protected the nucleic acid from degradation [115]. Such complexes of protamine and mRNA have even made their way into clinical trials where their safety, tolerability and immunogenicity was shown for cancer vaccination [116].

Another biodegradable polymer that is well characterized, also for nucleic acid delivery, is PLGA (poly(lactid-co-glycolid)) [117]. There are also reports about combinations of several polymers [118]. The large advantage of polymers is their high stability also in complexes. Only recently, a new mRNA vaccine made of poly( $\beta$ -amino ester) (PBAE) was reported to elicit an immune response after application via the harsh conditions of the gastrointestinal tract [119]. This supports the high potential of polymeric nanoparticles and may be the next candidate for a clinical study.

The breakthrough with the first approved mRNA-based vaccine came with solid lipid nanoparticles (SLNs) [120]. They are composed of lipids filling up the particle core as well instead of forming only bilayers [80]. The lipid content and thus the potential binding sites for electrostatically binding the nucleic acid is dramatically increased. Not only encapsulation efficacy is high but also the drug loading that correlates with the amount of nanocarrier that needs to be applied to reach the full dose.

Such solid lipid nanoparticles are produced with microfluidic devices under acidic conditions. The pH around 3 protonates the ionizable lipid that is responsible for the complexation and endosomal escape of the nucleic acid [81]. After preparation of the particles, the buffer is exchanged to reach physiologic pH-values where the ionizable lipid is neutral reducing its toxicity [121]. Next to the ionizable lipid, there are helper lipids to support both, endosomal escape and encapsulation, and structural lipids, mostly cholesterol that improves particle stability and membrane fusion [122, 123].

## 1 General Introduction

In most cases, a pegylated lipid is added to increase storage stability by reducing aggregation and immune cell opsonization [124, 125].

They can be loaded with different kinds of nucleic acids and engineered to target selected organs [126]. Without a targeting modification, more than 80% of mRNA is deposited in the liver after intravenous administration of an often-used SLN composed of C12-200, DOPE (1,2-dioleoyl-sn-glycero-3-phosphoethanolamine), cholesterol and DMG-PEG2000 (1,2-Dimyristoyl-sn-glycero-3-methoxypolyethylene glycol). The nucleic acid is locally detectable for up to 72 h, while produced protein is found for up to a week [91].

Based on this general structure, many modifications have been realized for every component to adapt the carrier for different purposes. Especially for the ionizable lipid, a large library of new candidates has been synthesized and patented with continuously less structure relationship to the originally used cationic lipids [127–129]. Such synthetic materials have a certain toxic potential and can accumulate mainly in the liver or spleen which was addressed for example by even more modifications [130, 131]. Cholesterol analogues were shown to improve endosomal escape but this modification was not widely implemented [132].

Helper lipids are mostly phospholipids like DOPC (1,2-Dioleoyl-sn-glycero-3-phosphocholine), DSPC (1,2-Distearoyl-sn-glycero-3-phosphocholine) or phosphatidylserine (PS) [122, 133]. Among them, DOPE has many well investigated benefits. It for example enhances the membrane fluidity resulting in a better protein adsorption such as apolipoprotein E in the blood. Binding this protein, leads to an enhanced liver delivery [122].

Widely used pegylation is always a compromise between benefits for particulate stability and the reduction of efficacy. Optimal concentrations are usually in the range of 0.5-5 mol% for nanoparticles in general [134]. For DMG-PEG2000 as part of solid lipid nanoparticles, the best results were generated with 1.5 mol% for siRNA [135] and mRNA delivery [136]. The attachment of long PEG chains onto the nanoparticle surface adds 3-5 nm of a hydrophilic barrier to the surface [100, 137]. As mentioned before, this reduces the interaction between nanocarriers before administration sterically and therefore increases the stability of the formulation. After application *in vivo*, the additional hydrophilic layer inhibits adsorption of plasma proteins [138]. The lack of opsonization reduces uptake into the liver and recognition by the immune system which both extend circulation time [127, 139].

Simultaneously, the interaction with cell membranes is influenced, too, which can jeopardize uptake or endosomal escape [100, 140]. Possible solutions are the reduction of the PEG content, chain shortage or releasing the PEG chain directly before uptake by the target cell when it is not needed anymore resulting in transfection-competent nanocarriers [99]. The longer the PEG chain, the less amount is needed to inhibit the complement activation [141]. PEG chains with a molecular weight above 2000 for instance reduce the interaction with the cells [142]. Depending on the chain length of the lipid anchor, the PEG chain desorbs from the nanoparticle as it is the case for DMG-PEG2000 (C14) or remain associated in circulation (C18 or C20) [143]. An anchor with a chain lengths below C10 diffuses too fast to elicit the wanted effect [99].

Despite these benefits of the solid lipid nanoparticles that allowed the approval for emergency use against Covid-19, there are also limitations. Especially a repeated administration of such solid lipid nanoparticles can elicit a so called cytokine release syndrome by the massive production of interleukin 6 in the spleen [144].

For all these nanoparticles based on this new, versatile group of carriers, the storage stability is a main issue. The first approved mRNA-based vaccines must be stored at -80°C which is a huge challenge for the supply chain and health care system.

The combination of the good transfection properties of lipids with the high stability of polymers has the potential to solve this problem of storage stability. It has been already shown that they

## 1 General Introduction

successfully delivery mRNA *in vitro* and *in vivo*. Hybrid nanoparticles made of PBAE and phospholipids successfully transfected about 30% of cells *in vitro* and even resulted in significant proteins level in mice after intranasal application [145]. Synergistic effects were reported by transfection rates of a combined hybrid nanoparticle that outperformed single component particles either made of protamine or DOTAP [146]. Yasar et al. proofed that this effect is associated with the hybrid combination of lipids and polymer as polymer-polymer-nanoparticles transfected less cells *in vitro* [147].

This lipid-polymer hybrid nanoparticle (LPN) is made of the biodegradable and well characterized PLGA and the cationic lipid DOTMA (1,2-di-O-octadecenyl-3-trimethylammonium propane) resulting in a positive surface charge that was used for the complexation of mRNA [117]. In general, these surface charges are related with toxic effects that often limit dosing and therapeutic effects [148]. For DOTMA in particular, necrosis was among the reported cytotoxic effects [149]. Another problem is the mentioned opsonization of cationic surfaces *in vivo* that leads to an immune stimulation and probably further adverse effects.

One strategy to cope with these limitations would be the reduction of cationic surface charge by reducing the cationic lipid content. Despite being responsible for nucleic acid interaction, the ionizable lipid in SLNs makes up maximum 50 mol% mainly next to helper lipids and cholesterol [150]. It needs to be investigated if such a composition might also work for lipid-polymer hybrid nanoparticles. A promising candidate for the partial replacement of DOTMA in the LPN is the phospholipid DOPE with many reported advantages. As mentioned before, it is known to enhance membrane fluidity [122]. DOPE promotes the transition to the hexagonal phase that is crucial for the endosomal escape and the release of the nucleic acid [151–153]. These properties end up in an improvement of mRNA transfection efficacy [81]. Furthermore, the combination of DOTMA and DOPE has been successfully investigated for nucleic acid delivery already and even commercialized as Lipofectin®. This transfection reagent is composed of a 1:1 mixture of the two lipids and has been used for over 30 years for DNA delivery [154] and mRNA transfection *in vitro* and *in vivo* [93, 155, 156]. The addition of DOPE to the hybrid lipid-polymer hybrid nanoparticle is therefore a feasible strategy of optimization.

### 1.5 Aim of This Thesis

The aim of this thesis was to develop a skin vaccination platform based on a minimally invasive application technique and mRNA-loaded nanocarriers. Due to the versatile properties of nucleic acids, an exchange of the sequence would enable vaccination against many different pathogens. Targeting immune cells in the upper layers of the skin with the laser-based administration, enhances the immunogenicity of the vaccine with the potential of dose reduction and simultaneously increases the compliance of the patients as application side effects like pain can be reduced.

mRNA-based vaccines have proven their potential to elicit a protective immune response in human beings. The first two vaccines of this new kind were approved and due to the Covid-19 pandemic they have been already applied to millions of individuals generating large data sets that will help in the development of similar vaccines. Despite this great success that paved the way in many directions, there are still drawbacks such as the storage stability of the solid lipid nanoparticles and the suboptimal application route via the muscle. The aim of this thesis was to address both of these topics that existed also before outbreak of the pandemic.

The first part of this work was the optimization of an existing carrier system for mRNA delivery that combined the good transfection properties of the cationic lipid DOTMA with the high stability of a polymer, namely PLGA. The focus was mainly on an improvement of the performance under stress conditions, in particular the protection against RNases, and a reduction of toxicity. The influence of the newly added phospholipid DOPE onto the particle characteristics was thoroughly investigated. In a next step, the effect of pegylation was assessed regarding a potential improvement of colloidal stability and tissue penetration properties.

This nanotechnological part was complemented by the evaluation of the best candidates for skin application to profit from high immune cell density and thus the potential to elicit protective responses with lower delivered doses. A minimally invasive administration technique using an ablative laser was selected to apply the mRNA-loaded nanocarriers in a two-step protocol. Created micropores by the selected P.L.E.A.S.E.<sup>®</sup> system are supposed to transiently disrupt the skin barrier attracting and stimulating immune cells and at the same time enabling particle penetration and antigen production in the skin tissue. This immunostimulatory potential of generated micropores with selected depth targeting the divers skin layers was tested in a mouse model. The microporation parameters were then adapted to human skin where particle penetration properties were compared between different application routes. An *ex vivo* human skin model was established to quantify the effect of the optimized nanocarriers for mRNA delivery over a course of one week. The focus was on the transfection rates and the ability to stimulate immune cells to migrate out of the skin tissue. The benefits of the laser-mediated application were tested against intradermal injection.

## 2 Materials and Methods

### 2.1 Nanoparticle Preparation and mRNA Loading Procedure

#### 2.1.1 Lipid-polymer Hybrid Nanoparticles

In this work, the lipid-polymer hybrid nanoparticles consist of a PLGA core (Resomer RG 503H, 50:50, Evonik Industries Ag, Germany) and a layer with different ratios of the lipids DOTMA and/or DOPE (both Avanti polar lipids, USA). The used ratios varied from DOTMA-only (labeled as LPN(0/100)) to DOPE-only LPNs (LPN(100/0)). The nomenclature of the nanoparticles refers to the molar percentages of DOPE (first number) and DOTMA (second number) as shown in Figure 1.

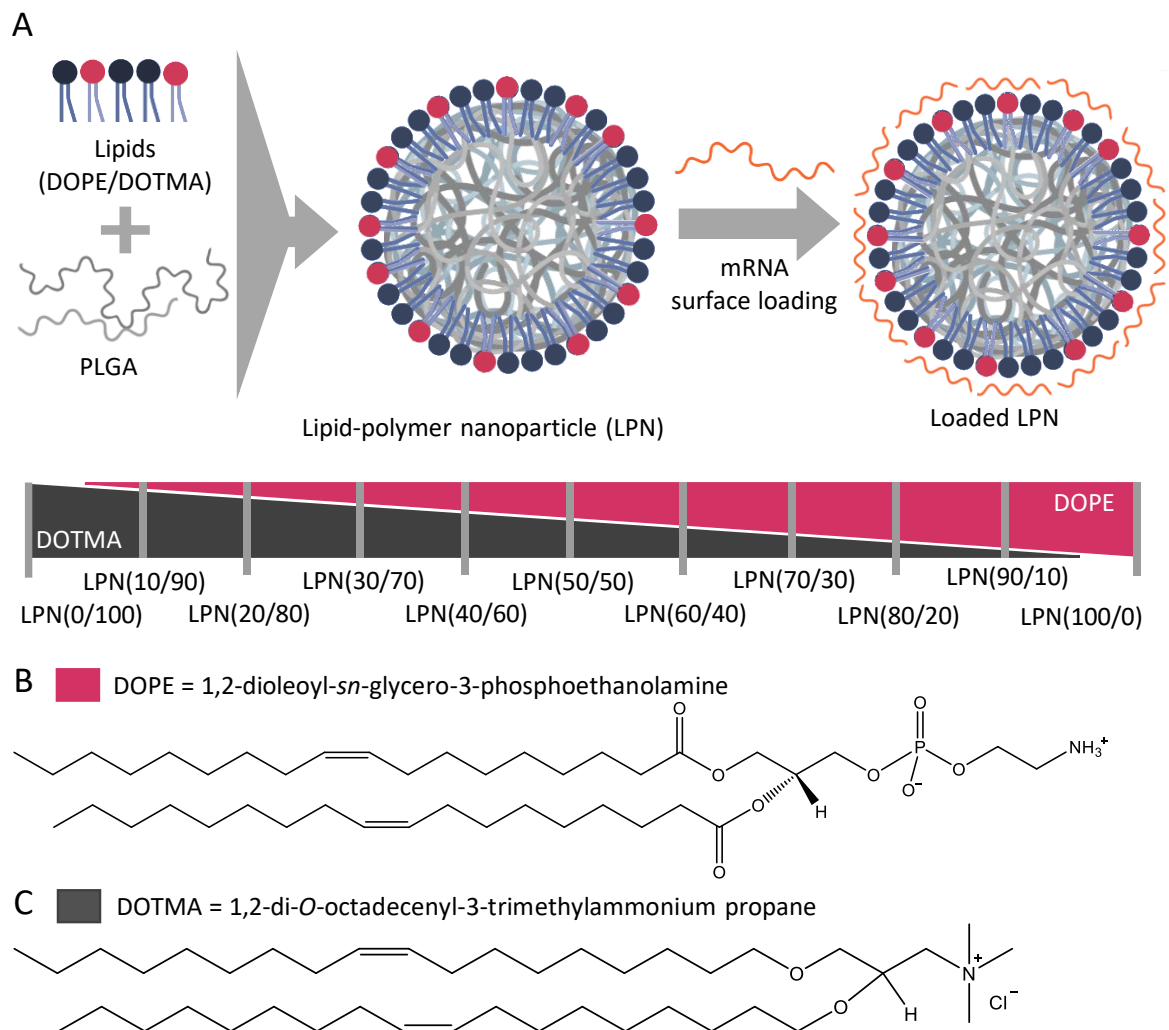


**Figure 1:** (A): Anticipated structure of nanocarriers. Nomenclature refers to the molar percentages of the DOPE (first number in brackets) and DOTMA (second number) amount in the lipid layer. (B): structure of DOPE (1,2-dioleoyl-*sn*-glycero-3-phosphoethanolamine), (C): structure of DOTMA (1,2-di-*O*-octadecenyl-3-trimethylammonium propane). Graph has been published in Kliesch et al. [157]

For the preparation of all nanoparticles, the same modified double-emulsion evaporation method was used based on the published protocol by Yasar et al. [147]. In brief, a stock solution of DOPE (25 mg/ml) was prepared using chloroform (Sigma-Aldrich, Germany). DOTMA was purchased as chloroform solution in the same concentration. Aliquots of lipids were mixed by vortexing while keeping the overall number of nitrogen atoms constant to ensure comparable numbers of potential binding partners for mRNA complexation. This lipid mixture was then combined with a PLGA solution

(30 mg/ml in chloroform) and diluted with chloroform to a total volume of 500  $\mu$ l. After thorough mixing by vortexing, 250  $\mu$ l ultra-purified water (Milli-Q<sup>®</sup>, Merck Millipore, Germany) (MQ) were added followed by ultrasound sonication for 30 s at an amplitude of 30% to create a water-in-oil-emulsion. Immediately 1 ml of polyvinyl alcohol (PVA) in MQ (2% w/v, Mowiol 4-88, Sigma-Aldrich, Germany) was added and again homogenized by ultrasonication. After pouring this emulsion into 5 ml PVA-solution, the water-in-oil-in-water double-emulsion was stirred for 3 h to evaporate the organic phase. LPNs were stored in the fridge until usage.

### 2.1.2 Pegylated LPNs

For the pegylation of the LPNs, a third lipid was added during the first mixing step of the protocol. The selected DMG-PEG2000 (CAS 160743-62-4, MedChemExpress, USA) replaced 0.5–5 mol% of DOPE by the new lipid. In this case, the concentration of the stock solution was 10 mg/ml in chloroform.

### 2.1.3 Fluorescence Labeled LPNs

Depending on the assay, I used two different ways of fluorescent labeling of the LPNs. First, fluoresceinamine (Sigma-Aldrich, Germany) was covalently coupled to PLGA as published in the protocol of Weiss et al. [158]. This modified PLGA replaced the non-labeled PLGA during the particle preparation procedure resulting in fluorescein isothiocyanate-labeled LPNs (FITC-labeled LPNs).

To generate a fluorescent label in the far-red spectrum, we selected DiD (1,1-dioctadecyl-3,3,3,3-tetramethylindodicarbocyanine, 10 mg/mL in ethanol, D7757, life technologies, Invitrogen, USA) and added 9  $\mu$ l of the dye solution to the unlabeled PLGA before mixing with the lipids. This resulted in a non-covalent incorporation into the LPNs. Unbound dye was removed by dialysis through a 100 kDa membrane for 24 h under light protection.

### 2.1.4 mRNA Loading and Release

For the electrostatic loading of mRNA onto the surface of the LPNs, appropriate amounts of nucleic acid were carefully pipetted into the nanoparticles' suspensions and incubated for one hour at room temperature (RT). Unless stated otherwise, mRNA encoding for the fluorescent reporter protein mCherry (CleanCap™ mCherry mRNA (5moU), 7203; TriLink BioTechnologies LLC, USA) with a stock concentration of 1  $\mu$ g/ $\mu$ L was used.

Yasar et al. showed that for DOTMA-only LPNs (LPN(0/100)) the optimal weight ratio is 1:20 which corresponds to a N:P ratio of 2.81 [117]. This N:P ratio was applied to all LPNs and used for all displayed experiments.

To later release the mRNA again from the nanoparticles by competitively occupying nucleic acids binding sites, two kinds of heparin were selected. Low molecular weight heparin (H3393-25KU, 119.1 mg solid) and high molecular weight heparin (H3393-100KU, 534.4 mg solid; both Grade I-A, Sigma-Aldrich, Germany) were dissolved in MQ in different concentrations. For the RNase exposure experiment, I finally added 375  $\mu$ g of dissolved heparin (30 mg/mL in MQ) per microgram mRNA for 30 min at RT.

## 2.2 Nanoparticle Characterization Without Cells

### 2.2.1 Dynamic Light Scattering

Dynamic Light Scattering (DLS; Zetasizer Nano, Malvern Instruments, UK) was used to characterize the nanoparticles' physicochemical properties such as hydrodynamic size, polydispersity index (PDI) and surface zeta potential. For that purpose, LPN stock solutions were warmed to room temperature, diluted 10 – fold with MQ and measured three times resulting in a mean value with standard deviation.

### 2.2.2 Nanoparticle Tracking Analysis

Nanoparticle tracking analysis (NanoSight LM10, Malvern Instruments, UK) enables the detection of fluorescent DiD-labeled LPNs against the background signal of the medium and thus the investigation of nanoparticle stability in more complex media. An incubation under gentle shaking at 37 °C in MQ was compared with the incubation in RPMI medium supplemented with 10% FCS, HEPES buffer, non-essential amino acids and  $\beta$ -mercaptoethanol representing the regular cultivation medium for the selected dendritic cell line DC2.4 (for details see 2.3.1). Nanoparticle concentrations and the time points were chosen to match the later established standard transfection protocols (see 2.3.6). After 0 h, 4 h and 24 h ongoing reactions were stopped by taking aliquots and diluting them 5-fold in MQ. For each sample three videos of 30 s were recorded in the fluorescence channel. These video tracks were analyzed with the NanoSight 3.3 software.

### 2.2.3 Cryo-TEM imaging

A 3  $\mu$ l droplet of the LPN sample was placed on a holey carbon supporting TEM (transmission electron microscopy) grid (Plano, Germany, type S147-4), blotted for 2 s and plunge-frozen in undercooled liquid ethane with a Gatan CP3 plunge freezer (United States) operating at  $-165$  °C. After transferring the vitreous sample under liquid nitrogen to a Gatan model 914 cryo-TEM sample holder, the samples were investigated by TEM (JEOL, Akishima, Tokyo, Japan, model JEM-2100 LaB6) bright field imaging at 200 kV accelerating voltage under low-dose conditions and imaged using a Gatan Orius SC1000 CCD camera and an exposure time of 4 s.

### 2.2.4 Lyophilization

For the stability study, aliquots of 1 ml plain LPN suspension were diluted with 4 ml trehalose solution in MQ (10 mg; final concentration 0.2%; D-(+)-trehalose dihydrate, CAS 6138-23-4, T0167, Sigma-Aldrich) and frozen at  $-80$  °C. In parallel, samples without trehalose were prepared the same way. Vessels were then covered with perforated parafilm and transferred to the precooled freeze drier. The automated drying program was run overnight. Lyo cakes were reconstituted with MQ.

For experiments with excised human skin, LPNs were first loaded with mRNA. After freezing at  $-80$  °C, samples were freeze dried over night with the standard program and parafilm. Samples were reconstituted with PBS on the day of the experiment.

### 2.2.5 RiboGreen® Assay and Binding Efficacy

To enable the quantification of bound fraction of mRNA, I used the Quant-iT™ RiboGreen® RNA quantification kit (Molecular Probes, Inc., USA) following the manufacturer's protocol. mRNA-loaded LPN samples were diluted 1:100 with Tris-EDTA (TE)-buffer to a volume of 100  $\mu$ l and mixed with 100  $\mu$ l RiboGreen® dye (1:200 in TE-buffer) in a black 96-well plate for 5 min. The plate reader (Infinite 200 Pro, Tecan Austria GmbH, Austria) measured the fluorescence signal with an excitation

wavelength of 480 nm and an emission of 520 nm. The binding efficacy of LPN samples was calculated relative to the fluorescence of the naked mRNA sample on the same plate.

### 2.2.6 Gel Electrophoresis

A gel retardation assay was used to confirm the successful loading of the mRNA onto the LPNs. The 0.7% *w/v* agarose gels (molecular biology grade, Serva, Germany) contained 35 µg ethidium bromide each (stock 10 mg/mL in water, Sigma-Aldrich, Germany) and a 1X Tris-Borate-EDTA (TBE) buffer. Samples were mixed with orange loading dye (Thermo Fisher Scientific, USA) and loaded into the gel (400 ng mRNA per pocket). After running the electrophoresis at 60 V for 30 min, the nucleic acids were visualized with a Fusion FX7 UV illuminator (Peqlab, Germany).

For the setup of gel electrophoresis after RNase exposure, see 2.2.8.

### 2.2.7 Artificial Interstitial Fluid (AIF)

To mimic the surrounding that LPNs face when applied to the skin after microporation, an artificial wound fluid (AIF) based on the composition of interstitial fluid as prepared [159]. PBS was diluted 1:15 in MQ. A carbonate buffer was added followed by potassium, sodium, magnesium and calcium accordingly resulting in an AIF-buffer with a measured pH of 7.02. Together with the intern Tobias Neu, we compared the reaction of LPNs in this buffer with the effect of the buffer including albumin (20.6 g/l). To do so, LPNs stock dispersions were diluted in the corresponding fluid and then mRNA was added. After 1 h incubation time, the binding efficacy was measured with the RiboGreen® dye and gel electrophoresis.

### 2.2.8 RNase Exposure and mRNA Protection

Based on the RiboGreen® assay described in section 2.2.5, I designed a kinetic experiment to measure the degree of protection of the loaded mRNA by the LPNs against RNase A representing a crucial property of nanocarriers. The readout was always based on the measured fluorescence values of the RiboGreen® dye. All samples and reagents were dispersed in TE-buffer.

I started with the adjustment of the RNase A (DNase and Protease free, EN0531, Life Technologies Inc., USA) amount. In the first setup, different amounts of naked mRNA in TE-buffer were prepared and mixed with the RiboGreen® dye (1:200 in TE-buffer) in a 96 well-plate. I then added the same amount of RNase A by simple pipetting. Realizing that the enzymatic degradation happens within seconds, I changed to the automatic dispensing function of the plate reader. This enabled me to avoid delays during the initialization process of the kinetic experiment and to measure in short intervals of 1 minute for 30 minutes starting immediately after dispensation. As before, the amount of RNase A dispensed per well was the same, but mRNA concentrations were varied resulting in different effective concentrations for the enzyme.

Next, the aim was to confirm that the amount of the specific RiboLock RNase Inhibitor (10 U/ng RNase protein, EO0381, ThermoFischer Scientific, Lithuania) is enough to stop the degradation. Before adding any components, I measured the fluorescence of the naked mRNA in all prepared wells as quality control to ensure comparable values. I then added RiboLock to one group followed by RNase A. The fluorescence was measured every minute for 30 minutes.

To release as much mRNA as possible from the LPNs, I tested different concentrations of low (119.1 mg, H3393-25 KU) and high molecular weight heparin (534.4 mg, H3393-100KU, Grade I-A, low-molecular weight, Sigma-Aldrich, Germany). Starting with loaded LPN samples diluted 1:100 with TE-buffer, I this time mixed them with higher concentrations of RiboGreen® dye (1:100 in TE-buffer)

## 2 Materials and Methods

in a 96-well plate. Again, components were diluted in TE-buffer and changes of fluorescence measured every minute for 30 minutes.

After optimizing all steps of the experimental set up, I finally tested selected LPNs and measured the three parts after each other in one experiment (every minute for 30 minutes each). Starting again with loaded LPNs (1:100 in TE-buffer) 1:1 mixed with RiboGreen® (1:100 in TE-buffer), RNase A was automatically dispensed to the samples leading to a final nuclease concentration of 0.0013 Kunitz (K)/ $\mu\text{g}$  mRNA. I added the RiboLock inhibitor and – after 30 minutes of measuring – added high molecular heparin to release the remnant mRNA from the nanoparticles.

After the experiment, all measured values were corrected with the one of the corresponding blank undergoing the same treatment. For LPNs, I used plain, unloaded nanoparticles with the same composition and TE-buffer in case of the naked mRNA. For every step, corresponding amounts of TE-buffer were added to keep a constant volume of all samples. With this procedure I tried to reduce the influence of unspecific dye binding as much as possible. In the last step, we compared the adjusted values of the group treated with RNase A with the results of the samples treated with TE-buffer instead (manually added before RNase). RiboLock and heparin were added to all samples independent of the first treatment.

For confirm and enable better interpretation of results, I used the same concentrations of additives with larger aliquots of loaded LPNs parallel to the plate reader assay but without RiboGreen® because the dye was added to the agarose gel (1:2000 in agarose (0.7% w/v)). I ran the gel at 60 V for 60 min and visualized the nucleic acids with the fluorescence lamp (Fusion FX7, Peqlab, Germany). For LPN(70/30), I had one sample that underwent only a part of the protocol separately.

## 2.3 *In vitro* Characterization

### 2.3.1 Cell Cultivation

Unless stated otherwise, the murine bone marrow derived dendritic cell line DC2.4 (SSC142, Merck Millipore, Germany) was used for cell-based experiments. Dendritic cells are the main target for our vaccination strategy as they play a key role in the initiation of the immune response by presenting an antigen and activating other immune cells. Cells were cultured at standard growth conditions (humidified incubator at 37 °C with 5% CO<sub>2</sub>). Following the supplier's recommendation, RPMI medium (Roswell Park Memorial Institute; 1640 1X, Ref 21875, Gibco/Life Technologies, UK) was supplemented with 10% FCS (fetal calf serum, Ref 10270106, Gibco, UK), HEPES buffer (4-(2-hydroxyethyl)-1-piperazineethanesulfonic acid; 0.01M, Ref 15630, Gibco, UK), non-essential amino acids (1X, REF 11146, Gibco, UK) and β-mercaptoethanol (0.0054X, Ref ES-007-E, Millipore, UK).

### 2.3.2 MTT with A549 Cells

In a first cytotoxicity test, I used a colorimetric assay based on the reduction of 3-(4, 5-dimethylthiazol-2-yl)-2, 5-diphenyltetrazolium bromide (MTT) to its purple formazan by metabolically active cells. These crystals inside the cells can be quantified by absorbance measurements and are proportional to the number of viable cells in the sample [160].

For this cell metabolism-based assays, I used the lung derived cancer cell line A549 cultivated in RPMI medium including 10% FCS in a humidified incubator at 37 °C with 5% CO<sub>2</sub>. 10,000 cells in 200 μl growth medium were seeded for three days in a 96-well plate. In parallel, I prepared dilution rows of LPNs (0/100 – 50/50) in HBSS buffer (Hank's Balanced Salt Solution) as these LPNs contain more of the cationic lipid DOTMA and are thus expected to be the most toxic ones. Dilutions covered a range from 7 μg/ml up to the stock concentration of 1700 μg/ml.

On the day of experiment, cells were washed twice with prewarmed HBSS and samples were then added. I used plain HBSS as live control and a Triton-X-solution (1% in HBSS) as dead control. After 4 h of slow shaking in the incubator (37 °C with 5% CO<sub>2</sub>, humidified) the supernatant was removed from the cell layer. Cells were washed once with HBSS. After diluting the MTT reagent (Thiazolyl Blue Tetrazolium Bromide, Sigma-Aldrich; stock: 5 mg/ml in PBS) in HBSS, an aliquot of 100 μl was added per well for 4 h while slowly shaking at 37 °C. After another washing step with HBSS, dimethyl sulfoxide (DMSO) was added for 10 minutes to lyse the cells and to dissolve formazan crystals. I measured the absorbance at 550 nm at endpoint of this colorimetric assay and calculated the viability relative to the live (100%) and dead control (0%).

### 2.3.3 Live-Dead-Staining

I used several different setups to distinguish live and dead DC2.4 cells after particle exposure. The general setup was the same, though. 50,000 DC2.4 were seeded for 2 days in 500 μl growth medium in a 24-well plate. After washing twice with HBSS, I incubated the cells for 4 or 24 h with nanoparticles, washed again, detached cells, incubated with the staining solution and finalized sample preparation for flow cytometry by washing the cell suspensions again. As a last step, samples were diluted in FACS-buffer (2% FCS in HBSS) and immediately analyzed with the flow cytometer (BD LSR Fortessa Cell Analyzer, Biosciences, Germany). At least 10,000 events per sample were acquired.

Applying a dual staining set up, I used fluorescein diacetate (FDA) (1:1000 in PBS, stock 5 mg/ml in acetone, CAS 596-09-8) to stain live cells. The diacetate can pass cell membranes and is cleaved inside metabolically active cells. The free acid is trapped intracellularly emitting a green fluorescent signal. For staining the dead cells, I used either DAPI (1:1000 in PBS, stock 1 mg/ml in water, 4',6-

## 2 Materials and Methods

diamidino-2-phenylindole, CAS 28718-90-3) as polar dye or 7-aminoactinomycin D (7-AAD, part of the Promokine Live/Dead cell staining kit I, PK-CA577-K315) as very large molecule. Both dyes can only pass cell membranes if the barrier is interrupted due to ongoing cell death processes. All dyes were mixed in PBS and incubation time of the single cell suspensions was 20 min unless stated otherwise. As live control, I used the plain medium – HBSS or growth medium -, and as dead control 5% ethanol in HBSS.

After data acquisition, I used the FlowJo Software (FlowJo 10.8.1, FlowJo, USA) to gate for the cell populations. Graphing the dead cell signal on the x-axis and the live cell signal on the y-axis, I found four populations. The debris that were excluded, live cells and cells with a dead cell signal. These last cells were either dead with only the dead stain signal or double positive for the live and dead cell staining. I counted the double positive cells as dead because the harmed membrane structure indicates the beginning of cell death processes in these metabolically active cells. Results are expressed as percentage of viable cells normalized to all cells without debris.

### 2.3.4 Uptake

The uptake was quantified using LPNs that contained the FITC-linked PLGA and thus a green fluorescent signal. The results are expressed as percentage of cells, that is associated with this FITC-signal and simultaneously lacking a DAPI signal for cell membrane damage. Details of the experimental setup are described in 2.3.6 because data sets were collected in the same experiment as the cytotoxicity and the transfection efficacy.

### 2.3.5 Transfection

mRNA encoding for the fluorescent protein mCherry was chosen to assess how many cells produce how much of protein. The resulting red signal of successfully transfected cells was quantified parallel to the uptake and cytotoxicity assessment in the same experiment as described in 2.3.6.

### 2.3.6 Combined Live-Dead-Staining, Uptake and Transfection Efficacy

As preparation for the combined experimental setup, 50,000 DC2.4 cells were seeded in 500  $\mu$ l growth medium per well in a 24 well plate. After two days incubation at 37 °C and 5% CO<sub>2</sub>, cells were washed twice with prewarmed HBSS under the laminar flow bench and added fresh medium. I used either plain RPMI (no phenol red, 1640, Ref 11835, Gibco, UK) or the regular cultivation medium with all supplements. After loading FITC-labeled LPNs with mCherry-mRNA, I added the nanoparticles to the wells under non-sterile conditions reaching a nucleic acid concentration of 2  $\mu$ g/ml per well. 5% ethanol in HBSS was used as dead, supplemented growth medium as live control. Cells were incubated for 24 h while slowly shaking the plate in the incubator. For the evaluation of influence of FCS addition (Figure 22), I prepared HBSS or Opti-MEM® including 1-10% FCS. I incubated the cells only for 4 h with the LPNs dispersed in different media, washed with HBSS and added fresh medium for 24 h.

The next day, nanoparticles were removed. Cells were washed twice with prewarmed HBSS and detached from the wells with trypsin-EDTA for 5 min. After stopping the reaction with FACS-buffer (2% FCS in HBSS), I transferred the cell suspensions to round-bottom FACS tubes. To collect the cells, samples were centrifuged for 5 min at 300 g at 4 °C and washed with PBS. In the next step, I stained the dead cells by adding the DAPI (1:1000 in PBS, stock 1 mg/mL) staining solution for 20 min at room temperature and light protection. Immediately after this incubation time, 20,000 cells were measured in the flow cytometer.

Data analysis was separately performed with the FlowJo Software and percentages for potential cytotoxic effects, uptake and transfection efficacy calculated. The gating strategy is shown in the

supplementary Figure S 3. For the first parameter, I excluded cell debris and DAPI-positive, dead cells from the entire measured cell population leading to the live cell population. The uptake as second parameter is expressed as live cells that show a green signal indicating successful uptake of the FITC-labeled LPNs. The third parameter, the transfection efficacy, was calculated in two ways. On the one hand, I calculated how many cells in the entire cell population express the mCherry protein. On the other hand, I measured the percentage of transfected cells within the live cell population.

I used two different commercial transfection reagents as positive controls for the setup. On the one side, JetMESSENGER® (REF 150-01, Polyplus, France) as polymeric compound and Lipofectin® (18292011, Invitrogen, USA) as liposomal mixture composed of a 1:1 ratio of DOTMA and DOPE. I prepared JetMESSENGER according to the manufacturer's recommendation. In brief, 100 µl of the reaction buffer was mixed with each microgram mRNA, vortexed shortly and incubated for 45 min to prepare this control in parallel to the LPNs. 15 min before use, the JetMESSENGER® reagent (2 µl for each microgram mRNA) was added and shortly vortexed as well.

For Lipofectin®, I diluted 6.19 µl of the reagent with 50 µl HBSS per microgram mRNA. This calculated amount of Lipofectin® had the same number of bindings site as the LPNs resulting in the same N:P ratio of 2.81. In parallel, mRNA was diluted in another 50 µl HBSS. After 45 min, both solutions were combined, gently vortexed and incubated for 15 min.

### 2.3.7 Live Cell Imaging with Lionheart: Transfection Kinetics

50,000 DC2.4 were again seeded in 500 µl growth medium for 48 h but this time I used an imaging 24 well plate. During the incubation time of the mRNA complexation, I adjusted the autofocus settings with the cells and selected three areas per well where the automated microscope (Lionheart FX Live Cell Imager, BioTek, USA) would take the images. I washed the cells twice with prewarmed HBSS and stained the nuclei with the Hoechst dye (20 min, 1:1000 in HBSS) under light protection to enable a faster and better autofocus. After another two washing steps with prewarmed HBSS, I added non-supplemented medium and the nanoparticles for 5, 15, 30 or 60 minutes. Then, LPNs were removed again by washing twice with HBSS and fresh, non-supplemented medium was added for 24 h. As comparison, there was one well per group where I did not wash away the LPNs but incubated for the full 24 h with the nanoparticles. We selected a 45 min imaging interval during this incubation time in the automated microscope and measured the number of fluorescent cells and fluorescence intensities in the Hoechst and the mCherry channel parallel to the bright field. For this first experiment, I tested only LPN(70/30) as favorite LPN from previous uptake studies and as comparison LPNs (0/100), (10/90) and (50/50) to cover the entire range of formulations. LPN(100/0) was excluded as we cannot expect transfection without mRNA attachment to the surface. There was only one well per condition for this preliminary study with the FITC-labeled LPNs.

The next day after the last images were taken, I washed again twice with HBSS, detached the cells (5 min with trypsin-EDTA) and prepared them for flow cytometry as described in 2.3.6. As cells were already stained with the Hoechst dye, I skipped the DAPI staining step during the sample preparation. Thus, I could not distinguish live and dead cells during the analysis and adjusted the gating strategy accordingly.

After selecting the 24 h incubation time for further studies, I repeated the experiment again with incubation in non-supplemented medium. This time I determined 7 spots per well and a 30 min imaging interval. Staining and washing step were the same.

Images were analyzed with the Gen5 software (BioTek, USA). I applied a preprocessing step to all images. For the bright field and the DAPI channel with the cell nuclei we selected a radius of 30 µm. Images in the mCherry channel were not processed. For deduction of numbers of transfected cells, I used 2000 as threshold in the mCherry channel and an object size of 10–300 µm.

## 2.4 Primary Bone Marrow Derived Dendritic Cells

### 2.4.1 Isolation and Peptide Presentation

All experiments with primary, mouse derived cells and mice were conducted in cooperation with Simon Delandre from the Department of Vaccinology and Applied Microbiology at the Helmholtz Centre for Infection Research (HZI) in Braunschweig. To collect the bone marrow cells, we flushed the femur and tibial bones of 6–8-week-old C57BL/6 mice (Envigo, Germany) with culture medium (RPMI 1640 supplemented with 10% fetal calf serum, 100 U/mL penicillin, 50 µg/mL streptomycin, 100 µg/mL gentamycin; Gibco, USA). Next, we lysed the erythrocytes in ACK lysing buffer (Ammonium-Chloride-Potassium, Sigma-Aldrich, Germany) and seeded the remaining cells at  $1 \cdot 10^6$  cells/mL in culture medium supplemented with 5 ng/mL murine GM-CSF (BD Pharmingen, USA). 7 days later the bone marrow derived dendritic cells (BMDCs) were ready for experimental use.

We used the cells in different setups. For all experiments, we loaded the LPNs with mRNA encoding for the model antigen ovalbumin (OVA) (CleanCap™ OVA (5 moU); TriLink BioTechnologies LLC, USA) in the same N:P ratio as for mCherry mRNA. This enabled us to quantify not only the transfection efficacy but later steps in the immune activation cascade such as the presentation of peptide fragments on the cell surface and the consecutive activation of specific T cells.

In a first scenario, we transfected the isolated cells with OVA-mRNA-loaded LPNs for 3 h in Opti-MEM®. After washing, we added fresh medium for 48 h and analyzed transfection rates by quantifying the SIINFEKL peptide presented on the MHC-II receptor on the surface of the cells with a specific antibody and flow cytometry. An added live-dead-staining kit enabled assessment of cytotoxicity. The second setup was the activation of OVA-specific T cells described in the following chapter.

### 2.4.2 Antigen-specific T Cell Activation

This study was based on OVA-T cell-receptor transgenic mice OT-I (C57BL/6-Tg(TcraTcrb)1100Mjb/J) bred at the animal facilities at the HZI under specific pathogen-free conditions. Thus, we again used OVA-mRNA to load the LPNs matching the specificity of the CD8<sup>+</sup> T cells isolated from spleen and lymph nodes of the transgenic mice.

We added the loaded LPNs to the BMDCs in Opti-MEM® (REF 31985) for 3 h. After this first step, tested different procedures that are described in the corresponding Figure caption. In short, we tested a lower dose of 0.5 µg mRNA. The CD8<sup>+</sup> T cells were labeled with 10 µM carboxy fluorescein succinimidyl ester (CFSE; Molecular Probes, USA) and added to the potentially transfected BMDCs for 4 days without a post-incubation time in between. Lacking reliable readouts, we increased the dose to 1 µg mRNA. After further cultivation for 20 h in culture medium (RPMI 1640 supplemented with 10% fetal calf serum, 100 U/mL penicillin, 50 µg/mL streptomycin, 100 µg/mL gentamycin; Gibco, USA), a co-cultivation time of 6 days followed. In both setups, all cells were then collected and analyzed by flow cytometry. We determined the loss of CFSE signal in CD8<sup>+</sup> T cells in response to OVA-peptide presentation by BMDCs.

## 2.5 *In vivo* studies with Mice

### 2.5.1 Evaluation of Skin Cell Behavior Following the P.L.E.A.S.E.<sup>®</sup> Microporation

#### 2.5.1.1 Handling of P.L.E.A.S.E.<sup>®</sup> System

We selected the P.L.E.A.S.E.<sup>®</sup> system by Pantec Biosolutions (Rugell, Liechtenstein) for our skin-based studies. The erbium:yttrium-aluminum-garnet (Er:YAG) laser has a wavelength of 2940 nm which is ideal to evaporate the water and thus the tissue. The user has many options to adapt the depth of the created pores to the application by changing several parameters during the laser setup. The only constant is the pore diameter which is 150  $\mu\text{m}$  according to the manufacturer. The laser beam parameters, repetition rate in Hertz (Hz) and pulse length in  $\mu\text{s}$ , determine the laser power and thus the energy per area (fluence,  $\text{J}/\text{cm}^2$ ). This fluence is responsible for the depth of one pulse that varies between 11 and 71  $\mu\text{m}$ . You can select the number of pulses per pore resulting in a theoretical maximum depth of 3500  $\mu\text{m}$  as depth per pulse is multiplied with number of pulses.

As last parameter, you can choose the size of the treated square with a maximum side length of 14 mm limited by the used adapter. We purchased two adapters that have direct contact with the skin piece and fully cover the area of treatment. The larger one had a side length of 14 mm, the smaller one for the mouse ear 8 mm. Pore densities and thus the number of pores can be varied between 1 and 15%.

#### 2.5.1.2 Application of P.L.E.A.S.E.<sup>®</sup> on Mouse Ear

All animal-based studies were conducted together with Simon Delandre, our collaboration partner at the HZI under the animal permission 16/2118-A. We selected 21 female wildtype B6 mice and distributed them equally in groups with three animals each. Mice were anesthetized with an intraperitoneal injection of ketamine and xylazine (0.1 ml/g bodyweight). We treated one ear at a time per mouse. As preparation, we fixed this one ear with a tape on a plastic support with the dorsal sit up. Using the smaller P.L.E.A.S.E.<sup>®</sup> adapter, we then treated an area of 8 x 8 mm on the back side of the ear. Laser settings were 75  $\mu\text{s}$  pulse length with a repetition rate of 200 Hz resulting in a fluence of 5.9  $\text{J}/\text{cm}^2$  and thus a calculated pore depth of 24  $\mu\text{m}$  per pulse. Pore density was 8%. A part of the animals was treated with so called shallow pores with only one pulse per pore targeting the epidermis. The second half of mice was treated with deep pores after two pulses per pore and 48  $\mu\text{m}$  theoretical pore depth.

In the first study the focus was on the effect of the P.L.E.A.S.E.<sup>®</sup> laser treatment. Therefore, we applied only 10  $\mu\text{l}$  of PBS buffer directly after laser treatment and massaged the ear with an inoculation loop. In the second study, we applied OVA-mRNA-loaded LPN(70/30) instead. These nanoparticles were loaded, freeze-dried, transported at RT to the HZI and reconstituted in PBS to increase the concentration. We applied 7.84  $\mu\text{g}$  mRNA per animal in twice 10  $\mu\text{l}$  nanoparticle suspension. The ear was then removed from the cartridge and covered with a transparent tape to avoid the immediate removal of the liquid during the self-cleaning procedure of the mice.

This described procedure was then repeated with the second ear of the animal to double the size of the treated area and thus enable later the application of more LPNs per animal. We treated groups of mice 24, 6 and 3 hours prior to the sampling. The control group was not treated at all.

#### 2.5.1.3 Overview Sampling Strategy

All samples were collected at the same time point. An overview of the sampling process is described in Figure 2. All samples were analyzed together with Simon Delandre in Braunschweig.

## 2 Materials and Methods

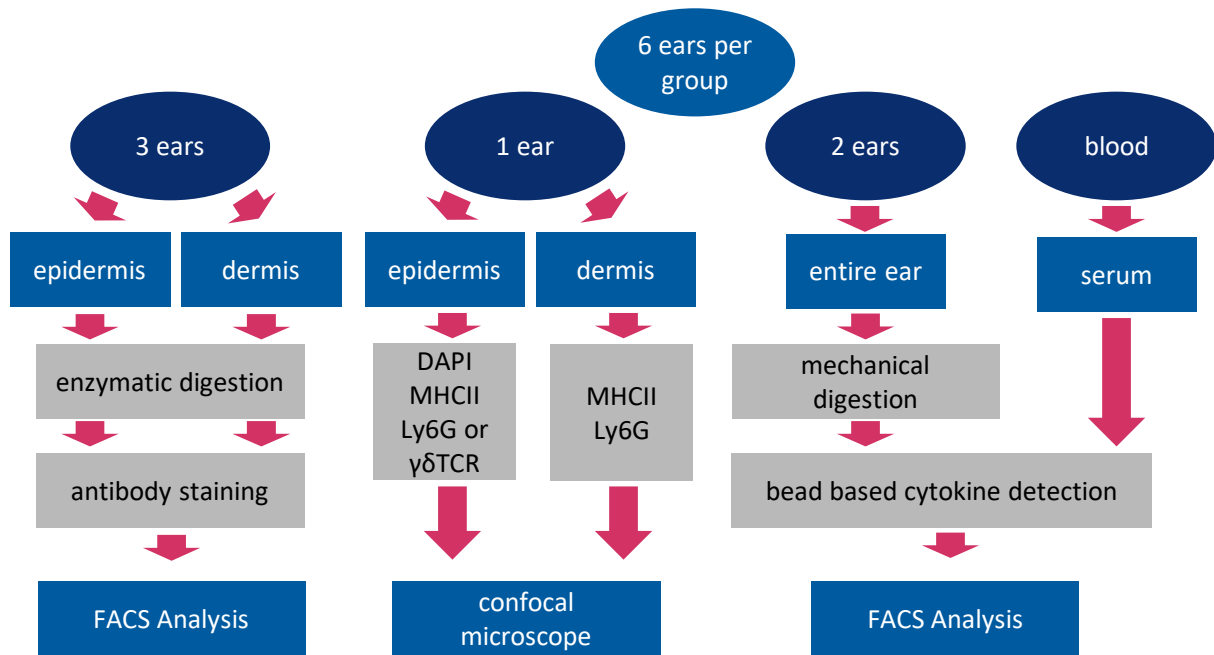


Figure 2: Overview of sampling methods and material for evaluation of P.L.E.A.S.E.® effect on skin cells. Three animals per group were microporated with shallow (24  $\mu\text{m}$ ) or deep (48  $\mu\text{m}$ ) pores. 10  $\mu\text{l}$  PBS buffer was applied with inoculation loop. Mice were treated 24, 6 and 3 hours prior to sampling.

### 2.5.1.4 Cytokine Analysis in Blood and Ear Tissue

The sampling started with the collection of the blood from the retrobulbar plexus of mice after anesthesia with isoflurane. Serum was immediately separated from red blood cells by centrifugation and stored for 24 h at  $-20\text{ }^{\circ}\text{C}$ . Then we transferred them to the  $-80\text{ }^{\circ}\text{C}$  freezer until analysis with the LEGENDplex™ mouse cytokine kit (ELISA, panel 2, 13-plex, cat. 740134, BioLegend, USA) following the manufacturer's protocol.

After blood collection, mice were sacrificed, and ears cut off at their base with scissors. We selected two ears of two different animals for the cytokine analysis of the tissue. The dorsal part of the ear was separated from the inner part with the cartilage using two forceps. After freezing in liquid nitrogen, ear parts were stored at  $-20\text{ }^{\circ}\text{C}$  for 24 h. The next day, cells were lysed with 1 ml NP-40 lysis buffer (150 mM NaCl, 50 mM Tris-HCl pH8, 1% NP-40; protease) in M-tubes for homogenization (for GentleMACS®, Miltenyi Biotec, Germany). Protease was added directly before the ear to protect the cytokines from tissue enzymes. After 1:20 min of mechanic digestion in the GentleMACS® and 10 min centrifugation, supernatants containing the cytokines were collected and stored at  $-80\text{ }^{\circ}\text{C}$  until analysis together with the blood cytokines and the cytokine kit. Results were normalized to the protein amount of one ear.

### 2.5.1.5 Tissue Digestion for Cellular Analysis with Flow Cytometry

For the cellular analysis with the FACS, we took one ear per animal and separated again the back part from the cartilage and the ventral part of the ear with forceps. To enable the separation of dermis and epidermis, dorsal ear parts were incubated dermis side down in trypsin GNK solution (0.1% glucose, 0.9% NaCl, 0.04% KCl, 0.29% trypsin in PBS, pH 7.6 with 1 M  $\text{NaHCO}_3$ ) at  $37\text{ }^{\circ}\text{C}$  for 45 min following the recommendation of Kashem und Kaplan [161]. Skin layers were separated carefully with a forceps and incubated simultaneously in different conditions to generate the single cell suspensions. The epidermis was incubated in DNase (0.1 mg/ml) in digestion medium (RPMI with 10% FCS, Pen/Step, 1% HEPES) for 30 min at  $37\text{ }^{\circ}\text{C}$  and vortexed every 10 min. The dermis needs a harsher chemical digestion. Next to the DNase, we therefore added collagenase XI (2.5 mg/ml) and

## 2 Materials and Methods

hyaluronidase (0.25 mg/ml) to the digestion medium for 45 min at 37 °C. All three samples of one treatment group were then filtered with the same 30 µm cell strainer and pooled in one Eppendorf tube resulting in one dermis and one epidermis tube per treatment group. After two washing steps with skin buffer (PBS supplemented with 2% FCS and 2 mM EDTA), IgG binding sites were blocked with  $\alpha$ CD16/ $\alpha$ CD32 at 4 °C for 10 min to prevent unspecific binding of staining antibodies. After centrifugation, the antibody panel and live-dead-staining in skin buffer was added to the cells for 30 min at 4 °C. After washing with plain skin buffer, samples were resuspended in the fresh skin buffer and analyzed with a BD symphony flow cytometer.

The FACS panel consisted of primary labeled antibodies against CD45 (labeled with BUV496) staining all hematopoietic immune cells. These cells were further sorted with CD3 (with BUV395) and NK1.1 (with Alexa700) for T cells, Ly6C (with BV785) and Ly6G (with PE-Cy7) for neutrophils and monocytes. Antigen presenting dendritic cells were labeled with an MHC-II antibody linked to BV421 and further specified with CD11b (with BV605) and CD24 (with APC-fire 750). CD40 (with A647) and CD86 (with BV650) were used to quantify the activation status of these dendritic cells. A  $\gamma$  $\delta$ TCR-antibody with PE stain labeled cells of the epidermis.

### 2.5.1.6 Spatial Analysis with Fluorescence Microscopy

After these sampling steps, there was one ear per group left that was reserved for the analysis with a confocal laser scanning microscope (CLSM). The first step was the depilation of the ears. Even though hair density is much reduced compared to the back of the mice, the mouse hair has an intense fluorescence and thus jeopardizes the microscopic evaluation. One drop of depilation creme was put on a paper tissue and the ear added for 1 min. Hairs were wiped away with the tissue followed by two washing steps with PBS. As before, the dorsal part was separate with forceps. The epidermis of this dorsal part was stucked to a crystal-clear tape to keep it spread out during sample preparation and microscopy. Following the same procedure as the cell suspension for the FACS, the basal membrane was digested for 45 min dermis side down in the trypsin containing GNK solution at 37 °C. After washing with PBS, dermis was carefully separated with forceps from the epidermis that remained on the tape. Both skin layers were fixed for 20 min at RT in 4% PFA and twice washed with PBS. One week incubation in a glycine solution containing bovine serum albumin (BSA) (1.5 g glycine and 3 g BSA in 100 ml PBS) at 4 °C reduced the background fluorescence.

The glycine was removed with one washing step of PBS followed by the staining procedure in staining buffer (PBS with 1% BSA and 0.25% saponin). For every antibody, the sheets were put in drop of antibody staining solution in a saturated humid chamber avoiding air bubbles. After incubation, samples are washed three times with PBS and the next antibody followed. We incubated the skin sheets overnight at 4 °C with an antibody against Ly6G and labeled this primary antibody for 1 h at RT with a secondary antibody linked to AF488. An antibody against MHC-II for 2 h at RT was marked with BV421 (1 h at RT). At the end, the sheets were placed on a glass slide with the tape facing downwards. Samples were encircled with a Pap-Pen, mounted with ProLong<sup>®</sup> Gold Antifade with DAPI and stored at 4 °C until microscopy.

## 2.5.2 Application of Loaded LPNs After P.L.E.A.S.E.<sup>®</sup> Microporation

### 2.5.2.1 Adoptive Transfer

The protocol for the adoptive transfer and the consecutive analysis was published by Lirussi et al. [162]. We will therefore describe the procedure only in brief. Transgenic mice with T cells specific for the model antigen ovalbumin were bred at the animal facility at the HZI. CD4<sup>+</sup> T cells were harvested from lymph nodes and spleens of OT-II mice, while CD8<sup>+</sup> T cells came from OT-I mice and were separately isolated. Cells from lymph nodes were collected using only a 100 µm cell strainer. For

## 2 Materials and Methods

lymphocytes of the spleen, erythrocytes were lysed in RBC lysis buffer first, then washed and also quantified. All cells from one type of animals were pooled. Next, T cells were isolated using an antibody-based kit by Invitrogen and a magnet to remove all unwanted, antibody-linked magnetic bead labeled cells. We isolated  $260 \times 10^6$  CD4<sup>+</sup> and  $160 \times 10^6$  CD8<sup>+</sup> T cells with a viability of 90%.

After combining OT-I and OT-II cells, we added the covalent label CFSE (carboxyfluorescein succinimidyl ester) for 5 min to follow the proliferation after stimulation [163]. With every mitotic cycle, the fluorescence signal per cell is reduced allowing an indirect quantification of the proliferation and thus the activation of the immune cells.  $5 \times 10^6$  labeled T cells were then transferred per mouse via intravenous injection into the tail vein. A quality control using a CD3 antibody as T cell marker for flow cytometry showed that 85% of injected cells belong either to the CD4<sup>+</sup> or the CD8<sup>+</sup> subpopulation.

### 2.5.2.2 Application of Samples

On the day after the transfer of the ovalbumin specific T cells, mice were treated with the same procedure as described in 2.5.1.1. This time we only used the deep settings with 2 pulses per pore and 48  $\mu$ m theoretical depth.

LPN(10/90) and LPN(70/30) were transported to the HZI in suspension on ice and loaded with mRNA encoding for ovalbumin on the day of experiment. We applied 3.13  $\mu$ g mRNA in total per mouse on both ears. We added a group with plain LPN(10/90) without mRNA to check if the nanocarrier itself has any toxic effects. For the ovalbumin control, 5  $\mu$ g in 50  $\mu$ l were injected subcutaneously together with cyclic di-AMP (CDA, cyclic di-adenosine monophosphate).

We had three animals per treatment group and only female mice in this study.

### 2.5.2.3 Isolation and Analysis of Single Cells

All mice were sampled 7 days after the transfer of T cells. The isolation of the ovalbumin specific T cells followed the same procedures as used before the transfer. This time samples were only pooled within the same treatment group and the same origin. Cells from lymph nodes and spleen were not mixed but analyses by flow cytometry after antibody staining to distinguish OT-I and OT-II cells.

## 2.6 *Ex vivo* Skin Model

### 2.6.1 Preparation of Human Abdominal Skin

The ethics committee of the Ärztekammer des Saarlandes approved the usage of human abdominal skin for LPN testing with the written consent of the patients. I picked up the skin directly after dissection from the patient during the plastic surgery. After short transport to the institute in a cooling box, the skin surface was cleaned with water and paper tissues. Next, the skin piece was fixed with epidermis side down on a cooling pack putting some tension on the tissue. I carefully removed the subcutaneous fat with a scalpel and changed the position of the clips stepwise to maintain the tension of the skin tissue. This ready-to-use skin was either directly treated and cultivated in medium or stored in foil at -20 °C. Frozen and stored skin was only used for the adjustment of pore density as cell viability was no criteria in that study.

### 2.6.2 Assessment of Optimal Pore Density

Stored human abdominal skin was defrosted and spread with clips at the edges. I used the large P.L.E.A.S.E.® adapter with a treatment array of 10x10 mm. Laser settings were 75 µs, 200 Hz per pulse theoretically creating a pore of 24 µm depth. After three pulses per pore the calculated total fluence was 17.8 J/cm<sup>2</sup> resulting in pores of 72 µm theoretical depth. I tested several different pore densities covering the entire range between 1 and 15% that is possible with the software. The pore density indirectly determines the number of pores because the size of pores and the treated array is constant. In a second step, I increased the contrast against the skin by applying 20 µl trypan blue dye (0.25% in PBS) per array to the freshly created pores and took a photo.

### 2.6.3 Transfer of Laser Parameters to Human Skin by Cryo-sectioning and Microscopy

I prepared fresh human skin as described in 2.6.1 and treated it with different laser settings to determine when pores reach the dermis. The fluence per pulse was the same as in mouse studies (5.9 J/cm<sup>2</sup>, 75 µs pulse length, repetition rate of 200 Hz) resulting in a calculated pore depth of 24 µm per pulse. I varied the number of pulses from 2 to 21 and had four biopsies per treatment group – two that were directly embedded and frozen and the other ones that was first cultivated for 24 h at 37 °C. For cultivation, skin pieces were freely floating in RPMI medium supplemented with 10% FCS and penicillin/streptomycin. Having two biopsies of every kind, I treated one of them with highly fluorescent polystyrol nanoparticles of a similar size as the LPNs. I applied 20 µl of undiluted FluoSpheres® (amine-modified microspheres, 200 nm, red fluorescence 580/605, 2% solid, Invitrogen, KatNo F8763, USA) immediately after laser microporation and massaged the tissue with the pipet tip.

At the selected time points, skin biopsies were cut in halves, embedded in Tissue-Tek® (O.C.T. Compound, Sakura, 4583) and frozen at -20 °C. Samples were cut in 10 µm slices at -20 °C using a cryotome with the blade moving from dermis towards epidermis to avoid a nanoparticle smear into the skin tissue. Skin cuts were stained with DAPI (0.5 mg/ml in PBS) for 20 min at RT, washed and mounted. Microscopy slides were stored in the fridge until analysis with the CLSM (Leica TCS SP 8, Germany).

### 2.6.4 Sample Preparation and Application Routes

LPNs were loaded with mCherry mRNA and lyophilized to increase the concentration and the viscosity by resuspending in less volume of PBS. I used different application routes and investigated the fate of LPNs (see next chapter 2.6.5). During the application, the skin was put under tension with

surgical clips.

The least invasive application method was pipetting the droplet of LPNs onto the fresh skin and massaging it for one minute with the pipet tip.

The second option was the P.L.E.A.S.E.<sup>®</sup> laser where we selected a fluence of 5.9 J/cm<sup>2</sup> per pulse (75  $\mu$ s pulse length, repetition rate of 200 Hz) and eight pulses per pore to theoretically generate 190  $\mu$ m deep pores. Treatment area was 8 x 8 mm. Immediately after microporation, LPNs were applied with pipet and massaged for one minute.

As comparison and most invasive method, I used intradermal injection with an insulin syringe (1 ml in 10 ml scaling steps, 26Gx0.5" (0.45x13 mm), Romed Holland, REF 3TS-1ML). Human abdominal skin was folded with a forceps to enable injection (about 2 mm deep) in a 10–15° angle. 20  $\mu$ l were injected per biopsy (11 mm diameter). After 10 s and the formation of a visible bulb on the skin surface, the needle was removed again.

After optimization with the positive control, I applied a dose of 8  $\mu$ g mRNA per skin biopsy in 20  $\mu$ l (0.4  $\mu$ g mRNA/ $\mu$ l). Next to the nanoparticles, I used PBS as negative and polyethyleneimine (PEI) as positive control. To have a fair comparison with the loaded LPNs, I complexed the mRNA in a weight ratio of 1:20 with PEI (branched, CAS 9002-98-6, Mw 25,000, water-free, Cat 408727, Sigma-Aldrich) in PBS. The final mRNA concentration was the same as in the reconstituted LPNs.

### 2.6.5 LPN Penetration Study

I prepared LPNs with a non-covalent DiD label as described in 2.1.3, loaded them with mRNA and resuspended them in PBS after lyophilization. Fresh skin was treated with these LPNs using all three described routes (2.6.4). Samples were either directly embedded in Tissue-Tek<sup>®</sup> or first cultivated freely floating in antibiotics containing medium for 24 h at 37 °C. Embedded skin biopsies were stored at -20 °C until they were cut in 10  $\mu$ m slices with the cryotome. The blade always moved from dermis to epidermis to avoid any artefacts by smearing the LPNs into the tissue. Cuts were mounted and stored until evaluation with confocal microscope.

### 2.6.6 Cultivation of skin samples and supernatant collection

Skin biopsies were cultivated in RPMI medium supplemented with 10% FCS. Directly before usage, 10% penicillin/streptomycin (15140122, Gibco, UK) were added. 11 mm skin biopsies were added to 2 ml medium in 24 well plate. Skin pieces floated freely on this medium without any support and cultivated at 37°C in the humidified incubator. After 24 h of cultivation, medium was collected with a pipet while flushing the bottom of the wells and replaced with fresh medium. Supernatants were always collected from the same wells with the samples with the longest incubation time, usually the 7 days samples.

### 2.6.7 MTT with Tissue Pieces

At selected time point, skin biopsies were taken out of the medium and cut in halves with a scalpel and forceps. One half was used for MTT, the other for digestion followed by FACS analysis. The procedure was adapted and optimized following the published protocols [164–167]. The MTT piece was minced in four approximately equal pieces and added to 500  $\mu$ l PBS in a black 24 well plate. After the last sample, 500  $\mu$ l MTT reagent in PBS were dispensed to all wells reaching a final concentration of 1 mg/ml. Incubation time was 3 h at 37°C under light protection. The reagent was then removed. Biopsies and the wells were washed twice with PBS. The formed purple formazan crystals were extracted with 1 ml isopropanol overnight at 37°C under slow shaking. A sticky cover foil prevented from evaporation. Three samples per well were then transferred to a 96 well plate and measured at 570 nm with the plate reader. Viability was calculated relative to the absorbance of the untreated sample on day 0. Isopropanol blanks were always subtracted.

### 2.6.8 Digestion with Skin Biopsies with Miltenyi Dissociation Kit

I used the Miltenyi Dissociation Kit and followed the manufacturers recommendations. Half of the 11 mm skin biopsies were cut in four pieces with scissors and forceps and added to 435  $\mu$ l digestion buffer (Whole Skin Dissociation Kit, human, 130-101-540, Miltenyi, Germany) in C-tubes (for GentleMACS<sup>®</sup>, Miltenyi, Germany). Enzyme A, D and P were added to a final volume of 500  $\mu$ l. Sample tubes were then incubated overnight in a 37°C waterbath under strong shaking. The next day, the reaction was stopped with 500  $\mu$ l RPMI + 10% FCS and samples put on ice. Tubes were inverted and samples flushed to the lids. Skin pieces were then mechanically digested for 35 seconds with the preset skin program of the Gentle-MACS. After collecting the sample at the bottom of the tube again by centrifugation (5 min at 4°C, 300 g), I filtered the sample through a 100  $\mu$ m strainer into FACS tubes. C-tubes and filters were flushed with another 4 ml medium and combined with the first sample resulting in 5 ml single cells suspension per half skin biopsy. After this filtration, I found pieces of epidermis in the cell strainer. These pieces were collected with a needle, spread out on a glass slide and directly covered with mounting medium. I used the brightfield and fluorescence channels of the Lionheart microscope to investigate the skin pieces.

### 2.6.9 FACS Analysis

Single cell suspensions after digestion and supernatant samples underwent the same FACS preparation procedure. All steps were performed on ice. Cells were collected by centrifugation (300 g, 4°C, 10 min for digested biopsies, 5 min for supernatants) and medium removed. Live-Dead-staining mix was added for 20 min per tube (200  $\mu$ l, 1:400 FDA/DAPI in FACS-buffer (2,5% FCS in PBS)). After washing with 1 ml FACS buffer with 5 min centrifugation each, samples were fixed in PFA (3% in PBS, 300  $\mu$ l for digested biopsies, 150  $\mu$ l for supernatants) and directly analyzed with the flow cytometer. 100.000 events were acquired for each biopsy. For the supernatants, the entire sample was analyzed.

## 2.7 Statistical Analysis

GraphPad Prism 9 was used to calculate a two-way ANOVA followed by a Tukey's multiple comparison test. We considered a  $p$  value below 0.05 as significant (\*  $p < 0.05$ ; \*\*  $p < 0.01$ ; \*\*\*  $p < 0.001$ ; \*\*\*\*  $p < 0.0001$ ). N represents the number of biological replicates in independent experiments and n the number of technical replicates for all the experiment.

### 3 Optimization of Nanocarriers

#### 3.1 Influence of Adding DOPE to the Lipid Layer of Lipid-polymer Hybrid Nanoparticles

##### 3.1.1 Preparation and Characterization

I used the same preparation procedure to prepare a panel of nanocarriers. To do so, I replaced different molar amounts of the cationic lipid DOTMA with the phospholipid DOPE in the lipid layer while added volumes and the amount of PLGA were constant. The LPNs are labeled accordingly. The first number in brackets refers to the molar percentage of the DOTMA content in the lipid layer, the second number to the DOPE amount. As introduced in section 2.1.1, Figure 1 shows a schematic drawing of the compositions and an anticipated nanocarrier structure.

Lipid-polymer hybrid nanoparticles had a size between 195-260 nm as shown in Figure 3. The batch-based particle preparation method resulted in a narrow size distribution with a PDI below 0.2 and a high reproducibility represented by the low standard deviations and the high degree of overlay for measurements of single batches (Figure 4). The zeta potential increased with the amount of DOPE and reached a maximum of 38 mV for LPN(70/30) before it dropped to negative values around -12 mV for DOPE-only LPN. Cryo-TEM imaging of representative samples confirmed the round shape of the nanocarriers (Figure 5). Table S 1 shows a summary of measured values for fluorescently labeled LPNs that had similar parameters like unlabeled ones.

### 3 Optimization of Nanocarriers

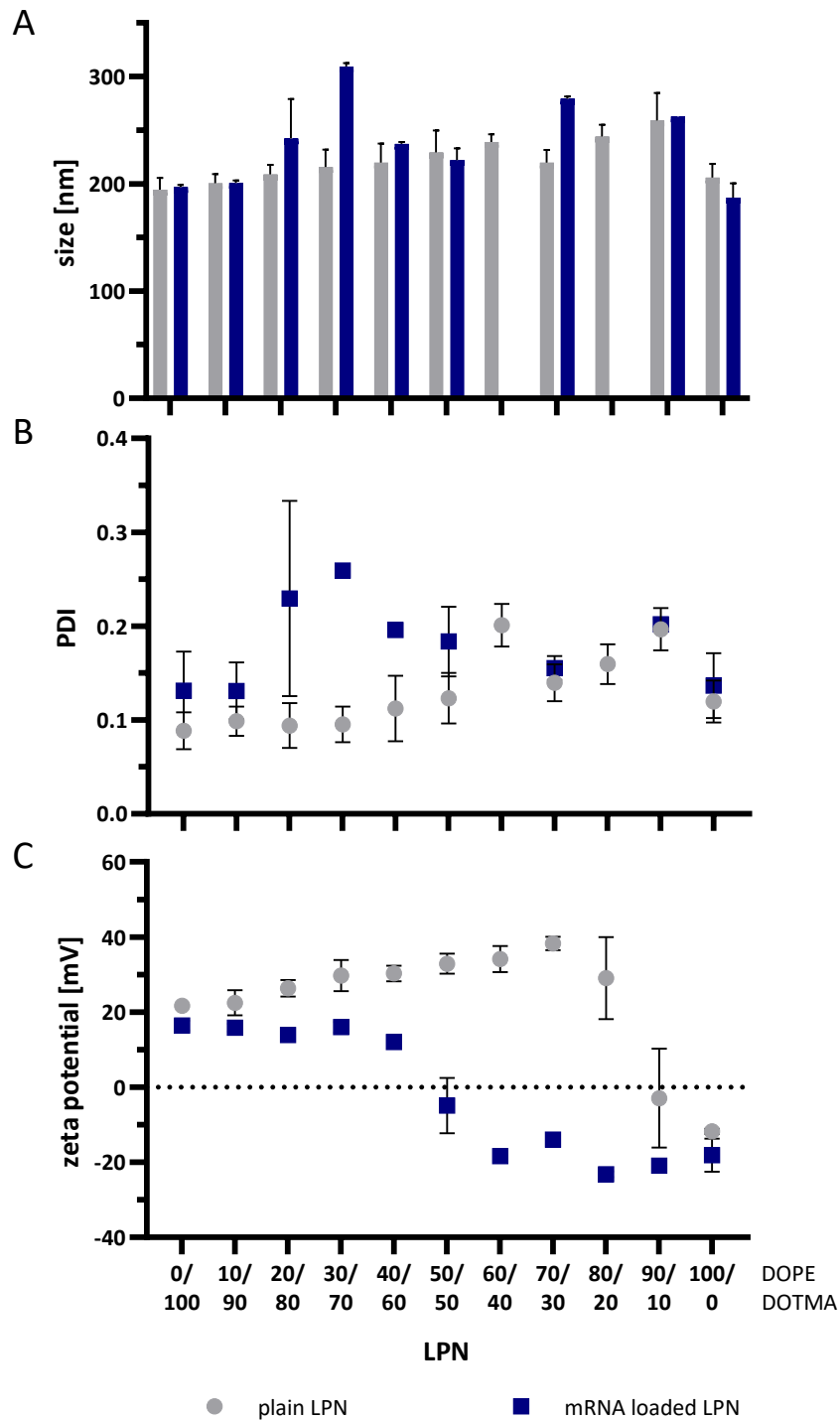


Figure 3: Overview of physicochemical parameters of plain and mRNA-loaded lipid-polymer nanoparticles (LPNs). (A): Size in nm, (B): Polydispersity index (PDI), (C): Zeta potential in mV. Data is displayed as mean and standard deviation between batches (3–5 batches for plain, 1–2 batches for loaded LPNs). Measured sizes and PDI are comparable for plain LPNs. The zeta potential of plain LPNs rises with the amount of DOPE in the lipid layer. For LPNs with at least 50 mol% of DOPE, the complexation of mRNA onto the surface leads to an inversion of zeta potential. Graphs have been published in Kliesch et al. [157]

### 3 Optimization of Nanocarriers

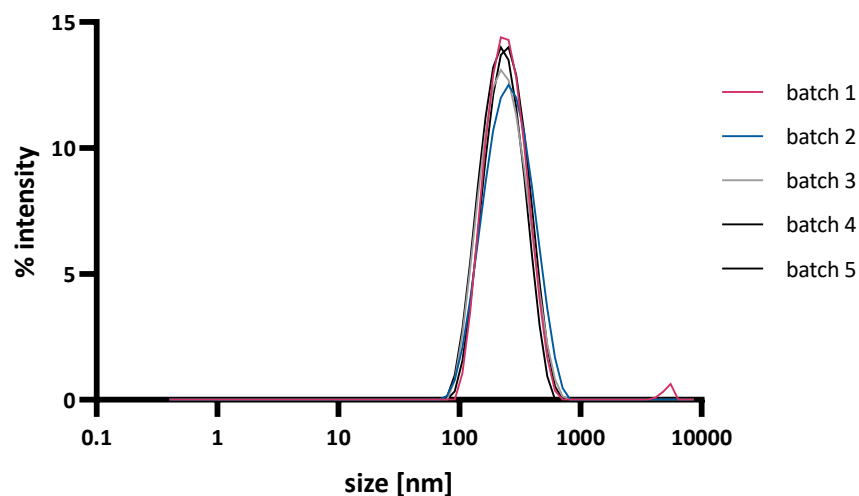


Figure 4: Overlay of size distributions for five batches of plain LPN(70/30). Each line represents a single measurement out of three measurements for one particle batch. High degree of overlap of curves confirms high reproducibility of the used batch-based preparation procedure. Graph has been modified from supplementary material of Kliesch et al. [157]

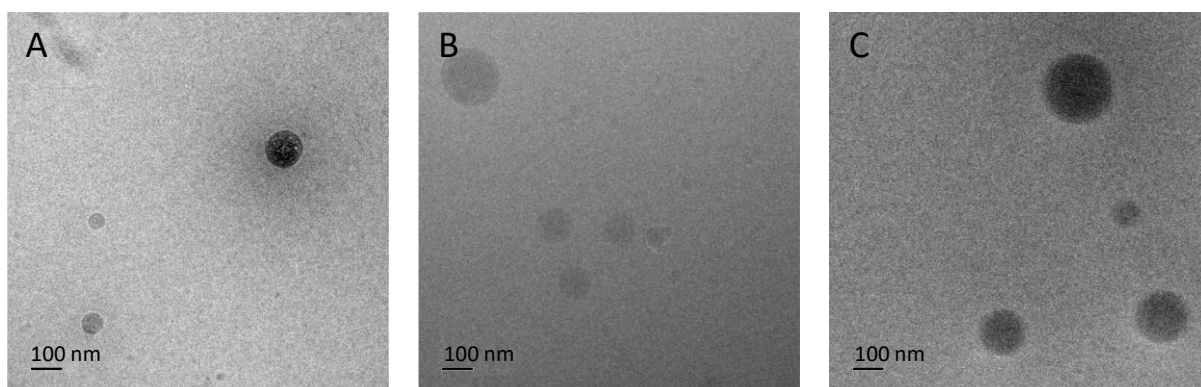


Figure 5: Cryo-TEM images of plain lipid-polymer hybrid nanoparticles. (A): DOTMA-PLGA-LPN (LPN(0/100)), (B): LPN(50/50), (C):DOPE-PLGA-LPN (LPN(100/0)). LPNs showed a spherical shape. Graph has been in Kliesch et al. [157]

#### 3.1.2 Stability

To investigate the colloidal stability of the nanoparticles, I stored aliquots of each LPN either at room temperature or in the fridge and measured size, PDI and zeta potential several times over the course of 21 weeks. Figures 6A-C show the results for LPN(70/30) as a representative example for the influence of storage onto colloidal parameters. The size was stable over time independent of the storage temperature (Figure 6A). Only at the last time point, the size was with 265 nm for the sample stored at room temperature larger than the fridge sample (220 nm) but with a large standard deviation. For this single batch the size on the production date was around 400 nm which differs from the five batch mean that is around 220 nm (Figure 3) and can therefore be ignored. After three month (12 weeks) the PDI increased for the aliquot stored at room temperature (Figure 6B) and went in hand with a loss of the positive surface potential (Figure 6C). These are indicators that LPN(70/30) loses its colloidal stability after 12 weeks of storage at RT. In the fridge, the zeta potential is reduced, too, but remained positive.

Figures 6D-F show the differences of the endpoints after 5 months (21 weeks) for all nanocarriers. Sizes remained below 250 nm for all LPNs stored in the fridge and thereby fulfilled the stability criteria. While storage at room temperature seemed to reduce the particle size for LPNs with lower

### 3 Optimization of Nanocarriers

DOPE content (0/100 – 50/50), sizes were increased for LPN(70/30) and LPN (100/0) to values of 265 nm and 285 nm, respectively (Figure 6D).

PDIs below 0.3 indicate a narrow size distribution. The smaller the values the better [97]. After 21 weeks of storage, all measured PDIs were under 0.3 but LPN(70/30) stored at RT (Figure 6E). For LPN(100/0) the PDI at RT was 0.15 higher than the values of the fridge aliquot. This might be a hint that nanoparticles with higher DOPE content are less stable.

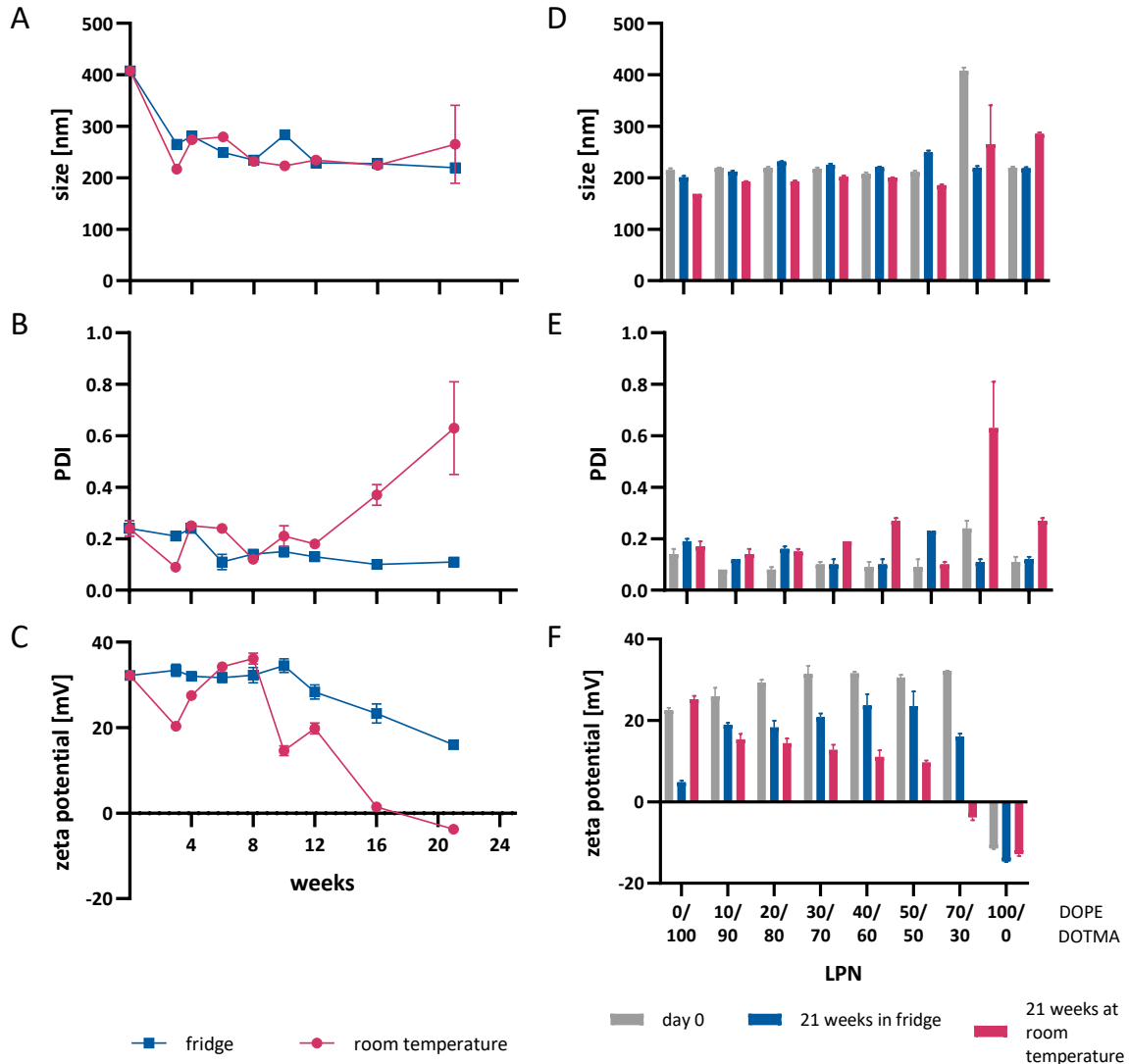


Figure 6: Stability assessment of plain LPNs over the course of 21 weeks. (A): Size of plain LPN(70/30) over time. (B): PDI of LPN(70/30). (C): Zeta potential of LPN(70/30). (D): Change of size of all LPNs at the endpoint of the observation period after 21 weeks. (E): PDI change for all LPNs. (F): Zeta potential measurement of all LPNs. LPN(70/30) shows signs of reduced colloidal stability when stored at RT longer than 12 weeks resulting in loss in surface charge and an increase in PDI. Size and PDI remain comparable for most LPNs with hints that higher DOPE content (e.g., LPN(70/30)) leads to instabilities after this extended period of time. Zeta potential is reduced with storage, especially if stored at room temperature.

Zeta potential measurements revealed the largest differences (Figure 6F). In general, the measured zeta potentials were the highest for the freshly prepared LPNs, storage in the fridge reduced it, storage at room temperature resulted in lowest values. LPNs (10/90 – 50/50) kept a positive surface charge of at least 10 mV after exposure to RT and at least 18 mV after fridge storage. LPN(0/100) behaved differently with a reduction of surface charge after fridge storage to 5 mV and slightly increasing charge at RT from 23 to 25 mV. We observed the largest difference for LPN(70/30) where

### 3 Optimization of Nanocarriers

zeta potential was reduced from 30.6 mV to -3.75 mV after storage at RT. For the electrostatic interaction with the cargo mRNA, this observation will be difficult. Thus, a storage in the fridge should be preferred.

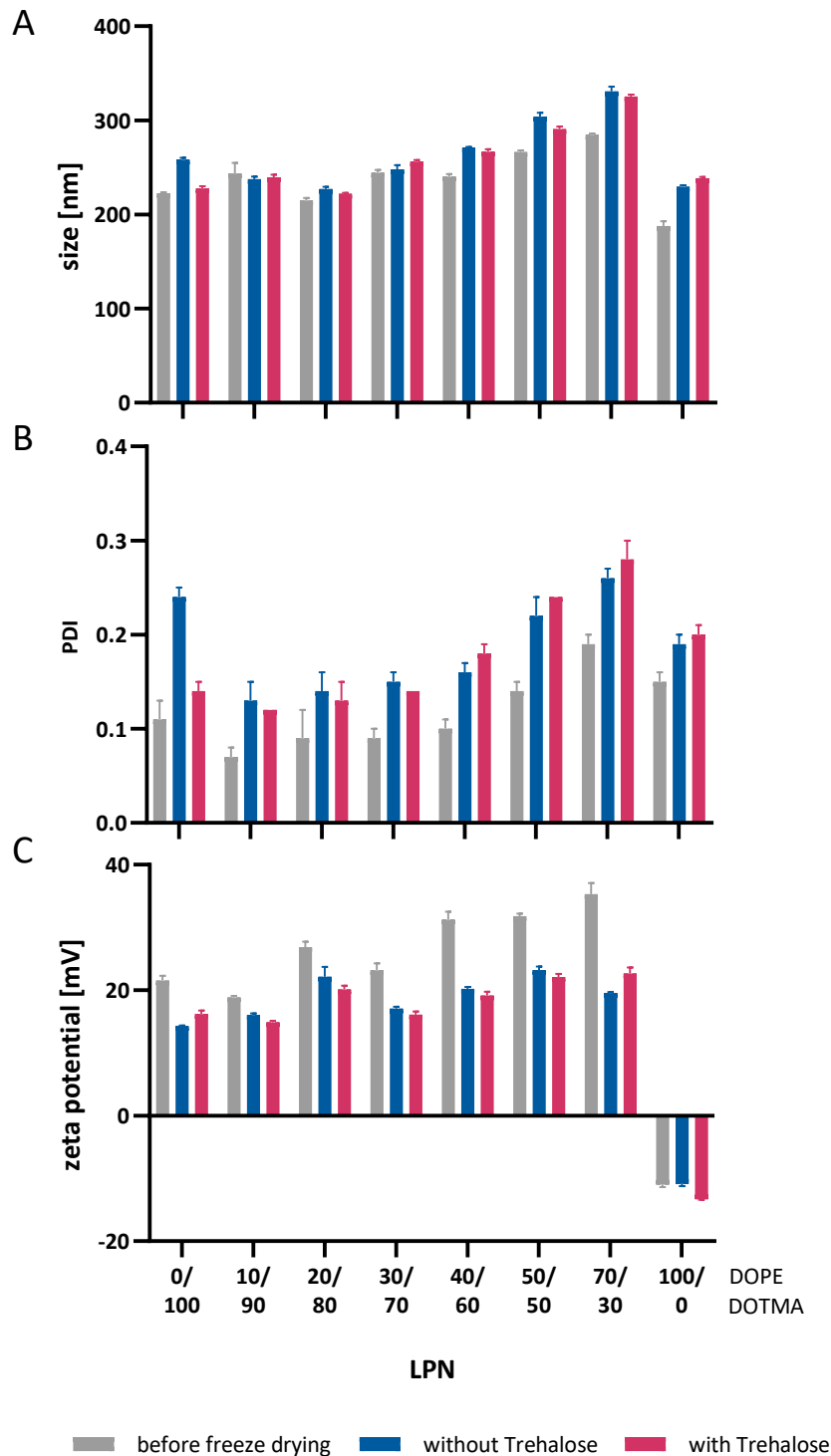


Figure 7: Lyophilization of plain LPNs. Comparison of LPNs before freeze drying with results after reconstitution in MQ to original volume. (A): Size measurements in nm. (B): PDI. (C): Zeta potential results. The procedure increased the PDI and reduced zeta potential. The cryoprotectant trehalose did not show an effect.

### 3 Optimization of Nanocarriers

In a next step, I tested if the nanocarrier structure is robust enough to survive the removal of water by freeze drying. This technique enables storage of nanoparticles not as liquid suspensions but as solid cake or powder. After storage, this lyo-cake has to be reconstituted again in liquid for the experiment. In theory, you can use any buffer or media and even reduce the added volume to increase the particles' concentration. As this process of water removal and reconstitution puts stress onto the LPNs, I investigated its effect with plain LPNs by comparing untreated ones with the lyophilized and reconstituted ones. Additionally, I added trehalose as cryoprotectant to a third group of samples.

After the reconstitution to the original volume with MQ, sizes were only minimally affected by the process (Figure 7A). PDI increased slightly independent of trehalose presence (Figure 7B). Zeta potential decreased through the treatment to still positive values but again, trehalose did not show an effect (Figure 7C). We can therefore conclude that lyophilization is possible with all tested LPNs and can be used for increasing the concentration. In our case, it is not needed to enhance storage stability as LPNs are stable also in suspension for several weeks. LPN(70/30) showed signs of instability when stored above 12 weeks.

#### 3.1.3 Cell Tolerability

I used the MTT-assay that is based on the cell metabolism to quantify the cytotoxic effects of plain LPNs with higher DOTMA content (LPN(0/100 – 50/50)). I selected these nanoparticles as cationic lipids such as DOTMA are known to harm cells [149]. I started with the stock concentration of 1700 µg/ml and went down to 7 µg/ml.

We observed clear concentration dependent effects with a cell viability of less than 20% for the highest concentration. We might overestimate the toxicity of these stock concentrations as they contain water as dispersant and no buffer like the other samples. For all tested LPNs, at least 50% of cells survived the lowest and second lowest concentrations but standard deviations were high. For LPNs (10/90 – 40/60) the three lowest doses (7-63 µg/ml) were tolerated well indicated by cell viabilities around 60%, above 75% for LPN(20/80) and LPN(30/70). This concentration range is important as we used similar amounts of LPNs for later transfection studies. The standard deviations are too large to draw conclusions, but we could not find hints for problematic cytotoxicity.

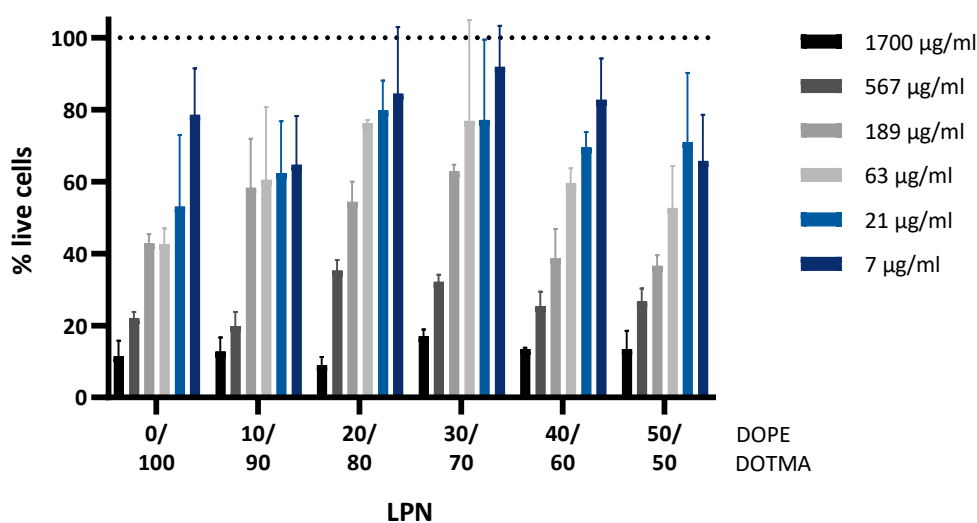


Figure 8: Cytotoxicity assessment of plain LPNs using A549 cells and MTT metabolism as colorimetric quantification method. 4 h incubation with plain LPNs in HBSS, 1 h incubation of cells with MTT salt, followed by cell lysis. HBSS was used as live, 1% triton-X in HBSS as dead control. Data display mean of two independent experiments (N=2 with n=1). We observed a concentration dependent effect and good tolerability for transfection relevant concentration range (21–63 µg/ml).

### 3 Optimization of Nanocarriers

In the next step, I changed the setup and used the dendritic cell line DC2.4 grown in a 24-well plate instead of A549 cells in the 96-well plate format. The readout was not colorimetric and plate reader-based but fluorescence and flow cytometry. I tested only the 40  $\mu\text{g/ml}$  concentration relevant for the transfection but this time also for LPN(70/30) and LPN(100/0) to cover the entire range of lipid compositions.

As shown in Figure 9, all LPNs were very well tolerated for the 4 h incubation time with percentages of live cells above 80%. Furthermore, there were no significant differences to the HBSS control and thus no harmful effects of the nanoparticles detected. I also tested half and double the number of LPNs with the DC2.4 but measured the same good tolerability (Figure S 1).

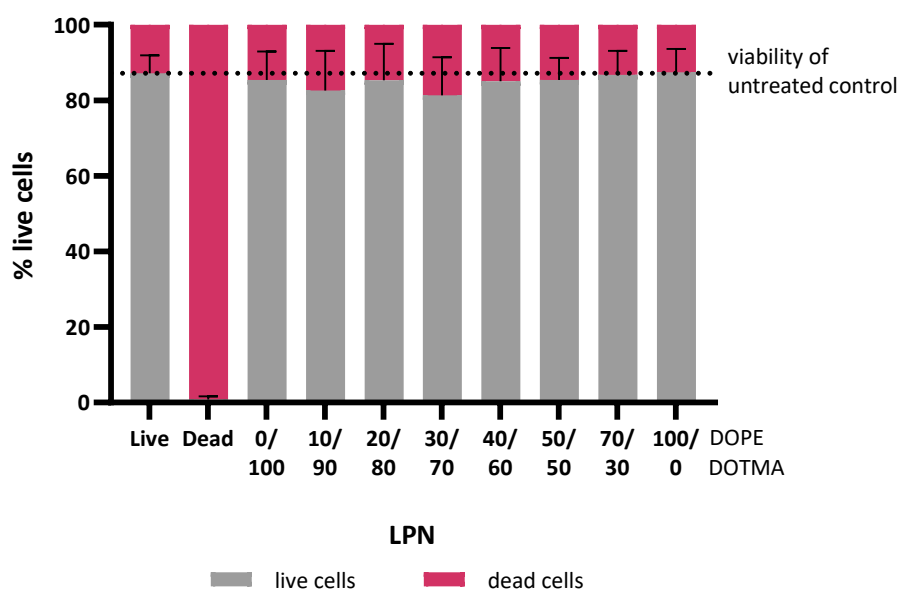


Figure 9: Cell viability assay. DC2.4 cells were incubated for 4 h with plain LPNs in HBSS. 7-AAD was used to stain dead, FDA for live cells in flow cytometry. Double positive cells were counted as dead. HBSS was used as live control, 5% ethanol in HBSS as dead control. N=3 with n=2 each. Cell viability was above 80% for all LPNs and comparable to the live control without any hints for toxic effects.

For our application on the skin, we will not wash away the nanoparticles. It is therefore important to prepare nanocarriers that are very well tolerated also after longer exposure times. Having the promising results after 4 h incubation time, we prolonged the incubation time to 24 h. This procedure revealed differences between the LPNs and a distinct trend. The more DOTMA the LPN contained, the less cells survived. This confirmed our hypothesis that the addition of DOPE reduces the cytotoxicity of the nanoparticle. We also observed a general problem of our setup. The live control with HBSS killed almost 50% of DC2.4. The buffer itself is already too harsh probably due to lack of nutrition. The cells might be more sensitive to the LPNs and the toxicity might be overestimated. To cope with this effect, we exchanged the buffer with growth medium.

### 3 Optimization of Nanocarriers

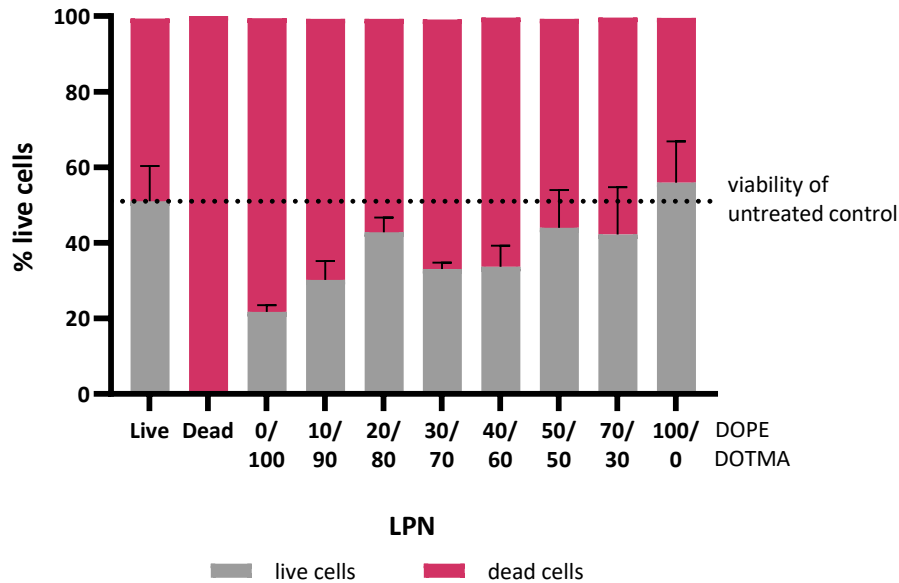


Figure 10: Cell viability assay. DC2.4 cells were incubated for 24 h with plain LPNs in HBSS. 7-AAD and FDA was used to distinguish live and dead cells in flow cytometry. Double positive cells were counted as dead. HBSS was used as live control, 5% ethanol in HBSS as dead control. N=2 with n=2 each. Cell viability was increased with the DOPE content in the lipid layer. The overall tolerability was reduced, also for the live control with only 50% viable cells.

After 24 h incubation of DC2.4 cells dispersed in RPMI medium without any supplements, the viability of the live control improved to 88%. Again, the LPNs did not harm the cells with viability values comparable to the control (Figure 11). The addition of supplements like 10% FCS, HEPES-buffer (0.01M), non-essential amino acids (1X) and beta-mercaptoethanol (0.0054X) did not enhance the viability of the live control further. For LPN containing samples, there seems to be little improvement but still values are in the same range. Testing different conditions, we can conclude that all plain LPNs are well tolerated by DC2.4 that survive the particle treatment as well as in the plain medium controls.

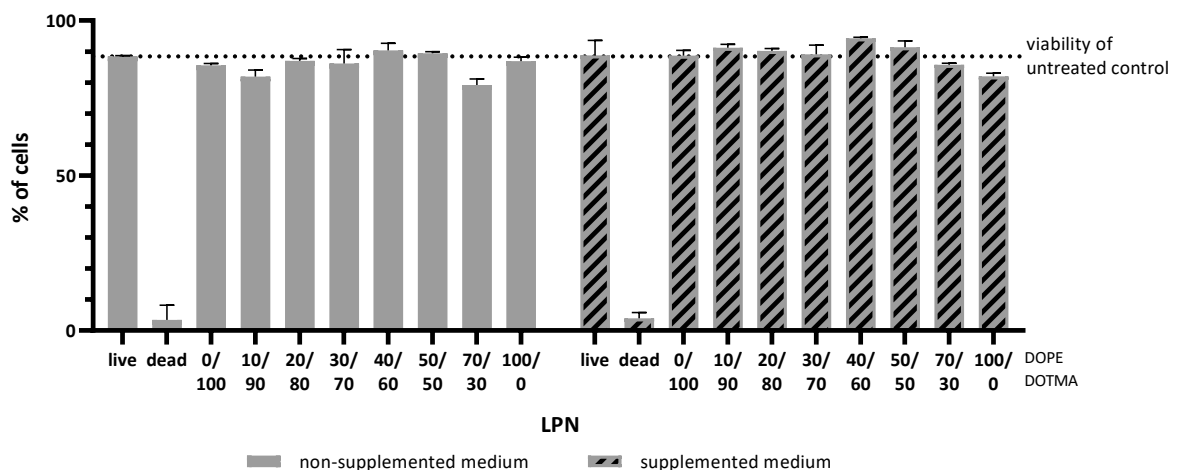


Figure 11: Cell viability after 24 h incubation of DC2.4 with plain LPNs dispersed in medium. We compared non-supplemented RPMI medium with one that included 10% FCS, HEPES-buffer, non-essential amino acids (1X) and  $\beta$ -mercaptoethanol (0.0054X). FDA and DAPI was used to distinguish live and dead cells in flow cytometry. Double positive cells were counted as dead. The corresponding medium was used as live control, 5% ethanol in HBSS as dead control. N=1 with n=2. All LPNs were well tolerated with values in the same range as the medium control. Supplementation of the medium only minimally improved the cell viability.

## 3.2 Evaluation of mRNA-loaded LPNs

### 3.2.1 Hydrodynamic Parameters

On the day of experiment, LPNs were warmed to RT and loaded LPNs with mRNA encoding for mCherry. To have the best possible comparability between the different LPNs, I used a constant N:P ratio of 2.81 for all of them. I added appropriate amounts of mRNA to the nanoparticles and mixed by carefully pipetting. Incubation time at RT was one hour.

Figure 3 on page 34 shows the results of the DLS measurements of the loaded LPNs next to the plain nanocarriers. mRNA loading led to slightly higher PDIs and comparable sizes. We saw some hints for instabilities as the PDI of LPN(20/80) and LPN(30/70) was higher and the mean size increased to 240 nm and 310 nm, respectively. LPN(70/30) had a larger size as well (280 nm) but maintained the low PDI of 0.14 pointing towards homogenous and stable nanocarriers. The loading of the negatively charged nucleic acids onto the surface of the positive LPNs led to the expected reduction of measured zeta potentials (Figure 3C). We measured reduced, but still positive values for LPNs (0/100 – 40/60), neutral values of -5 mV for LPN(50/50) and negative ones for LPNs with more DOPE content. The difference between plain and loaded LPNs got larger the more DOPE the LPN contained. For LPNs (60/40 – 80/20) the zeta potential reversed to negative values resulting in differences of 52 mV each. The zeta potential of the DOPE-only LPN (LPN(100/0)) remained in the negative range.

### 3.2.2 Binding and Release of mRNA

In the next step, I visualized the mRNA with the RiboGreen<sup>®</sup> assay following the manufacturer's protocol. By binding the accessible fraction of mRNA, the included dye exhibits a green fluorescence signal that is detectable with a plate reader. The measured fluorescence intensities are displayed in Figure 12 together with the values for the binding efficacy which was calculated relative to the naked mRNA.

As expected, we measured the highest fluorescence values for the naked mRNA samples as all nucleic acid molecules are accessible for the dye. DOPE-only LPNs showed a similarly high signal due to a large fraction of free mRNA resulting in a low binding efficacy (BE). All other LPNs followed a clear trend. The more DOTMA the LPNs contained, the smaller the accessible fraction of mRNA, the smaller the measured signal, the higher the binding efficacy. The addition of 30 mol% DOTMA to DOPE-only LPN doubled the BE from 21% (LPN(100/0)) to 42% (LPN(70/30)) and then another time from 42% to 85% (LPN(40/60)). LPNs with more than 80 mol% of DOTMA (LPNs (0/100 – 20/80)) had a BE of more than 98%.

To further confirm the association of mRNA with the LPNs, I performed a gel electrophoresis and found a similar trend. For LPNs with the highest DOTMA content (LPNs (0/100 – 20/80)), there was no signal visible – neither in the gel nor in the pockets. Adding more DOPE, a signal in the pocket appeared that increased with the DOPE amount. Continuing the row of increasing DOPE concentrations, we saw a signal in the gel for LPN(70/30) at the same height as the naked mRNA. This signal got stronger for LPN(100/0) while the pocket signal almost disappeared for this DOPE-only LPN. This observation goes in line with the results of the RiboGreen<sup>®</sup> assay and confirms that the mRNA does not bind to a large extend to the LPN(100/0).

I released the mRNA from the nanoparticles by adding heparin as competitor for the nucleic acid. This is possible because the polyvalent anionic polymer has a twofold higher charge density [168]. After a 30 min treatment, we saw a signal in the gel pockets for all but the LPN(100/0) and another band at the height of the naked mRNA. This confirms that the mRNA was present in the first gel, too, but not accessible for the ethidium bromide for intercalation.

### 3 Optimization of Nanocarriers

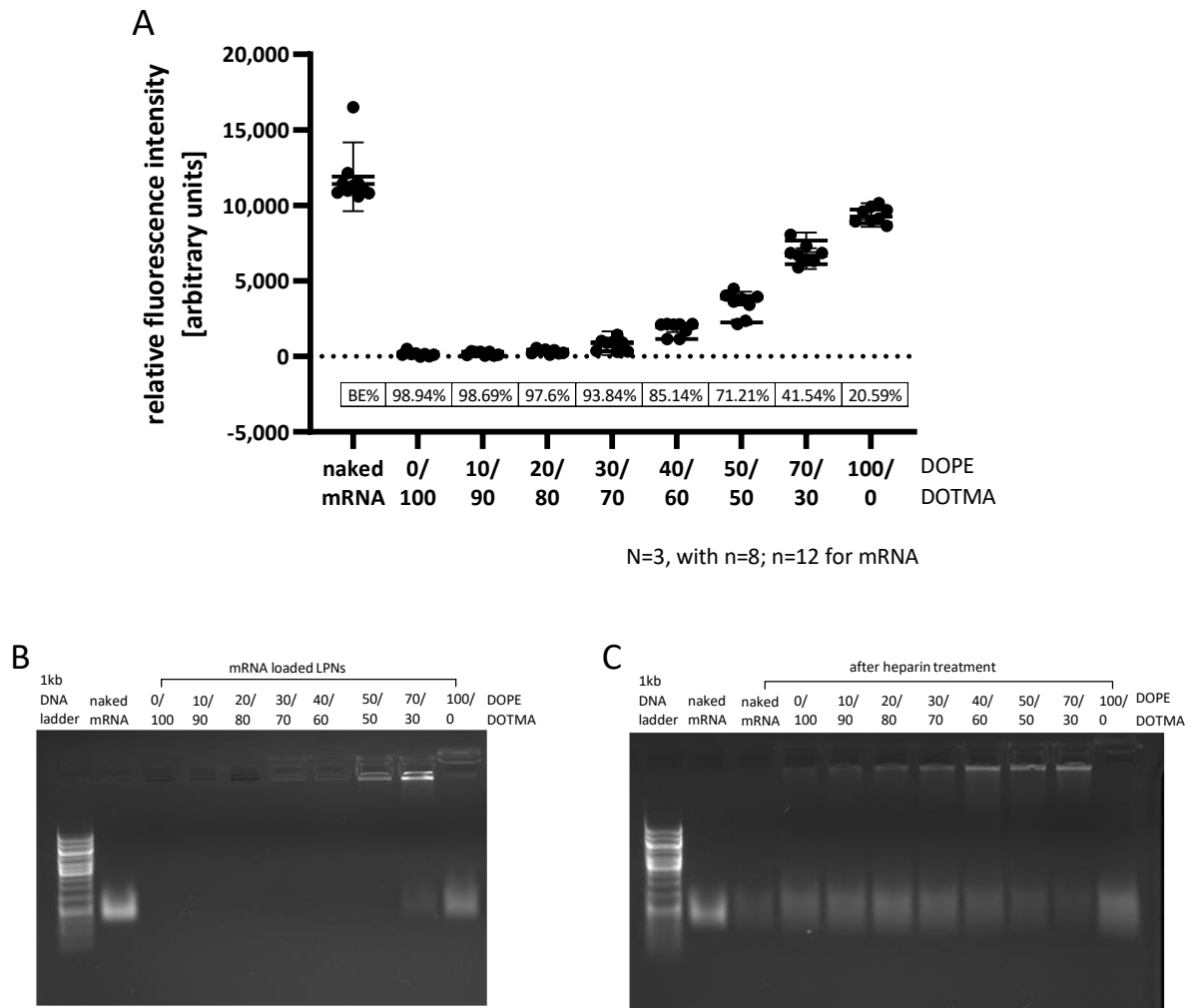


Figure 12: Assessment of mRNA binding efficacy. (A): Quantification of binding efficacy of mRNA by measuring fluorescence of RiboGreen® dye after successfully binding accessible fraction of mRNA. Binding efficacy is calculated relative to the fluorescence of naked mRNA. (B): Gel electrophoresis of loaded LPNs. (C): Gel electrophoresis of loaded LPNs after heparin treatment to release the complexed mRNA. Graphs have been published in Kliesch et al. [157]

#### 3.2.3 Stability of Interaction Against Medium Additives

Gel electrophoresis confirmed the successful loading of mRNA onto the surface of the nanocarriers (see previous chapter 3.2.2). In this part, I tested how stable this interaction is when exposed to additives like salts or proteins. Such supplements occur naturally everywhere in the body and are therefore needed for the cultivation of cells *in vitro*. In our case, we aim for an application of LPNs onto the skin after microporation with the P.L.E.A.S.E.® laser. The created pores represent little wounds that lead to the secretion of wound fluids. Mimicking this fluid, I prepared an artificial wound fluid (AIF) based on the interstitial fluid.

I diluted the plain LPNs with the different fluids and added the mRNA afterwards. I then measured the binding efficacy with gel electrophoresis and RiboGreen®. I used nuclease-free water and PBS as control and compared it to AIF with and without the addition of albumin.

### 3 Optimization of Nanocarriers

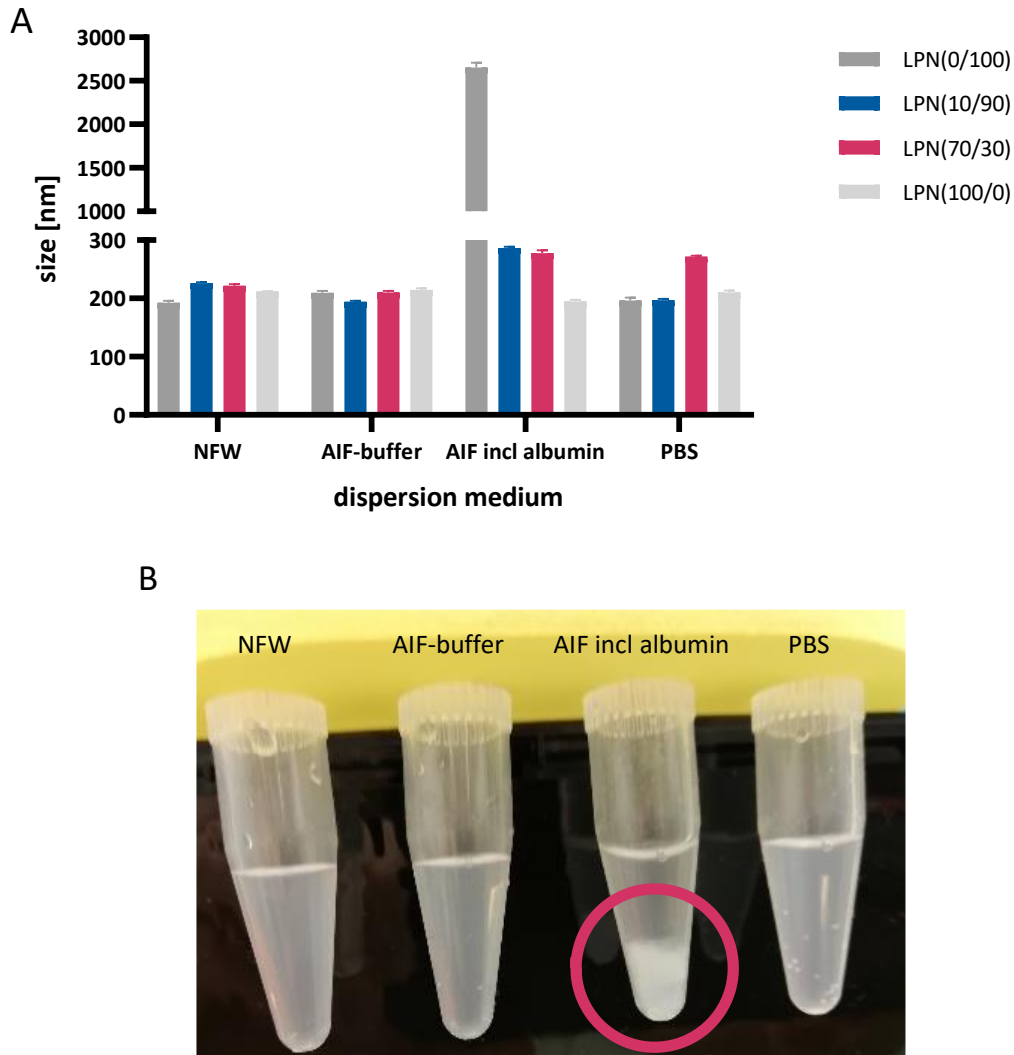


Figure 13: Effect of salts and proteins onto size of loaded LPNs. LPNs were diluted in buffers or NFW prior to adding the mRNA for complexation. Artificial interstitial fluid (AIF) with and without albumin was used to mimic surrounding in micropores of the skin. (A): Results of size measurements by DLS. (B): Macroscopic differences of LPN(0/100) after dilution. LPN(0/100) lost colloidal stability as soon as albumin was present and aggregated. Other LPNs remained below 300 nm.

As soon as albumin was part of the sample, LPN(0/100) lost its colloidal stability indicated by a 10-fold increase in size leading to values above 2500 nm (Figure 13). These aggregated LPNs are visible with the bare eye and not suitable for the application *in vivo*. After gel electrophoresis, we saw two new bands for the albumin containing sample of LPN(0/100) (Figure 14C). One at the height of free mRNA, the other one in the middle between that band and the pocket. In the case of LPN(100/0), the size was not influenced but in the gel the intensity of the band of free mRNA was reduced in the presence of albumin and a new band above appeared (Figure 14D). LPN(10/90) and LPN(70/30) showed an effect of albumin, too, but sizes remained below 275 nm. LPN(10/90) again had a tight interaction of LPN and mRNA resulting in low signals in gel and RiboGreen® assay (Figure S 2). Only with albumin, we observed a faint band at the height of free mRNA (Figure S 2B). For LPN(70/30) the amount of free mRNA increased with any fluid that diluted the LPNs prior to mRNA addition but remained on a comparable level with similar intensities on the gel (Figure 14A). For nuclease free water and albumin-containing fluid we saw a brighter signal in the pocket. For the latter, we also saw an increased fraction of free mRNA. The RiboGreen® had the highest signals for the NFW sample and an AIF including albumin confirming the observations of the gel (Figure 14B).

### 3 Optimization of Nanocarriers

As described, albumin showed the highest impact. Added salts and the changes of pH had only minor influence on the binding efficacy when compared to the dilution in nuclease-free water.

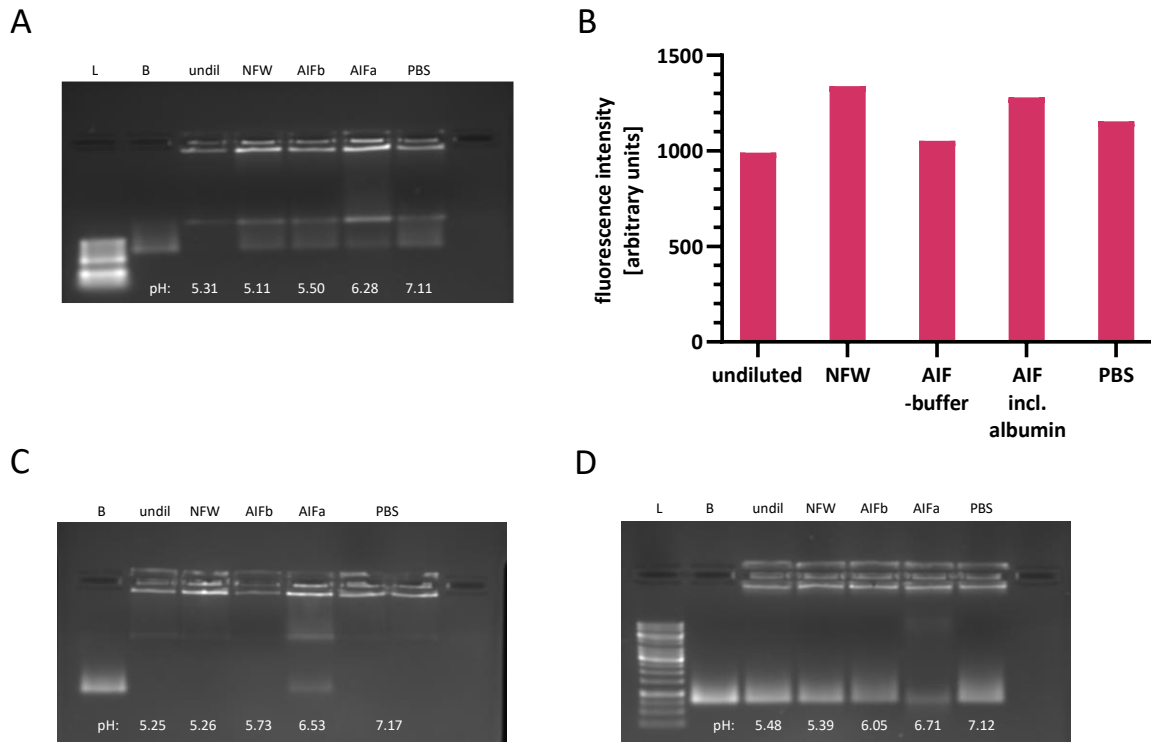


Figure 14: Effect of salts and albumin on binding efficacy of LPNs. (A): Gel electrophoresis of LPN(70/30). (B): Measured fluorescence intensities of RiboGreen® dye mixed with LPN(70/30). (C): Gel electrophoresis of LPN(0/100). (D): Gel electrophoresis of LPN(100/0). Nanoparticles were diluted in buffers or NFW prior to adding the mRNA for complexation. Addition of albumin led to an additional band between naked mRNA and the pocket. It increased the fraction of free mRNA for LPN(70/30) and (0/100) but reduced it for LPN(100/0). AIFb: artificial interstitial fluid – buffer only; AIFa: artificial interstitial fluid including albumin.

I then tested if nanoparticle size changes if loaded LPNs are incubated in normal growth medium (Figure 15). The medium components did not harm the colloidal stability of the selected LPNs when compared to the incubation in MQ. We thus continued with the first cell-based experiment, the evaluation of cell tolerability.

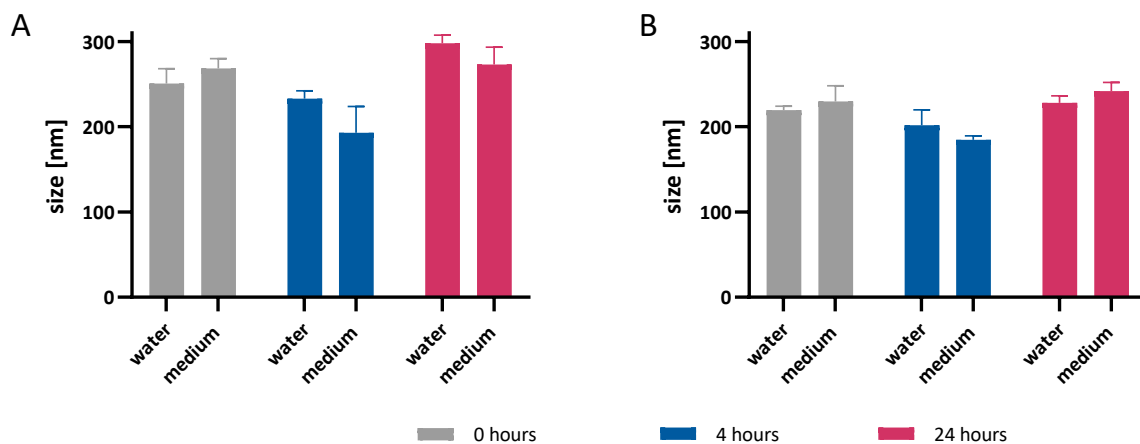


Figure 15: Colloidal stability of LPN(10/90)(A) and LPN(70/30)(B) in demineralized water and supplemented medium (supplemented with 10% FCS, HEPES-buffer (0.01M), non-essential amino acids (1X) and  $\beta$ -mercaptoethanol (0.0054X)). DiD-labeled LPNs were loaded with mRNA and incubated for 4 and 24 h and analyzed by Nanoparticles Tracking. The analysis revealed no signs of instability for none of the LPNs. Graph has been modified from supplementary material of Kliesch et al. [157]

### 3.2.4 Cell Tolerability

Having proved that mRNA can be successfully loaded onto the surface of the LPNs, I tested the influence of this modification onto the cell tolerability. We expected an even better cell viability as the nucleic acids reduced the positive and thus potentially toxic surface charge of the LPNs. The experimental setup was this time based only on a DAPI staining of the dead and dying cells. I did not use a live cell dye because we decided to test FITC-labeled LPNs and to measure their uptake in parallel to the cytotoxicity and the transfection efficacy. Preparation procedure and hydrodynamic parameters were comparable despite the fluorescence labeling (see material and methods section 2.1.3 and Table S 1). The gating strategy is depicted in Figure S 3. The mRNA concentration was 2 µg/ml for all LPNs.

I again compared the cell viability of DC2.4 after 24 h incubation in non-supplemented medium with incubation in regular growth medium with fetal calf serum, HEPES buffer, β-mercaptoethanol (0.0054X) and non-essential amino acids (1X). Figure 16 displays the results showing the same trend as for plain LPNs. In non-supplemented medium, the LPNs containing more DOTMA have a certain cytotoxic potential but the lower viability after LPN(0/100) and LPN(10/90) treatment were not statistically significant. The less DOTMA the LPNs contain, the better they are tolerated by the DC2.4 cell line. Adding the mentioned supplements to the medium, all LPNs showed a survival rate comparable to the one of the untreated control.

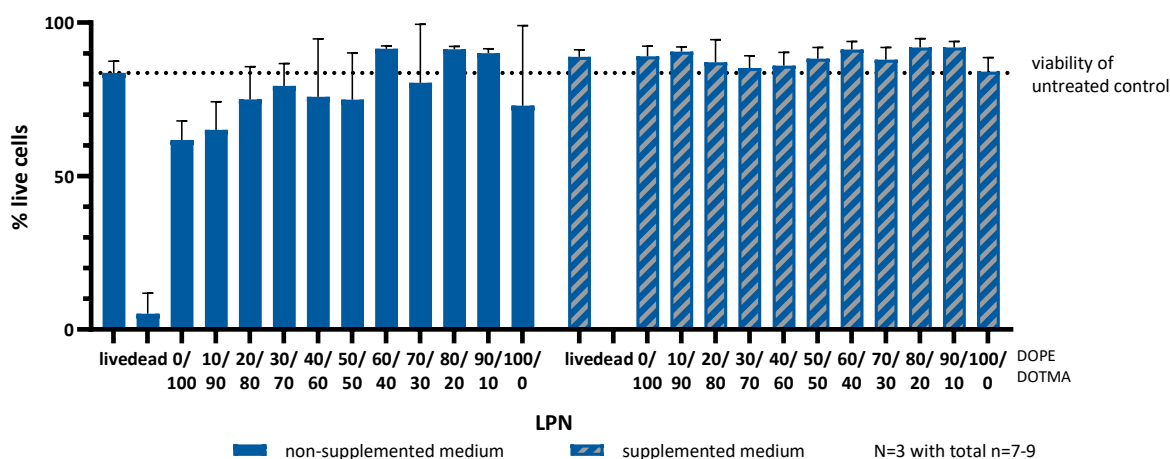


Figure 16. Cell viability of DC2.4 after 24 h incubation of mRNA-loaded LPNs dispersed in non-supplemented and fully supplemented cell growth medium. Investigation of a reduced cell membrane integrity as indicator for cell damage by DAPI staining and flow cytometry analysis. Medium without nanoparticles was used as live, ethanol (5% in HBSS (v/v)) as dead control. LPNs were covalently labeled with FITC and mRNA concentration was 2 µg/ml. Uptake and transfection efficacy were measured in parallel. Only LPNs with high DOTMA amount in the non-supplemented medium showed signs of cell damage. All other LPNs were tolerated comparably well as the live controls. Graph has been modified from Kliesch et al. [157]

## 4 Testing Nanoparticle Performance Under Stress Conditions

### 4.1 Uptake

In the previous section, I described the influence of the lipid composition on the nanoparticles' characteristics and on the survival of cells. In the following part, I will concentrate on the performance of the LPNs, in particular on the ability to cause protein production by successful mRNA delivery. For that purpose, the loaded nanocarriers have to cross the cell membrane. I quantified this uptake of LPNs into DC2.4 cells by using FITC-labeled LPNs in the same experiment as the previously shown cytotoxicity study. This combined readout made it possible to compare the uptake only into the live cell population as these viable cells have the highest chance to produce the protein encoded on the mRNA.

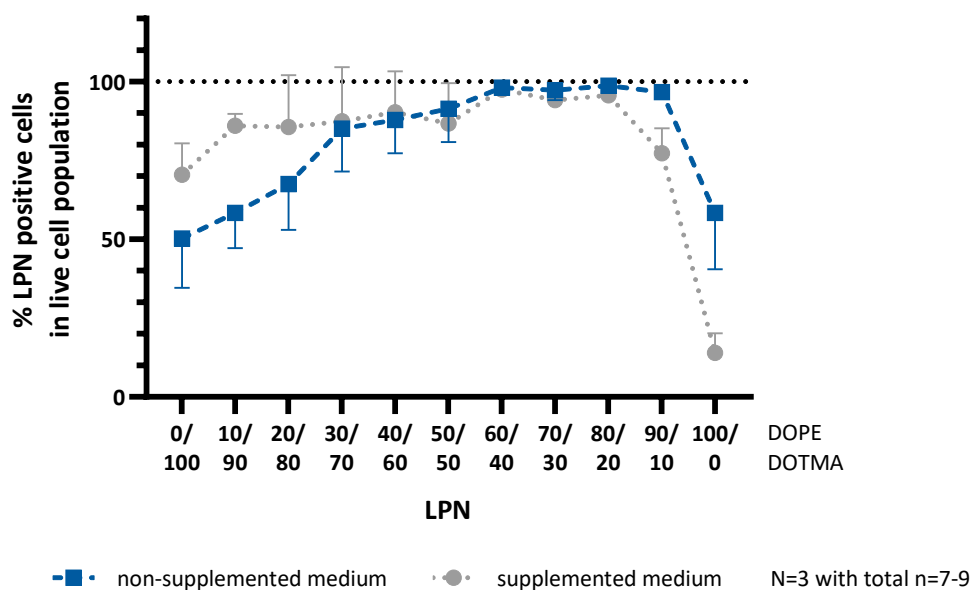


Figure 17: Cellular uptake of LPNs into DC2.4. Graph shows the percentages of live cells that have a green fluorescence signal after 24 h incubation with FITC-labeled, mRNA-loaded LPNs. DAPI staining for dead cell exclusion. N=3 with total n=7-9. Data collected in same experiment as cytotoxicity and transfection rates and amounts. A high DOPE content in combination with DOTMA is beneficial for the uptake with highest values for LPN(80/20) and LPN(90/10) for non-supplemented and supplemented medium, respectively. DOPE-only LPN (LPN(100/0)) showed a reduced uptake independent of the dispersion medium. The medium conditions revealed significant differences only for the edges of the row - high DOTMA (LPNs (0/100 – 20/80)) and high DOPE LPNs (LPNs (90/10 – 100/0)). Graph has been modified from Kliesch et al. [157]

Figure 17 shows how the uptake improved parallel to the DOPE amount with maximum values of 99% (LPN(80/20) in non-supplemented medium) positive cells until a decline in general uptake for DOPE-only LPN. In the lower nutrition condition with non-supplemented medium, the uptake was higher for LPNs with high DOPE content (LPNs (90/10) and (100/0)). For LPNs with maximum 20 mol% DOPE (LPNs (0/100) – (20/80)), we saw the opposite phenomenon with better uptake in supplemented medium. Between these two extremes, almost all live dendritic cells were associated with the LPNs without a difference for the two conditions with values above 85% for LPNs (30/70 – 50/50) and 94% for LPNs (60/40 – 80/20), respectively. Analyzing the measured fluorescence intensities (MFI), I could indirectly investigate the amount of nanocarriers the cells were associated with (Figure 18). Standard deviations were high, but the overall trend fits to the one of the percentages of fluorescent cells. Nevertheless, in the MFI measurement, the row ended earlier with the maximum already at LPN(70/30) while the percentages of cells were still high for LPN(80/20).

#### 4 Testing Nanoparticle Performance Under Stress Conditions

Combining these two readouts, LPN(70/30) might be a good candidate for further evaluation as the uptake reached almost 100% independent of the dispersion medium and the particle amount is the highest compared to other LPNs.

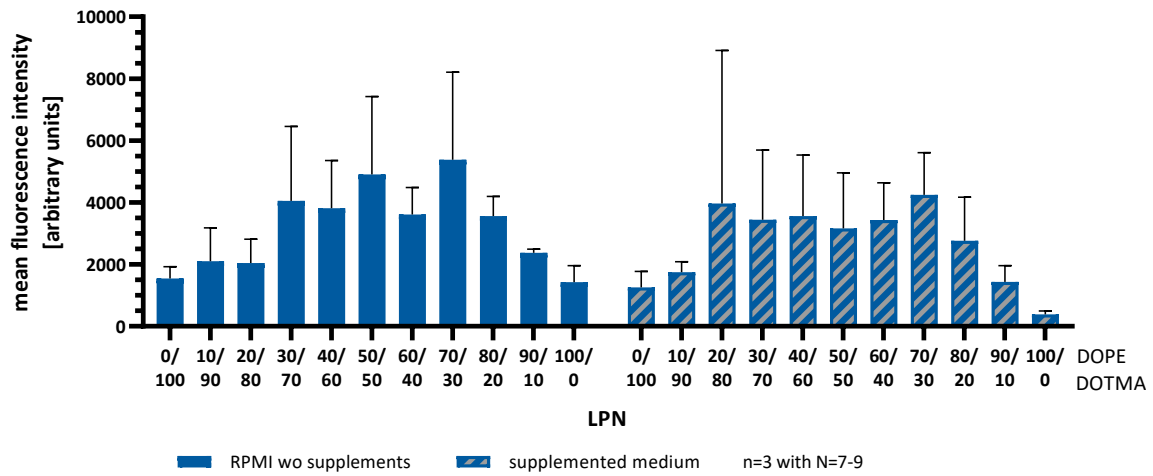


Figure 18. Amount of LPN uptake indirectly measured by fluorescence intensities of live cells after 24 h incubation with FITC-labeled, mRNA-loaded LPNs. The highest fluorescence values and thus the largest amounts of LPNs associated with the DC2.4 cells were found for the same LPNs (LPNs (30/70 – 80/20)) that led to the highest uptake rates. Graph has been modified from supplementary material of Kliesch et al. [157]

## 4.2 Transfection Efficacy

### 4.2.1 Kinetic Evaluation of Optimal Incubation Time

From previous experiments we know that the LPNs are well tolerated and associated with the cells to a high extend after 24 h incubation. After this successful uptake, the mRNA needs to reach the cytosol where it will be translated into the protein. In our case, we used mRNA encoding for the fluorescent protein mCherry to enable an easy readout by flow cytometry or fluorescence microscopy.

In a first setup, I investigated how much incubation time is needed to detect protein production. I incubated the DC2.4 cells for 5, 15, 30 or 60 min, removed them afterwards by washing and added new cell medium for further 24 h to give the cells enough time for protein synthesis. As comparison, I incubated one well per group 24 h with the LPNs dispersed in non-supplemented medium without a washing step in between (Figure 19). I followed the upcoming red fluorescence signal with an automated fluorescence microscope imaging every 45 min and additionally measured the fluorescence values by flow cytometry at the end of the experiment.

For DOTMA-only LPN (LPN(0/100)) we found a clear correlation between incubation time and measured fluorescence intensity (Figure 19A). Already with a 15 min incubation time, we found a faint but constant signal showing up after 3 h. With 30 min incubation, the red fluorescent signal appeared within one hour reaching the plateau after 3 h. These measured values were more than threefold as high as for the shorter incubation time. Doubling the incubation time again to 60 min, doubled the fluorescence intensities. For continuous incubation with LPN(0/100) we found a different profile than before with a steep rise within 6 h, a plateau until 12 h followed by a decline. The maximum value was about twofold as high as the plateau of the 60 min curve. For LPN(10/90), the fluorescence intensity increased after 30 min incubation (Figure 19B). Longer incubation reduced the time until we saw the first signal. 60 min and 24 h incubation resulted in similar curves. For LPN(50/50) we saw fluorescence values similar to the 30 min of LPN(0/100) already after 15 min (Figure 19C). It was yet not possible to compare this line further with the other curves of LPN(50/50) because a lack of focal plane during imaging did not allow any reliable readout. Same occurred to the wells of LPN(70/30) (Figure 19D). As we found transfected cells in the flow cytometer, the problem was only at the imaging part and not caused by a bad performance of the LPNs.

## 4 Testing Nanoparticle Performance Under Stress Conditions

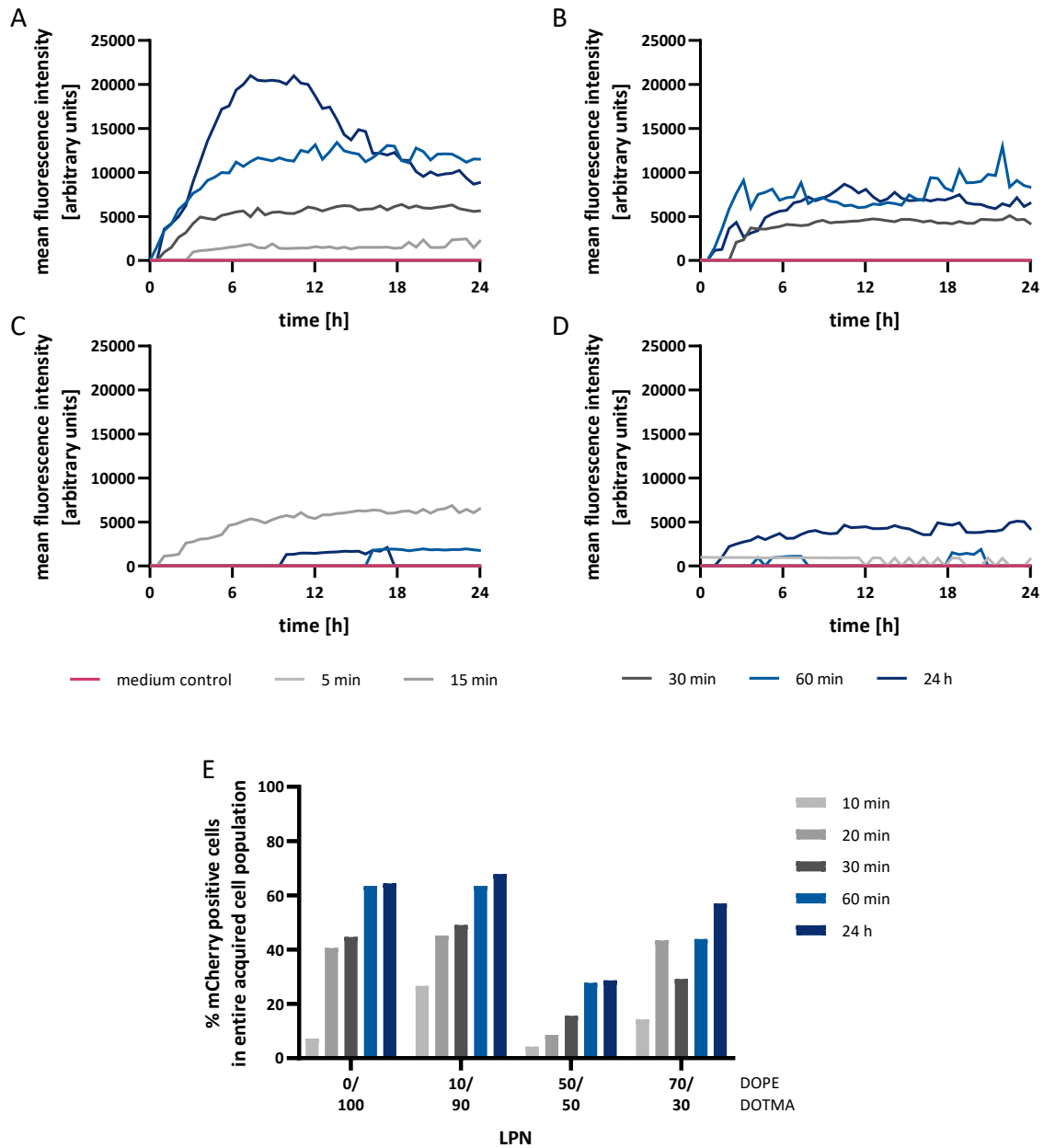


Figure 19: Evaluation of transfection efficacy as a function of incubation time. DC2.4 cells were incubated with FITC-labeled, mCherry-mRNA-loaded LPNs in non-supplemented medium for displayed time intervals. After washing and adding new medium, cells were imaged every 45 min for 24 h with an automated microscope. One well per condition with three imaging spots per well. Hoechst staining for better autofocus. Imaging-based quantification of mCherry related fluorescence intensities after incubation with (A): LPN(0/100). (B): LPN(10/90). (C): LPN(50/50). (D): LPN(70/30). LPN(0/100) showed a clear correlation of incubation time and measured fluorescence intensity while results for LPN(10/90) were similar for three longest incubation times. For LPNs (50/50) and (70/30) the measurement was jeopardized by suboptimal autofocus and thus not conclusive. (E): Results of flow cytometric analysis after last all images were taken with automated microscope. All LPNs showed a correlation of incubation time and measured fluorescence intensity but on different levels. Longest incubation time for 60 min and 24 h resulted in highest transfection rates.

In the flow cytometric analysis, we found the same trend that the longer the incubation time, the higher is the percentage of transfected cells (Figure 19E). For LPN(10/90) and LPN(70/30) this trend continued for all time steps with the exception of 20 min for LPN(70/30). For LPN(0/100) and LPN(50/50) we found similar percentages for 60 min and 24 h incubation time. This fits to the results of the microscope curves for LPN(0/100). LPNs with lower DOPE amount transfected more cells than the other nanocarriers. LPN(50/50) showed the lowest effect. As the percentage of successfully

#### 4 Testing Nanoparticle Performance Under Stress Conditions

transfected cells were the highest after 24 h and the LPNs are tolerated well enough, we decided to fix this incubation time for further experiments.

I optimized the autofocusing parameters and repeated the experiment with the automated microscope. DC2.4 cells were incubated for 24 h again with FITC-labeled LPNs in non-supplemented medium. Figure 20 shows the number of transfected cells in A and the mean fluorescence intensities in B. As comparison, I added jetMESSENGER®, a commercial polymer-based transfection reagent, and Lipofectin®, a liposomal transfection reagent composed of DOTMA and DOPE (1:1). These commercial controls successfully transfected DCs with the fastest arrival of the first positive cells. The Lipofectin® sample had a little slower onset than the JM sample and generally a lower MFI. For LPN(0/100) the MFI curve was comparable to the one of the previous experiment with maximum values around 20,000 after 10 h and a decline after 15 h. In contrast, the maximum cell count was already reached after 5 h. This might be an indicator that there are few cells that produce the protein very efficiently.

We observed a similar curve combination for LPN(10/90) with overall smaller cell numbers and intensities compared to DOTMA-only LPN. The level of cell counts of LPN(50/50) was comparable to the commercial controls with an onset like Lipofectin®. The MFI differed with a flat increase reaching its plateau after 18 h on a lower level than the controls. LPN(70/30) had the slowest increase of transfected cells. Still the MFI reached its plateau already after 2 h and remained its level. The LPNs seem to have different kinetic transfection profiles that might be beneficial for different applications. Anyways, this single experiment gives only hints of the transfection profiles but confirms the selection of 24 h as good time point to analyze cell counts with the flow cytometer.

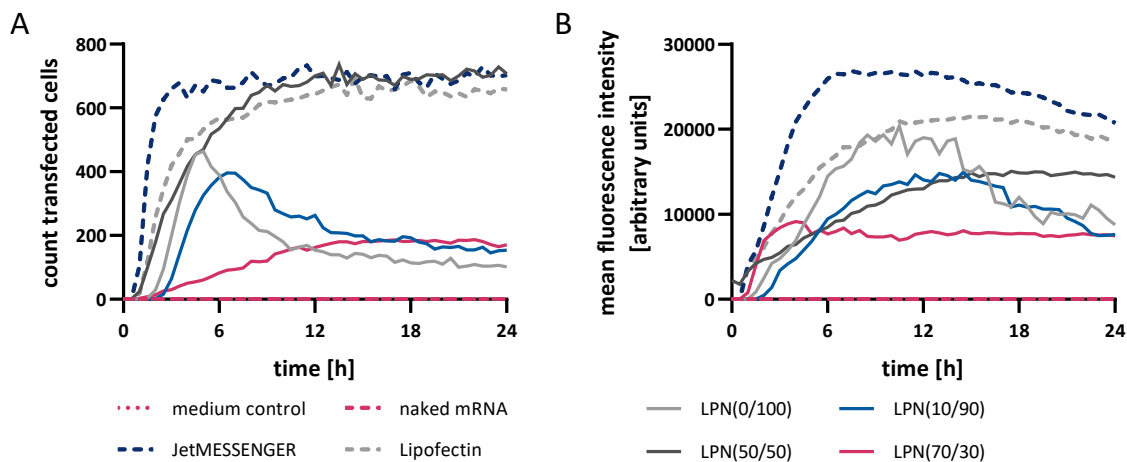


Figure 20: Imaging-based, kinetic evaluation of transfection efficacy. FITC-labeled, mCherry-mRNA-loaded LPNs were added to non-supplemented medium for 24 h. DC2.4 cells were imaged every 30 min with an automated microscope. One well per condition with seven imaging spots each. Hoechst staining improved autofocusing. (A): Count of transfected, fluorescent cells. (B): Mean fluorescence intensity of transfected cells. LPN(0/100) and LPN(10/90) show similar profiles with a delayed maximum of MFI compared to the cell count curves. LPN(50/50) had cell counts comparable to controls but lower MFI plateau. LPN(70/30) had slowest onset of transfected cells but still with a constant MFI over 24 h.

### 4.2.2 Assessment of Dose Dependency

In the next step, I investigated if the protein expression is already saturated and if it could be reached with a lower dose after 24 h incubation. I compared doses of 1  $\mu\text{g}$  mRNA per well as previously used with half the amount. I also added the LPNs (20/80 – 40/60) to see if there is a linear decline parallel to the DOPE content. DOPE-only LPNs were investigated as well to proof the theory of no transfection for these LPNs. This hypothesis was confirmed as Figure 21 shows. The transfection rates of DOTMA-only LPN (LPN(0/100)) and the transfection controls were not affected by the dose and could be realized with less mRNA as comparably high percentages indicate. For all other LPNs but LPN(100/0), the experiment revealed a clear influence of the mRNA amount. The overall transfection efficacy did not show a linear trend with one maximum and one minimum. The effect decreased from LPN(0/100) to a minimum at LPN(30/70) and increased again with a maximum at LPN(50/50) and decreased again to no transfection for DOPE-only LPN. These results do not fit to the previous findings where we had only one well per condition. But this time the data set is based on up to five wells out of two experiments and is thus more trustable. Nevertheless, we would need more repetition for solid conclusion. We anyways gained hints that the transfection efficacy profits from a higher mRNA dose.

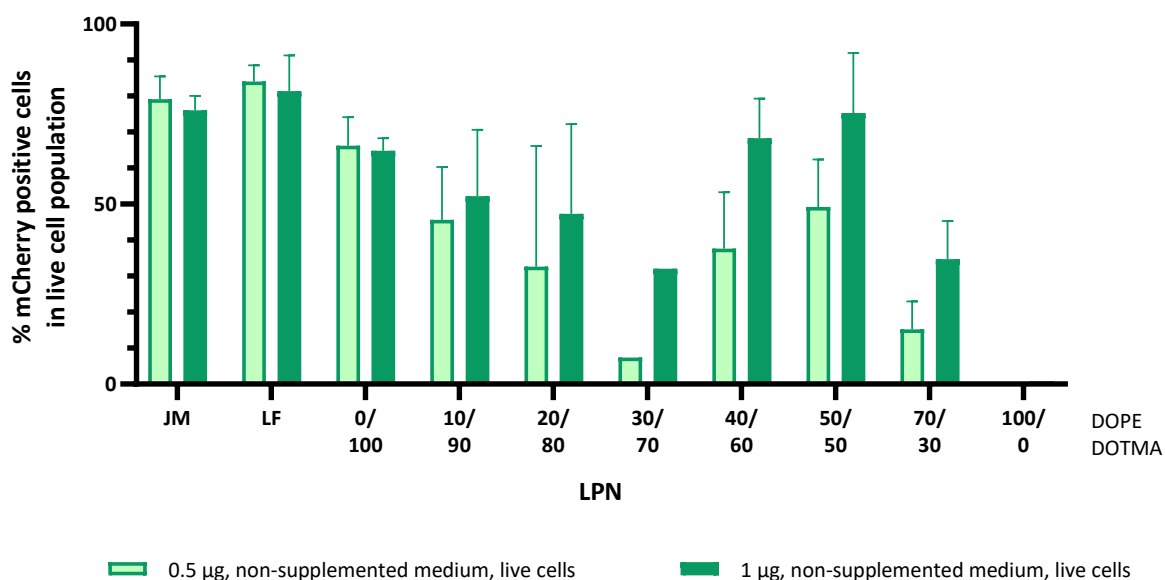


Figure 21: Comparison of transfection efficacy for different LPN amounts. DC2.4 cells were incubated for 24 h with FITC-labeled, mCherry-mRNA-loaded LPNs dispersed in non-supplemented medium. For dose reduction half the number of loaded LPNs was added to the medium. DAPI staining for dead cell exclusion.  $N=2$  with total  $n=1-5$ . Commercial transfection reagents: JM: JetMESSENGER®, LF: Lipofectin®. Controls and LPN(0/100) showed comparable transfection rates for both doses while other LPNs profited from higher mRNA dose resulting in higher percentages of protein producing cells.

### 4.2.3 Influence of Medium Supplements on Transfection Efficacy

Having set the incubation time to 24 h and the mRNA dose to 1  $\mu\text{g}$  per well, I investigated how robust the transfection is. Standard transfection protocols often use buffers or medium with a reduced serum amount for nanocarrier incubation because additives have the potential to reduce the transfection efficacy [139]. These protocols recommend a washing step after incubation followed by a post-incubation time in medium to give the cells the time to produce the protein. In the following experiment, I followed this recommendation and incubated the DC2.4 for 4 h with LPNs in different media, washed away the nanoparticles and let the cells grow for further 24 h. We selected LPN(70/30) as favorite candidate in the uptake study and as comparison LPN(10/90) with good transfection results in the preliminary experiments. As shown in chapter 3.2.3, LPN(0/100) is not

#### 4 Testing Nanoparticle Performance Under Stress Conditions

colloidally stable in protein containing media and will be therefore excluded from closer analyses. I compared HBSS with Opti-MEM®, a common medium for transfection studies, and investigated the effect of FCS addition.

For LPN(10/90), we found a drastic reduction in transfection efficacy as soon as 1% FCS was added (94% to 14% transfected live cells) while numbers were high for samples incubated without FCS (Figure 22). In contrast, the percentage of protein producing cells was still high for LPN(70/30) when FCS was added and generally higher than in the previous experiments. 10% FCS in HBSS reduced the result for LPN(70/30) from 92% in plain buffer to 73%, respectively. In combination with medium, the transfection efficacy was reduced to 34%. The more FCS the medium contained, the higher was the challenge for the nanocarriers. This influence was higher if the loaded LPNs were incubated in supplemented medium than in buffer (HBSS) or special transfection medium (Opti-MEM®).

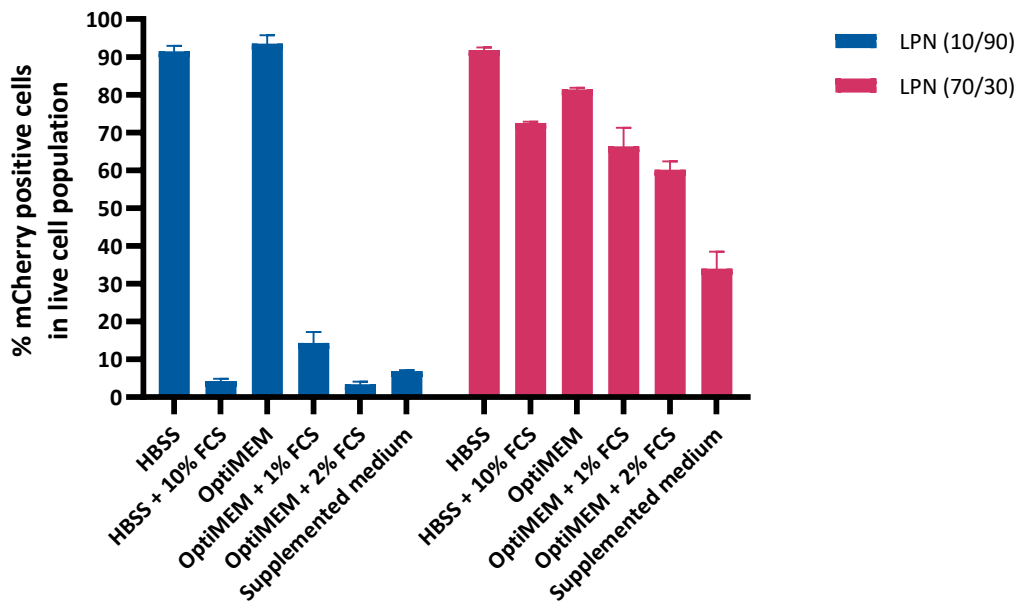
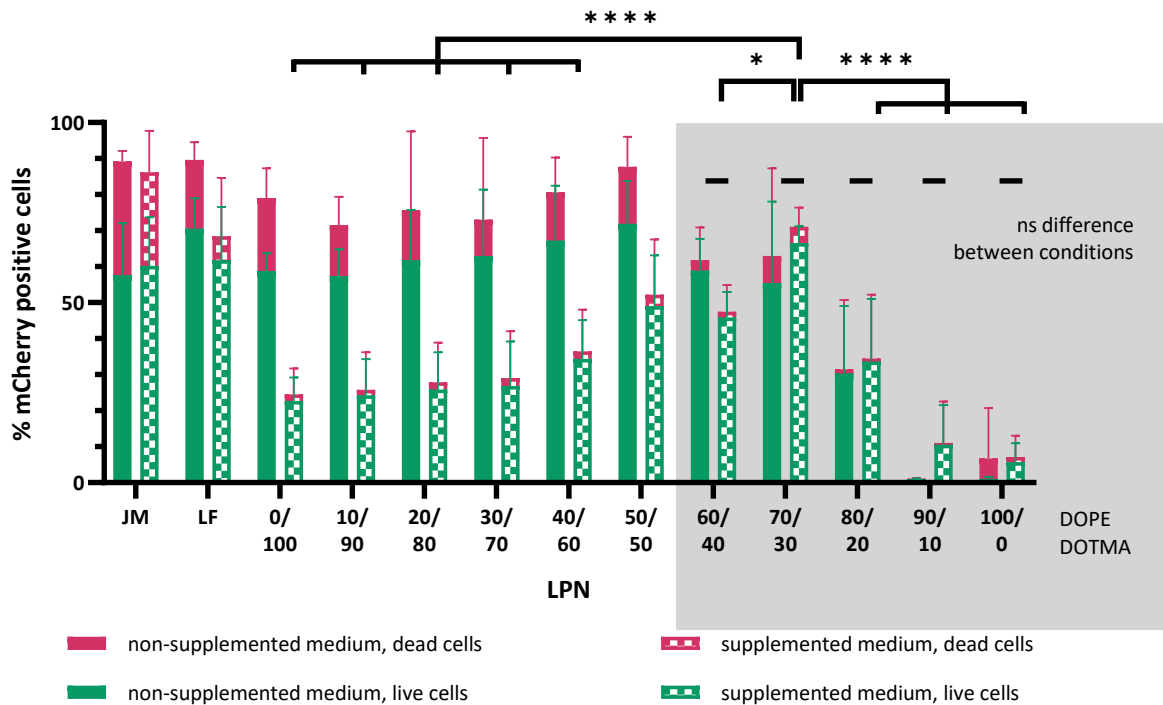


Figure 22: Quantification of the influence of FCS addition onto transfection efficacy of LPNs. DC2.4 cells were incubated for 4 h with FITC-labeled, mCherry-mRNA-loaded LPNs, washed and then grown for another 24 h with regular growth medium (RPMI supplemented with 10% FCS, HEPES, non-essential amino acids (1X),  $\beta$ -mercaptoethanol (0.0054X)). Nanoparticles were dispersed in different media to test the influence of FCS addition. N=1 with n=2. LPN(10/90) showed a distinct reduction of transfection efficacy as soon as FCS was added while transfection rates were more stable for LPN(70/30).

After completing the described optimization steps for the transfection conditions, I finally investigated the transfection efficacy of all prepared LPNs. I compared plain RPMI medium with regular growth medium for DC2.4 cells that is supplemented with  $\beta$ -mercaptoethanol (0.0054X), non-essential amino acids (1X), HEPES-buffer (0.01M) and 10% serum. I incubated the FITC-labeled LPNs for 24 h in these media and added DAPI for the dead cell exclusion during the preparation for flow cytometry. Figure 23 shows the transfection results that were acquired in the same experiment as data sets in Figures 16 (cytotoxicity) and 17 (uptake). Our gating strategy is shown in Figure S 3. I displayed the data as overlay of live transfected cells (green bars) and mCherry-positive cells in the entire, acquired cell population (pink bars).

#### 4 Testing Nanoparticle Performance Under Stress Conditions

Testing all LPNs for the first time, we found several trends connected with the DOPE content. In non-supplemented medium, we saw a difference between total transfected cells and live transfected cells with a maximum value of 20% for LPN(0/100). This difference was drastically reduced when cells were incubated with LPNs with at least 60 mol% DOPE but on the same time the transfection rates was much lower. The percentage of live transfected cells in non-supplemented medium increased from 59% for LPN(0/100) to a maximum of 72% for LPN(50/50).



N=3 with total n=7-9

Figure 23: Evaluation of transfection efficacy depending on the supplementation of the medium. DC2.4 cells were transfected with FITC-labeled, mCherry-mRNA-loaded LPNs for 24 h dispersed in plain RPMI or supplemented medium (RPMI supplemented with 10% FCS, HEPES, non-essential amino acids (1X),  $\beta$ -mercaptoethanol (0.0054X)). DAPI was added to enable exclusion of dead cells. Green bars represent live transfected cells as overlay to red bars that show all transfected cells in the entire, acquired cell population. N=3 with total n= 7-9. (\*  $p < 0.05$ ; \*\*\*\* $p < 0.0001$ ). Data collected in same experiment as cytotoxicity, uptake and protein amounts (MFI). Commercial transfection reagents: JM: JetMESSENGER®, LF: Lipofectin®. Beginning with a DOPE content of 60 mol%, the differences between medium conditions are insignificant represented by the grey box. LPN(70/30) shows highest transfection efficacy independent of the medium. Graph has been modified from Kliesch et al. [157]

In supplemented medium, the differences between efficacy values in live and the entire cell population were much smaller or not present at all. Transfection rates profited again from the DOPE content even though the values were at a lower level. For LPN(0/100), measured percentages of transfected cells in the entire population dropped from 79% in the lower nutrition condition to 25%. The more DOPE the LPNs contained, the better the transfection efficacy climaxing in 67% of live transfected cells after incubation with LPN(70/30). LPNs with at least 80 mol% DOPE (LPNs (80/20) – (100/0)) had a reduced or no transfection. LPN(70/30) performed significantly better than all other LPNs but LPN(50/50) in the full medium condition. The measured live cell transfection for these two LPNs was as good as the one of the commercial controls while all other LPNs transfected less cells. For jetMESSENGER® and Lipofectin® we observed similar numbers in both conditions but with more dead cells compared to the LPN results. For LPNs with more than 50 mol% of DOPE (LPNs (60/40) – (100/0)) the performance did not depend on the medium anymore and was stable for both conditions. We can conclude that the LPN(70/30) showed the best performance with highest and on

#### 4 Testing Nanoparticle Performance Under Stress Conditions

the other side also most stable transfection rates. The evaluation of the fluorescence intensities revealed the same trends for produced protein amounts and is displayed in Figure 24.

As indicated before, the lack of colloidal stability might be the reason for the limited efficacy of LPN(0/100) in complex medium but for the other LPNs we did not find an explanation for the performance differences yet. One option is the presence of nucleases in the added serum that degrades the mRNA cargo. The results of the systematic evaluation are described in the following part.

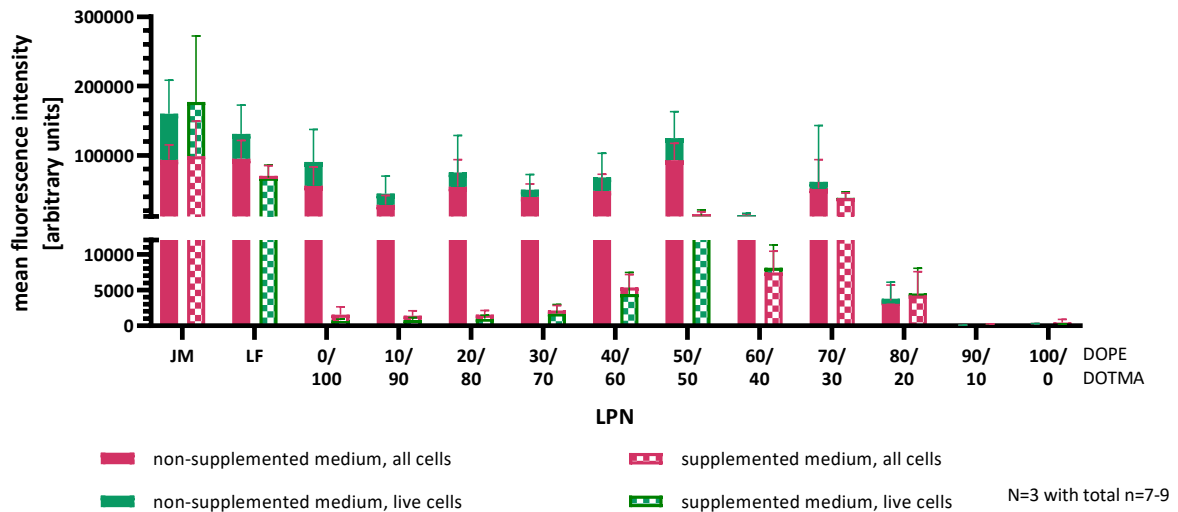


Figure 24: Mean fluorescence intensities of transfected cells in dependence of the used medium. DC2.4 cells were transfected with FITC-labeled, mCherry-mRNA-loaded LPNs for 24 h dispersed in plain RPMI or supplemented medium (RPMI supplemented with 10% FCS, HEPES-BUFFER (0.01M), non-essential amino acids (1X),  $\beta$ -mercaptoethanol (0.0054X)). DAPI was added to enable exclusion of dead cells. Green bars represent live transfected cells as overlay to red bars that show all transfected cells in the entire, acquired cell population. N=3 with total n= 7-9. Data collected in same experiment as cytotoxicity, uptake and transfection rates. Commercial transfection reagents: JM: JetMESSENGER®, LF: Lipofectin®. MFI results confirm LPN(70/30) as optimal nanocarrier generating high and comparable amounts of mCherry protein in both media conditions. All other LPNs showed considerably reduced protein production in supplemented medium. Graph has been modified from supplementary material of Kliesch et al. [157]

### 4.3 RNase Stability

#### 4.3.1 Optimization of Experimental Setup

The addition of serum reduced the transfection rates of our LPNs as shown in the previous chapter. In the following part, I investigated if the included nucleases might be the reason for our observations.

Our aim was to establish an experimental setup where we could follow the mRNA degradation over time. I added again the RiboGreen® dye that exhibits a fluorescent signal after binding mRNA to the samples in a 96-well plate. After dispensing RNase A, I measured the fluorescence over time with the plate reader. To later be able to evaluate the amount of protected mRNA and thus release it from the nanoparticles, I needed to stop the enzymatic process. I optimized all components of the planned protocol stepwise as described below.

#### 4 Testing Nanoparticle Performance Under Stress Conditions

First, I tested how much RNase A I could add to naked mRNA to be able to still follow the degradation. Our first try confirmed that the enzymatic process happened within seconds (Figure 25A). We also observed that already the first measured fluorescence value was reduced depending on the RNase concentration. To save as much time as possible and to avoid any handling delays, I used the automatic dispensing function of the plate reader and varied the mRNA amount in the plate. The second study showed that RNase concentration should be below 0.031 K/ $\mu$ g mRNA because this enzyme amount degraded more than 50% in 5 min (Figure 25B). We decided to set the RNase A concentration to 0.0013 K/ $\mu$ g mRNA.

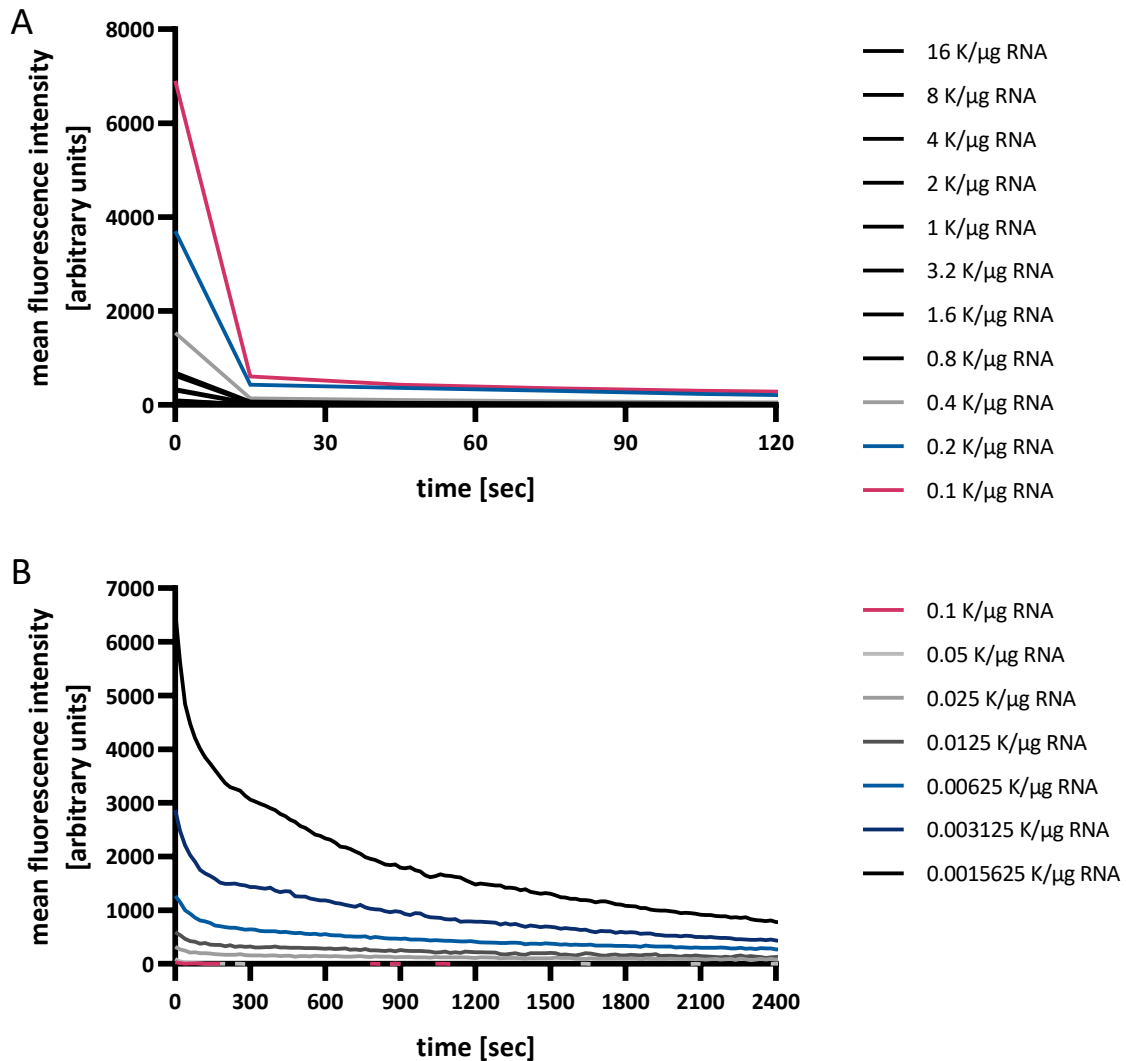


Figure 25: Evaluation of RNase A amount needed to degrade mCherry-mRNA within 30 min. Visualization of mRNA by adding RiboGreen® dye exhibiting fluorescence after binding nucleic acid. Constant amount of RNase was added to different amounts of mRNA in a 96 well-plate. TE-buffer blank is subtracted from measured values. One well per sample. (A): Addition of RNase A by pipetting with hand. (B): Dispensation of RNase A by automated dispensing function of plate reader with immediate initiation of measurement intervals (every min for 30 min). RNase A concentration needs to be below 0.0031 K/ $\mu$ g mRNA to be able to follow the degradation over time. Higher concentration led to a faster loss of mRNA signal.

#### 4 Testing Nanoparticle Performance Under Stress Conditions

The second step of our kinetic experiment is to stop the enzymatic digestion. For that purpose, I added the specific inhibitor RiboLock and tested if 10 U/ng RNase protein is enough to protect the naked mRNA. Comparing a naked mRNA sample with one exposed to RNase added after RiboLock showed no differences while mRNA was degraded without the inhibitor (Figure 26). The mRNA was still present and not degraded. The added amount of inhibitor is therefore enough to stop the reaction timely.

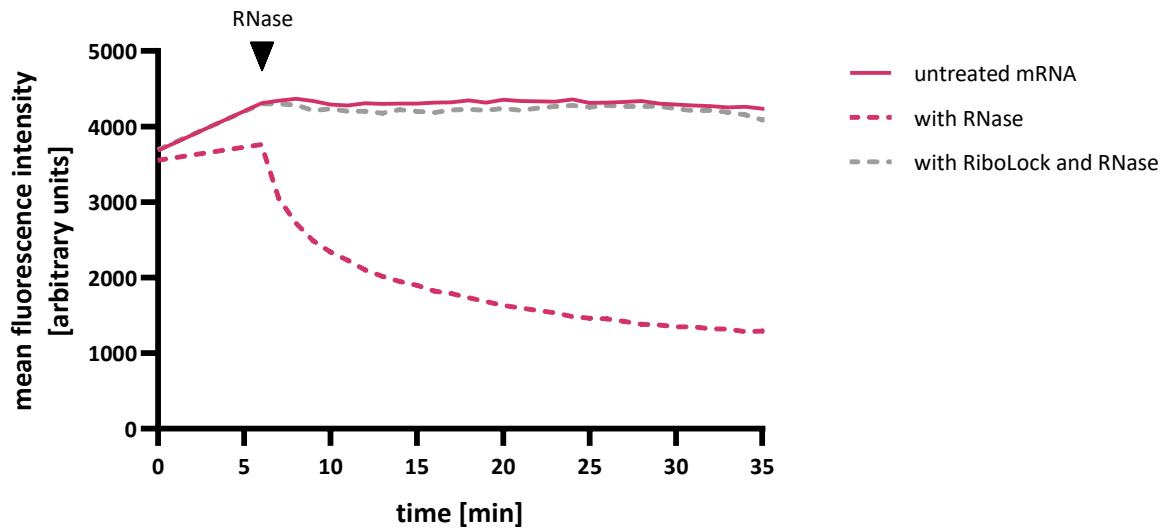


Figure 26: Confirmation of RiboLock amount to sufficiently stop degradation of mRNA by RNase A. Concentration of RNase A 0.0013 K/ $\mu$ g mRNA and the specific inhibitor RiboLock 10U/ng RNase protein. mCherry mRNA was visualized by adding RiboGreen<sup>®</sup> dye. One well per sample. After quality control measurement, RNase A was added and fluorescence measured every minute for 30 minutes. RiboLock was added to mRNA prior to RNase A and successfully protected mRNA from degradation.

After successfully stopping the digestion with the specific inhibitor, I wanted to detach the mRNA from the nanocarriers to see if it was still intact. I used heparin as negatively charged polymer to compete with the nucleic acid for the positively charged nitrogen-atoms on the LPN surface thereby releasing the mRNA. I tested low and high molecular heparin in different concentrations (119.1 mg and 534.4 mg solid, respectively).

## 4 Testing Nanoparticle Performance Under Stress Conditions

With none of the treatments, it was possible to release the entire amount of mRNA indicated by the plateau (Figure 27). The reached fluorescence values were comparable for all treatments. Therefore, we decided to use a medium concentration of 50 mg/ml of high molecular weight heparin that corresponds to 3200  $\mu\text{g}$  heparin/ $\mu\text{g}$  mRNA.

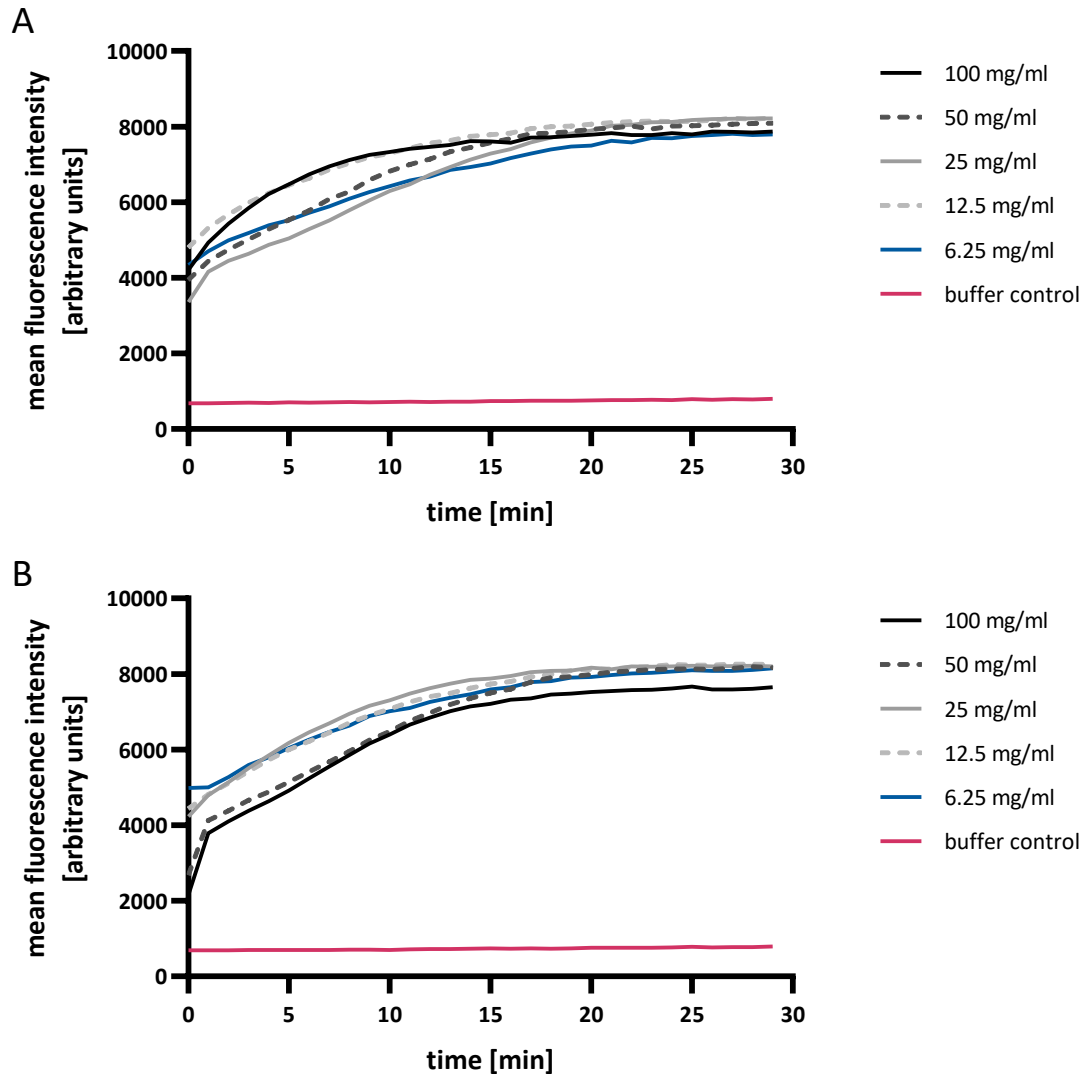


Figure 27: Titration of heparin amount to release the bound mRNA from LPN(10/90). RiboGreen® dye to visualize mCherry-mRNA. For the control group, TE-buffer was added to mRNA-loaded LPNs instead of heparin. One well per sample. (A): Effect of low MW (25KU). (B): High MW heparin (100 KU). All heparin concentrations and types show similar effect and reach a plateau.

### 4.3.2 Kinetic Study of RNase Degradation

Putting the three described steps together, I challenged the mRNA-loaded LPNs with RNase A and followed the change in fluorescence signal on the plate reader. After stopping the digestion and releasing the mRNA from the nanocarriers, I compared RNase treated with samples that underwent the same protocol but were treated with only buffer in the first step.

DOTMA-only LPNs (LPN(0/100)) showed similar values for both samples indicating well protection capabilities for this lipid (Figure 28). On the other side, the differences of DOPE-only LPN (LPN(100/0)) were even larger than the ones for naked mRNA. From previous experiments we know that the majority of mRNA is not bound at all to this nanoparticle and can therefore be easily

#### 4 Testing Nanoparticle Performance Under Stress Conditions

degraded by the enzymes. The other tested LPNs revealed comparable degrees of protection as indicated by similar differences of endpoints even though we saw some RNase effects in the first part of the kinetic experiment for LPN(70/30).

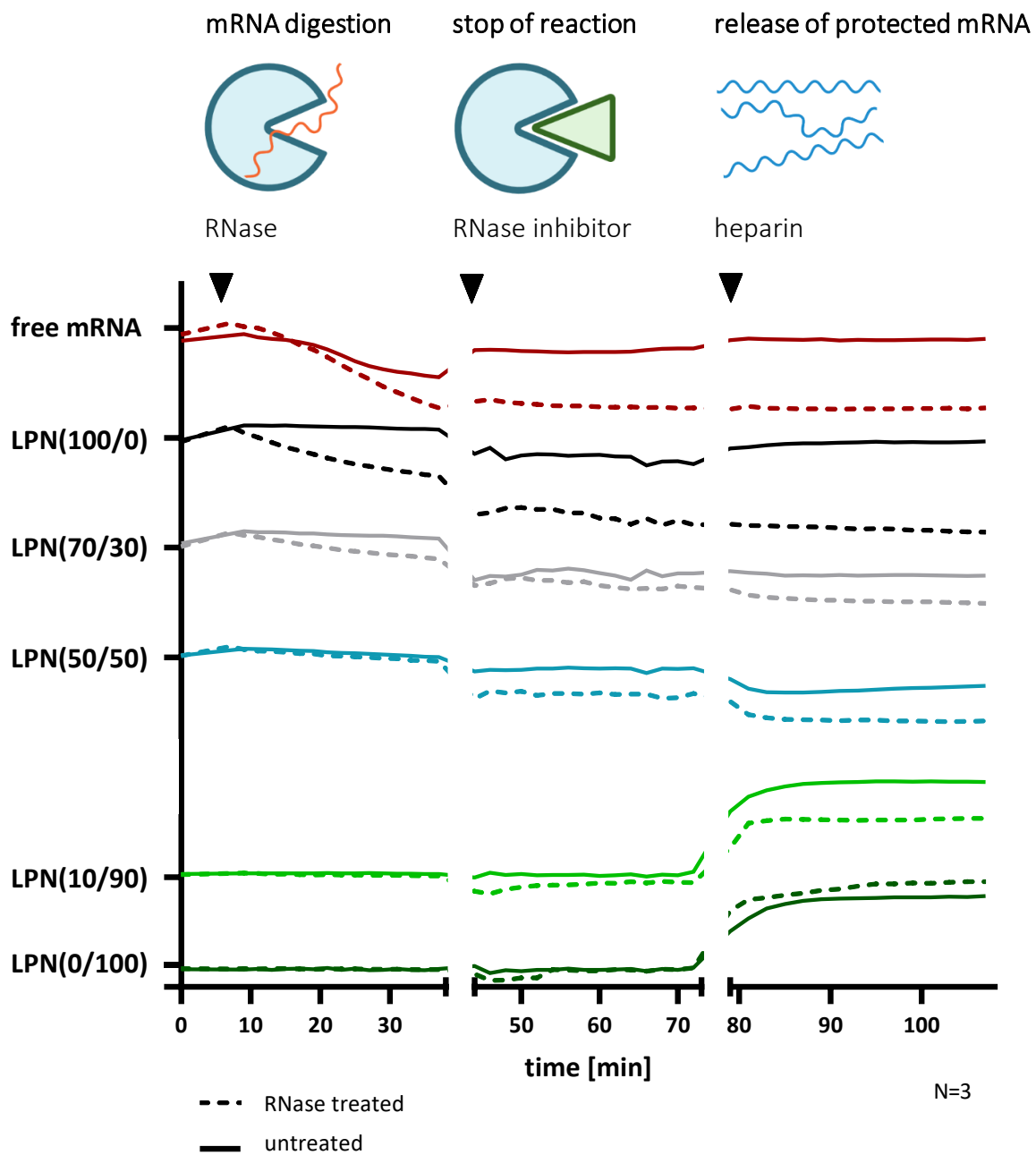


Figure 28: RNase degradation based on fluorescent RiboGreen® dye. mRNA-loaded LPNs were exposed to RNase A and after stopping the reaction to heparin to detach the nucleic acid from the LPN. Measured fluorescence intensities are displayed on the y-axis in arbitrary unit for each LPN separately to facilitate comparison. There is no connection between the height and the measured values. Colors represent the LPN. Solid lines the untreated and dotted lines the RNase treated sample. DOTMA content is beneficial for mRNA protection. Graph has been modified from Kliesch et al. [157]

#### 4 Testing Nanoparticle Performance Under Stress Conditions

In parallel, samples were treated with the same concentrations and protocol but without RiboGreen® and afterwards transferred to a gel containing the dye. For LPN(0/100) and LPN(10/90) we found bright bands with a smear ending at the height of the band of naked mRNA (Figure 29A). In the second gel, this band was more precise for LPN(10/90) and therefore confirmed that the released mRNA is still intact (Figure 29B). LPN(50/50) had a smear in the first gel, too, but darker than the first described LPNs (Figure 29A). For LPN(70/30), there was a faint signal and none for LPN(100/0) supporting the finding of lacking protection by this latter nanoparticle. All the free mRNA that was present in the LPN(100/0) sample before is degraded (compared to Figure 12B).

Looking at the in-process controls of LPN(70/30), we observed a distinct band of free mRNA for the untreated sample (Figure 29B). As soon as heparin is added, this band gets smeared with a weakened intensity. RiboLock does not further change the appearance. We did not find a band on the same height in the gel after RNase treatment whereas there was a faint signal in the first gel. The signal in the gel pocket was reduced as well. In contrast to the results from the plate reader, there seems to be a lack of protection by the LPN(70/30) at least for the fraction that is visible without treatment in the gel.

The comparison with all tested LPNs showed a trend that the more DOTMA the LPN contained, the stronger is the signal of intact mCherry mRNA in the gel after RNase exposure. These LPNs with higher DOTMA and less DOPE content seem to protect the mRNA from RNase A.

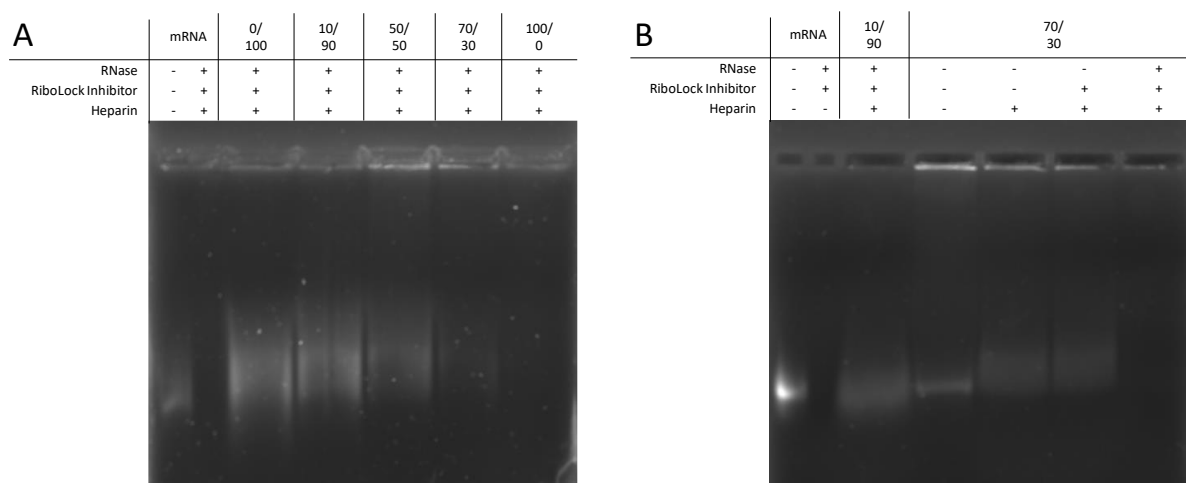


Figure 29: Gel electrophoresis to assess degree of protection of mRNA against RNase A. mRNA-loaded LPNs were exposed to RNase A, followed by the specific inhibitor RiboLock to stop the reaction. To visualize the remnant mRNA in the gel, nucleic acid was released from the LPNs by heparin. Fluorescence dye RiboGreen® in the gel enable visualization. (A): Samples after undergoing all steps of the protocol in a row. (B): Process controls of LPN(70/30) that underwent only a part to the protocol. RNase addition led to disappearance of mRNA band for LPN(70/30). We found a clear correlation between DOTMA content and brightness of band after release.

Gel electrophoresis did not explain why transfection rates are lower in serum containing media for LPNs with higher DOTMA content. Thus, I performed again a transfection study and tested if the established RNase exposure before incubation or serum addition during incubation has the higher impact. As Figure 30 shows, the influence of RNase was much lower than the one of FCS and reduced the transfection rate in this single experiment only a bit. FCS resulted again in a very drastic reduction of transfection efficacy. Putting all our findings together, we decided to test the LPNs in a more complex setting to include also unknown factors in our evaluation.

#### 4 Testing Nanoparticle Performance Under Stress Conditions

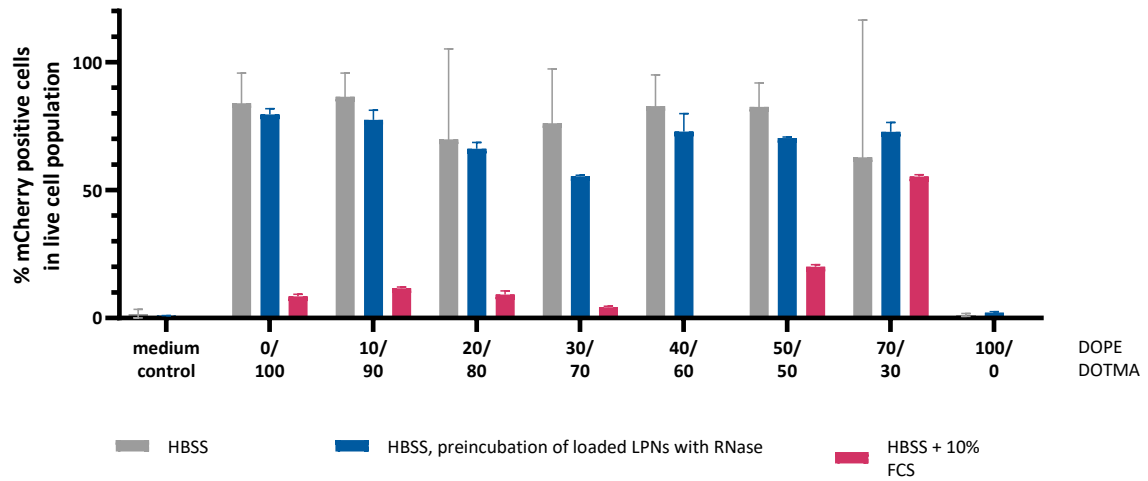


Figure 30: Transfection efficacy under the exposure of RNase A preincubation or FCS addition during incubation. mRNA-loaded LPNs were preincubated with RNase A (0.0013 K/ $\mu$ g mRNA) for 30 minutes at 37 °C and then added to the DC2.4 cells in HBSS. For the other samples, LPNs were directly added to the cells cultivated in HBSS or HBSS including 10% FCS. After 4 h incubation, all LPNs were removed, cells washed and fresh medium added for 24 h. Flow cytometry and DAPI allowed dead cell exclusion. N=1 with n=2. Effect of FCS addition is much higher than the influence of RNase preincubation.

#### 4.4 Performance in Primary Immune Cells

We increased the challenge for the LPNs by exchanging the dendritic cell line with primary bone-marrow derived DCs. All following experiments were conducted in collaboration with Simon Delandre at the HZI. As primary murine cells can be more sensitive to treatments [106], we first investigated the toxicity of mRNA-loaded LPNs after 3 h incubation in Opti-MEM® and 48 h post-incubation time in full medium. As expected, the viability of the cells was reduced indicated by a percentage of live cells in the medium control of only 30% (Figure 31). LPN(0/100) and LPN(70/30) were as well tolerated as this medium control. The other tested LPNs showed more toxic effects leading to a viability that was only half as high (around 15% for LPNs(10/90), (40/60) and (50/50)).

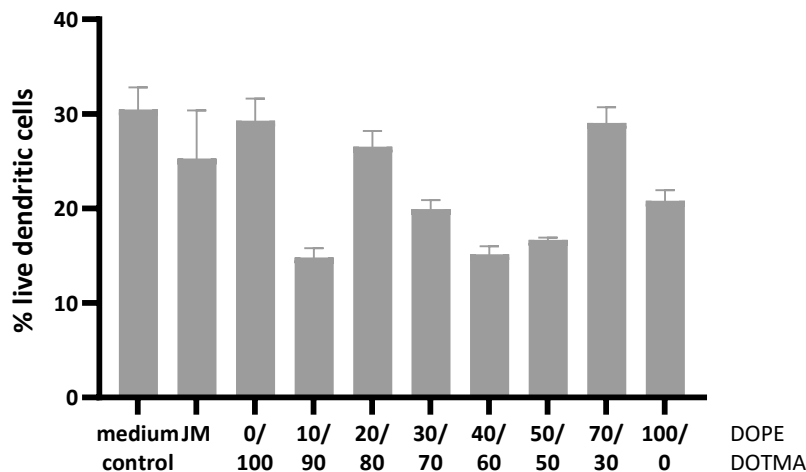


Figure 31: Toxicity assessment of OVA-mRNA-loaded LPNs incubated with primary bone-marrow derived DCs for 3 h in Opti-MEM®. mRNA amount was 1 µg/well. After washing, cells were incubated for further 48 h in regular growth medium and analyzed by flow cytometry. JM: JetMESSENGER®, commercial transfection reagent. N=1 with n=3. Data kindly provided by Simon Delandre, HZI. Overall viability was low with maximum value around 30% for live control, LPN(0/100) and LPN(70/30). Other LPNs halved the viability further.

#### 4 Testing Nanoparticle Performance Under Stress Conditions

Next, we evaluated the performance in these cells and decided to measure not only the transfection rate but the percentage of cells that present parts of the produced protein on their surface. LPNs were loaded with mRNA encoding for the model antigen ovalbumin in the same N:P ratio used for mCherry loading. The successful mRNA delivery and consecutive protein production causes presence of the ovalbumin in the cytosol which leads to its presentation as the eight amino acids (1X) long peptide SIINFEKL on the MHC-I complex that can be quantified with an antibody [17]. After 3 h with the LPNs and another 48 h without, we found SIINFEKL positive cells for all LPNs, but the level was very low compared to the one of the positive control, the ovalbumin protein itself. Only LPN(0/100) and LPN(20/80) showed better values of around 6% positive cells (Figure 32).

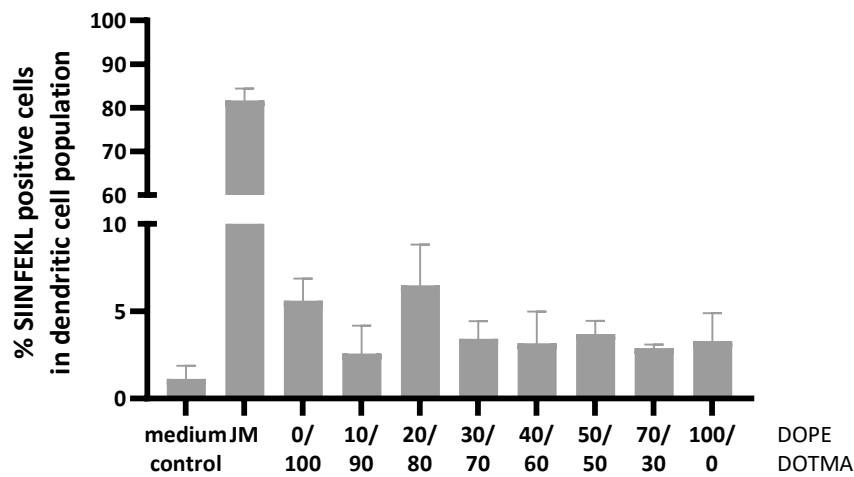


Figure 32: Antibody-based quantification of SIINFEKL presentation on MHC-II receptors of BMDCs. Primary cells were incubated 3 h with OVA-mRNA-loaded LPNs in Opti-MEM® and after washing further 48 h in complete medium. OVA-protein was used as positive control. mRNA amount was 1 µg/well. MC: medium control without mRNA. N=1 with n=3. Data kindly provided by Simon Delandre, HZI. LPN(0/100) and LPN(20/80) showed increased levels of peptide presentation but on a very low level compared to the positive control.

From these values we cannot judge if the number of positive cells is enough to elicit an immune response. To assess how many immune cells are activated, we co-cultivated the transfected BMDCs with ovalbumin-specific, naïve T cells for 4 days. With activation, these T cells start to proliferate resulting in a measurable reduction of the included staining with every mitotic cycle. LPN(70/30) led to about three times more proliferation of CD8<sup>+</sup> T cells than the medium control (Figure 33A). Most CD4<sup>+</sup> T cells were stimulated after treatment with LPN(30/70). We cannot draw any solid conclusions from this experiment as standard deviation of most stimulative samples were high and the positive control with the protein did not work and unexpectedly did not cause a great CD4<sup>+</sup> T cells proliferation. Additionally, LPN(100/0) did stimulate CD8<sup>+</sup> T cells which should not be possible with the results from the cell line experiments.

#### 4 Testing Nanoparticle Performance Under Stress Conditions

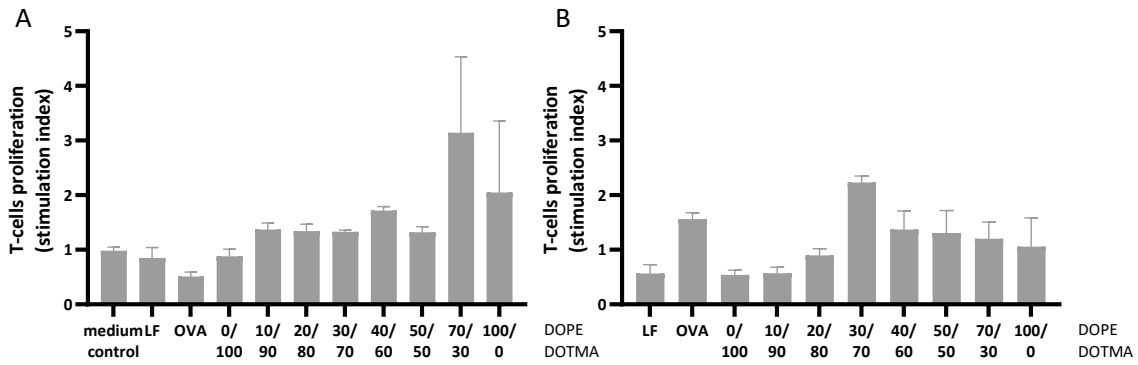


Figure 33: T cell proliferation index after incubation with transfected BMDCs. Proliferation of OVA-specific CD8<sup>+</sup> T cells (A) and CD4<sup>+</sup> T cells (B). Dose of mRNA-loaded LPNs was 0.5  $\mu$ g of OVA-mRNA for 3 h in Opti-MEM<sup>®</sup>. Directly after washing OVA-specific T cells were added for 4 days in complete medium. LF: Lipofectin<sup>®</sup>. N=1 with n=3. Data kindly provided by Simon Delandre, HZI. OVA-protein was used as positive control but lacked in CD4<sup>+</sup> T cells proliferation. LPN(70/30) and LPN(100/0) led to at least twofold higher proliferation of CD8<sup>+</sup> T cells, while LPN(30/70) stimulated most CD4<sup>+</sup> T cells.

Therefore, we repeated the experiment and doubled the applied dose to 1  $\mu$ g mRNA per well for 3 h. We added a post-incubation time of 20 h for the BMDCs alone and extended the co-cultivation time with T cells from 4 to 6 days. We tested LPN(70/30) against jetMESSENGER<sup>®</sup> and LPN(10/90) and found that LPN(70/30) and the commercial transfection reagent caused more proliferation than the medium control (Figure 34). LPN(70/30) as our favorite nanocarrier from the previous studies with the DC cell line led to almost three times more proliferating cells compared to LPN(10/90) and confirmed its status.

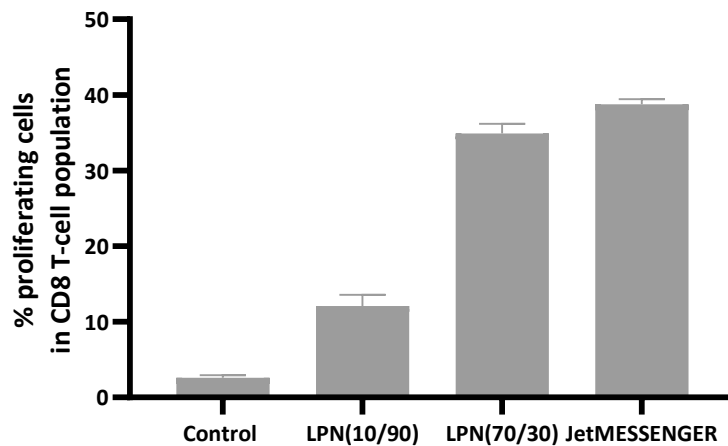


Figure 34: OVA-specific CD8<sup>+</sup> T cells proliferation. Primary BMDCs were transfected with LPNs that were loaded with mRNA encoding for the model antigen ovalbumin. By successfully expressing the protein, these cells activated co-cultured OVA-specific T cells and caused their proliferation. N=1 with n=3. Data kindly provided by Simon Delandre, HZI. LPN(70/30) led to more proliferation than LPN(10/90) indicating again the benefit of this higher DOPE content. Graph has been modified from Kliesch et al. [157]

## 5 Minimally Invasive Application of LPNs to the Skin

### 5.1 Evaluation of P.L.E.A.S.E.® Laser Device

#### 5.1.1 Pilot Study in Excised Human Skin

After optimizing the nanocarriers and thoroughly testing them in different conditions, I concentrated on the method of application for our potential vaccine candidate in this third part of the thesis. Aiming for a minimally invasive application technique, we chose the P.L.E.A.S.E.® system by Pantec Biosolutions that allows the creation of micropores of a distinct depth to target a certain skin layer. In general, we planned a two-step application protocol. First, the micropores are created. In the second step the mRNA-loaded LPNs are applied. You can see a schematic drawing in Figure 35.

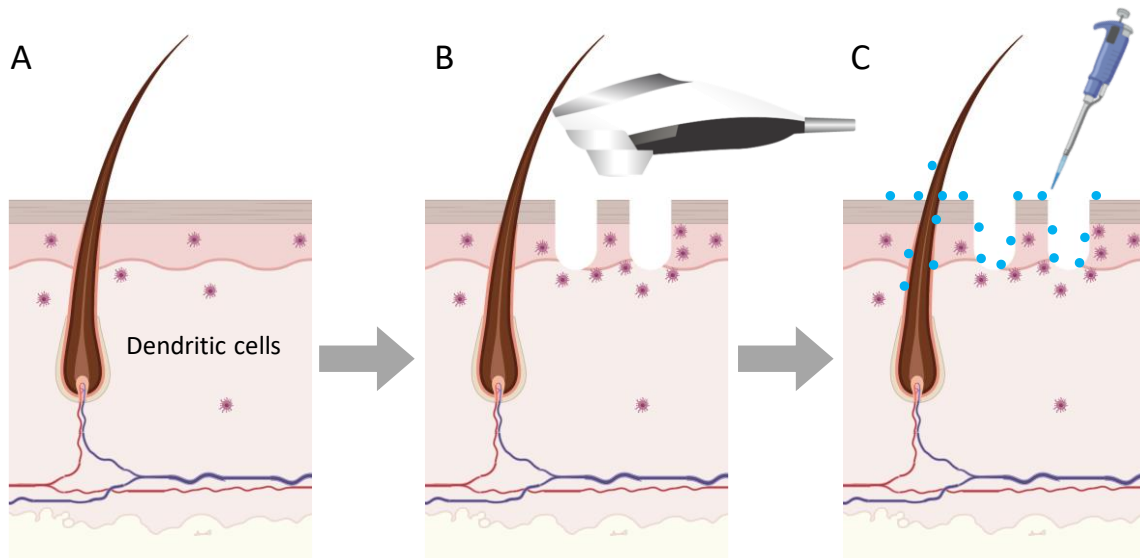


Figure 35: Schematic of the two-step application method of the P.L.E.A.S.E.® laser. (A): Skin with intact barrier before the application. (B): The creation of micropores of distinct depth with the P.L.E.A.S.E.® device attracts dendritic cells. (C): Then the application of mRNA-loaded LPNs.

## 5 Minimally Invasive Application of LPNs to the Skin

We started the experimental series with the P.L.E.A.S.E.<sup>®</sup> system with human abdominal skin and tested the different pore densities. First, I created the pores and then applied trypan blue (0.25% in PBS) to enhance the contrast against the skin and to visualize the pores. We found that medium densities between 7.5% and 10% are a good compromise as many pores are created but there is still room left between the pores (Figure 36). We believe that this aspect is important to initiate an immune reaction later and might save time for future applications as number of pores directly correlates with the time the machine needs to treat the skin. Furthermore, 8% was shown to work for targeting dendritic cells via microporation at the mouse ear [67].

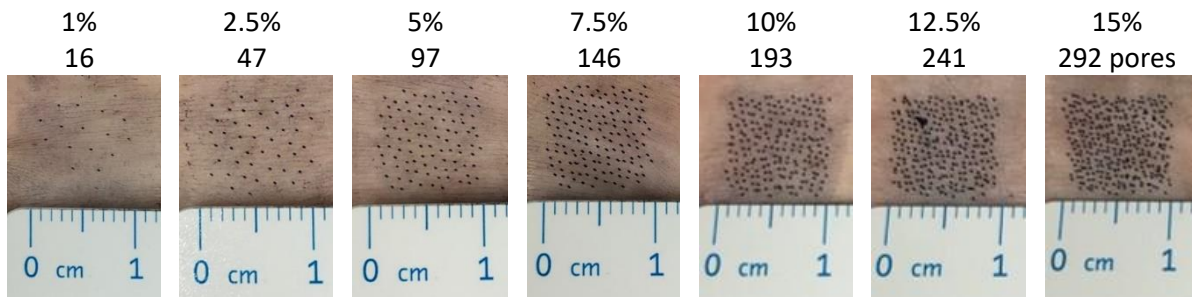
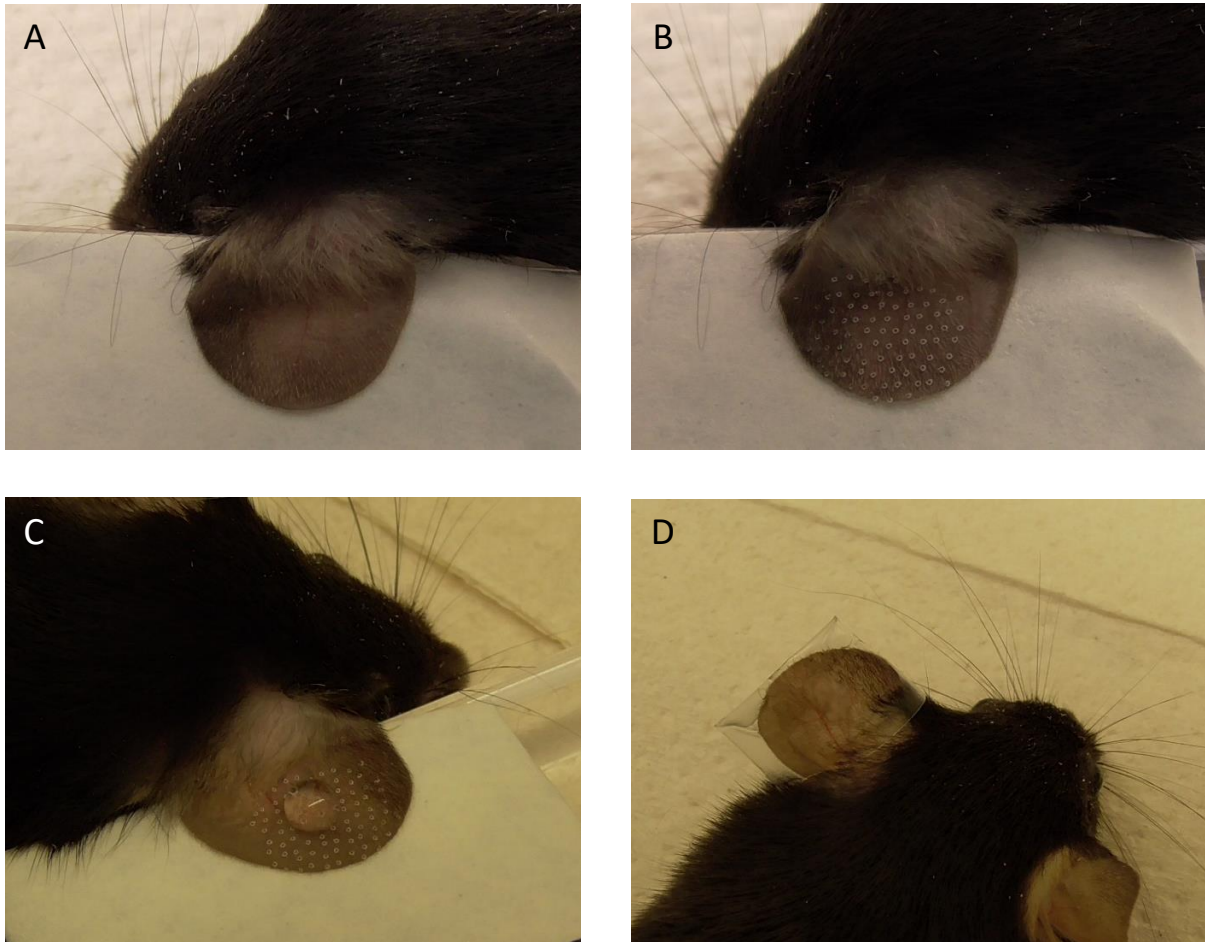


Figure 36: Visualization of pore density of P.L.E.A.S.E.<sup>®</sup> treatment. An area of 10x10 mm of human abdominal skin was treated with different density settings generating pores in a different number but with the same calculated depth of 72  $\mu\text{m}$ . P.L.E.A.S.E.<sup>®</sup> settings: fluence 17.8 J/m<sup>2</sup> (pulse length 75  $\mu\text{s}$ , repetition rate 200 Hz, 3 pulses per pore; resulted in calculated pore depth of 72  $\mu\text{m}$ ). Pore number was counted manually after staining.

### 5.1.2 *In vivo* Studies with Mouse Model

In the next step, our aim was to investigate if the application with the P.L.E.A.S.E.<sup>®</sup> system has an immune stimulatory effect itself. To be able to compare the reactions of the immune system, we decided to do an animal study with mice. As the laser needs direct contact with the skin, the fur of mice might negatively influence the outcome of the experiment. There are protocols of how to treat the back of mice for transfollicular vaccination approaches where the largest area possible is needed. A disadvantage of this application site is that mice need to be shaved and depilated the day before treatment [169]. Hair follicle density was not a problem in our pilot study as the skin came from human abdomen where hair density is generally very low (6-11 follicles/cm<sup>2</sup> versus 658 on mouse back [170–172]). We wanted to avoid any additional factors or treatments like shaving for our mouse study and therefore decided to treat not the back but the ear of mice where the hair density is reduced about 3-fold compared to the back [173]. The area is smaller with a maximum array size of 8 x 8 mm but still large enough for laser microporation without depilation. The mouse ear requires only minimal preparation before treatment like fixation on the tape and a detailed characterization of its immune system is available [174]. Figure 37 shows the single steps of the procedure on the mouse ear including the application of a 10  $\mu\text{l}$  buffer drop and the consecutive massage with an inoculation loop.

## 5 Minimally Invasive Application of LPNs to the Skin



*Figure 37: Stepwise application procedure of P.L.E.A.S.E.® device at the ear of mice. (A): The ear of anesthetized mice was stuck to a tape with dorsal side up. (B): Microporation with P.L.E.A.S.E.® laser (pulse length 75  $\mu$ s, repetition rate 200 Hz, 1 or 2 pulses per pore with calculated pore depth of 24 and 48  $\mu$ m; pore density 8%, treated area 8 x 8 mm). (C): Application of 10  $\mu$ l of PBS and massage with inoculation loop (not shown). (D): Mouse ear was detached from tape and covered with transparent bandage. The treatment of second ear followed. Pictures kindly provided by Simon Delandre, HZI.*

In our study, we compared the immune reaction of two different P.L.E.A.S.E.® settings and applied only PBS buffer without any LPNs or mRNA. The shallow pores had a calculated depth of 24  $\mu$ m representing the successful parameters for the delivery of vaccibodies [67] and targeted only the epidermal skin layer. For the second group, we created micropores of 48  $\mu$ m theoretically reaching through the epidermis down to the dermis. After selected time points, we analyzed the mouse ears with confocal microscopy and digested the skin tissue looking for recruited cells and cytokines.

Confocal microscopy confirmed that the shallow pores do not reach the dermis but end in the epidermal layer as indicated by the lack of pores in the according images (Figure 38 F-H). Without microporation (A, E), there are only a few MHC-II positive cells present in the epidermis while the dermis has many resident immune cells displayed in green. Looking onto the epidermal surface of the ear, we saw hair in white and the first recruited MHC-II positive cells after 3 h. Their number increased with time, climaxing in bright signals after 24 h surrounding a hole in the center of the image for both pore depths (D, K). In the dermis, there is no change in fluorescence signal for shallow pores confirming again that this skin layer has not been reached by these laser settings (F-H). 24 h after deep pore creation, we saw in the dermis a concentration of MHC-II-positive cells building a circle. Even though cells were present in that layer before microporation as well, they did not assemble in this pattern indicating that the laser treatment did attract these cells (N).

## 5 Minimally Invasive Application of LPNs to the Skin

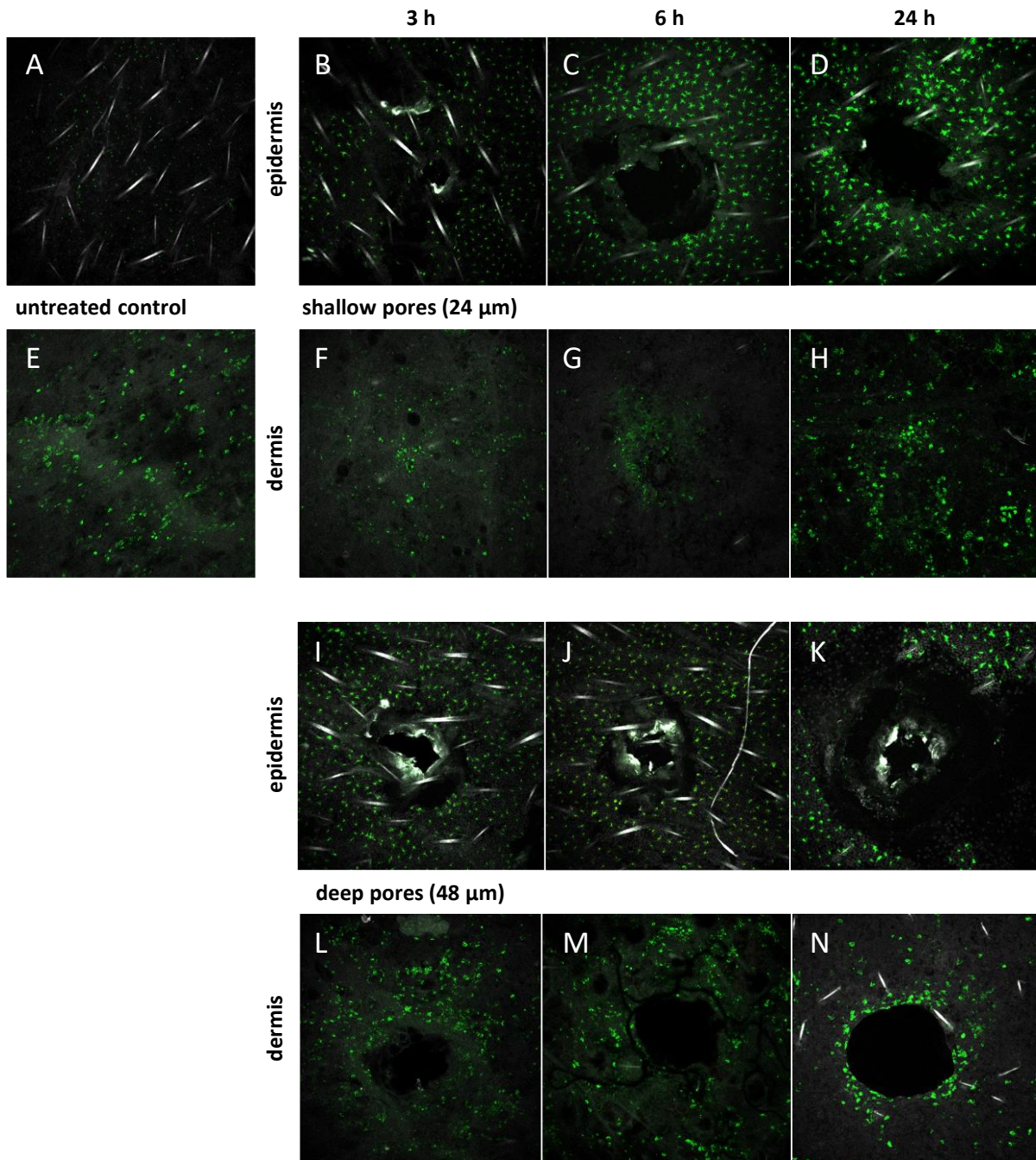


**Figure 38:** Recruitment of MHC-II positive cells after P.L.E.A.S.E.<sup>®</sup> microporation and PBS application. A-D and I-K show images of epidermal skin layer. E-H and L-N show images of dermis. BV421-mediated antibody staining against MHC-II displayed in green. Autofluorescence of mouse hair is shown in white. (A, E): untreated control group. (B-D): Epidermis 3 (B), 6 (C) and 24 h (D) after microporation with one pulse per pore and theoretical pore depth of 24  $\mu\text{m}$  (pulse length 75  $\mu\text{s}$ , repetition rate 200 Hz, pore density 8%, treatment area 8 x 8 mm). (F-H): Dermis of the same ear 3 (F), 6 (G) and 24 h (H) after microporation. While fluorescent signal increased in epidermis with time, the differences were low in dermis compared to the untreated control. We found no hints of a pore in the dermis and concluded that pores hit only the epidermal skin layer of the mouse ear. (I-K): Epidermis 3 (I), 6 (J) and 24 h (K) after microporation with two pulses per pore and theoretical pore depth of 48  $\mu\text{m}$  (pulse length 75  $\mu\text{s}$ , repetition rate 200 Hz, pore density 8%, treatment area 8 x 8 mm). (L-N): Dermis of the same ear 3 (L), 6 (M) and 24 h (N) after microporation. These deeper pores reached down to the dermis. MHC-II positive cells were recruited by the microporation and assembled around the shape of the pore after 24 h. All microscopic cuts of samples K and N are shown in Figure S 7. Data kindly provided by Simon Delandre, HZI.

Flow cytometry analysis revealed some trends but few significant differences. The same is true for the analyses of the cytokines in blood and skin tissue. We therefore decided to concentrate only on the results of cellular analysis. Focusing first on the epidermis, we found invading monocytes and

## 5 Minimally Invasive Application of LPNs to the Skin

neutrophils for both P.L.E.A.S.E.<sup>®</sup> settings after 24 h while percentage of Langerhans cells within the CD45<sup>+</sup> positive cell population decreased (Figure 39). For the neutrophils we even found a significant difference with more cells after deep pores. The second significant improvement was observed in the activation index for monocytes (Figure 40). 3 h after deep pore creation, we found about five times more activated cells compared to shallow pores and the untreated control. After 24 h both groups performed similar well. The activation of Langerhans cells in the epidermis increased over time for both P.L.E.A.S.E.<sup>®</sup> settings.

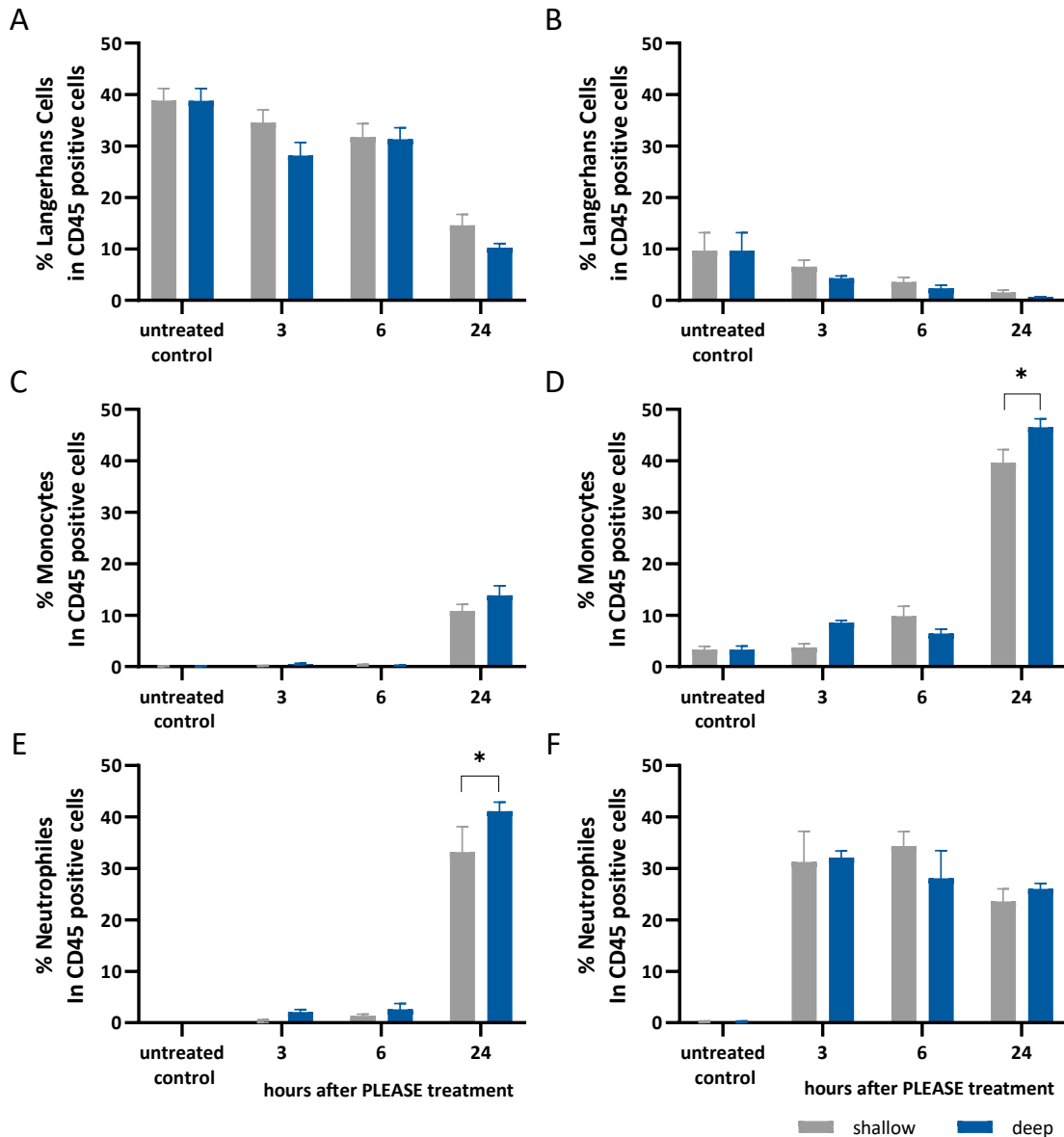


Figure 39: Recruitment of skin cells after P.L.E.A.S.E.<sup>®</sup> microporation and the application of 10  $\mu$ l PBS buffer. (A, B): Langerhans cells in epidermis (A) and dermis (B); (C, D): Monocytes in epidermis (C) and dermis (D); (E, F): Neutrophils in epidermis (E) and dermis (F). Treatment at the dorsal part of the mouse ear (pulse length 75  $\mu$ s, repetition rate 200 Hz, 1 or 2 pulses per pore with calculated pore depth of 24 ('shallow') and 48  $\mu$ m ('deep'); pore density 8%, treated area 8 x 8 mm). Data kindly provided by Simon Delandre, HZI. Microporation leads to a reduction of percentage of Langerhans cells in the epidermis, while number of monocytes was increased in both skin layers after 24 h. Significant improvement for the deeper pores (\*) were detected after 24 h for monocytes in the dermis. Neutrophils invaded the epidermis after 24 h with significant benefits for the deeper pores and stayed on a high level in the dermis.

## 5 Minimally Invasive Application of LPNs to the Skin

Looking at the dermis, we found increased numbers of monocytes up to 40 and 50% of the CD45<sup>+</sup> cells for shallow and deep pores respectively (significant difference) with 3 to 4 times higher activation markers. The neutrophil number increased already after 3 h and stayed high for the 6 h time point and showed a little decrease after 24 h (Figure 39F).

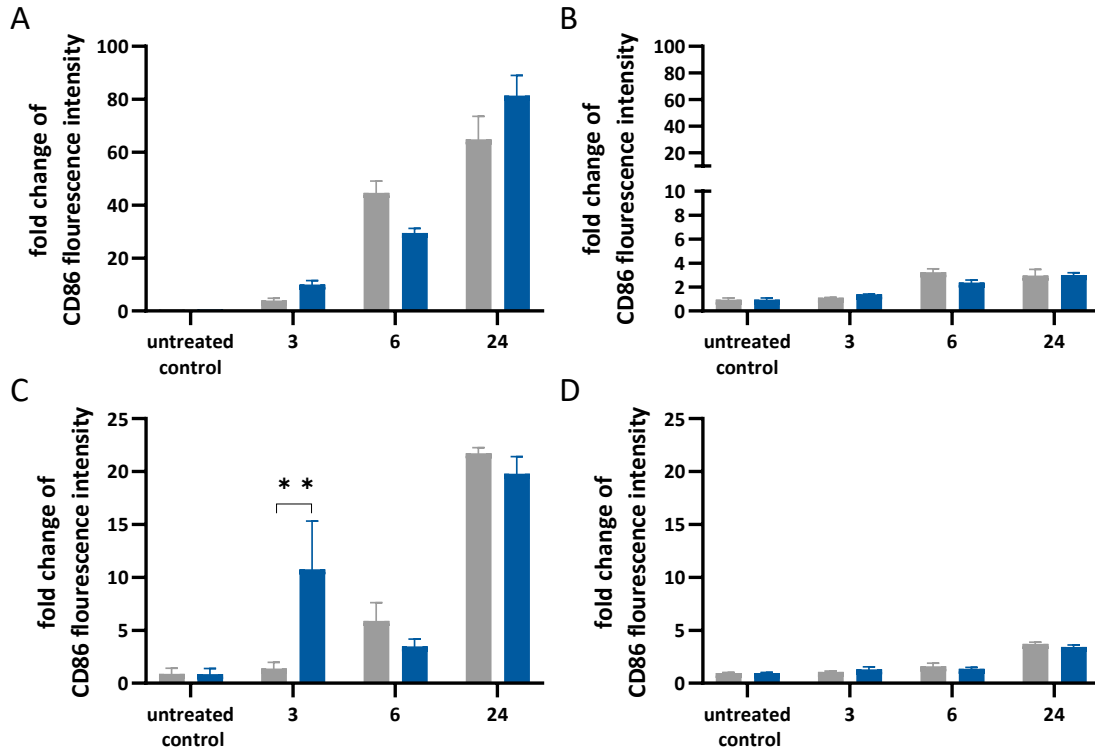


Figure 40: Activation of skin cells after laser microporation. (A, B): Langerhans cells in epidermis (A) and dermis (B); (C, D): Monocytes in epidermis (C) and dermis (D). Treatment at the dorsal part of the mouse ear (pulse length 75  $\mu$ s, repetition rate 200 Hz, 1 or 2 pulses per pore with calculated pore depth of 24 ('shallow') and 48  $\mu$ m ('deep'); pore density 8%, treated area 8 x 8 mm). Data kindly provided by Simon Delandre, HZI. Change of activation especially for the Langerhans cells was observed in the epidermis beginning already after 3 h.

Taking the results from this first mouse study together, we saw several indicators that hitting the dermis with the deeper micropores is advantageous for the immune answer. Furthermore, the processes of invasion and activation happened especially at the latest time point after 24 h. Testing only this time point, we evaluated in the next step if we observe similar benefits of the laser treatment when application is combined with the LPN(70/30). We compared both pore types (shallow/deep) in combination with the OVA-mRNA-loaded LPNs or buffer with an untreated control group and collected the samples after 24 h.

## 5 Minimally Invasive Application of LPNs to the Skin

In both tested skin layers, the application of the P.L.E.A.S.E.<sup>®</sup> system attracted monocytes and neutrophils while number of Langerhans cells was again reduced (Figure 41). For the deep pores in combination with LPNs, the cell movements were comparable to the buffer control with a slight increase in neutrophil numbers in epidermis and monocyte numbers in dermis. The combination of LPNs with shallow pores, showed a reduced immune activation in the epidermis as indicated by a number of Langerhans cells that remained about double as high compared to the deep pores. While less monocytes and neutrophils invaded the epidermis, their number rather increased in the dermis even though the shallow pores did not reach this skin layer.

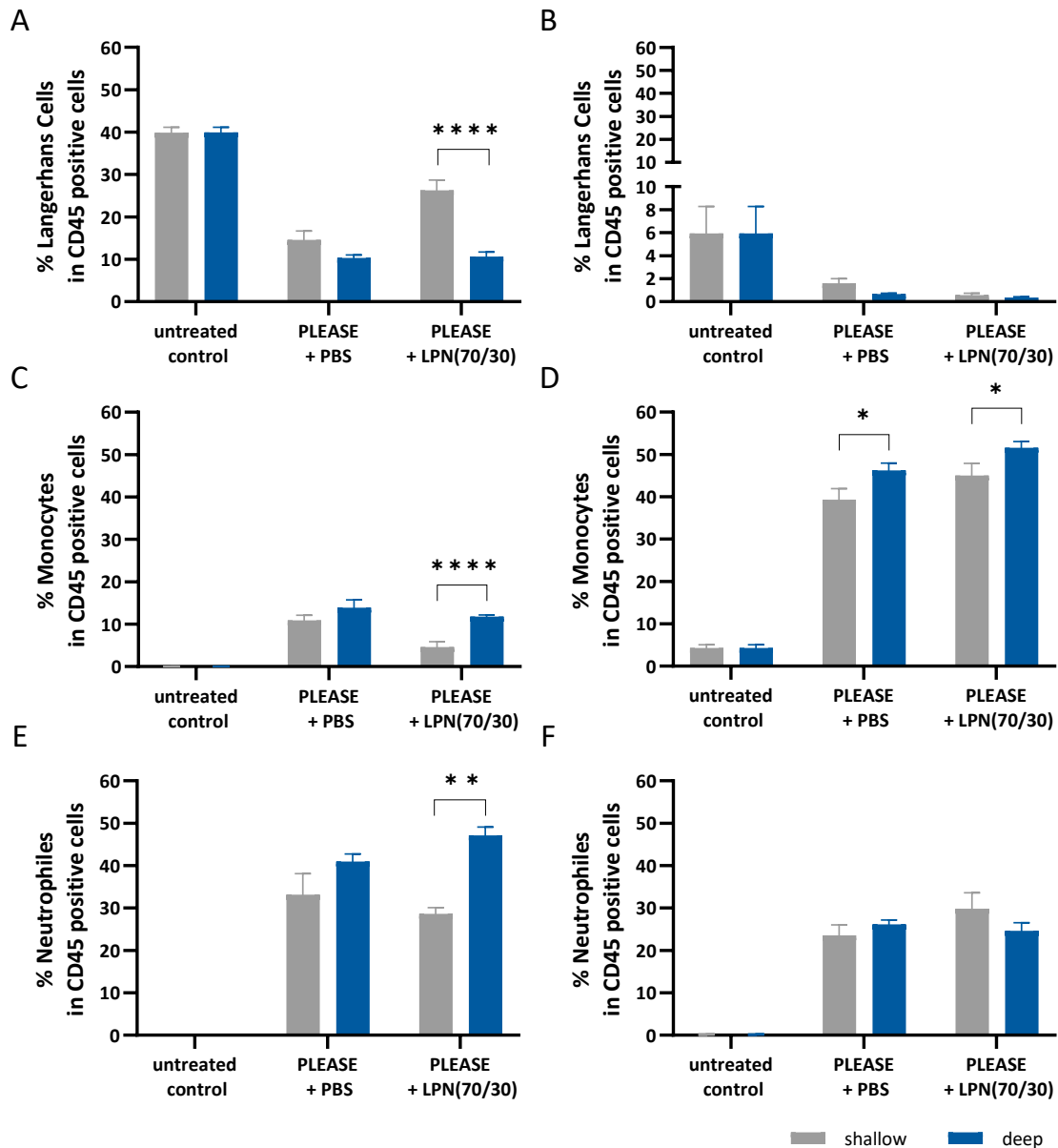


Figure 41: Recruitment of skin cells after P.L.E.A.S.E.<sup>®</sup> microporation and the application of OVA-mRNA-loaded LPN(70/30). (A, B): Langerhans cells in epidermis (A) and dermis (B); (C, D): Monocytes in epidermis (C) and dermis (D); (E, F): Neutrophils in epidermis (E) and dermis (F). Treatment at the dorsal part of the mouse ear (pulse length 75  $\mu$ s, repetition rate 200 Hz, 1 or 2 pulses per pore with calculated pore depth of 24 ('shallow') and 48  $\mu$ m ('deep'); pore density 8%, treated area 8 x 8 mm). Dose per animal 7.84  $\mu$ g mRNA. Data kindly provided by Simon Delandre, HZI. Shallow pores combined with LPN(70/30) led to a reduced immune stimulation compared to deep pores and PBS controls as indicated by more remaining Langerhans cells and less invading monocytes and neutrophils in the epidermis.

## 5 Minimally Invasive Application of LPNs to the Skin

Looking at the cell activation in the epidermis, the markers for LPNs were about double as high as for the buffer control (Figure 42). In the dermis, we saw the same trend for Langerhans cells but the opposite for monocytes. There were no differences between deep and shallow pores in any population.

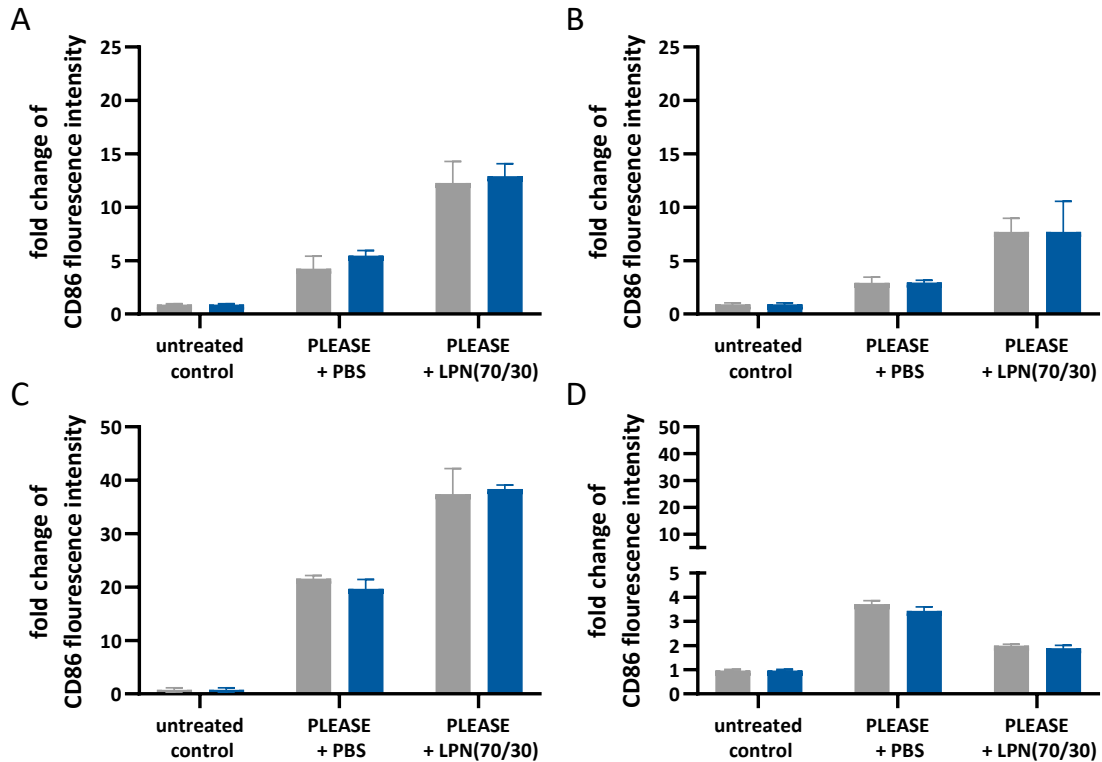


Figure 42: Activation of skin cells after laser microporation and the application of OVA-mRNA-loaded LPN(70/30) or PBS. (A, B): Langerhans cells in epidermis (A) and dermis (B); (C, D): Monocytes in epidermis (C) and dermis (D). Treatment at the dorsal part of the mouse ear (pulse length 75  $\mu$ s, repetition rate 200 Hz, 1 or 2 pulses per pore with calculated pore depth of 24 ('shallow') and 48  $\mu$ m ('deep'); pore density 8%, treated area 8 x 8 mm). Dose per animal 7.84  $\mu$ g mRNA. Data kindly provided by Simon Delandre, HZI. LPN treatment doubled the activation of all selected cell populations with the exception of monocytes in the dermis.

As the experiment was not continued beyond the 24 h time point, we do not know if the LPN elicit a sufficient immune reaction or if our observations and the stimulations are still under the needed threshold of the immune system. We therefore decided to use an adoptive transfer model for our next *in vivo* study. For that model, transgenic mice with CD4<sup>+</sup> or CD8<sup>+</sup> T cells specific for the model antigen ovalbumin were bred. These T cells were transferred to a third group of mice with a regular immune system resulting in OVA-sensitized mice that react within a week instead of four weeks with several stimulations with regular, non-sensitized mice. Another advantage of this mouse model is that we have a good control group showing the optimal response. In our case, this was the protein ovalbumin together with the adjuvant cyclic-di-AMP (c-di-AMP, CDA) via subcutaneous injection. The application route for the other treatment groups was P.L.E.A.S.E.<sup>®</sup> microporation using only the deep settings from the previous experiments.

## 5 Minimally Invasive Application of LPNs to the Skin

One day after the treatment, the pores were visible as red dots on the ear skin. After sampling on day 7, the OVA-protein control met our expectations with more than 90% specific CD4- and CD8<sup>+</sup> T cells in spleen and lymph nodes (Figure 43). The P.L.E.A.S.E.<sup>®</sup> did as well show adjuvant effects especially for CD4<sup>+</sup> T cells when applied in combination with the OVA-protein. In lymph nodes, we found more than 85% CD4<sup>+</sup> and around 60% CD8<sup>+</sup> OT cells, in spleen 50% and 25%, respectively. This observation confirms our general strategy with the P.L.E.A.S.E.<sup>®</sup> application replacing needles and shows the proof of concept for this minimally invasive application route. LPN(70/30) did not stimulate the OT cells above the levels of the negative and buffer controls. As the protein control with the P.L.E.A.S.E.<sup>®</sup> system worked well, the problem seems to be on the side of the LPNs. We therefore took a step back and modified the LPNs adding a pegylated lipid.

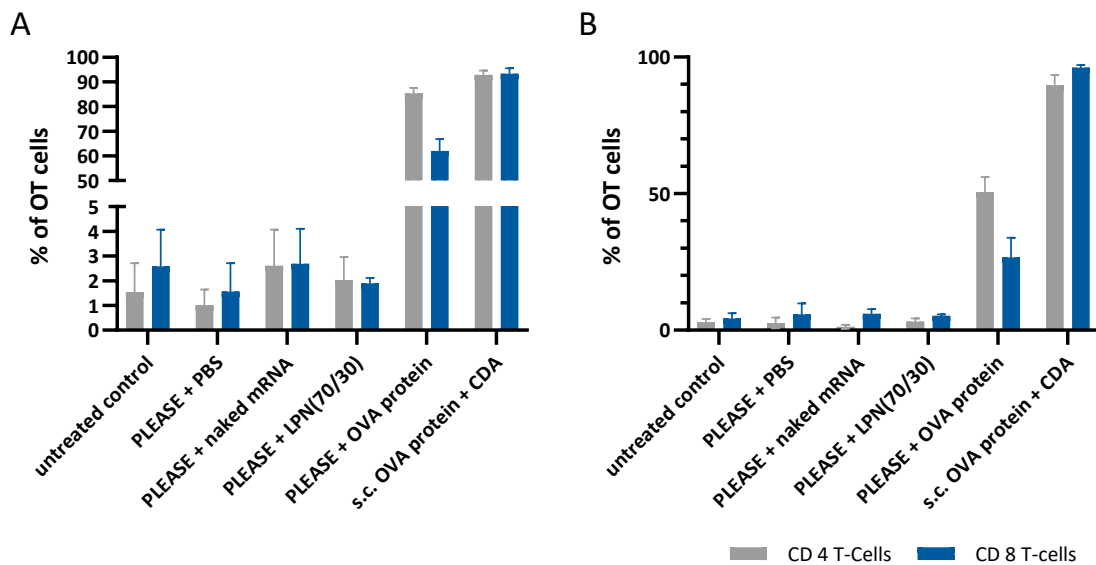


Figure 43: Effect of P.L.E.A.S.E.<sup>®</sup> microporation in combination with LPN(70/30) in adoptive transfer mouse model. Graphs show frequencies of ova-specific T cells (OT cells) in lymph node (A) and spleen (B). Treatment of dorsal parts of the mouse ear (pulse length 75  $\mu$ s, repetition rate 200 Hz, 2 pulses per pore with calculated pore depth of 48  $\mu$ m ('deep'); pore density 8%, treated area 8 x 8 mm). Dose per animal 3.13  $\mu$ g mRNA encoding for ovalbumin. Control group with 5  $\mu$ g ova-protein. Transfer of ova-specific CD4<sup>+</sup> and CD8<sup>+</sup> T cells, vaccination the next day and sampling at day 7. Data kindly provided by Simon Delandre, HZI. The combination with P.L.E.A.S.E.<sup>®</sup> showed an adjuvant effect onto the proliferation of ovalbumin specific T cell almost as high as the adjuvant c-di-AMP (CDA) and subcutaneous injection in the lymph node. This effect was less pronounced in the spleen. LPNs did not elicit a stimulation above the untreated control.

## 5.2 Pegylation of LPN

### 5.2.1 Preparation and Characterization

After testing the P.L.E.A.S.E.<sup>®</sup> laser in combination with the LPNs *in vivo*, we decided to change the composition of the LPNs as results did not fulfil our expectations. I again modified our standard preparation protocol and added the pegylated lipid DMG-PEG2000 at the beginning to the lipid mixture. The previous experiments showed that the DOTMA is more important for the interaction with the mRNA. Furthermore, I wanted to have a good comparability with the non-pegylated LPNs and thus decided to keep the molar amount of DOTMA constant. As a results, I replaced different molar fractions of DOPE with the pegylated lipid.

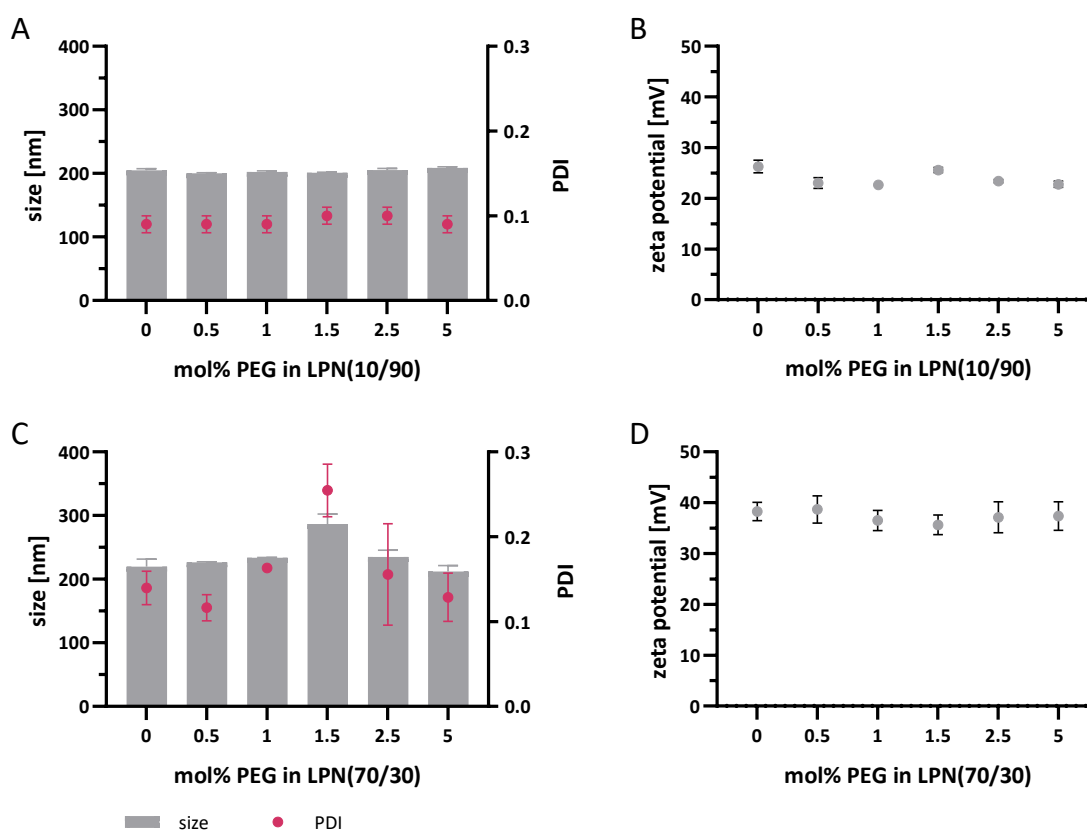


Figure 44: Hydrodynamic parameters of plain, pegylated LPNs. (A): Bars represent size in [nm], dots the mean PDI of LPNs based on LPN(10/90). (B): Zeta potential in [mV] of LPN(10/90) family. (C): Bars represent size in [nm], dots the mean PDI of LPNs based on LPN(70/30). (D): Zeta potential in [mV] of LPN(70/30) family. Each data point represents the mean and the standard deviation of 1–5 batches. The addition of DMG-PEG2000 resulted in comparable particles properties. Only 1.5 mol% PEG in LPN(70/30) showed a deviation from the other LPNs in terms of size and PDI.

We selected again LPN(70/30) as our favorite nanocarrier and for comparison LPN(10/90) and modified both by the addition of 0.5–5 mol% DMG-PEG. The hydrodynamic parameters were constant for all particles with sizes between 200–235 nm and PDI below 0.18 except for 1.5 mol% PEG in LPN(70/30) (Figure 44A, C). The zeta potentials were comparable to the non-pegylated LPNs (Figure 44B, D) and remained stable for the tested time frame of 4 weeks with only marginal losses of surface charge and little increase in size (Figure S 4). The complexation of mRNA by the PEG-LPNs worked as successful as without the pegylation resulting in the same band pattern in the gel electrophoresis (Figure S 5). I then investigated the stability of the LPN(70/30) in supplemented medium for 24 h and observed the same behavior as before without any hints for instabilities for all tested LPNs (Figure 45). The sizes of non-pegylated LPNs rather decreased than

## 5 Minimally Invasive Application of LPNs to the Skin

increased. Measured sizes were generally much larger than in the Zetasizer, especially for LPNs with 5 mol% PEG. As described in chapter 3, we then continued with cell culture-based experiments using the cell line DC2.4.

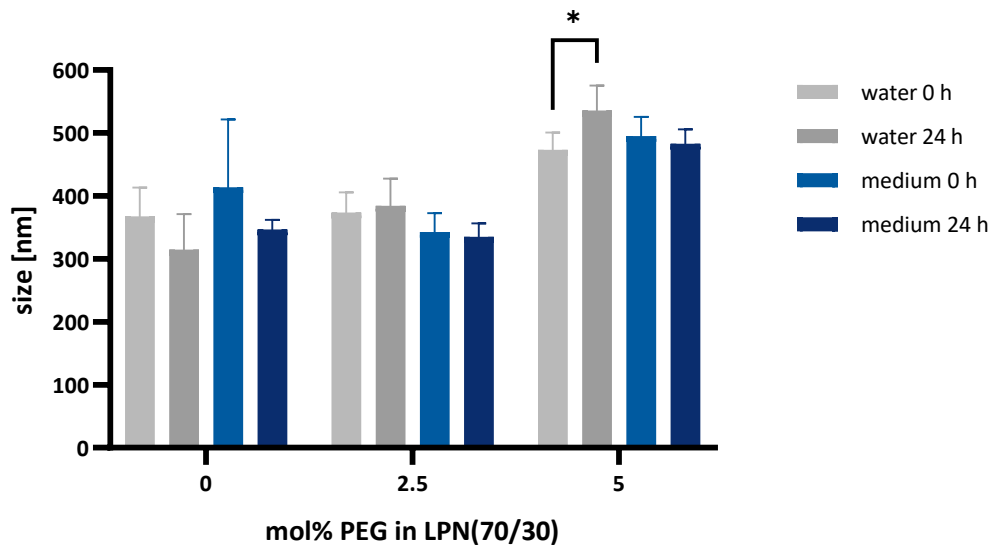


Figure 45: Assessment of influence of medium components onto size of pegylated LPN(70/30) using nanoparticle tracking analysis. DiD-labeled LPNs were loaded with mRNA and incubated for 24 h in demineralized water or medium supplemented with 10% FCS, HEPES-buffer (0.01M), non-essential amino acids (1X) and  $\beta$ -mercaptoethanol (0.0054X). Graph displays size in [nm] at the beginning of the experiment and after 24 h of incubation at 37 °C. Measured sizes in water and medium were comparable independent of the pegylation. The size of the sample with 5 mol% PEG increased from 473 to 535 nm in water representing the only significant difference ( $p < 0.05$ ).

### 5.2.2 Cell Viability

In a first experiment, I incubated DC2.4 cells separately for 4 and 24 h with all mRNA-loaded LPNs in plain RPMI medium analyzed the viability by flow cytometry. After 4 h, we saw a trend that the more DMG-PEG the LPNs contained, the less cells survived resulting in about 40% of live cells for 5 mol% of PEG for both LPNs while non-pegylated LPNs had a survival rate of 90%. Extending the incubation time to 24 h, this trend almost disappeared with viabilities above 80% for all tested nanoparticles but the 5 mol% PEG in LPN(10/90).

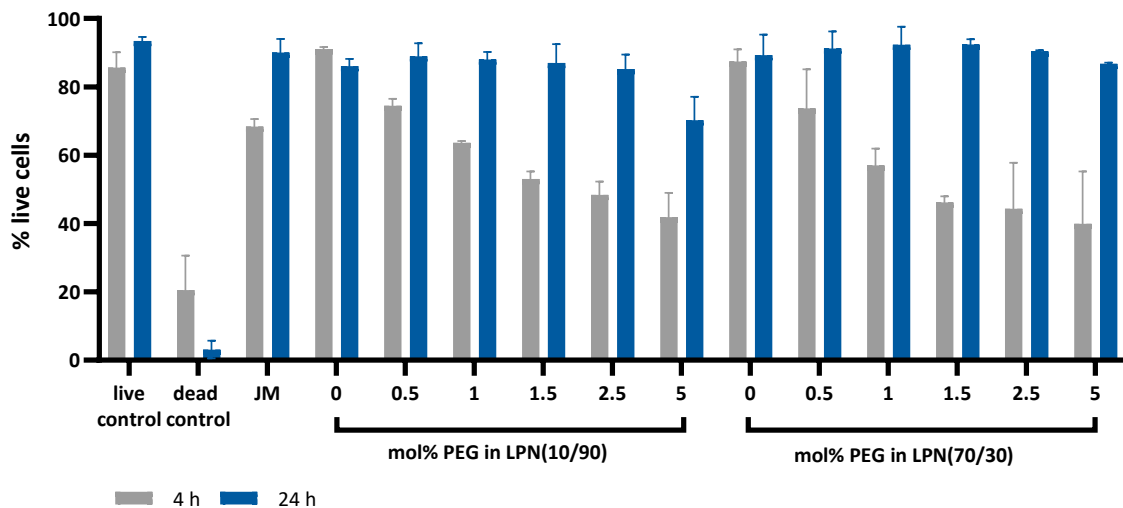


Figure 46: Viability of DC2.4 after incubation with mRNA-loaded, pegylated LPNs for 4 and 24 h in non-supplemented RPMI medium. FDA and DAPI were added to distinguish live and dead cells. Medium without nanoparticles was used as live, ethanol (5% in HBSS (v/v)) as dead control. JM: JetMESSENGER®, commercial transfection reagent. N=1 with n=2. The more PEG the LPNs contained, the less cells survived after 4 h. After extended incubation time cells mostly recovered even though nanocarriers were not removed.

Next, I tested LPNs in the two medium conditions that I previously used with 24 h incubation time (Figure S 6). Again, all LPNs were well tolerated with values above 90% of viable cells, only 5 mol% PEG in LPN(70/30) in plain medium had a lower value of 70%. To solidify these observations of this preliminary experiment by measuring more wells in three independent experiments, I repeated the experiments with selected LPNs covering the entire range of pegylation. As Figure 47 shows, the percentages of live cells were comparable to the medium control. The viability in supplemented medium was always significantly better than in plain medium. We confirmed that the highest amount of PEG reduces the viability but on a well acceptable level (minimum 78% viable cells in plain medium).

## 5 Minimally Invasive Application of LPNs to the Skin

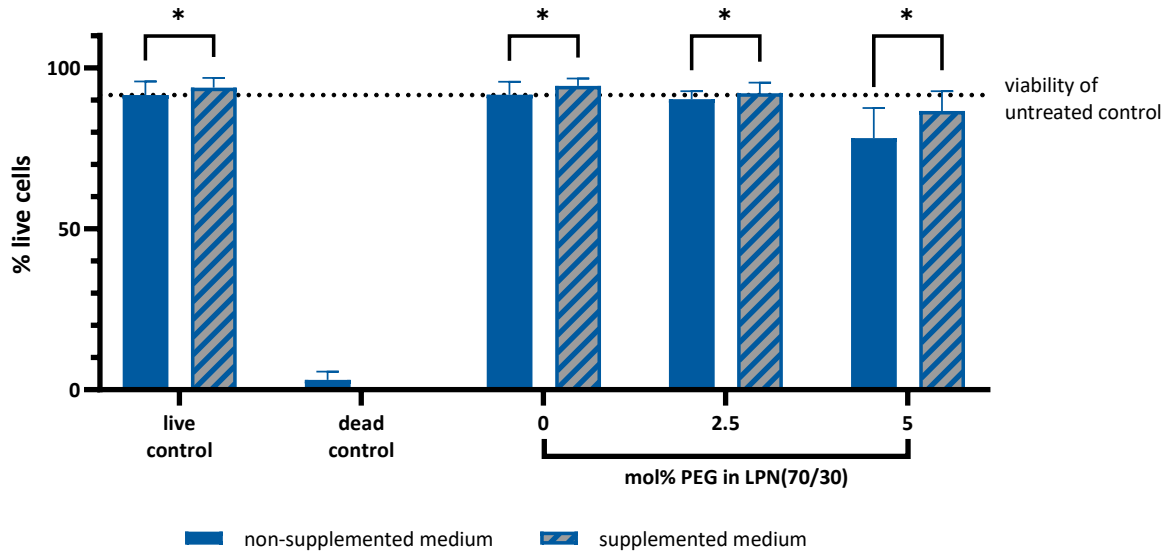


Figure 47: Viability of DC2.4 cells after 24 h incubation with mCherry-mRNA-loaded, pegylated LPN(70/30). Nanocarriers were either dispersed in non-supplemented RPMI medium or full growth medium with 10% FCS, HEPES-buffer (0.01M), non-essential amino acids (1X) and  $\beta$ -mercaptoethanol (0.0054X). Medium without nanoparticles was used as live, ethanol (5% in HBSS (v/v)) as dead control. Live cells were gated using FDA and DAPI staining. N=3-4 with total n= 9–12. LPNs were as well tolerated as the medium control with the exception of 5 mol% PEG-LPN(70/30) that slightly reduced the cell viability.

### 5.2.3 Uptake

The uptake of pegylated and non-pegylated LPN(70/30) was the same for all tested nanocarriers and conditions (Figure 48). We observed a trend this time that the uptake is better in non-supplemented medium but without a significant difference. In the previous study where I tested all LPNs, the uptake was above 90% for LPN(70/30) in both conditions (Figure 17).

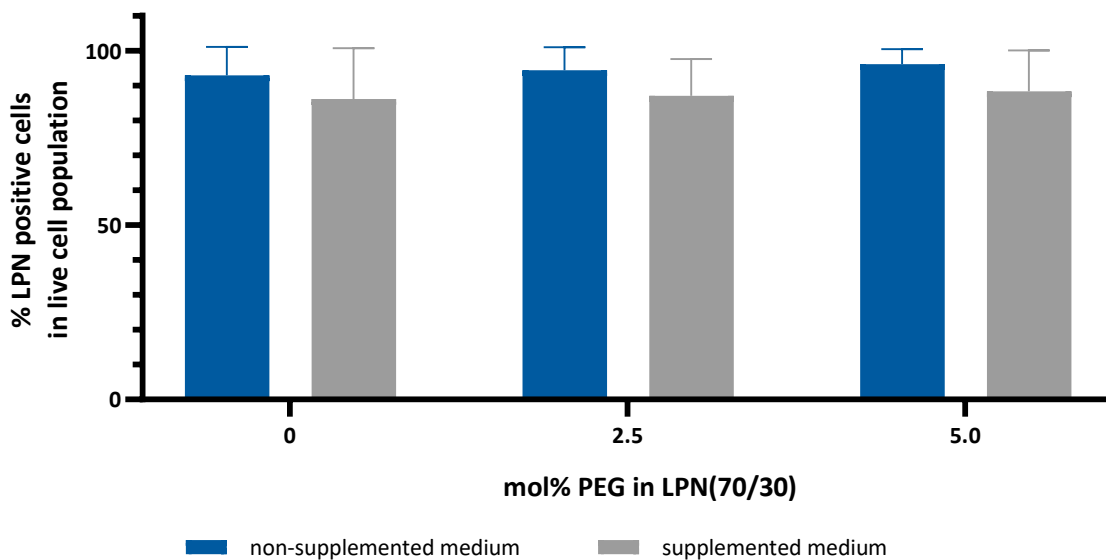


Figure 48: Uptake of LPN(70/30) into DC2.4 depending on the degree of pegylation. Cells were incubated with mRNA-loaded, FITC-labeled LPNs for 24 ihhh h in plain or supplemented RPMI (with 10% FCS, HEPES-buffer (0.01M), non-essential amino acids (1X) and  $\beta$ -mercaptoethanol (0.0054X)). N=3 with total n=9. The uptake was comparable for all conditions and LPNs, with a trend towards reduced uptake in supplemented medium.

### 5.2.4 Transfection

Parallel to the viability data of chapter 5.2.2, I acquired the percentages of live cells that express the fluorescent mCherry protein. For LPN(10/90), the experiment revealed a clear correlation between the degree of pegylation and the transfection rate (Figure 49). The more PEG the LPN(10/90) contained, the lower the transfection rate with minimal values for 5 mol% PEG (7 and 5% transfected cells after 4 and 24 h, respectively). For all other nanoparticles, the percentages increased with the incubation time. Pegylation of LPN(70/30) did not affect transfection rate of the nanocarriers as much. After 4 h, I measured values around 70% positive cells, after 24 h above 90% independent of the PEG content of LPN(70/30). The only exception was again the 5 mol% PEG in LPN with reduced values of 40% and 68% indicating that this PEG amount hinders transfection.

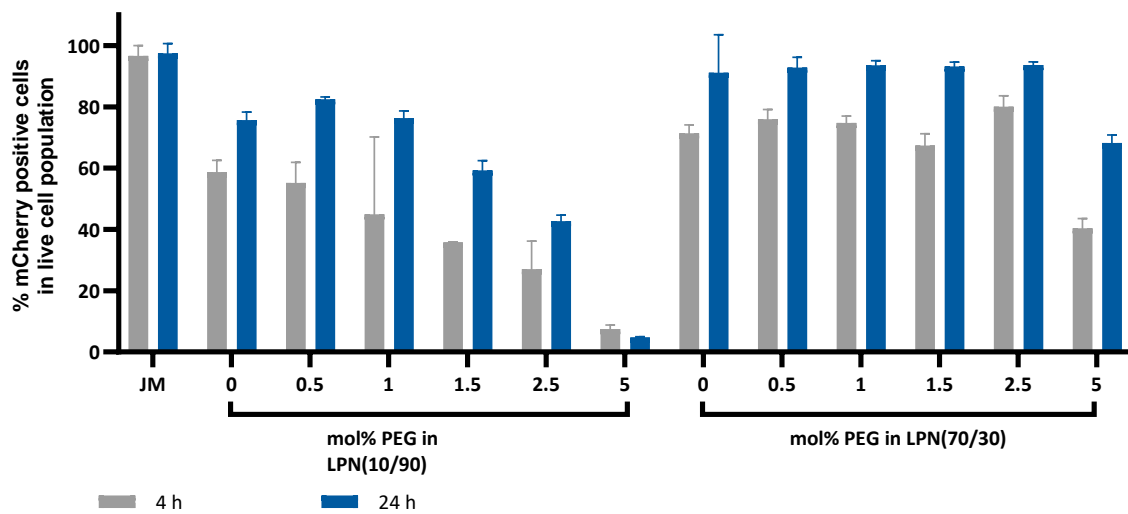


Figure 49: Transfection efficacy of mRNA-loaded, pegylated LPNs after incubation of DC2.4 for 4 and 24 h in non-supplemented RPMI medium. JM: JetMESSENGER®, commercial transfection reagent. N=1 with n=2. The more PEG the LPNs contained, the less cells expressed the mCherry protein. Extension of the incubation time to 24 h improved that percentage. Nanoparticles deduced from LPN(70/30) generally showed higher transfection rates than the ones from LPN(10/90).

## 5 Minimally Invasive Application of LPNs to the Skin

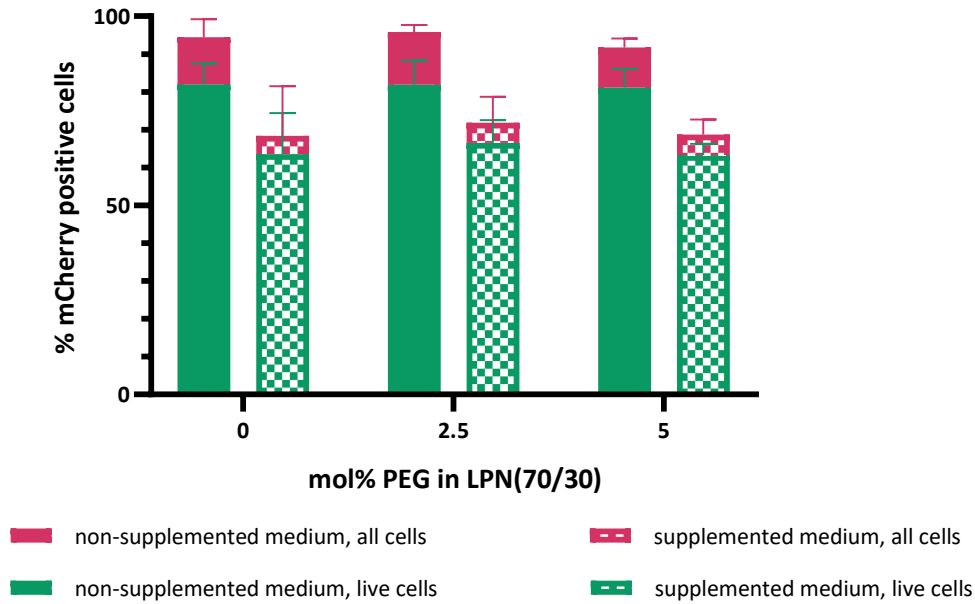


Figure 50: Transfection of DC2.4 cells after 24 h incubation with mCherry-mRNA-loaded LPNs in two medium conditions. Nanocarriers were either dispersed in non-supplemented RPMI medium or full growth medium with 10% FCS, HEPES-buffer (0.01M), non-essential amino acids (1X) and  $\beta$ -mercaptoethanol (0.0054X). DAPI was added to enable exclusion of dead cells. Green bars represent live transfected cells as overlay to red bars that show all transfected cells in the entire, acquired cell population.  $N=3$  with total  $n=9$ . Supplementation of the medium reduced the transfection efficacy for all LPNs. Pegylated nanoparticles performed as well as the non-pegylated one.

These results confirmed again that the composition of the LPN(10/90) is not optimal and finally led to its exclusion from further studies. More repetitions with the selected LPN(70/30) candidates in the two media conditions for 24 h went in the same direction as before even though 5 mol% PEG LPN performed better than in the pivotal study (Figure 50). For all three tested LPNs, we found a reduced transfection rate in the supplemented medium. We can conclude that the addition of the pegylated lipid did not jeopardize the good transfection efficacy of the LPN(70/30) but on the same time there was no improvement detectable. If pegylation has an effect on the penetration properties into the skin tissue, cannot be tested in cell culture. I therefore started to work with excised human skin.

### 5.3 Development of *Ex vivo* Human Skin Model

#### 5.3.1 Transfer of Laser Parameters from Mouse Model

In this part of the thesis, I concentrated on the development of a skin model to investigate the effect of the LPNs in combination with the laser application in the skin. From the mouse study with our collaboration partner at the HZI (described in chapter 5.1.2), we know that the immune reaction is stronger if created pores hit both, epidermis and dermis. For the mentioned animal study, we selected the dorsal part of the mouse ear as application site because the low hair density allows a treatment without depilation. For our skin model, I planned to work with human abdominal skin where hair density is very low, too, but skin is much thicker compared to the mouse ear. According to literature, the stratum corneum of human abdominal skin is 13-19  $\mu\text{m}$ , the epidermis 26–60  $\mu\text{m}$  and the whole skin is around 3 mm thick [170, 171, 173]. For mouse skin, there are only a few but very different numbers available. Khiao In et al. measured 6  $\mu\text{m}$  stratum corneum and 13  $\mu\text{m}$  epidermis with a total thickness of 840  $\mu\text{m}$  for the skin at the back of mice [170], while Ibrahim et al. claimed only 280  $\mu\text{m}$  skin thickness at the back and 90  $\mu\text{m}$  at the ear [173]. Having these contrary numbers underlines the importance of laser parameter optimization. Therefore, the first step was to investigate which laser settings are needed to reach the dermis in the human skin.

We decided to keep the general laser setup as in the mouse study and simply vary the number of pulses per pore between 2 and 21 pulses. The treated skin pieces were cut directly after treatment or 24 h later, stained with DAPI and imaged with a confocal microscope. To get an estimation of where the LPNs might end up, I applied beads with a very strong fluorescence after laser microporation in a second group of samples. All images are shown in Figure 51.

The skin samples in the first row (Figure 51 A-D) were treated with two pulses which are exactly the settings of the mouse study. As expected, the pores did not reach the dermis but were even hard to detect because they interrupted only the outermost layer, the stratum corneum (A, B). The creation of pores of double the size (4 pulses) led to pores in the epidermis (E-H). After eight pulses (I-K), I hit the dermis for the first time as indicated by a full interruption of the epidermis (I). 24 h later, the epidermis already regenerated and covered the pore leaving a little cavity (J). If nanoparticles were applied, the pores were still open the next day but with already prolonged edges of the epidermal layer (K). For the deepest pores with 21 pulses (L-O), we found black areas at the edges and the bottom of the pores as indicator for burned cells (L). This might be the reason why these pores were still open after 24 h, too (M).

For pores created with 2 and 4 pulses it was very difficult to see where the nanoparticles ended up (Figure 51 C,D and G,H). We hypothesized that the pores were too shallow to hold them back and therefore the NP are wiped away during sample preparation steps like cutting and staining. After 21 pulses we found NP at the bottom of the pore (N) and thus in contact with dermal cells but the bad quality of the sample after 24 h made an interpretation difficult (O). For 8 pulses we found some NP in the cavity below the newly build epidermal edges expected to have a good chance for uptake by the cells (K). Still, the majority of NP remained at the surface. These observations indicate that deeper pores increase the duration of nanoparticles in the skin and thus the contact time with the cells.

As the aim of this experiment was to transfer parameters from mouse to human skin, the 8 pulse-setup fulfilled the criterium to hit the dermis and the epidermis. Thus, we selected this setup for the next experiments.

## 5 Minimally Invasive Application of LPNs to the Skin

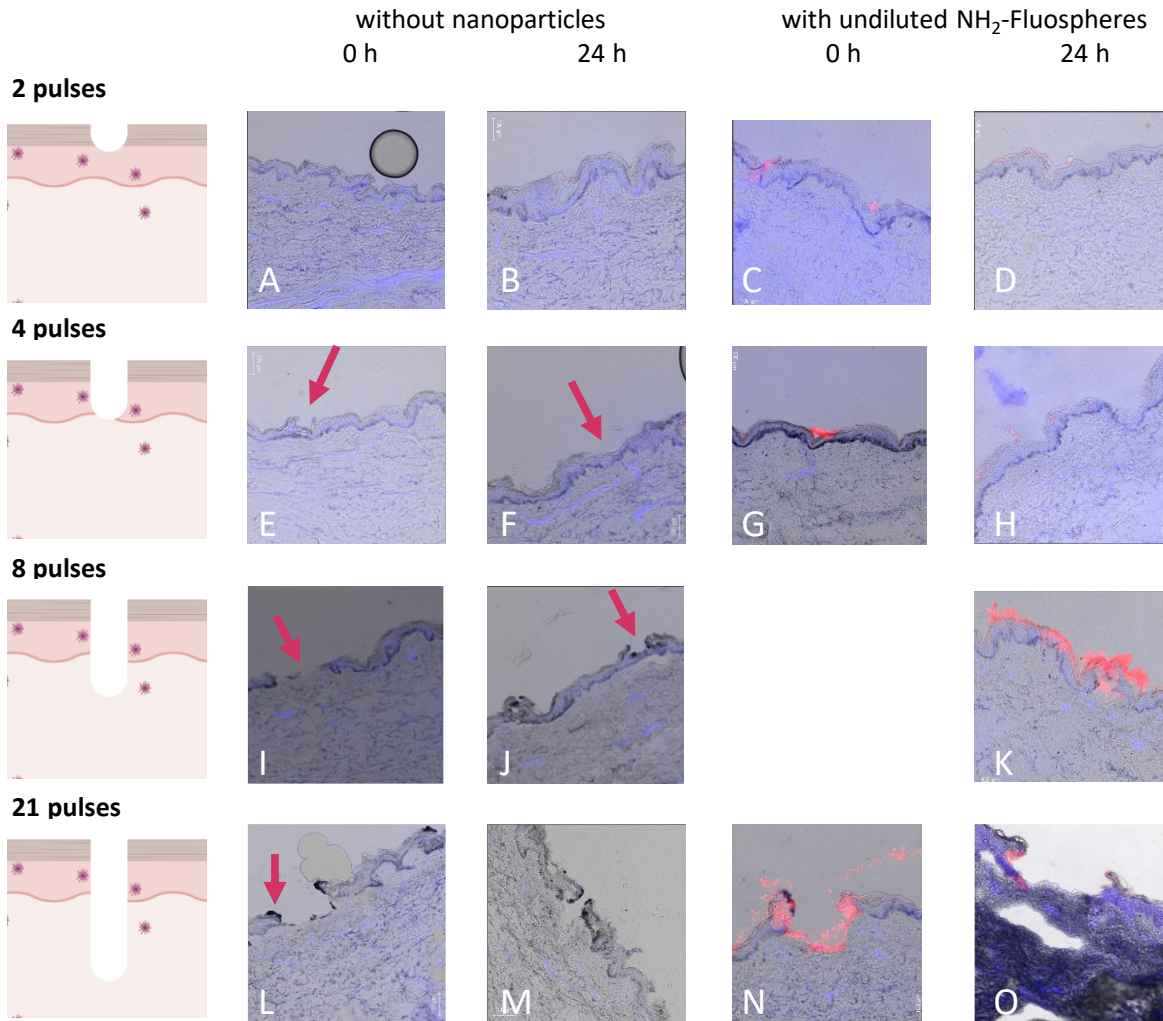


*Figure 51: Confocal images of human abdominal skin after microporation with different laser settings. One biopsy per group was cultivated freely floating in medium with antibiotics for 24 h. All samples were frozen, cut, stained with DAPI and imaged using confocal fluorescence microscopy. FluoSpheres® were applied to get an estimation of the fate of nanocarriers when applied directly after microporation. Large circle outside of the skin piece in image A is an air bubble. 2 and 4 pulses led to superficial pores that were hard to identify under the microscope and reached only the epidermis (A-D for 2 pulses, E-H for 4 pulses; arrows indicate location of epidermis interruption). 8 pulses deep pores reached the dermis (I, arrow indicate interruption of epidermis) and were closed within 24 h (J, arrow indicate formation of new epidermal layer). 21 pulses led to deep pores but also burned the edges of the epidermis (L, arrow indicates burned tissue) extending the time until pore closure beyond 24 h (M).*

### 5.3.2 Penetration of LPNs Into Tissue

Having selected 8 pulses per pore as laser settings, I tested in the next step how the LPNs behaved after application. I wanted to investigate if the pegylation is beneficial for the penetration and how the exposure of skin cells changes with the application route. For each selected LPN, I compared the application of the same amount of nanocarriers either onto the intact skin with massage, intradermal injection or after laser microporation. LPN(70/30) with and without PEG were labeled with DiD and loaded with mRNA resulting in a negative surface potential (for overview of hydrodynamic parameters, Table S 2).

Intradermal injection of 20  $\mu$ l PBS or LPN suspension created a bulb on the surface of the skin biopsies recognizable with the bare eye (Figure 52). Next to this macroscopic observation, the exposure after injection differed a lot from the other two application routes. As example, Figure 53 A-C show the skin cut images directly after applying 5 mol% PEG in LPN(70/30). In the first image (A), there are hardly any LPNs visible in the skin piece but a few outside of the tissue. It is unlikely that any nanoparticle passed the barrier of the stratum corneum and if they did, the number is very limited and below the detection limit. In contrast, the skin cuts after intradermal injection showed a very bright area of fluorescence crossing the entire height of dermis (B). This dot was also visible with the bare eye as blue shining dot in the center of skin piece during cryo-cutting (not shown). We observed some signals in the epidermis, too, but this might be an artefact as the concentration of nanoparticles was that high that especially the cutting process could lead to a smear of nanoparticles. In comparison to that high exposure in the dermis but lower density in the epidermis, we found the opposite phenomenon in laser microporated skin (C). There was a high concentration of nanoparticles around the pores, but only a few deeper down in the dermis. Comparing these three images, the exposure is by far the highest after injection, much lower but still well detectable for laser microporation and around zero on intact skin.



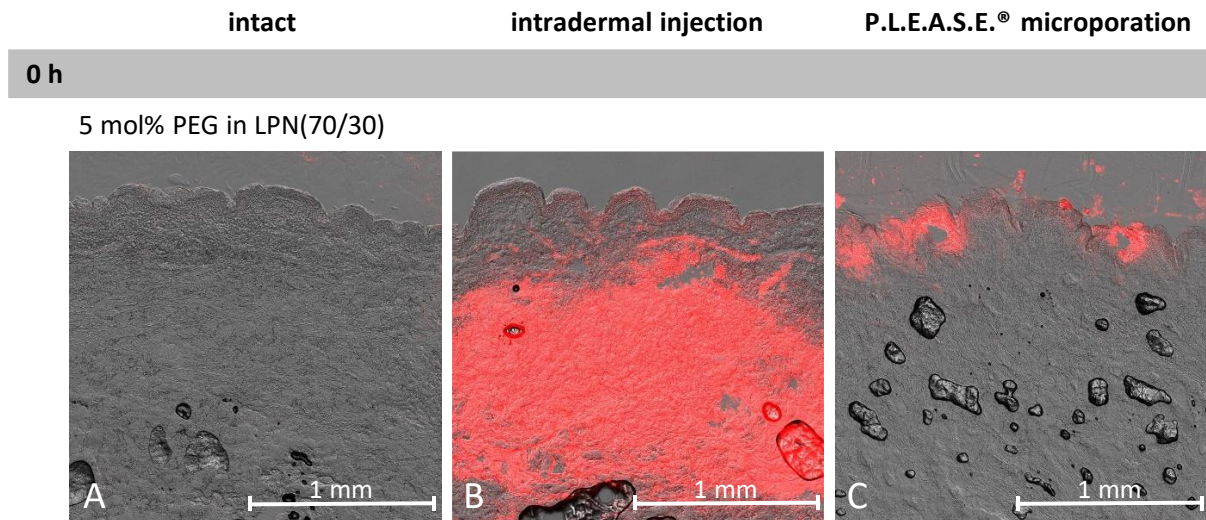
Figure 52: Photos of skin biopsies after intradermal injection of PBS. Skin surface forms a visible bulb (indicated by the arrow).

This order was constant for all tested LPNs and time points. While we did not find clear nanoparticle signals after 24 h for LPN(70/30) on intact skin (D), there were spots of fluorescence for both pegylated LPNs, especially at the bottom of skin folds (G, J). For laser microporated skin, we observed faint signals in the dermis for all nanoparticles (F, I, L) but as mentioned before, it is difficult to judge if this is not an artefact of skin processing. I cut the skin from dermis to epidermis so at least this processing step could not cause the red signals in the dermis. The concentration of LPNs remained high after injection (E, H, K). For LPN(70/30), we observed also high amounts in the epidermis (E). This might be connected with a smaller injection angle compared to the others rather than particle

## 5 Minimally Invasive Application of LPNs to the Skin

movement because the nanoparticles did not spread as much in the other directions. Image M shows the entire skin cut as example to get an impression of the exposure in relation to the tissue. The morphology of the skin was not changed by the treatment and is at least from our microscopic images comparable to the ones of the untreated and PBS control (Figure S 8).

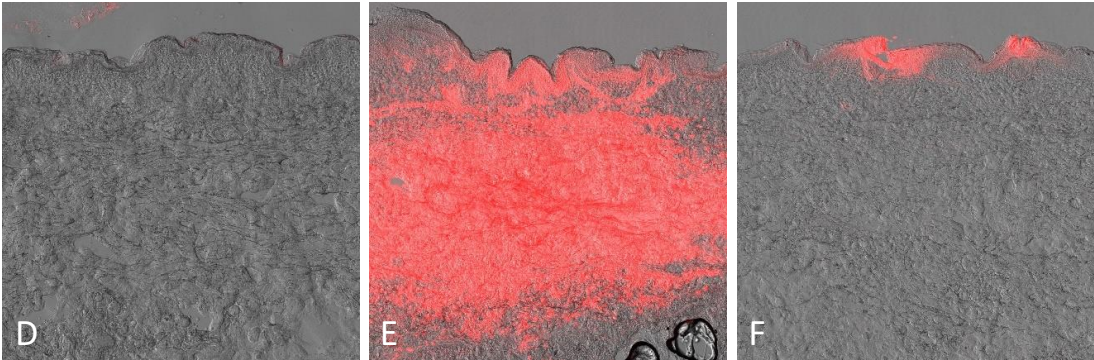
It was not possible to quantify our observations as we expect a high inter sample variability but still had only one skin biopsy per treatment. Anyways, the experiment helped us to get an impression of the exposure of skin cells in the different application route. The invasive method of intradermal injection is the most promising candidate to see an effect of the LPNs even though we aim for a comparable result for laser-based application.



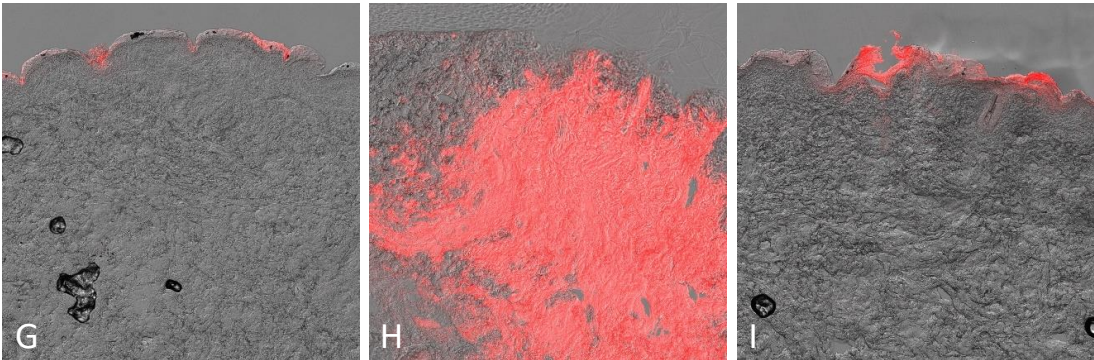
5 Minimally Invasive Application of LPNs to the Skin

24 h

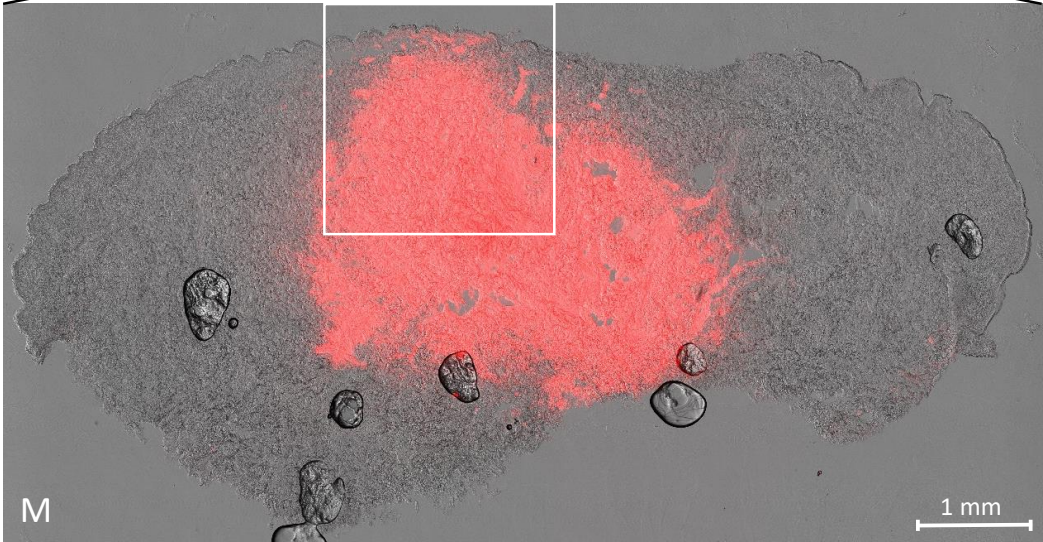
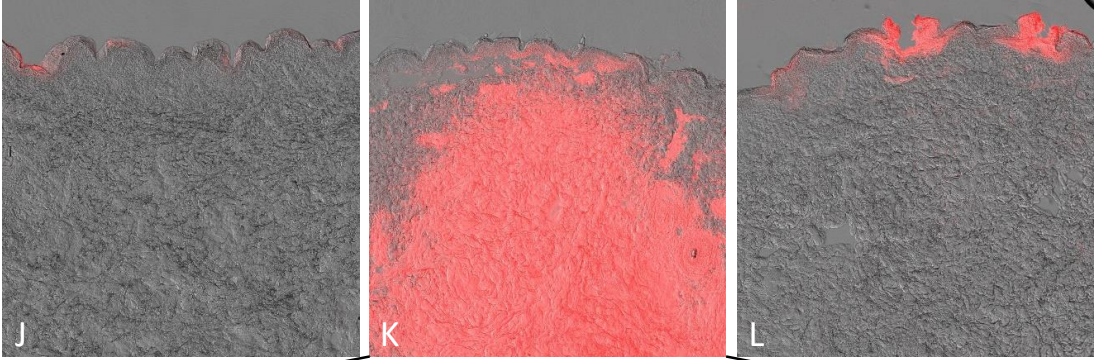
LPN(70/30)



2.5 mol% PEG in LPN(70/30)



5 mol% PEG in LPN(70/30)



## 5 Minimally Invasive Application of LPNs to the Skin

Figure 53: LPN exposure of human abdominal skin after three different application routes: on intact skin, by intradermal injection or after microporation with P.L.E.A.S.E.<sup>®</sup> laser (pulse length 75  $\mu$ s, repetition rate 200 Hz, 8 pulses per pore, 8 x 8 mm treatment area). I applied 20  $\mu$ l of DiD-labeled, mRNA-loaded LPNs per sample. Directly after treatment (A-C) or after 24 h cultivation, samples were embedded, frozen, cut at -20 °C and imaged using a confocal microscope. Exposure of tissue was highest after intradermal injection (E, H, K) especially in the dermis. After laser microporation (F, I, L), we found more LPNs in the epidermis and overall less than after injection. The exposure after application on intact skin did not lead to detectable nanoparticles in the tissue (D, G, J). This is valid independent of the LPN composition.

### 5.3.3 Ex vivo Cultivation of Human Skin

I started establishing the human skin model from the scratch but profited from the experience in our lab with previous nanoparticle penetration and skin barrier studies with frozen skin. In our case, we aimed for the biosynthesis of the protein encoded on the delivered mRNA. I therefore needed viable skin tissue and a successful cultivation strategy to give the nanocarriers and the cells enough time to show an effect. Collaborating with a plastic surgeon in a hospital close by enabled us to get the skin as fresh as possible directly after dissecting from the patient with a short transportation time. After removal of the subcutaneous fat, the skin was ready for treatments and cultivation.

Every step of the model needed several optimization steps until I could test the LPN(70/30) with and without pegylation. We decided to use the same 8x8 mm applicator for the P.L.E.A.S.E.<sup>®</sup> handpiece that we used for our mouse study on the ear. This square sized plastic piece fitted onto round 11 mm punch biopsies of the human skin. Handling and treating the skin as fast as possible with a non-interrupted cooling chain needed simply practice. For application and cultivation protocols, I had to test several options. Literature research and preliminary tests confirmed that high doses of antibiotics are needed to prevent bacterial growth during cultivation.

In a first set up, I cultivated skin biopsies freely floating in medium for up to 9 days and assessed the viability of the tissue using an adapted MTT protocol. For each time point, I compared one sample of untreated skin with one where I injected PBS intradermally. We observed a drop in viability after 3 days of cultivation (Figure 54). For untreated skin, this reduced viability of around 50% after 3 days was comparable until the end of the experiment after 9 days. PBS injection led to a reduction of viability for all time points ending in a value of 18% after 9 days. Exceptions were the values of day 3 and 7 where PBS injection showed higher viabilities than the untreated samples.

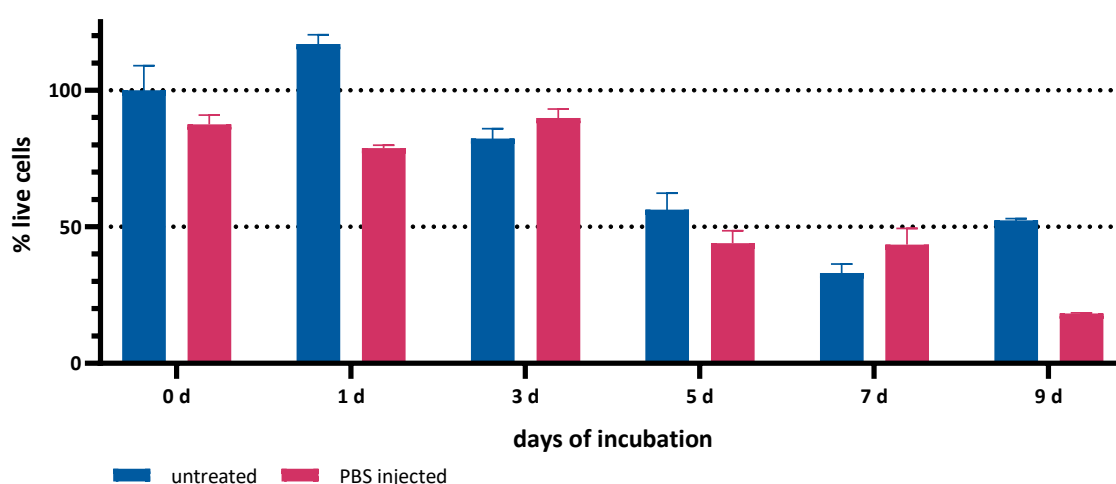
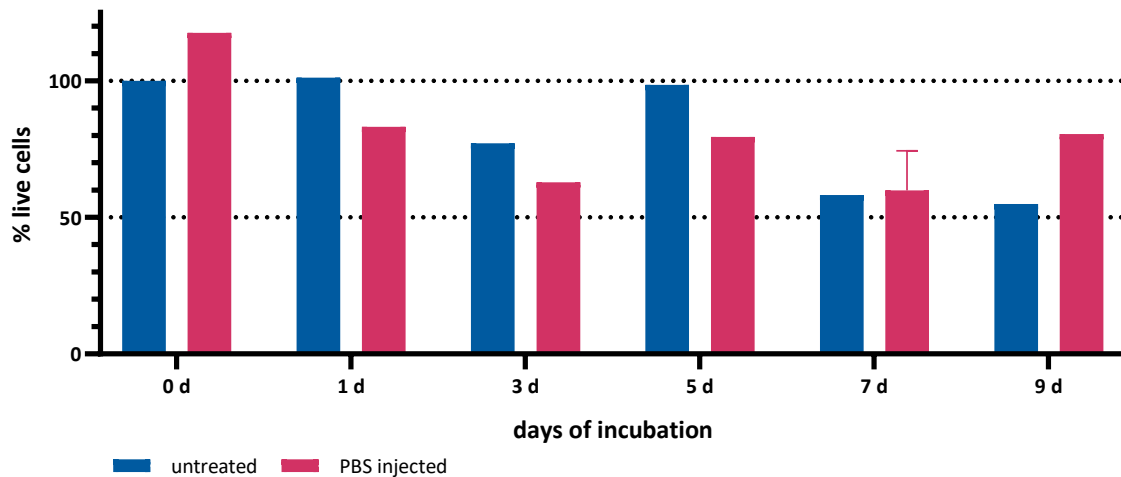


Figure 54: Viability of skin biopsies over the course of 9 days quantified by MTT. Data expressed relative to the absorbance of the untreated sample on day 0. Data acquired in one experiment with one biopsy per treatment. Half a skin piece used for MTT, split up in three wells; the other half was digested for FACS analysis. Viability dropped after 3 days of cultivation and stabilized on a lower level for untreated control. Intradermal injection of PBS reduced viability of skin.

## 5 Minimally Invasive Application of LPNs to the Skin

I digested the second half of the skin biopsies and analyzed the viability by flow cytometry. I measured 48,000 viable cells out of 100,000 counted events for the untreated sample on day 0 and expressed the results relative to this sample (Figure 55). After 9 days, the viability of the untreated samples was again about 50% reduced compared to day 0 but in this readout the values were higher for day 3 and 5 and dropped on day 7. This might be an indicator that the MTT measures rather the viability at the edges of the tissue and underestimates the viability inside the tissue. We might still profit from MTT as complementation of the FACS analysis, though. For day 1 to 5, PBS injection reduced the viability about 20%, but at day 0 and 9 it increased it to the same extend. There seems to be no adverse effects of the injection of PBS. In this pivotal study, we saw that the skin viability is stable for several days with our cultivation protocol even after injection of PBS.



*Figure 55: Viability of skin biopsies over the course of 9 days quantified by flow cytometry. Data expressed relative to the viability of the untreated sample on day 0. Data acquired in one experiment with one biopsy per treatment (exception PBS after 7 days with n=3). Half a skin piece was enzymatically and mechanically digested; the other half was used for MTT. The single cell suspension was stained with DAPI and FDA to distinguish between live and dead cells.*

### 5.3.4 Evaluation of Transfection Reagents as Positive Control

For the application of the model as test system for mRNA-loaded nanocarriers, we need to know if the measured viability is high enough to see successful transfection. In the next step, I therefore tested commercial transfection controls after intradermal injection to see the highest possible effect. As in our cell culture experiments, we selected again jetMESSENGER®. Additionally, I used PEI in three different doses to check how the skin pieces react to this potentially toxic substance [175] and for what mRNA dose I see a protein production.

We found a correlation of PEI dose and reduced viability for all time points compared to PBS (Figure 56). Especially the highest dose with 12 µg mRNA showed toxic effects in MTT (Figure 56A) and even more pronounced in the FACS analysis (B) where viability directly after treatment at day 0 was reduced to less than a third (118% for PBS to 36%). In MTT analysis, there was a difference between the 4 and 8 µg doses, too, but this was not confirmed in FACS analysis where both treatments were tolerated about half as good as PBS (except 7 d). JetMESSENGER® was comparably well tolerated as PBS in FACS analysis.

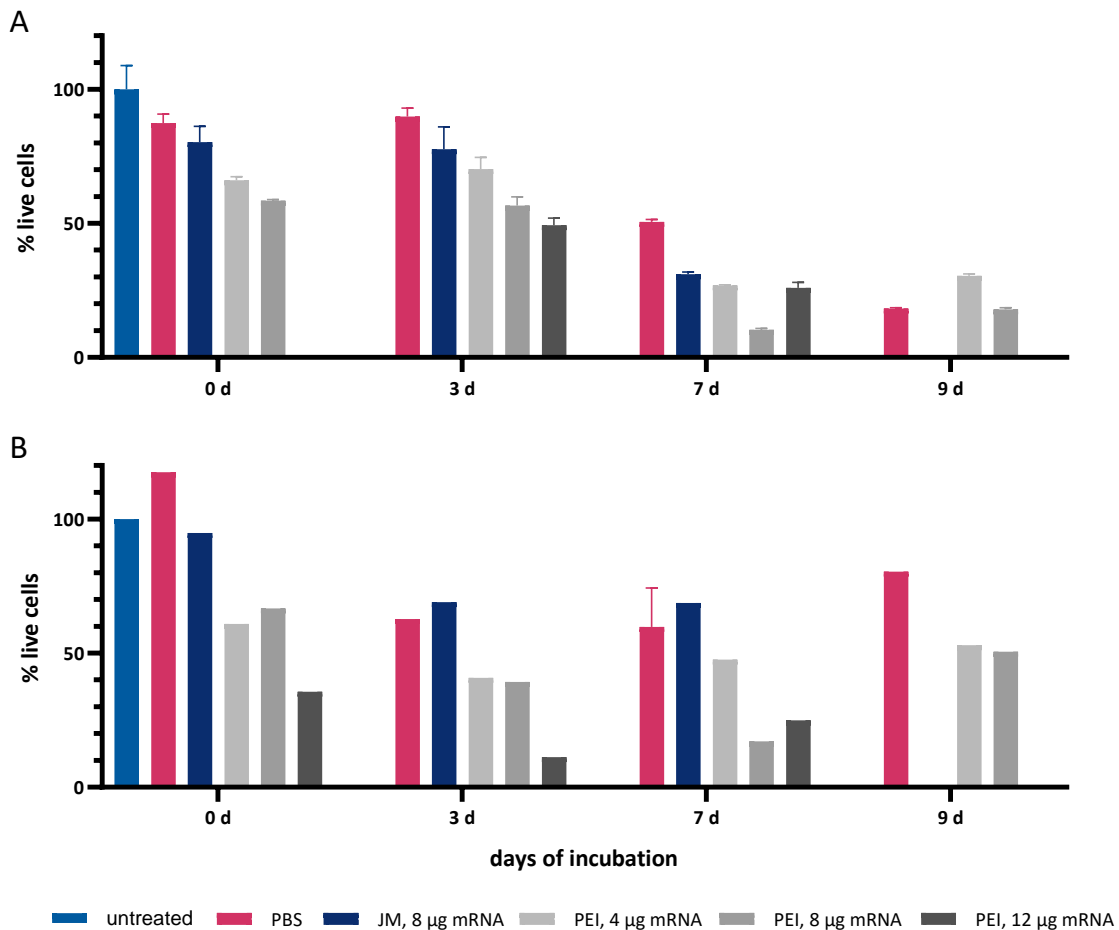
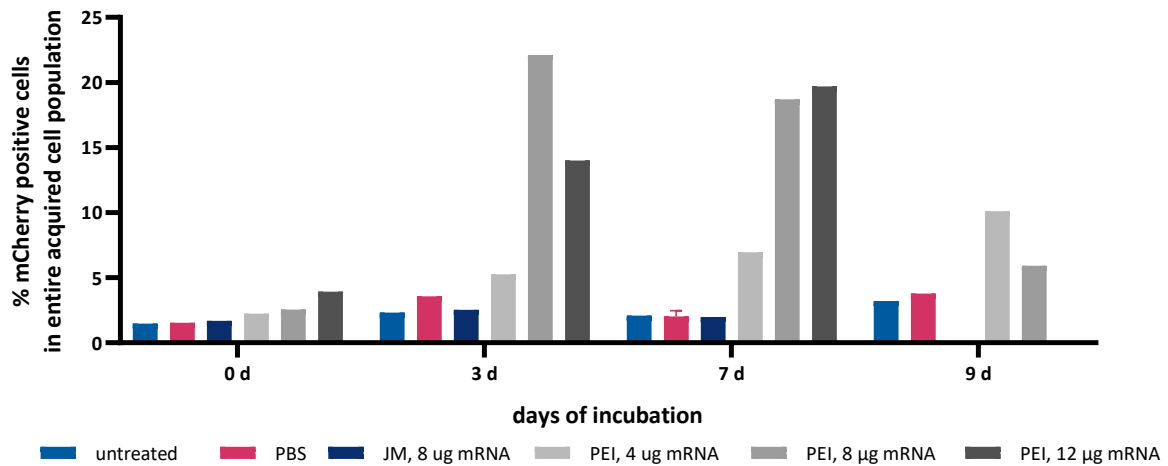


Figure 56: Tissue viability over the course of 9 days after intradermal injection of transfection controls. (A): evaluation by MTT, (B): Flow cytometry analysis. Half a skin piece was analyzed with MTT, the other half was enzymatically and mechanically digested for flow cytometry. The single cell suspension was stained with DAPI and FDA to distinguish between live and dead cells. Data acquired in one experiment with one biopsy per treatment (exception PBS after 7 days with  $n=3$ ). Data expressed relative to the viability of the untreated sample on day 0. JM: JetMESSENGER®, commercial transfection reagent. Dose dependent toxicity was observed for PEI, while JM was almost as well tolerated as PBS after intradermal injection.

## 5 Minimally Invasive Application of LPNs to the Skin

Looking now for the first time on the percentage of cells that express the mCherry protein encoded on the delivered mRNA, we measured increasing numbers for PEI after 3 days of cultivation (Figure 57). A dose of 8  $\mu\text{g}$  mRNA complexed with PEI transfected about 20% of events after 3 days while the higher dose resulted only in 15% positive cells. This might relate to the higher toxicity of this treatment and thus no intact cells during FACS analysis. After 7 days, both doses performed similar with transfection rates of 20% and a viability below 25%. PEI with 4  $\mu\text{g}$  mRNA had slower slope of transfection ending in a maximum transfection efficacy of 10% after 9 days. JetMESSENGER<sup>®</sup> did not show any mCherry expressing cells. From this first study, we decided to choose a dose of 8  $\mu\text{g}$  mRNA PEI intradermally injected as positive control and to cultivate the skin biopsies for 7 days as longer incubation did not improve the results further.



*Figure 57: Assessment of transfection efficacy of control samples expressed as percentage of mCherry expressing events in all acquired events. Data acquired in one experiment with one biopsy per treatment (exception PBS after 7 days with n=3). Skin biopsies were enzymatically and mechanically digested and analyzed with flow cytometry. JM: JetMESSENGER<sup>®</sup>, commercial transfection reagent. After 3 days, the number of mCherry positive cells increased for samples treated with 8 or 12  $\mu\text{g}$  mRNA complexed with PEI. These numbers remained high until day 7 and dropped afterwards. 4  $\mu\text{g}$  mRNA with PEI had a later maximum at day 9. JM did not lead to fluorescent cells.*

## 5.4 Results *Ex vivo* Skin Model

### 5.4.1 Viability

The previous chapter showed how I set up the skin model. In the following part, I will describe the results using skin of five different donors coping with inter individual variations. Furthermore, we finally compared the intradermal injection that was tested so far to the application after P.L.E.A.S.E.<sup>®</sup> laser microporation.

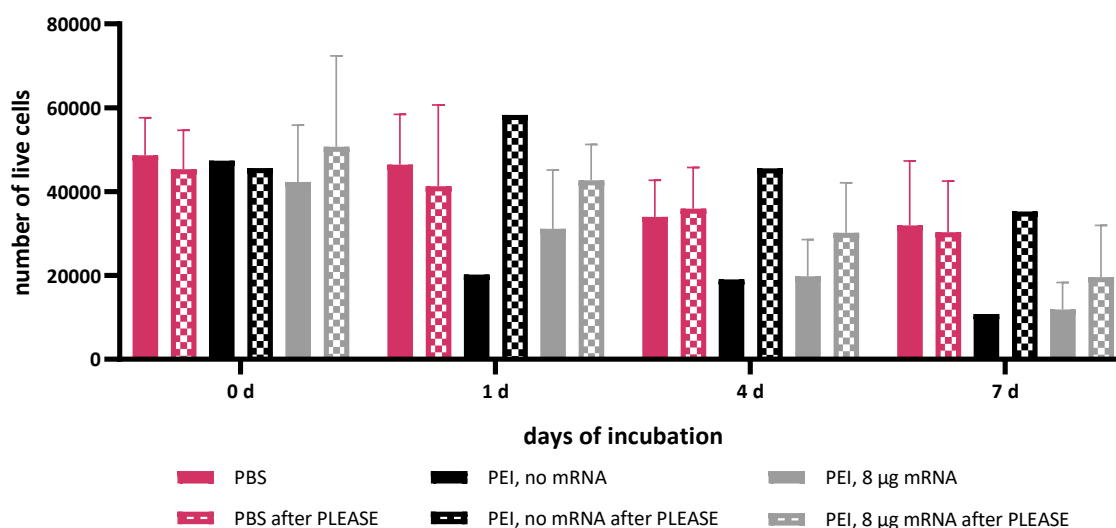


*Figure 58: Absolute viability of skin biopsies after treatment with process controls either by intradermal injection (solid bars) or after P.L.E.A.S.E.<sup>®</sup> microporation (bars with pattern) (pulse length 75 µs, repetition rate 200 Hz, 8 pulses per pore, 8 x 8 mm treatment area). PBS was used as negative, PEI with mRNA as positive control (8 µg mRNA per biopsy). PEI without mRNA was added to assess toxic effects of polymer itself. 100,000 events counted in flow cytometer. DAPI and FDA addition enabled gating for live cells. Data acquired in five independent experiments with up to eight biopsies per treatment group in total (PEI without mRNA had only 1 data point per time point). The application of PEI (with/without mRNA) after P.L.E.A.S.E.<sup>®</sup> microporation drastically reduces the toxicity compared to intradermal application.*

Figure 58 displays the number of viable cells in the control groups, measured in flow cytometry. The untreated control (not shown) lost around 33% of viability over 7 days (45000 viable cells to 35000), so did the PBS control (minus 35% and 33% respectively). Analyzed by MTT, the tissue did not lose any viability after PBS treatment (Figure S 9) during the experiment. I applied PEI either as blank polymer or complexed with mRNA and observed comparable toxic effects when injected intradermally. On day 0, both were as well tolerated as PBS because samples were digested directly after treatment. Thus, we can conclude that we did not see any acute toxic effects of the treatments. After 24 h, PEI with mRNA was better tolerated (31000 viable cells vs. 20000) than the blank polymer but after 4 days there was no difference anymore. If formulations were applied after P.L.E.A.S.E.<sup>®</sup> treatment, more cells survived compared to the intradermal injection. We observed this trend for all time points but the start of the experiment. The longer the skin was cultivated, the larger the benefit of the combination with the P.L.E.A.S.E.<sup>®</sup> (+38% day 0 to +66% day 7 for PEI-mRNA). But the highest difference was observed for the blank PEI polymer where the combination with the P.L.E.A.S.E.<sup>®</sup> resulted in a triplication of live cells after 24 h. This might relate to the general exposure of the cells to the polymer as shown in chapter 5.3.1. As less cells get in contact with the polymer after P.L.E.A.S.E.<sup>®</sup> treatment, we see fewer toxic effects.

The corresponding bar charts of FACS and MTT analyses for the LPN treatments are shown in Figures S 10 and S 11. In this main text, I wanted to emphasize the comparability of the LPNs and PBS in terms of toxicity and therefore displayed the FACS results as follows (Figure 59). The green lines are

## 5 Minimally Invasive Application of LPNs to the Skin

the number of live cells in the PBS samples with their standard deviation marked in grey. All samples are within this area and therefore as well tolerated as the PBS control. Only injection of PEI with and without mRNA caused more cells to die as described before (brown lines). We observed a trend that P.L.E.A.S.E.<sup>®</sup> sample have rather higher viability values than the injection samples.

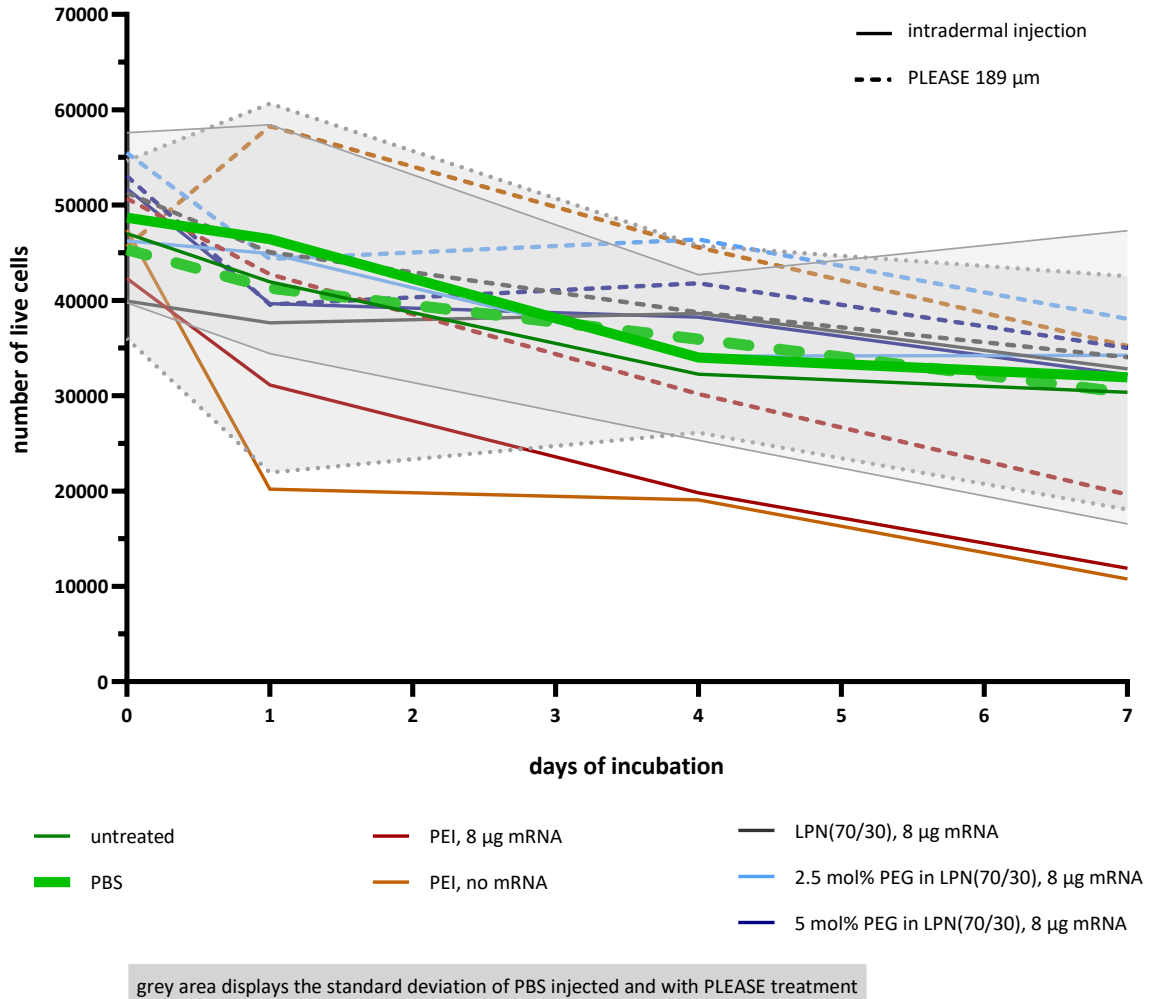


Figure 59: Overview of skin viability after application of mRNA-loaded LPNs either by intradermal injection (solid line) or after P.L.E.A.S.E.<sup>®</sup> microporation (dotted line) (pulse length 75  $\mu$ s, repetition rate 200 Hz, 8 pulses per pore, 8 x 8 mm treatment area). PBS was used as negative control, PEI with mRNA as positive control. PEI without mRNA was added to assess toxic effects of polymer itself. Dosing: 8  $\mu$ g mRNA per biopsy. DAPI and FDA addition enabled gating for live cells. 100,000 events counted in flow cytometer. Data acquired in five independent experiments with up to eight biopsies per treatment group in total (PEI without mRNA had only 1 data point per time point). Grey area displays standard deviations of PBS controls. All measured values of the LPNs are within this area emphasizing the good tolerability of the LPNs. Intradermal injection of PEI (with and without mRNA) harms the tissue as indicated by brown lines outside the grey area.

### 5.4.2 Nanoparticle Testing

I tested LPN(70/30) with and without pegylated lipid on the human abdominal skin of five different donors. As controls, I always used PBS and PEI. I applied all samples with intradermal injection and after using the P.L.E.A.S.E.<sup>®</sup> laser to create pores of 189  $\mu$ m depth targeting the dermal skin layer. I collected the medium surrounding the skin biopsies every day and looked for evading cells in addition to digestion of the skin biopsies themselves. Our gating strategy for both sample groups in the flow cytometer is displayed in Figure 60.

## 5 Minimally Invasive Application of LPNs to the Skin

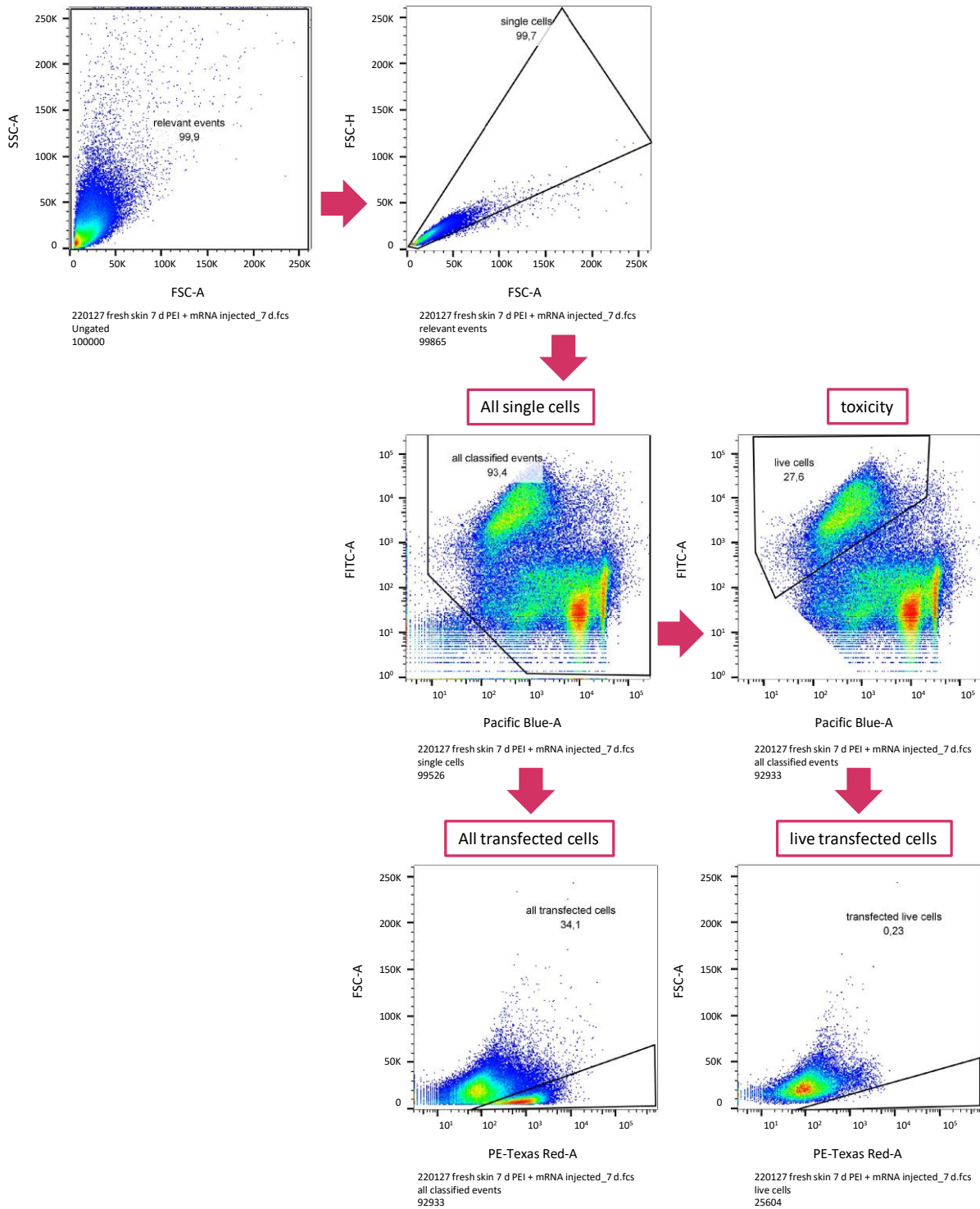


Figure 60: Gating strategy for digested skin samples after data acquisition by flow cytometry. DAPI and FDA were added to assess live cell populations. The used mRNA encoded for the fluorescent protein mCherry enabling gating for successfully transfected cells. FSC: forward scatter, SSC: sideward scatter. Graph shows results for incubation of skin for 7 days after intradermal injection of mRNA complexed with PEI as example.

## 5 Minimally Invasive Application of LPNs to the Skin

The number of live cells in the supernatant decreased with the incubation time (Figure 61). Within the first 48 h of cultivation most cells left the tissue and ended up in the medium. The highest number was found for the blank PEI polymer 24 h after intradermal injection but PBS and the untreated control had comparable numbers at day 2. 2,5 mol% PEG in LPN(70/30) led to the migration of a similar number of live cells on day 2 but declined again after that. This observation applies also to the number of all – live and dead – cells in the supernatant (Figure S 12). After 5 days almost no live cells were detectable in the medium.

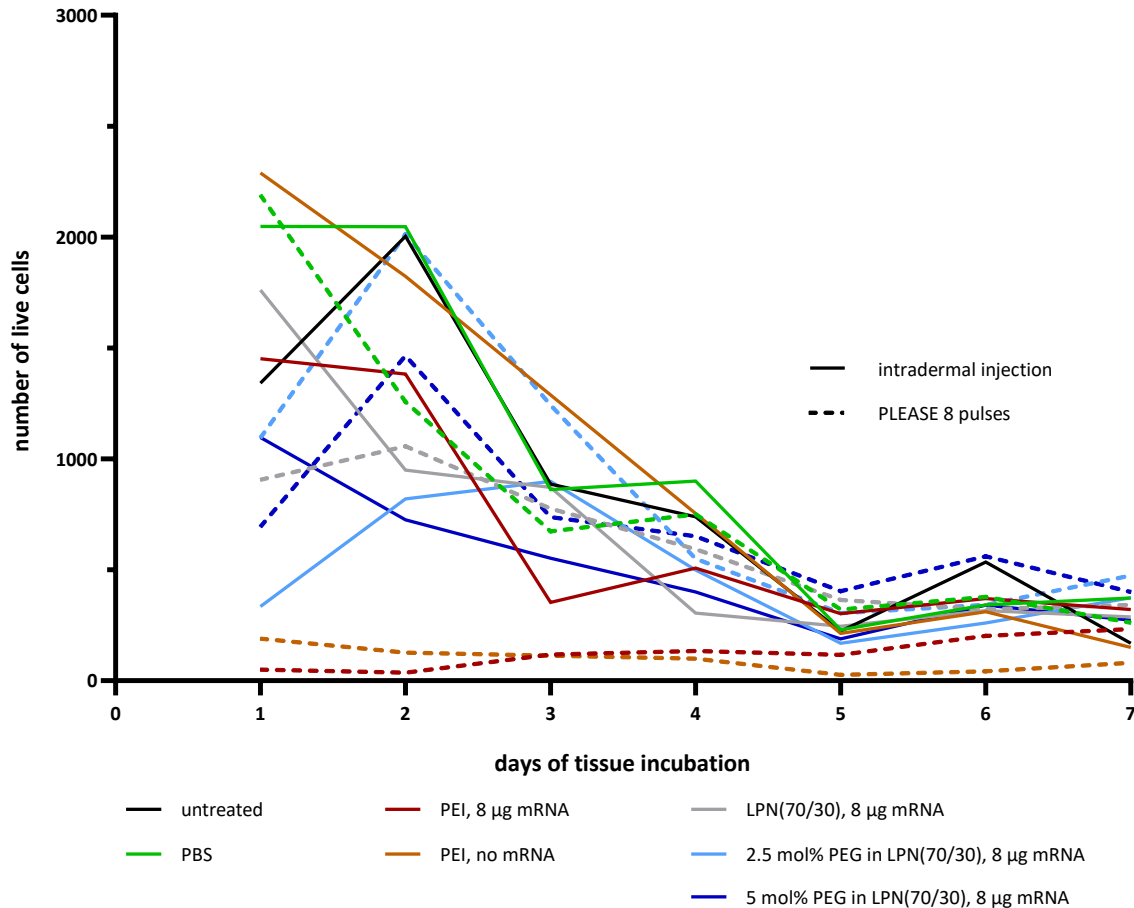


Figure 61: Overview of number of live cells in the supernatant of cultivated skin biopsies over the course of one week. After daily collecting medium from the same biopsy, medium was replaced. Samples were analyzed by flow cytometry. DAPI and FDA were added to gate for live cells. Solid lines represent skin biopsies after intradermal injection, dotted line after P.L.E.A.S.E.<sup>®</sup> microporation (pulse length 75 µs, repetition rate 200 Hz, 8 pulses per pore, 8 x 8 mm treatment area). Most cell evaded the tissue within the first 48 h of cultivation.

Looking at the number of live transfected cells in the supernatant, we observed generally a very low number below 100 cells per sample (Figure 62). Highest numbers were again measured for samples without mRNA, namely PBS and blank PEI polymer but this time also for PEI with mRNA 48 h after intradermal injection. On day 2, we found about 50 live transfected cells for the 2.5 mol% PEG in LPN(70/30) sample, too. If we focus only on the P.L.E.A.S.E.<sup>®</sup> samples, the 2.5 mol% PEG sample led to the evasion of about double the number of cells compared to PBS after 2 days (54 vs 29). This might be an indication for successful transfection by the LPN but already the next day (3 days) the order of sample and control was reversed. On that day (day 3), LPN(70/30) showed little more live transfected cells after intradermal injection compared to the injected PBS control (39 vs 36, respectively). For the later time points, PBS and plain PEI showed highest values.

## 5 Minimally Invasive Application of LPNs to the Skin

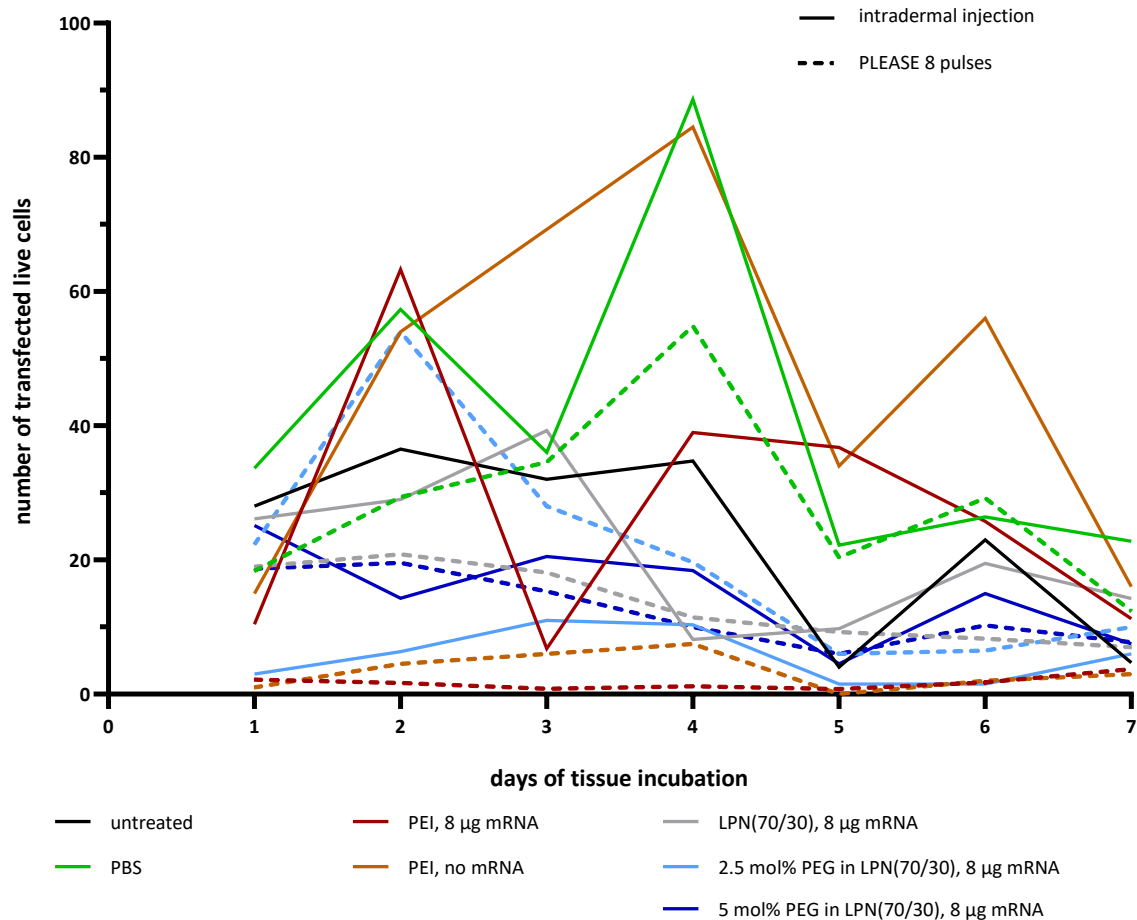
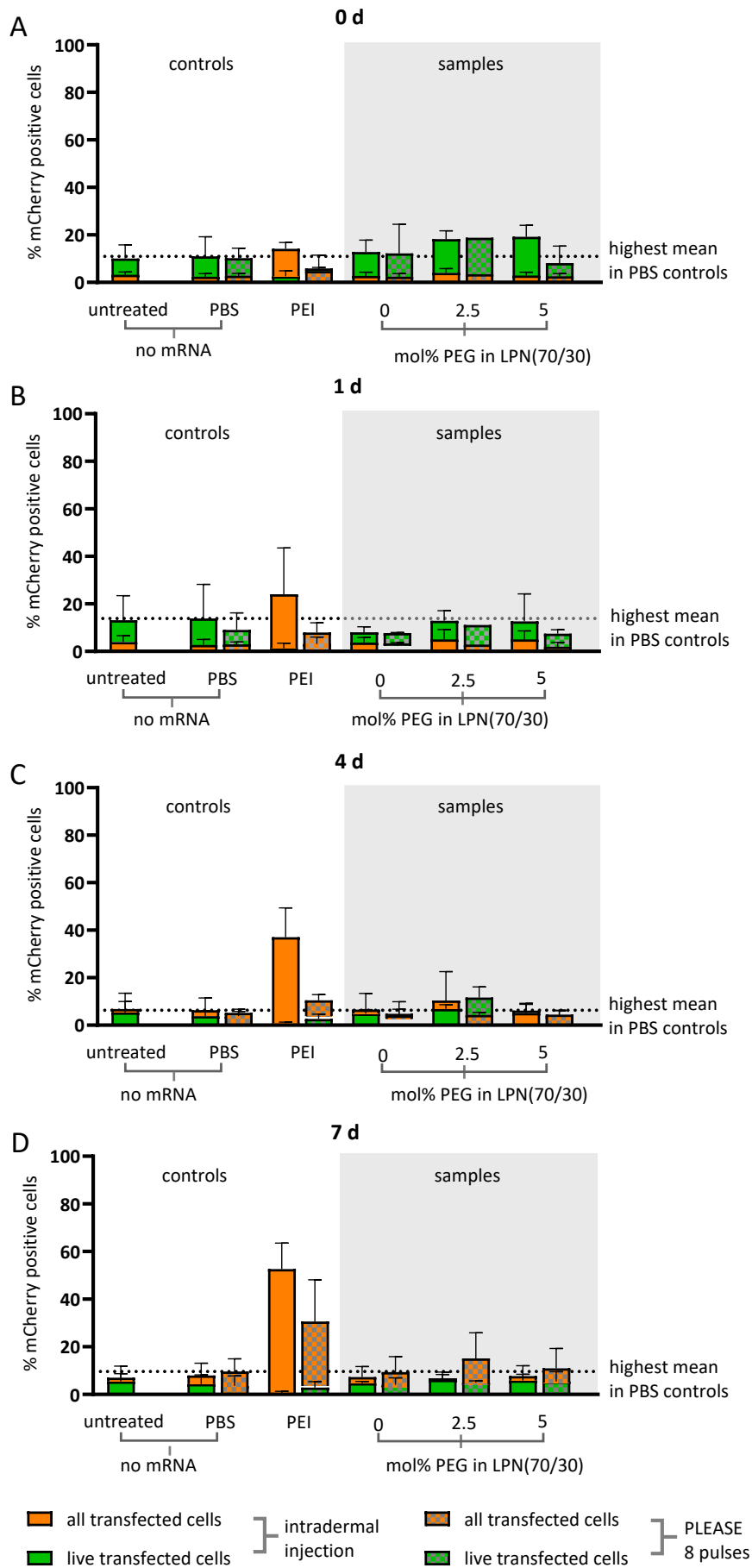


Figure 62: Overview of live transfected cells in the supernatant of cultivated skin biopsies over the course of one week. After daily collecting medium from the same biopsy, medium was replaced. Samples were analyzed by flow cytometry. DAPI and FDA were added to gate for live cells. Solid lines represent skin biopsies after intradermal injection, dotted line after P.L.E.A.S.E.® microporation (pulse length 75 µs, repetition rate 200 Hz, 8 pulses per pore, 8 x 8 mm treatment area). Samples without mRNA (PBS and blank PEI polymer) had the highest number of live cells with a fluorescent signal. Values were generally on a low level.

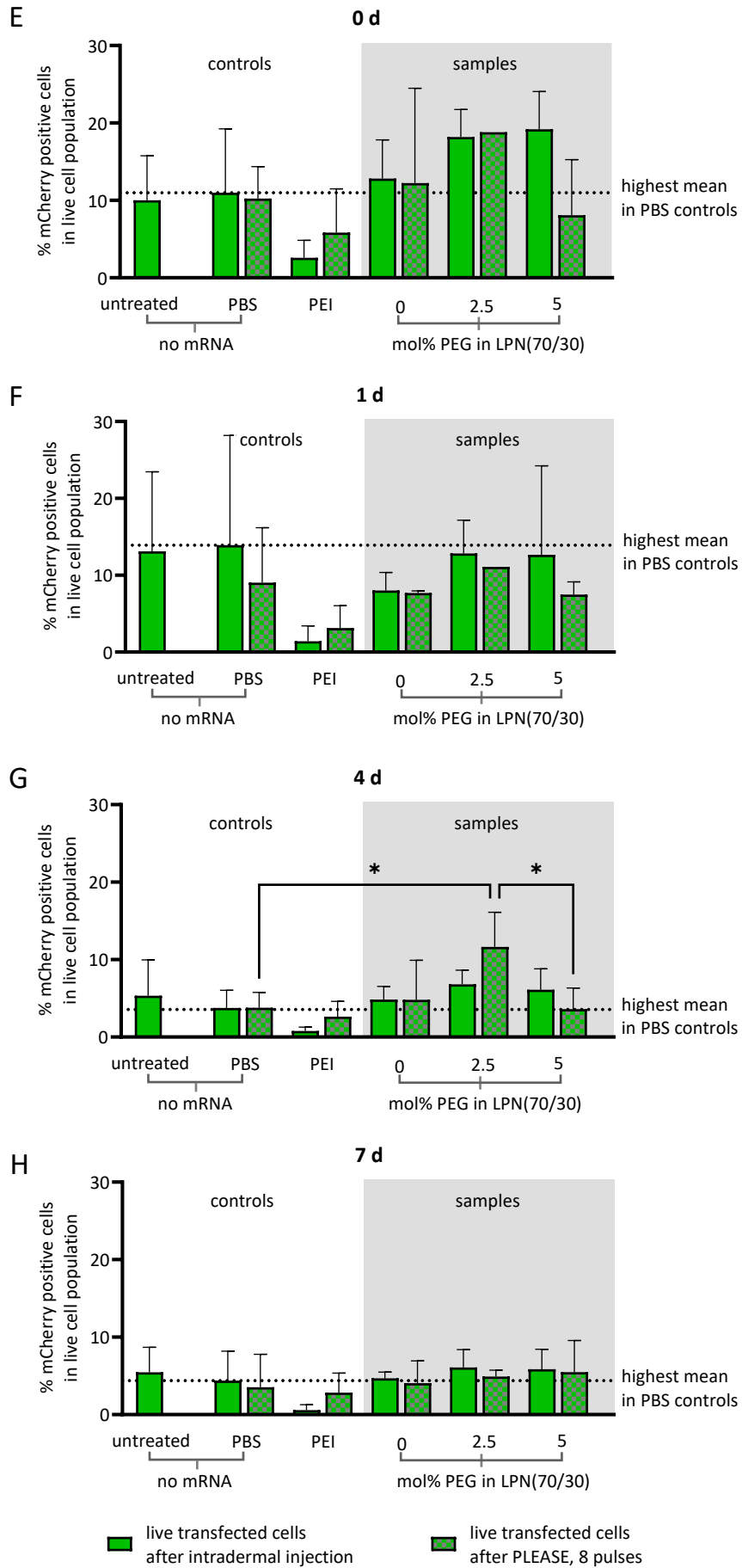
Next to the medium, I also collected the biopsies and analyzed the cells after digestion. Figure 63 shows the results for the single days of analysis as all transfected cells (orange bars) and the transfected live cells (green). Dotted lines represent the highest values measured for the PBS control and is the threshold to cross.

We observed an increasing percentage of cells with mCherry signal for PEI beginning at day 1 with 24% (Figure 63A) and ending on day 7 with 53% (D) but as the color indicates and the diagrams at the right show, all these cells were dead. In a separate experiment, I measured the fluorescence of cells after exposure to PEI without mRNA. As displayed in Figure 64, we measured similar values for PEI samples with and without mRNA in the mCherry channel. We will discuss possible reasons later but for now, we can conclude that the PEI results are not dependable in the context of transfection and that we should concentrate on the live cell population only. The entire setup needs further evaluation but still we can get hints which LPN composition might be the optimal.

## 5 Minimally Invasive Application of LPNs to the Skin



## 5 Minimally Invasive Application of LPNs to the Skin



## 5 Minimally Invasive Application of LPNs to the Skin

Figure 63: Overview of transfection efficacy after application of mRNA-loaded LPNs either by intradermal injection (solid bars) or after P.L.E.A.S.E.<sup>®</sup> microporation (bars with square pattern). Laser parameters: pulse length 75  $\mu$ s, repetition rate 200 Hz, 8 pulses per pore, 8 x 8 mm treatment area. PBS was used as negative control, PEI with mRNA as positive control. Dosing: 8  $\mu$ g mRNA per biopsy. DAPI and FDA addition enabled gating for live cells. 100,000 events counted in flow cytometer. Green bars represent transfected cells in live cell population, while orange bars show percentage of fluorescent cells in total acquired population. Data acquired in five independent experiments with up to eight biopsies per treatment group in total. Untreated and PBS samples had a high background signal rendering LPN results insufficient. There was only one significant difference when 2.5 mol% PEG combined with P.L.E.A.S.E.<sup>®</sup> treatment transfected cells after 4 days of incubation.

Focusing on the fluorescence signals in the live cell population, we measured percentages around 20% at day 0 for both 2.5% PEG LPN(70/30) samples and 5% PEG LPN(70/30) injected (Figure 63E). One day later (day 1, F), the values were around 10% but standard deviations for the PBS negative control was very high. At the end of the studies on day 7 (H), all values were around 5% and comparable to the negative controls. Only after 4 days (G), we saw some differences for the LPN treated samples that deviated from PBS. 2.5% PEG LPN(70/30) in combination with the P.L.E.A.S.E.<sup>®</sup> system, transfected 12% of live cells while PBS had values below 4% for both application routes, which is a significant difference. After intradermal injection, we found 7% of live transfected cells after treatment with this LPN but this was not significant. This observation after a reasonable time after application might be a hint that these nanocarriers indeed transfected skin cells and that the P.L.E.A.S.E.<sup>®</sup>-mediated application increases the potential effects. We will discuss this topic in the next part in more detail.

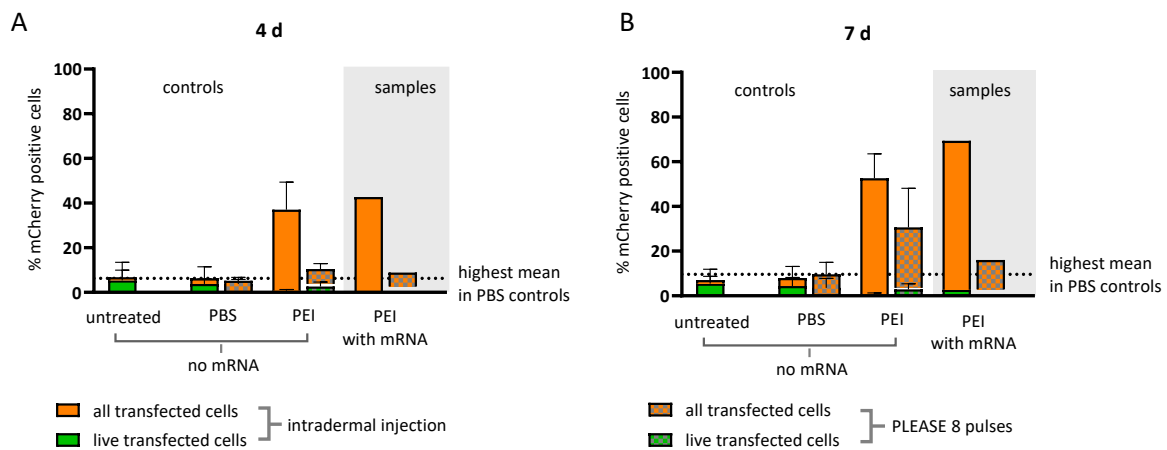


Figure 64: Assessment of percentage of fluorescent cells in the mCherry channel after 4 (A) and 7 days of incubation (B). PBS application by intradermal injection or after P.L.E.A.S.E.<sup>®</sup> treatment was compared to the application of PEI, either complexed with mCherry-encoding mRNA or as blank polymer. Dosing: 8  $\mu$ g mRNA per biopsy. DAPI and FDA addition enabled gating for live cells. 100,000 events counted in flow cytometer. Green bars represent transfected cells in live cell population, while orange bars show percentage of fluorescent cells in total acquired population. Data acquired in five independent experiments with up to eight biopsies per treatment group in total (only one data point for blank polymer per time point). Samples without mRNA have comparably high signals in mCherry channel as PEI complexed with mRNA. This is clear hint that we did not measure transfection but unspecific reactions to PEI application.

## 6 Discussion

### 6.1 Lipid-polymer Hybrid Nanoparticles as Delivery System for mRNA

#### *Relevance of messenger RNA as Therapeutic Entity*

The history of mRNA as therapeutic began with its discovery in the early 1960ies [176]. Since then, scientists believed in the therapeutic potential of messenger RNA but the molecular properties made its realization difficult and raised the need for a delivery vehicle.

Successful transfection *in vitro* was first realized with liposomes in 1978 [177, 178]. The first report about protective CTL response *in vivo* after subcutaneous application of liposomal mRNA was published already in 1993 [93], followed by the observation of antibody titers after intramuscular injection in mice [179]. The sensitivity and the ubiquitous degradation enzymes, namely RNases, made the transition to application in humans difficult. Understanding the structure and function of all parts of the mRNA in more detail enabled specific modifications and therefore the production of more stable nucleic acid molecules [180–183]. Commercialization of the manufacturing process increased the availability of mRNA for more researchers being a catalyst for detailed knowledge and all kinds of delivery systems. The breakthrough came with Covid-19 pandemic when worldwide efforts and expenses were concentrated on the development of a mRNA-based vaccine being ideally suited for such a pandemic threat with its high production speed and scale [184]. Researchers profited especially from earlier findings about the combination of modified mRNA with lipid nanoparticles for individualized cancer therapy [185]. This development led to the rapid approval of the first mRNA-based therapeutic in December 2020, namely the first vaccine against SARS-Cov2 less than a year after the viral sequence was published [186]. Starting a new era in medicine, these vaccines opened the door for any thinkable application of mRNA. The approved vaccines deliver the mRNA complexed with a lipid mixture as solid lipid nanoparticles but other application routes than intramuscular injection may require other delivery systems [80].

#### *Hydrodynamic Parameters and Shape of plain DOTMA-DOPE-PLGA LPNs*

For the application to the skin, we aimed for a lipid-polymer hybrid nanoparticle (LPN) combining the good transfection properties of lipids with the high stability of the polymeric core. Such LPNs were shown to elicit significant protein levels in mice after intranasal application [145]. Yasar et al. proofed that it was possible to produce lipid-polymer hybrid nanoparticles made of DOTMA and the well-established polymer PLGA [147]. We decided to add the zwitterionic phospholipid DOPE to reduce the potential toxic effects, to profit from its ability to increase endosomal escape and to enable a more robust transfection efficacy [187]. I modified the published protocol to prepare a panel of LPNs with increasing amounts of DOPE in the lipid layer.

Cryo-TEM imaging confirmed the round shape and the presence of PLGA reacting specifically to the electron beam (Figure 5) [188]. The absence of liposomal structures allowed the conclusion that lipids and polymer were successfully associated even though it was not possible to visualize the core-shell structure itself nor the arrangement of the lipids. The sizes of 195-260 nm were within the range optimal for *in vivo* DNA delivery [189] and typical for polymeric nanoparticles (100–300 nm) [97]. The measured zeta potentials were positive indicating a clear difference to nanoparticles only made of PLGA as these typically have a negative surface charge of about – 30 mV [57]. We therefore assume that the PLGA core interacts with the hydrophobic tails of the lipids with the consequence that the charged lipid head groups point to the surface of the nanoparticle and can interact with the mRNA.

We observed higher surface charges for LPNs with increasing DOPE content with a maximum of 38 mV for LPN(70/30) (Figure 3). We would expect a decline of surface charge transferring the observations made for the addition of neutral phospholipid to cationic DOTAP liposomes [107]. In contrast, the observed increase of zeta potential might be caused by the structural arrangement of the lipids. A tight packaging of the lipids might fully cover the phosphate and thus hinder its contribution to the surface charge. A second option would be a complete change of the lipid arrangement with increasing DOPE amounts. For our application none of the options would be a problem as the zeta potential measurements were very reproducible over several batches and the loading of mRNA worked well, too.

Beginning with 80 mol% (LPN(80/20)), higher percentages of DOPE reduced the surface charge ending in negative values for DOPE-only LPNs (LPN(100/0)). The phospholipid DOPE is zwitterionic with a negatively charged phosphate and a positively charged primary amine for pH values below 8 resulting in a neutral lipid [190]. Using only fluids and buffers with a maximum pH of 7.4, the neutral DOPE most probably leads to neutral LPNs measured as negative. Mura et al. made a similar observation when measuring a zeta potential of -5 mV for PVA-coated PLGA nanoparticles that are supposed to be neutral [191].

### *Storage Stability of plain LPNs*

In our stability study with plain LPNs over the course of 21 weeks, we saw a reduction of surface charge with time, especially when LPNs were stored at RT (Figure 6). The observed losses of surface charge happened mainly for storage at room temperature while fridge temperatures showed less effect. For LPN(70/30), the reduction of surface charge started already after 16 weeks of storage at RT. Lacking repulsion forces between nanoparticles, this LPN aliquot lost its colloidal stability indicated by an increased PDI.

The general reduction of cationic surface charge needs to be considered as it is needed for the complexation of the mRNA. We concluded that LPNs should be as fresh as possible for experimental use and stored not longer than 12 weeks in the fridge as LPN(70/30) started to lose stability after this time point. We assume that the combination with the polymeric core is responsible for that result as liposomes or solid lipid nanoparticles show shorter shelf lives or need reduced storage temperatures [80, 192, 193].

There seems to be some potential for extended storage in the fridge that I did not investigate. Nevertheless, the studied proofed the stability and consistent quality of the nanocarriers during the 12-week interval most relevant for conducting experiments like transfection studies. For such experiments in a laboratory set up, the stored LPNs can be loaded with the mRNA directly before the experiment in a RNase free working area. In a later phase of preclinical development, an extended storage stability study of loaded LPNs should be performed instead. This is particularly important to warrant the intactness and thus the therapeutic effect of the mRNA molecule. If stored separately from LPNs, naked mRNA is not protected from degradation by ubiquitous nucleases raising the need for RNase-reduction procedures and trained health care professionals. Additionally, pure mRNA is stored at -20 or even -80 °C requiring the corresponding freezer infrastructure.

### *Stability of mRNA-loaded LPNs*

The stability study with plain LPNs allowed a storage in the fridge up to 12 weeks. On the day of experiment, LPNs were loaded with mRNA and directly used. It is at this point not necessary to investigate the long-term storage stability of loaded LPNs. Nevertheless, colloidal stability should be at least maintained during the course of the experiment and therefore stability assessment should focus on these time intervals.

The complexation of mRNA onto the surface of the LPNs changes the surface properties of the nanocarriers with potentially strong effects for the particle stability. For LPNs (0/100 – 40/60) the surface charge is reduced but still positive, for LPN(50/50) around zero and starting with LPN(60/40) I measured negative values below -14 mV (Figure 3). In general, measured values between -10 mV and +10 mV are generally considered as neutral [194]. The closer the zeta potential gets towards zero, the lower are the repulsion forces and potentially also the storage stability. This might be a problem for LPN(50/50) where the nucleic acids completely neutralized the lipid charges, but we did not observe hints for instabilities during any of our experiments with this LPN.

To get a good impression of the stability of loaded LPNs without performing an extended stability study, we decided to systematically test selected challenging conditions that the nanoparticles might face during experiments. Common medium components like salts and especially polyanionic serum proteins are known to be a challenge for nanoparticles [139]. The longest incubation time of the cells with loaded LPNs and therefore also the stability test interval was 24 h.

In our experiment, LPN(0/100) immediately aggregated in protein containing media with sizes above 2500 nm (Figure 13B) probably due to binding of the negatively charged albumin to the DOTMA-only LPN [195]. In the mRNA-loaded state, this LPN has the highest positive zeta potential and is therefore most prone to bind the protein. For cell culture use, the larger agglomerates might even be beneficial as they microprecipitate to the cell layer increasing the local concentration and thus the chance of uptake. As DCs are antigen presenting cells, they can even take up such large components leading to good transfection results. In other setups than cell culture with professional antigen presenting cells, this instability might be a problem and should be avoided. For the other LPNs, we did not observe such an agglomeration tendency.

Next to the agglomeration, we observed a reduced mRNA loading capacity for this LPN(0/100) as indicated by the apparel of a band for free mRNA (Figure 14C). Due to the increased size after albumin addition the LPNs lose surface area resulting in a lower number of mRNA binding sites and furthermore the albumin might cover the surface changing the charge and thus the prerequisite for loading [196–198]. Additionally, a new band between the band of free mRNA and the pocket appeared in the gel electrophoresis of LPNs (0/100) and (100/0). As this mRNA did not migrate as far as the free mRNA, it might be associated with proteins. In contrast to the albumin addition, the tested salts and buffers did not change the degree of complexation with mRNA. The reason for that might again be the pH as all used fluids have a pH below 7.4 maintaining the charge of DOPE. Increasing the challenge further, I incubated mRNA-loaded LPNs (10/90) and (70/30) in cell culture medium supplemented with buffers and most importantly 10% fetal calf serum for 24 h and directly measured the effect using nanoparticle tracking analysis (Figure 15). We found hints for a slightly increased size in medium for LPN(70/30), but measured values were comparable with samples in MQ. The serum proteins might have attached to the surface in a similar process as members of the complement system in the blood do when in contact with cationic DNA-lipid-complexes [199]. This trend would explain an increased size but on the other hand, Crook et al. observed a decrease in size of DNA-loaded liposome when exposed to 50% serum. Furthermore, they found no difference of type and amount of bound serum proteins between two liposomal formulations (DOTAP with and without cholesterol) [139]. Due to the polymeric core of the LPNs, such a reduction is not likely but these observations might explain the little effect onto the measured sizes. At this point, we can

conclude that all LPNs with at least 10 mol% DOPE are sufficiently stable in biological relevant media. It will be later discussed how the opsonization of proteins influences the interaction with the cells.

### *mRNA Complexation and N:P Ratio*

Having discussed the stability topic, there is now room for mRNA complexation aspects. As mentioned before, zeta potential measurements showed the expected reduction of surface charge after mRNA binding. Beginning with LPN(50/50), the loaded LPNs had a neutral or negative surface charge. The difference between plain and mRNA-loaded LPNs increased parallel to the DOPE content with a maximum of 52 mV for LPNs (60/40 – 80/20) before it decreased rapidly. Gel electrophoresis and RiboGreen<sup>®</sup>-based quantification showed that the fraction of accessible mRNA increased in the same way (Figure 12). But for most LPNs, especially for those with a low DOPE content, both dyes did not lead to a detectable signal neither in the pocket nor in the gel until heparin was added to compete with the nucleic acid for binding sites. Adding heparin successfully released the mRNA from the LPNs which was confirmed by new signals after gel electrophoresis. We hypothesized that the interaction of mRNA and nucleic acid is so tight leaving no room for the dyes to intercalate and thus no detectable signal. This goes in line with the established observation that DNA is not accessible to ethidium bromide as soon as it is complexed with lipids resulting in a loss of signal on the gel [139, 200].

The visible signals in the gel pocket might be caused by a fraction of mRNA that is attached to the surface of LPNs tightly enough to prevent its movement into the gel but simultaneously loosely enough to make room for the interaction with dyes. DNA complexed with DOTAP in liposomes had similar signals in the pockets [200]. The fact, that the intensity of this kind of signal increased a lot after heparin addition underlines the relevance of this possible explanation as the mRNA is partly detached from the LPNs by heparin. These hypotheses explain the outcome of the visualization process but not the fact that more DOPE leads to more accessible and finally free mRNA.

One reason for more free mRNA with reduced DOTMA content might be a different strength of interaction of the lipids with the mRNA backbone. To have the best possible comparison between nanocarriers, we decided to use the N:P ratio for mRNA loading instead of the weight ratio. For the calculation, I counted all positively charged amine groups as potential binding partners for the phosphates in the mRNA backbone and kept this molar amount constant while varying molar fractions of DOTMA and DOPE. As a result, the number of quaternary ammonium groups of DOTMA was reduced while the primary amines of the phospholipid DOPE were increased. From our experiments it seems that these two kinds of binding partners are not equally strong in the interaction with the mRNA. Methylation of the head group led to a loss of transfection favoring properties [153, 201]. We can thus assume that DOPE interacts directly with the nucleic acid but seemingly weaker maybe because of the proximity of its own phosphate to the amine. If DOTMA is the better complexing lipid and its number is reduced, good binding sites get saturated. mRNA molecules will not find several binding sites anymore but instead only a few resulting in a looser attachment and more room for the intercalating dyes. This explanation would also fit to the signals in the gel electrophoresis where we found bands in the pockets for LPNs with higher DOPE content. DNA complexed with DOTAP in liposomes showed a similar trend that the addition of the cationic lipid reduces the ethidium bromide signals in the gel pockets [200]. The cloud of nucleic acid chains with their negative charge around the high-DOPE nanocarriers and some free mRNA molecules in the suspension will also reduce the measured surface charges and therefore explain the inversions of zeta potentials to negative values.

Using the N:P ratio for mRNA complexation has recently become the most common way in the field. Alternatives are the ratio of weight or charge. For *in vivo* gene therapy, a charge ratio of 5:1 is typically used [202]. In many cases, DOPE is part of the formulation of mRNA but often it is

considered only as helper or structural lipid and not counted for mRNA complexation [81, 122, 153, 203]. If we adapt our N:P ratio of 2.81 to this strategy and count only the DOTMA molecules, the ratio is around 2 for LPN(30/70) and reversed beginning with LPN(70/30) with more mRNA-phosphates than amines (N:P of 0.84). In other words, if N:P ratio is below 1, we need less nanocarriers to complex the same amount of mRNA. Kranz et al. tested similar N:P ratios with DOTMA/DOPE liposomes while counting only DOTMA for mRNA complexation and confirmed an inversion of zeta potential to negative values for N:P ratios below 1 resulting in the best transfection rates. In their study, ratios between 2.5 and 0.9 resulted in instable liposome-mRNA complexes which is in contrast to our stable LPNs [203]. Malone et al. found that a N:P ratio around 0.6 (weight ratio 2.5:1) works best for transfection of RNA with Lipofectin® (1:1 DOTMA/DOPE) if only DOTMA is counted (1.15 for DOTMA+DOPE) [156]. Being able to use N:P ratios below 1 is very helpful for a potential application as a smaller number of nanoparticles needs to be applied for a sufficient dose. Next to reducing toxicity concerns, less material is needed that might be limited especially during situations like a pandemic. With applying smaller volumes, transport and material costs could be reduced and patients will benefit from smaller edema and less pain at injection site. Even if we lose some of the nucleic acid during loading of LPN(70/30), we know from RNase protection and transfection studies that this LPN is the best performing one of our panel and the most promising candidate. The looser way of complexation seems to be enough as naked mRNA does not elicit protein production and cannot be accounted for the effect of this LPN. Crook et al. observed free DNA on the gel as well for their optimized transfection formulation [139].

For LPN(90/10) the N:P ratio would be 0.28 and zero for LPN(100/0) but with increased amounts of free mRNA in the gel and minor performance in transfection studies. These N:P ratios seem to be beyond the optimum resulting in larger fractions of free mRNA that cannot contribute anymore to the performance.

The loaded LPN(50/50) had a zeta potential around zero indicating that with this corrected N:P ratio of 1.4 all the mRNA can be bound without left free mRNA. Showing also very stable transfection results, this or a similar LPN could be another candidate for further evaluation. A calculated N:P ratio of 1 needs an LPN with 64.4 mol% DOPE and 35.6 mol% DOTMA and would be called LPN(64/36). We would expect a slightly negative zeta potential and good transfection results.

### *Cell Tolerability and Cytotoxicity*

Looking now in more detail onto cell-based experiments, we found that all LPNs were well tolerated. There were some signs for toxicity of plain LPNs after starving the cells in HBSS for 24 h but the medium control showed a reduced viability as well. In the more relevant setups with cell culture medium either with or without cell supplements like FCS, both, plain and mRNA-loaded LPNs were tolerated well by the dendritic cell line DC2.4. As complexation with DNA is known to reduce the toxicity of cationic lipids [204, 205], we hypothesized that loaded LPNs will be better tolerated but the results did not confirm this expectation. In contrast, we even observed slightly reduced viabilities in non-supplemented medium for loaded LPNs with their not as positive or even negative surface charge but not for the plain LPNs. In general, we aimed for an improvement of cell viability by adding DOPE as the phospholipid is known to reduce cytotoxic effects of cationic lipids like DOTMA [154]. We saw an effect of this modification for loaded LPNs after 24 h in non-supplemented RPMI medium but 20 mol% DOPE was already enough to see a difference (Figure 16). In the supplemented medium, there was no difference anymore probably because cells were cultivated under optimized nutrition and thus less sensitive to treatments [206, 207]. This good tolerability is important for the later application to the skin as nanocarriers will not be removed but remain in the tissue.

### *Cellular Uptake*

For the uptake study we instead saw a clear benefit of the DOPE addition resulting in the highest uptake for LPNs with at least 60 mol% of DOPE independent of the medium (Figure 17). There was a linear trend in non-supplemented medium that the more DOPE, the more uptake climaxing around 100% positive cells for LPNs (60/40) – (90/10) until it dropped for DOPE-only LPN (LPN(100/0)). In supplemented medium, the uptake was increased for LPNs (0/100) – (20/80) compared to the non-supplemented medium which might be due to an adsorption of proteins to the surface of these positively charged LPNs mediating and thus improving the uptake. The uptake of the other LPNs did not improve after the addition of supplements because it was already around 100% before, leaving no room for further improvement. One would expect that positively charged nanoparticles bind better and in an higher extend to the rather negatively charged cellular membrane facilitating their uptake [208, 209]. In contrast, Song et al. claimed that any charge either positive or negative is needed for the electrostatic interaction with carbohydrates and proteins on the cell surface [100]. After binding, cellular entry mostly happens via different endocytic pathways [210]. Stimulating factor of the serum like insulin might also increase the rate of endocytosis to increase nutrient delivery [211]. Furthermore, with the detection of fluorescently labeled PLGA in the flow cytometer, we can only measure how many cells are associated with LPNs but we cannot distinguish if the nanoparticle is outside or inside the cells. There are anyways several reports that show that uptake and transfection do not directly correlate [107, 212]. The focus should therefore be on the protein production as a consequence of uptake and endosomal escape.

### *Parameter Optimization for Transfection Studies in DC2.4 Cell Line*

Tolerability and successful uptake are important features for nanocarriers, but they are only checkpoints on the way to successfully transfecting nanoparticles. We started the evaluation of this pivotal property with an automated microscope and got an impression of the transfection kinetics of our LPNs. In a first setup I varied the incubation time of DC2.4 with the LPNs and found a clear time dependency with the highest transfection rates after the longest incubation time of 24 h. While measured time profiles were conclusive for LPN(0/100) and to some extend for LPN(10/90), the other tested LPNs (LPN(50/50) and LPN(70/30)) did not lead to signals in the microscope but in the flow cytometric analysis. As we found signals in the FACS, the lack of data points in the microscope is most probably caused by the measurement technique. The used Lionheart microscope is equipped with an autofocus module to find the plane where the cells are. After autofocusing, brightfield and fluorescence values are measured, and the plate moves to the next preset position where the machine again starts with focusing. If the autofocusing process fails for example due to low contrasts of the cells, no data points can be generated in the measurement channels. Furthermore, the optical evaluation relies only on a few positions within a well. We selected these regions of interest carefully to have comparable cell numbers and densities, but the general cell count is limited and DC2.4 cells are rather mobile and move in and out of the imaging window. The data base for the presented kinetic curves is therefore not constant. For flow cytometry, all cells are detached from the wells and an aliquot of several thousand cells is measured resulting in a much broader sample for analysis.

Nevertheless, I optimized the measurement parameters and repeated the experiment with the microscope and an incubation time of 24 h. This helped us to get an impression of the kinetic profiles of the transfection. For LPN(0/100), we found a broad peak of fluorescence intensity in the channel of the mCherry protein that was encoded on the delivered mRNA while the number of protein-producing cells declined after a sharper peak. There seemed to be some cells that very effectively produce the protein and thus enhance the fluorescence signal. On the other hand, the rest of cells successfully transfected at the beginning reduced or stopped the protein production.

LPN(50/50) showed a very stable transfection. We found as many protein producing cells as for the controls but a rather low fluorescence intensity pointing to low protein amounts per cell. Both curves showed a steady and parallel increase without a decline at the end of the experiment. In comparison to LPN(0/100), the cell counts were much higher, and the protein amounts remained high after 24 h. This might be a hint that LPN(50/50) leads to a very homogenous transfection and a longer lasting expression of the protein. There might even be some potential for more protein production if incubation time was extended. When Karikó et al. evaluated the kinetic profile of DOTMA/DOPE-mRNA-lipoplexes *in vitro* with a cell line, they found an signal onset after 15 min, the maximum after 8 h and a decline to 4 and 1% of maximum after 24 and 48 h, respectively [205]. It is therefore likely that the selected observation time covers the interval with the highest effect.

LPN(70/30) had a slow but constant increase of number of positive cells. Protein production appeared very early after a few hours and stayed on the same, rather low level for the entire measuring time. This MFI profile of LPN(70/30) was the most constant but lowest of the samples. We hypothesized that few super producing cells are responsible for this observation. Depending on the application, either profile might be beneficial.

As I performed the FACS analysis only at the end of the experiment, we might underestimate the performance of LPN(0/100) while overestimating the transfection rates of LPN(50/50). Another aspect of the selected 24 h setup is the chance to generate unrealistic uptake rates. When applied to the skin or other tissues where physiologic cleaning processes are in place, the cells will not have such a long time and so many chances to take up the nanocarriers. From this perspective, the traditional two-step transfection protocols with an incubation time with nanoparticles followed by a particle free period may be more realistic. During this extended second episode the cells have enough time to produce the protein. Such procedures were especially needed for DNA transfection experiments where time until protein production is longer and cells thus need new nutrition. Without the need of delivery and transcription in the nucleus, mRNA translation to the encoded protein is generally faster, so the selected 24 h were enough to see an effect.

Next to evaluating the best time point for the FACS analysis, I also tested typical medium supplements with selected LPNs in a preliminary experiment. We found that the transfection efficacy of LPN(10/90) is drastically reduced to less than 15% as soon as FCS (independent of the amount) is part of the medium while the effect is lower for LPN(70/30) (Figure 22). This effect beginning with 1% serum addition was shown before for DNA [134]. As mentioned before, the uptake of LPN(10/90) is improved with supplementation, and we hypothesized that an adsorption of proteins to the surface might be responsible. If protein adsorption changes the uptake mechanism, it may also influence the intracellular fate of the nanocarriers leading to the fast removal of the LPNs from the cells. This process might happen as digestion or exocytosis as most common options [102]. Additionally, the adsorbed proteins might represent a barrier for the interaction with the endosomal membrane and could therefore hinder endosomal escape of the mRNA. Another reason for the reduced transfection efficacy would be the degradation of the cargo by the nucleases in the serum but our later discussed RNase exposure experiment did not give us hints in that direction. We therefore think that the adsorption of proteins is responsible for the behavior of LPN(10/90).

In contrast to these observations, the uptake of LPN(70/30) was not changed by the medium supplements, but the RNase exposure showed little enzymatic digestion of mRNA. This degraded fraction is probably the same that is only loosely attached to the nanocarrier and visible in the gel pocket. If there is enough space for the intercalating dyes, the enzymes may also fit and digest the nucleic acids. Nevertheless, the remaining mRNA onto the particle is enough to successfully transfect the cell also in the presence of serum.

### *LPN mediated RNase Protection*

Looking now in more detail onto the RNase exposure experiment, we saw little effect of the enzyme for LPNs (0/100), (10/90) and (50/50). While mRNA signal of LPN(70/30) was reduced during RNase incubation, the final difference between treated and untreated samples were comparable to the other LPNs indicating a similar degree of protection. As hypothesized before, the LPNs with higher DOTMA content have a tighter packaging of the nucleic acid resulting in a lack of dye binding but also protection against enzymes. LPN(100/0) did not protect the mRNA resulting in a difference at the end that was larger than the one of the naked mRNA. This goes in line with the findings of Koshizaka et al. who observed that liposomes containing only phospholipids like DOPE did not protect DNA from nucleases whereas liposomes with a cationic lipid did sufficiently [213].

For the interpretation of these observations, we need to discuss the relevance of the challenge. There is only little known in literature about the total, physiological amounts of RNases as quantification is difficult and large differences are reported depending on the tissue or compartment [214–217]. There is for example RNase T2 in lysosomes to cleave RNA at acidic pH [218]. In most articles where mRNA-loaded nanocarriers were systematically exposed to nucleases researchers tested different concentrations and evaluated results with gel electrophoresis. Our tested concentration is for example in the same range as Zhang et al. [219]. We wanted to investigate not only the endpoints but to follow the degradation in a kinetic setup. Our focus was on the comparison of the LPNs to find the best possible protection of the mRNA cargo. I started the setup with the naked mRNA control and adjusted the RNase amount accordingly to still be able to follow its degradation. The ubiquitous presence of nucleases made handling in the lab difficult. From the calibration curves I had a theoretical fluorescence of sample before the addition of RNase but I could hardly reach this value. The unwanted digestion happened within seconds. Furthermore, we know from the gel electrophoresis that heparin addition does not detach all the mRNA from the nanocarriers. Using the RiboGreen® dye for visualization, we only get one mixed signal for free and the loosely attached mRNA. If heparin leads to a looser complexation of mRNA, we cannot see a difference in the kinetic signal which seems to be true for LPN(50/50) and LPN(70/30). For high DOTMA-LPNs (LPNs (0/100) and (10/90)) the heparin showed a distinct effect with RiboGreen® when invisible mRNA suddenly had a signal (Figure 28). Interpreting the electrophoresis bands after RNase treatment, we can still say that there is intact mRNA after heparin addition that was protected by the LPN. A transfection study with preincubation of the samples with RNase confirmed that the remaining mRNA led to protein production. We do not know if the invisible rest is still intact on the LPN or degraded and out of the gel.

We were therefore not able to compare absolute numbers between experiments but only the difference values between treated and untreated samples. Additionally, the selection of the low RNase amount due to the high sensitivity of the naked mRNA may have two contrary consequences. On the one hand, it is unclear if the nanocarriers would protect the cargo also against higher nuclease amounts and might therefore underestimate the protection. On the other hand, if we directly transferred these results to *in vivo* and if the physiologic amounts were higher, this reduced challenge might lead to an overestimation of the protection.

From our first transfection experiments in FCS containing medium we know that this protein mixture is a high challenge for the LPNs. We decided to compare this challenge to the preincubation with the selected RNase concentration and found that the FCS has the higher effect (Figure 30). Due to the high background signal of the serum on the gel, it was not possible to investigate the effect of FCS directly [219]. But with the transfection results, we can assume that our kinetic study rather led to an overestimation of protection but as discussed before, the other FCS and medium components might also have an effect. Our other preliminary experiment indicated that enzymes are not the only hurdle for the nanoparticles because the transfection rates in HBSS + 10% FCS were much higher than the

one in supplemented medium (RPMI + 10% FCS and others). The complexity of FCS in combination with medium cannot be modeled with a single parameter. Nevertheless, our RNase exposure study confirmed that a nanocarrier is generally needed to protect the mRNA as naked nucleic acid is degraded fast even with this limited setup. *In vivo*, there will also be several aspects that might challenge the nanocarrier. The higher the challenge *in vitro*, the better and more dependable is the selection of best performing nanoparticle. We therefore decided to judge the effect of LPNs only with and without the FCS in medium.

### *Parallel Investigation of Tolerability, Uptake and Transfection Efficacy in DC2.4 cells*

For the final experiment I combined a live-dead staining with uptake evaluation and the transfection efficacy (Figure 23). This setup enabled us to present the fraction of live transfected cells and protein producing cells in the entire measured population. This second value gives an estimation how the cells react to the nanocarriers and if the treatment has a cytotoxic potential.

We observed differences of live and total cell population only in the non-supplemented medium going in line with the hypothesis that in this way cultivated cells are more sensitive. The transfection rate of this dead cell population is higher for almost all particles. So nanocarriers must have also hit these cells which might lead to their death.

For the selection of the best candidate, we concentrate on the population of transfected live cells. In non-supplemented medium, we measured increasing transfection rates in the live cell population from around 60% for LPN(0/100) up to 72% for LPN(50/50) followed by a decline. This benefit of the increasing DOPE content was much more pronounced in supplemented medium when values increased from 25% (LPN(0/100)) to 67% for LPN(70/30). As mentioned before, serum is known to reduce the transfection efficacy of nanoparticles but it was also recently shown that the effect depends on the components of the carrier [220]. There are several aspects to be considered. The first LPN in the row (LPN(0/100)) has the most positive surface charge in the loaded state and it is thus most likely that serum proteins adsorb to the surface. The addition of serum causes a loss of colloidal stability leading to aggregation. These larger particles might be rather degraded when taken up by the cells without delivering the mRNA to the cytosol. In contrast, LPN(10/90) is stable in the serum containing medium but still transfects only 24% instead of 57% of live cells as without the supplements. As surface charge of all LPNs until LPN(50/50) is positive after mRNA complexation, the adsorption of serum proteins might change surface properties directing them towards lysosomal degradation after endocytosis. This redirection was for example observed by Wang et al. for positively charged polystyrene particles [111].

Another explanation of the reduced transfection efficacies is the lack of intact mRNA in the cytosol. On the one side, the nuclease activity of the serum might degrade released mRNA. In direct comparison of transfection efficacy in serum containing medium with RNase preincubation the nuclease activity seems to play a minor role as transfection was more reduced with serum. As mentioned before, the presence of serum proteins adsorbing and thereby changing the nanocarriers surface properties has probably the stronger influence. Nevertheless, the fraction of mRNA that is only loosely attached to the nanocarriers might be degraded. On the other hand, releasing the mRNA from the nanocarrier might not only be a challenge in experimental setups. For DSPC (1,2-Distearoyl-sn-glycero-3-phosphocholine), as phospholipid with quaternary amine, it was postulated that the stronger complexation of mRNA compared to DOPE might hinder the release from the nanocarrier once inside the cells [81].

Measuring comparably high uptake rates for all LPNs, the differences seem to be inside the cells. After endocytosis, the loaded LPNs need to escape the endosome and deliver the mRNA to the cytosol where the protein can be produced. If this process is disturbed or not fast enough, the nanocarriers are degraded or exocytosed without the chance to generate a protein signal. For this escape, the cationic lipid and its buffering capacity is important to activate proton pumps. As the

proton sponge theory claims, the presence of lipids leads to chloride influx, raises osmotic pressure resulting in swelling of the endosome and thus enables the endosomal escape [102–104]. I did not quantify the ability of endosomal escape of the LPNs but DOPE is known to enhance this process [187]. The phospholipid has a conical shape and therefore promotes transition to the less stable hexagonal phase which is crucial for nucleic acid release, reduces the membrane stability and at the end facilitates endosomal escape [99, 152, 212]. Kauffman et al. found that the addition of DOPE is the strongest predictor of *in vivo* mRNA delivery to the liver. The molar amount of ionizable lipid was with 35 mol% close to our optimal 30 mol% DOTMA but their highest used percentage of DOPE was only 28% (and up to 50 mol% cholesterol) [81]. In the commercially available transfection reagent Lipofectin<sup>®</sup>, DOTMA and DOPE are used in equal proportions [151]. From our data, we would expect that the maximum transfection is reached for even higher DOPE amounts around 70 mol% which is in concordance with the findings of Pinnaduwege et al. and Zhang et al. who found 20 mol% cationic lipid in DOPE to be optimal for *in vitro* transfection of DNA [221, 222]. In our study, these benefits of a higher DOPE content led to high and stable transfection rates without any risks for cell toxicity due to the cationic lipid. For LPNs with at least 50 mol% of DOPE there was no difference anymore between non-supplemented and serum containing medium. LPN(70/30) showed the highest transfection of live cells and was therefore selected for further evaluation.

### *LPN Evaluation in Primary Cells with Focus on Immune Cell Activation*

For the application for vaccination purposes also dying transfected cells might enhance the elicited immune response because the produced protein or the delivered mRNA can be taken up by attracted immune cells, a process called cross-priming [46]. These professional antigen presenting cells like DCs can then process the antigens by themselves, present it to other cells and start the cascade after this little detour [10, 17]. Recognizing mRNA as foreign to the body, leads to the presentation via MHC-I and activation of CD8<sup>+</sup> T cells which was also shown *in vitro* [23, 223]. If immune cells take up the produced protein and detect it as antigen, the pathway goes via MHC-II towards stimulation of CD4<sup>+</sup> T cells. Common vaccines often lack the CD8<sup>+</sup>-response and thus the cellular effector and memory cells resulting in an insufficient protection against the antigen after some time. In contrast, nucleic acid-based vaccines are known to induce weaker antibody titers compared to proteins but instead a stronger cellular immunity in mice [86]. With applying mRNA as cargo, almost every cell in the body can produce the protein and present the mRNA via MHC-I to immune cells. For our planned intradermal application, we target the immune cells of the skin. If these cells are transfected first, they can start both pathways and the immune reaction is supposed to start earlier and more efficient [46]. For the vaccination application both MHC-pathways are reasonable, and we can at this time point not decide which one is more important

In a first experiment, we quantified the presentation of the SIINFEKL peptide via MHC-II by primary dendritic cells and found high percentage of positive cell for the ovalbumin protein control while LPNs showed percentages less than 10% (Figure 32). As we did not find many SIINFEKL presenting cells the chance to stimulate CD4<sup>+</sup> T cells in the next step is low. In the following stimulation experiment we instead observed stimulation only of CD8<sup>+</sup> T cells via MHC-I presentation. There was maybe a mistake in the setup, for example the threshold of proliferation might not have been reached or the selection of antigen-specific CD4<sup>+</sup> T cells did not work as good as for the CD8<sup>+</sup> T cells because the protein control did not stimulate CD4<sup>+</sup> T cells as expected [57]. Probably, our time point of analysis with 48 h was simply too early. We can assume that the metabolism of primary cells is reduced under such artificial cultivation conditions and the process from nanocarrier uptake to the translated protein followed by its presentation may take much longer. It is known that primary cells are harder to transfect than cell lines [106, 122] and that the maximal effect is lower [224].

For the control, we applied the protein avoiding all these steps. It makes sense, that this protein control did not stimulate CD8<sup>+</sup> T cells as proteins are processed via MHC-II stimulating CD4<sup>+</sup> T cells. In

## 6 Discussion

the final experiment with the optimized setup, LPN(70/30) stimulated almost as many T cells as the commercial reagent jetMESSENGER® (Figure 34). It needs to be investigated if both values are enough to activate the immune cascade and provoke its reaction. Even though there was no antigen protein production detectable via a CD4<sup>+</sup> T cell stimulation, the mRNA was successfully delivered as indicated by CD8<sup>+</sup> T cell stimulation.

## 6.2 *Ex vivo* Human Skin Model to Test mRNA delivery

### *Pegylation of LPNs*

After the best candidate LPN(70/30) failed in stimulation of primary CD4<sup>+</sup> T cells and in the adoptive transfer model, I modified the composition by adding a pegylated lipid while maintaining the DOTMA amount. The sizes were comparable to non-pegylated LPNs. The zeta potential was not influenced by the PEG addition which is in line with the findings of Smith et al. [194]. As discussed before, this DOTMA part is probably more relevant for the complexation of mRNA which is again confirmed by the good binding efficacies of the pegylated LPNs. Replacing the well tolerated phospholipid DOPE, the pegylation resulted in some acute toxic effects with viabilities below 40% after 4 h. After 24 h the cells could recover from the treatment and produce the protein successfully (Figure 46).

We found a clear correlation between the amount of PEG and a reduction of transfection rates which is in line with findings of Harvie et al. for DNA delivery [137]. For LPN(10/90) that I added as comparison for LPN(70/30), the percentage of protein producing cells went from 80% down to less than 10% for 5 mol% PEG in non-supplemented medium (Figure 49). We hypothesize that the uptake is jeopardized but did not quantify that number for LPNs deducted from LPN(10/90). In contrast, the transfection rates of modified LPN(70/30) are stable except of the highest PEG (5 mol%) with a rate of 70% instead of 90% positive cells. The quantification of the uptake for this LPN did not show an effect of the pegylation for these LPNs. For DNA delivery by liposomes it was shown that PEG has minimal influence on uptake but can severely hinder endosomal escape and thus the gene transfer [100, 137]. Mui et al. showed that for siRNA delivery by solid-lipid nanoparticles a DMG-PEG amount of 1.5 mol% is the threshold and the best compromise between beneficial effects on biodistribution and pharmacokinetics and minimal harm of siRNA effect [143]. In theory, 2–3 mol% of pegylated lipid are needed to fully cover both sides of a lipid bilayer [225]. Assuming that the long PEG-chains arrange only in the outer lipid layer of the solid lipid-nanoparticles [128], the mentioned 1.5 mol% can fully cover the surface and elicit the maximum effect. Below this number there will be too much space between PEG-chains and above this threshold, the molecules will extend away from the membrane. This is also the reason why the approved SARS Cov2 vaccines contain 1,5 mol% of DMG-PEG [80]. With the polymeric core of the LPNs the surface to size ratio is different compared to this lipid-only nanoparticles. It is therefore reasonable that the necessary PEG amount is higher.

Even though we did not see a benefit of the pegylation with our dendritic cell line *in vitro*, we observed a reduction of transfection efficacy with high PEG amounts. As pegylation might still influence the tissue penetration, we continued with a more complex test system discussed in the next chapter.

### *Rational behind Development of an Ex vivo Skin Model*

The discussed experiments showed that we cannot explain and quantify all observations by systematic tests *in vitro* with our dendritic cell line DC2.4. Especially when it comes to the questions of immune reaction, tissue penetration and the benefit of the application in combination with the P.L.E.A.S.E.<sup>®</sup> microporation, we need the skin as target tissue.

One option was to perform *in vivo* studies with established vaccination mouse models. With the help of our collaboration partners, we could successfully show that the P.L.E.A.S.E.<sup>®</sup> microporation has an immunostimulatory effect *in vivo*. We will discuss this in more detail in the next chapter 6.3. In general, the mouse is just a surrogate and a handy model to understand the ongoing processes in preclinical studies but results are not always transferable [226, 227]. Bahl et al. for example showed that needed inhibitory antibody titers differ a lot between mouse and humans after mRNA-mediated influenza vaccination (100–1000 vs < 100, respectively) [184, 228]. Overall, our aim is to develop a

new cutaneous vaccine for human beings and working with human tissue is thus the most relevant option. Especially for the penetration into tissue we expect differences, as human skin is a lot thicker than mouse skin [170]. There are reports that the general architecture of the skin and innate sensing mechanisms might be different as well [228, 229]. On the other side, there are reports that the antigen expression kinetics in human skin explants correlate well with the profile in a mouse model when the same DNA vaccine is intradermally applied by a tattooing technique [50, 230]. Thus, provided that cultivated tissue behaved similar to the *in vivo* situation, excised human skin is the better option to investigate the performance of the nanocarriers. Avoiding excessive animal studies, we can still later confirm the results in the mouse model. We therefore decided to concentrate on the transfection efficacy of the LPNs first and to optimize this prerequisite in human skin before focusing on the immune response *in vivo*.

I tested mRNA-loaded LPN(70/30) in the original form and after adding 2.5 and 5 mol% PEG to the lipid layer. We found some indicators for successfully transfected cells especially after 4 days of incubation with the 2.5 mol% PEG in LPN(70/30) sample, but several circumstances such as the high background signals of the PBS sample made the interpretation difficult. We will now discuss the drawbacks and possible improvements of the *ex vivo* skin model and then end this chapter with a detailed evaluation of the LPN results.

### *Viability of Ex vivo Cultivated Human Skin*

I started with the development of the excised human skin model for vaccination purposes from the scratch in our lab but profited from published reports [76, 228]. The first step was to receive skin pieces as fast as possible after dissecting from the patient and to maintain its viability. Stored and thawed skin was not an option because the viability is dramatically reduced within 24 h which is probably not enough time for successful transfection [231]. High doses of antibiotics in the medium were necessary to avoid bacterial growth during cultivation. This enabled us to refrain from extensive cleaning procedures of the skin surface to remove the natural microbiome. Such measurements might destroy the barrier properties and thus artificially enhance particle penetration. There were no signs of bacterial growth or change of indicator color observed when medium was daily exchanged.

Messager et al. recommend to use at least two methods to quantify the skin viability [232]. They used microscopy, quantified the amount of used oxygen and MTT for example. The MTT assay is an established method and recommended by the OECD to test for example ingredients of cosmetics or other chemicals for acute toxic reactions [167]. For this purpose, artificial skin surrogates made of keratinocytes can even be used. The MTT assay with whole skin was for instance used as quality control for wound repair [231].

In our case, the incubation of the entire skin piece with MTT led to the formation of the visible formazan crystals only at the edges of the biopsies. When culturing the biopsies, these cells on the edges are exposed to the new environmental conditions instead of neighboring skin cells but simultaneously get most nutrients from the medium. On the other side, one would expect that especially the cells in the center of the biopsy are exposed to the applied LPNs, but it is probably exactly these cells that will not get in contact with the MTT reagent. If the formulations harm these cells in the center, there is a good chance that we will not measure a decline in optical density and thus underestimate the toxicity. I tried to cope with this problem by cutting the biopsies in eight smaller pieces with scissors to expose also the cells in the center, but this process cannot be standardized as much and will probably lead to different sizes of contact areas facing the MTT reagent.

Another difference to the setup in cell culture, is the fact that cells are not lysed but formed crystals are extracted with isopropanol. This process happens overnight bearing the risk of evaporation of

diluent and thus changing the concentration which has a direct influence on the measured optical density. Despite these limitations, the MTT is a rather fast and easy to apply method to get a first impression of the skin quality and its change during cultivation. We observed for example that viability of untreated skin is reduced after 5 days to 50% compared to original value and that PEI exhibits a dose dependent cytotoxicity (Figure 54).

The second method was a live-dead staining of the single cell suspension after digestion of the biopsies (Figure 55). The plan was to quantify the protein expression on the single cell level and the combination with the viability staining was a feasible step to report the transfection rate in the live cell population as well. I tested different published digestion protocols but found the highest number of live cells with the commercial skin dissociation kit that is based on enzymatic and additionally mechanic digestion overnight. This long incubation time and harsh conditions might lead to additional cell death but was needed to separate the cells and assess viability in the center of the skin piece. Nevertheless, this procedure led to a high proportion of debris in the sample interfering with gating process in the FACS. Unable to sufficiently separate the population of cells from other signals, I enlarged the gate and thereby the number of relevant events. Expressing the viability relative to this population led to percentages of viable cells around 50% which is much lower than reported 98% [228]. For a fair comparison, the gating process and the size of populations need to be considered. The gating strategy in the mentioned paper included for example only 59% of total events in the first step. 85% of these cells were single cells. They express their viability as percentage of this selected population making up only 50% of the entire measured events. At the end, 98% of these 50% are viable which correlates to 49% of all measured events. This calculation shows that our viability values at the beginning are comparable to the published data even though it seemed to be much lower from the first look.

In the first published human *ex vivo* skin model, tissue viability was 50% after 60 h and cultivation was stopped after 72 h [50]. After 10 days of culture, Blakney et al. report 45% viable cells in total events (reported as 90% of single cells) and 35% after 21 days [228]. We had only 26% live cells after 9 days in the pivotal study and decided to culture only up to 7 days with 28% viability. Viabilities of untreated skin and after PBS injection were similar in this pivotal study. Cumulating data points of all our skin experiments, we had a final viability of PBS injection samples of 49% at the beginning, 46% after 24 h, 34% and 32% after 4 and 7 days, respectively.

We can conclude that the viability of our tissue was comparable to the published reports at the beginning but cultivation for the extended 3 weeks period was not possible. One reason might be in the medium and the nutrient supply. They used 10 ml instead of 1 and replaced it only every third day. Sizes of biopsies were similar. On the other hand, there are protocols available that recommend a medium exchange every or every second day [76]. We would expect that the more frequent exchange and the supply of nutrition is beneficial but handling the biopsies so often might also disturb ongoing processes and cell homeostasis.

To show the effect of cultivation over time and to have an easier comparison with the MTT results, we expressed the viability relative to the value of the untreated control at the beginning of the experiment (day 0). For most time points, the measured values in the FACS were comparable to the MTT results with a tendency to higher viability percentages for the controls in the FACS. After 7 days of incubation of untreated skin, differences were the highest when FACS showed about 60% viable cells while MTT had only 30%. This fits to the mentioned theory that the MTT assay is mainly influenced by the cells at the edges that are more exposed to the environment.

The PEI that I used as transfection control, showed dose dependent toxic effects in both assays. For the highest dose of 12  $\mu\text{g}$  mRNA, the viability was reduced to 36% at the first time point already. This PEI-mediated cell death is probably caused by acute reactions of the cells instead of the mRNA cargo and the transfected protein. The skin tissue did not recover from the exposure but continuously

showed reduced viability number after PEI application. In contrast, the LPNs were as well tolerated as PBS confirming the good results from cell line experiments.

### *Selection of best time point to measure transfection efficacy*

After the cultivation setup, the next step was to select and optimize the readouts. The quantification of transfected cells is most commonly performed on day 3 [32, 175]. With our good viability after 4 days, there is a chance that skin cells produce the encoded protein. This signal might also be detectable already after 24 h with the FACS because at least for DNA tattooing, first luciferase signal appeared after 2 h, had a maximum after 20 and diminished after 72 h in *ex vivo* skin and mice [50, 230]. Probst et al. detected the encoded antigen for several days after intradermal injection of mRNA and claimed that the uptake mechanism differs from that of tattooed DNA [234]. In any case, the presence of endonucleases of the skin is a problem for such naked nucleic acids and compensated with high doses [235] that I avoided by complexation on the LPNs which might even increase transfection rates.

The selection of the best time points for the readout remains difficult as this effect is also dependent on the used nanocarrier, nucleic acid and application route. Profiting from our experience with the LPNs *in vitro*, we decided to use the fluorescent protein mCherry again and to digest the skin tissue keeping the option to later add an antibody panel to specify the cell populations in more detail. Despite reports about successful detection of GFP transgene in human skin explants [32, 175], we found high autofluorescence signals in the green spectrum and decided against this option. If the focus is only on the quantification of protein expression, using luciferase-encoding mRNA would be more straight forward. One could measure the signal of the same biopsy every day to find the best time point for the more detailed analyses.

In our case, I digested the skin sample for analysis and thus needed a new biopsy for every condition and every day. This is time, cost and material consuming and has the risk of additional variations due to unequal skin conditions. If only one skin piece is needed per condition with the luciferase readout, the saved material can be used to have triplicates of every group and consolidate the findings. Next to this easier readout, luciferase and the measured luminescence intensity has the advantage to have a smaller background signal without any interference with autofluorescence and enables spatial resolution. It is therefore commonly used in mouse studies, especially for systemic administration protocols when site of transfection is not predictable.

### *Benefits and Limitations of the Skin Digestion Protocol*

Digesting the tissue had some advantages, too. As mentioned before, it can be combined with a live-dead staining to quantify the viability and by adding a panel of antibodies, cell populations can be specified. Next to this detailed differentiation, it is also possible to separate skin layers prior to digestion to specify findings. The border between epidermis and dermis, the basal membrane, is most sensitive to enzymatic digestion. We used this property in our mouse study to show the immune response in more detail. This would also be possible with the human abdominal skin. Indeed, the applied digestion procedure with the kit resulted in some kind of unwanted separation of the skin layers. For most biopsies, we found three or more (out of four in theory) larger pieces of epidermis in the cell strainer after filtration of the single cell suspension. I transferred these epidermis pieces with a needle to a glass slide, spread it out and fixed it immediately with mounting medium. The areas seemed larger than the original 11 mm diameter of biopsies, maybe because of swelling of the tissue or simply the lack of little skin folds that were now spread out. For P.L.E.A.S.E.<sup>®</sup> treated samples, pores were visible as empty squares without cells with the bare eye. Microscopic analysis did not allow any conclusions as imaging parameters in the fluorescence channel did also exhibit signals in the PBS controls. In this case, I did not use the confocal microscope to have a larger

imaging window and an overlay with the bright field image but analyses clearly indicate that autofluorescence is a problem for the mCherry readout.

For epidermis samples, an endogenous fluorescence in the red spectrum between 610–680 nm next to the strong blue fluorescence was published [236] which interferes with the mCherry emission wavelength at 610 nm. Depending on the excitation source, others reported the maximum autofluorescence around 480 nm with a long decline above 600 nm [237, 238]. A decrease in autofluorescence with cultivation time was reported [239] which fits to our findings of reduced background signal for the PBS controls at day 4 and 7. It is also known, that the microbiome, diseases like diabetes and lifestyle factors such as diet or flavonoid intake can increase the skin's autofluorescence and thus increase the variations between donors [236]. At the end, this might be the reason for the high standard deviations of the PBS control after pooling the data sets.

Similar problems with a lack of signal in FACS and microscopy after intradermal injection was published for DNA encoding for the green fluorescent protein [240], as well. One reason for their observation might be the quenching of signal under acidic condition in the endosomes [50, 241]. For the mouse ear, there are reports that a protein signal is detectable already 1 d after intradermal injection of naked DNA when using fluorescently labeled antibodies for microscopy [35]. Expecting the mRNA to show an even faster effect, the mCherry signal intensity might also be the problem. An antibody-based analysis would solve both problems, the probably low signal intensity and the interference with autofluorescence and maybe enable the detection of produced protein.

As a consequence of the observation of epidermis pieces, the kit digested mainly the dermis and FACS data represent dominantly these cells. Due to the higher layer thickness, the epidermal cells would anyway have only a minor influence on results when analyzed together with the entire tissue. Though, analyzing the epidermis separately has a better chance to see an effect of the P.L.E.A.S.E.<sup>®</sup> because the microporation will cross this entire layer and will therefore affect a higher proportion of cell in the population.

In the dermis, this situation is completely the opposite. Aiming for a minimally invasive application, we want to apply the P.L.E.A.S.E.<sup>®</sup> laser as superficial as possible. Compared to the total thickness of the skin, the P.L.E.A.S.E.<sup>®</sup> microporation hits only the upper parts of the tissue. In the dermis, the number of affected cells is probably very limited which might be a problem for the transfection evaluation as not even all of these cells with LPN contact will be transfected. van den Berg et al. showed that about 2% of epidermal cells express the encoded antigen after DNA tattooing and that the vast majority of these cells that are keratinocytes and less than 1% Langerhans cells [50]. Blakney et al. reported a maximum transfection rate of 2% for the entire skin tissue [32]. If this is the maximum effect to expect, it is very difficult to detect differences because our background signal was already higher than that, probably due to regular autofluorescence as discussed above. Expecting only small differences of treated and untreated samples, these high variations jeopardized any conclusions. One possible strategy to cope with this problem would be a separate analysis of epidermis or the selection of another smaller population where expected transfection rates and signal-to-noise ratios are supposed to be higher. Additionally, an alternative readout signal like luminescence with a smaller background might finally show the effect of the LPNs. More biopsies per treatment group might further reduce the standard deviations.

### *Cell Counts in Collected Medium Supernatants after Skin Cultivation*

Following the same principle to reduce the population size, I collected the medium of the biopsies and analyzed the number and characteristics of the cells. In theory, the activated immune cells of the skin migrate to the draining lymph node to stimulate antigen-specific T cells. After application of mRNA-containing formulations and successful transfection, stimulated immune cells would end up in the medium. We would expect that their number increases especially at the beginning as they initiate the adapted immune response and that their number correlates with the intensity of signal of transient antigen expression. It can be considered as sign of immune activation and works well as supported by the following reports.

Machado et al. for instance specified the cells collected 48 h after epidermis targeting PLEASE microporation and intradermal injection in explant human skin. In their case, 50% of migratory cells with an MHC-II receptor were dermal DCs and only 1–2% LCs [242]. With similar results, Tajpara et al. evaluated the effect of tape stripping in *ex vivo* cultured skin and observed migrating DCs after 48 h. For another study, they incubated untreated, separated epidermal sheets in medium and collected Langerhans cells with a purity of 92–95% in the supernatant after 24 h [76]. After intradermal injection of DNA into the mouse ear, 80% of non-adherent cells in the supernatant after 3 days were MHCII-positive and able to stimulate CD4<sup>+</sup> T cells *in vitro* [35, 243]. Larsen et al. counted the cells they found in the supernatant of rat ears. In the first 24 h, they found up to 10,000 cells per ear, a number that none of our samples reached. The suspension cells, mainly LCs, had a 25-50 times on day 1 and 75-100 times on day 3 higher activity than spleen extracts [243].

In our case, the number of live cells in the medium decreased with time ending in less than 500 cells per biopsy after 5 days (Figure 61). Most cells migrated within the first 48 h which is in concordance with the mentioned reports. The most potent epidermal APCs were found in the second interval (1–3 days) which fits to our results at day 2 with most live transfected cells after mRNA exposure. Overall, this confirmed our expectations that the acute reaction of immune cells happens fast, but the used setup showed some limitations.

Surprisingly, highest numbers were detected for the naked PEI polymer without mRNA and PBS. Observed hints for the cytotoxicity of PEI in our viability assays might explain this stimulation. The intradermal exposure to the strongly charged polymer might hit a threshold for danger signals leading to the migration of cells. If PEI is applied after microporation, skin is not as much exposed, and this threshold is not reached. In contrast, PEI with mRNA that showed toxic effects in viability assay, too, did not lead to enhanced migration of cells.

We can only speculate why number of migrating cells after PBS application was that high. One reason might be the general application techniques of injection and microporation but untreated skin samples had comparable numbers after 48 h. In that case, the reason might be the general handling of the skin after surgery as hypothesized by Machado et al. [242].

If all other samples show less cells, there might be an issue with the collection of cells as well. Activated, migrating immune cells change their shape and become more adherent [244] which is in contrast to the cited references that report 80% of non-adherent cells in the supernatant to express the MHC-II receptor [35, 243]. Before collecting the supernatant, the medium itself was used to flush the wells. Maybe this procedure was not enough to detach cells from the bottom of the wells. We might have missed most of these relevant cells but collected the non-specifically moving ones instead. An easy way would be to check the wells under the microscope for left-over cells after supernatant collection which was not done. Alternatively, one could transfer the biopsy to a new plate with fresh medium to get an empty plate containing the supernatants instead of simply replacing the medium. In general, larger biopsies or pooling of samples might help to increase the number for more reliable analysis.

### *mCherry Positive Cells in the Supernatants*

Taking a closer look onto live transfected cells in the supernatants, we found again highest values for PEI without mRNA and PBS controls (Figure 62). Only after 2 days, there was a peak of live transfected cells for PEI complexed mRNA after injection that was little higher than the one without mRNA and the PBS control. We will later discuss how dependable such PEI signals are.

For LPN(70/30) without PEG, we measured little more live transfected cells in the medium after 3 days as for the PBS control (39 vs 36, respectively). Besides that, 2.5 mol% PEG in LPN(70/30) combined with P.L.E.A.S.E.<sup>®</sup> resulted in about 50 live transfected cells in the medium. That was little less than the injected PBS control but about double as high as PBS combined with P.L.E.A.S.E.<sup>®</sup> (54 vs 29). Intradermal injection of this LPN did not cause any migration. This might be a hint for successful stimulation of immune cells by this LPN.

24 h after naked DNA on gold nanoparticles was applied with a gene gun to the epidermis, there were 50–100 transfected DCs found in draining lymph nodes while total number of DCs was above 20,000 [245]. Our low number of live transfected cells in the supernatant seems to be at least in the range of this report.

### *mCherry Positive Cells in the Single Cell Suspensions of the Skin Biopsies*

If live transfected cells ended up in the medium between 24 and 48 h after treatment (sampling of supernatant after 2 days), there should be a signal of live transfected cells in the digested biopsies after 24 h. The highest transfection rates were found at the first analysis time point (0 d) though (Figure 63). Percentages were almost double as high as the PBS controls (10 vs 19% of live cells) but insignificant due to the high standard deviations of the PBS controls. These 0 days-samples were never in contact with the medium because digestion process was started directly after application of formulations. The biopsies were only cut in 8 pieces and 4 of them were incubated overnight in the enzyme mixture. The skin cells apparently took up the formulation and produced the protein also in this submerged state until they were fixed in PFA directly before FACS analysis on the next day.

After 1 and 4 days of cultivation, we found a stable number of 10% transfected live cells after 2.5 mol% PEG in LPN(70/30) and P.L.E.A.S.E.<sup>®</sup> application. The graphs of these time points still appeared very different, because of the high background signal of the PBS samples at days 1. At 4 days, the 10% live transfected cells of the 2.5 mol% LPN(70/30) was double as good as the PBS control representing the only significant difference in this study. This statistical test can only give hints as number of samples per group was not equal. For the 2.5 mol% PEG in LPN(70/30), there were only one data point for 0 and 1 day each, and 2 for 4 and 7 days while PBS controls had 5 or 6 values per time point. Especially at day 0, other groups with several samples had high standard deviations. This lack of replicate for 2.5 mol% PEG in LPN(70/30) may therefore lead to an overestimation of transfection potential. After 7 days, the number of live transfected cells decreased to 5%. For the first time in this study, the number of transfected cells in the entire population (including cells with membrane damage) was higher than in the live cell population.

For the other LPNs, there was not such a clear sign for successful transfection. For LPN(70/30), the only positive signal was the high standard deviation of P.L.E.A.S.E.<sup>®</sup> combined sample at day 0 generated by one data point above 20%. All other readouts were on the level or below the PBS control. For 5 mol% PEG in LPN(70/30), the injection led to about 19% live transfected cells at the first time point but due to the variation of PBS control it was not significant. The next day, this transfection rate was still on the level of PBS and on day 4 little above PBS (5.9 vs 4.4) but variations did not allow conclusions. In contrast to the 2.5 mol% PEG in LPN(70/30), these results were generated after intradermal injection whereas the P.L.E.A.S.E.<sup>®</sup>-assisted application led to values that were only half as high.

Focusing only on the numbers of the 2.5 mol% PEG sample, the stable percentage of live transfected cells might be caused by transfected keratinocytes. With 83%, they make up by far the highest cell population in the skin whereas immune cells comprise only about 7% (0.8% DCs and 3.8% LCs) [32]. It was published that these keratinocytes are mainly transfected without the chance to migrate. At least for DNA vaccines it was reported that such transfected keratinocytes are responsible for inducing the T cell response [50, 246–248]. They can produce the protein and present it via the MHC I receptor towards immune cells, a process called cross-priming, or antigen presenting cells could uptake the produced protein after death of transfected keratinocytes [247, 249]. From our observations, we could hypothesize that 2.5 mol% PEG in LPN(70/30) successfully transfected keratinocytes and maybe directly primed some immune cells within the first hours after application. The protein production stimulated immune cells either by cross-presentation via keratinocytes or by direct transfection. These activated cells were found mainly in the supernatant after 2 days. The keratinocytes that stayed in the skin continued production of the protein until tissue viability decreased. The shift towards more dying transfected cells after 7 days at the expense of live transfected cells might be an indicator for this process. This transient protein production would probably end shortly after.

This hypothesis is underline by reports in literature. After epidermal application of DNA by skin scarification, the nucleic acid was mainly taken up by the keratinocytes that expressed the antigen for up to 12 weeks after three vaccinations [22, 247]. This expression of antigen may serve as reservoir for immune cells as their stimulation is critical for the response [23, 250]. After a single application, Akbari et al. found first transfected cells after 3 and a maximum after 10 days in the entire skin which is in line with findings after gene gun bombardment [18, 247]. In contrast after one month, the signal was only present in the dermis. Activated immune cells had left the tissue to the lymph node where they expressed the antigen as well for 2 weeks. They attributed the transient expression of the dendritic cells to their half live of less than a week [247, 251]. Using mRNA will probably shorten the time of expression but the circumstances might be similar in our case. The general principle, that a small number of activated DCs was enough to generate a protective immune response can be certainly applied to any skin vaccination [247]. Maybe even the live transfected cells in the supernatant are enough.

### *Exposure of the Skin Tissue after Different Application Routes*

As mentioned before, these observations apply only to 2.5 mol% PEG in LPN(70/30) combined with P.L.E.A.S.E.<sup>®</sup> microporation. After intradermal injection, we did not find transfected cells in the supernatant. In the digested biopsies, numbers after injection of 2.5 mol% PEG in LPN(70/30) were comparable to the P.L.E.A.S.E.<sup>®</sup> sample but injected PBS controls had an even higher standard deviation. The results of the other LPNs were even closer to the PBS controls. After 4 days, when we saw significant differences in the P.L.E.A.S.E.<sup>®</sup> sample with 2.5 mol% PEG, the percentage of injected sample was much lower (7% vs. 12% with P.L.E.A.S.E.<sup>®</sup>; both PBS controls at 4%). These observations emphasize the superiority of epidermal application that was shown before in several of the mentioned studies (see 1.2.2). Details of the P.L.E.A.S.E.<sup>®</sup> administration will be discussed in the next chapter 6.3. In any case, it underlines the importance of comparing only to the controls with the same application method.

This lack of transfection signal after injection in digested skin biopsies contrasts with the exposure of the skin tissue (Figure 53). For laser-assisted application, the signal of DiD-labeled nanoparticles led to high fluorescence in the epidermal layer and less in the upper dermal layer. This trend was the opposite for the intradermal injection with only little signal in the epidermis but an intense signal in the dermis on a generally much higher lever. This low epidermal exposure after intradermal injection is in concordance with published findings for the double-stranded RNA analog p(I:C) [76].

Furthermore, Machado et al. already published that general skin exposure is 50times less after

P.L.E.A.S.E.<sup>®</sup> administration when using 4 pulses per pore instead of 8 as we did [242].

We did not observe changes within 24 h of cultivation for any formulation. The nanoparticles seemed to stay at their macroscopic position. As discussed before, the purpose of the pegylation was to improve tissue penetration and reduce adsorption of proteins. We did not get the impression of an improved distribution and penetration of the tissue but did neither quantify the observations nor the cellular uptake into skin cells. When nanocarriers were applied on intact skin, the stratum corneum prevented their penetrations. Even for the much smaller p(I:C), the skin is an unbreachable biological barrier [76].

The intradermal injection exposes many more cells to the formulation but this did not lead to a stimulation of an immune response in our setup. This might be because of methodological limitations in the cultivation or the readout leading to oversteering the signal but it might be as well due to toxic effects. The high exposure after intradermal injection might generate such a high danger signal that the innate immune system is stimulated and clears the tissue from LPNs instead of eliciting adaptive responses. The nanoparticles might be digested without the chance to deliver the mRNA.

### *Limitations of PEI as Positive Control for the Experimental Setup*

Such an acute reaction might be caused by the application of PEI as well as we observed a dose dependent cytotoxic effect in the human abdominal skin model (Figure 56). In contrast to the 2.5 mol% PEG in LPN(70/30) signal at day 4, the mCherry positive population did not metabolize the live cell dye FDA. One could speculate that such cells are successfully transfected after the PEI application and produce so much protein that it reaches harmful cytosolic levels which then stops the metabolism of FDA and a lack of live cell signal. A second possible explanation is related to the well-known toxicity of the polymer. On the one side the presence of the polymer strongly activates the complement system which fits to the high number of migrating cells in the supernatant [175, 199]. On the other side, dying cells undergoing apoptosis would change their characteristic profile in forward and sideward scatter in the FACS. Additionally, these cell death processes might change the autofluorescence pattern of the cells leading to high signals in the far-red spectrum overlapping with mCherry fluorescence. Thus, the high signal in the mCherry channel might be false positive.

I thus performed a control experiment with PEI but without any nucleic acid and observed similarly high percentages of “transfected” cells (Figure 64). We can conclude that the PEI-mediated signals in the mCherry channel are rather artefacts than truly positive cells.

In literature, there is one report about successful transfection of cells after intradermal injection of PEI complexing self-amplifying RNA into human skin explants [175]. Best results with 8% GFP expressing cells were generated with a weight ratio of 20:1 of polymer to nucleic acid which corresponds to our preparation procedure. They do not report about viability status or observed toxic effects in their skin model. Maybe the problem with worse results with our PEI is associated with the lower quality of the raw material as they used a special transfection grade and observed no acute toxic effects. Another difference is the higher molecular weight of 40,000 instead of our 25,000 but for linear PEI it was shown that this does not affect good transfection properties at least *in vitro* [113]. It needs to be tested if reported findings about PEI quality and transfection efficacy apply also to mRNA.

The purpose of adding PEI was to have a well working positive control for our skin model. With the findings of the naked PEI polymer, our model lacks such a process control. This is also the case for published skin models that report, if any, only the effect of naked mRNA [32]. Our results clearly support the importance of standard negative controls for background fluorescence like untreated skin or PBS undergoing same application procedures. Furthermore, a comparison with unloaded versions of the LPNs would be reasonable.

Coming back to the implementation of a better positive control, the application of the control with

the P.L.E.A.S.E.<sup>®</sup> system would be the best reference but to our knowledge this is the first time, that the laser system was used to apply mRNA-loaded nanocarriers. Alternatively, the intradermal injection of an optimized carrier from a published report might be an option as well. The solid lipid nanoparticles of Blakney et al. seem to be the appropriate candidate because they showed its ability to transfect cells in human skin explants by delivering mRNA [233]. I could also test if the approved Covid-19 vaccines that are usually intramuscularly injected, elicit a signal in skin. The applicability of approved vaccines with the P.L.E.A.S.E.<sup>®</sup> instead of intramuscular injection was shown before at least for protein antigens [64].

### *Evaluation of the Applied mRNA Dose per Skin Biopsy*

A last point to consider, is the applied dose in our *ex vivo* human skin model. A regular human dose for the BioNTech Covid-19 vaccine is 30 µg mRNA [252]. In our human abdominal skin model, I injected 8 µg mRNA per biopsy. This is even 3 µg more than Blakney et al. for successful intradermal injection [233] but much less than the approved vaccine. This difference is reasonable as the skin itself is much more immunogenic than the muscle. We have discussed that important benefit of targeting the skin in more detail in the introduction (see 1.2.2).

### *Short Summary of General Evaluation of Ex Vivo Human Skin Model*

Summarizing the described experiences with the human abdominal skin model, we saw several signs that 2.5 mol% PEG in LPN(70/30) after P.L.E.A.S.E.<sup>®</sup> microporation successfully transfected keratinocytes and stimulated immune cells to migrate out of the tissue. This degree of pegylation is expectedly the optimum as discussed in chapter 6.1 even though it was not possible before to show the benefits of this modification *in vitro*. The problem seemed to be mostly on the side of the presented *ex vivo* skin model that had some drawbacks jeopardizing any other solid conclusions. Most promising ways to improve it are changing the readout to luminescence, reducing population size, analyzing the epidermis separately, using antibodies for microscopic analysis and the addition of a better positive control to ensure skin quality and viability. It would also be possible to quantify transfection potential of the LPNs in primary cells again. Instead of bone-marrow derived DCs, one could use epidermal Langerhans cells that migrate into the medium after separation from dermis [76]. After such optimizations, the performance of the LPNs should be reevaluated to check if the faint signal is due to the bad performance of the tissue model or the carrier. In the next chapter, I will concentrate on the immunologic effects of the laser-assisted application with the P.L.E.A.S.E.<sup>®</sup> system.

### 6.3 The P.L.E.A.S.E.<sup>®</sup> Laser as Minimally Invasive Application Strategy for Nanoparticles

#### *Rational for the selection of the P.L.E.A.S.E.<sup>®</sup> system*

I will now address the benefits and the general potential that the combination of mRNA-loaded LPNs with the P.L.E.A.S.E.<sup>®</sup> system has and discuss how far we got on the way to a minimally invasive application of mRNA-based vaccines.

The original idea of a non-invasive application to the skin without harming its barrier function, is a fascinating approach but has not been realized yet due to some limitations. The main purpose of the skin is to form a barrier and to protect the body from its environment with its many resident immune cells that scan the tissue and maintain the integrity. As a potential entry port for pathogens, the hair follicle is an immune privileged organ within the skin and thus suitable for the non-invasive application of a vaccine. Larger and more solid structures like the one of polymeric nanocarriers were beneficial to deliver more antigen and to reach the deeper areas by a gear pump mechanism of the hair [57, 253]. With protein as antigen, it was not possible to deliver enough material to elicit a protective immune response. An adjuvant is needed in any case for this transfollicular vaccination strategy [169].

Exchanging the protein antigen to its mRNA has the potential for signal amplification and intracellular presence of foreign nucleic acid molecules will enhance the elicited CD8<sup>+</sup> T cell response. With these mechanisms, the limited intrafollicular delivery of nanocarriers might be enough for a sufficient immune response. This approach was tested in our lab with our collaboration partner at the HZI but T cell proliferation was only found after subcutaneous injection. The transfollicular route, even with adjuvantation, did not lead to specific T cell stimulation. Believing in the versatility of mRNA, we decided to change to a more invasive but still minimally invasive application method creating a higher available volume for the nanocarriers compared to the hair follicle. With the P.L.E.A.S.E.<sup>®</sup> system, we can create micropores of a distinct depth and number and clinical studies proved that this microporation is painless for human beings and pores are re-epithelized quickly [65]. In a second step, we can then apply our mRNA-loaded nanocarriers as liquid or creme.

#### *The Mouse Ear as Application Site for In Vivo Studies*

Next to the higher accessible volume of the micropores, the application process with the laser is more straight forward compared to the non-invasive route. For the transfollicular vaccination procedure, it is important to have as many hair follicles as possible and treat a large area to compensate for the low delivery of a single follicle. Furthermore, mice need to be shaved the day before to gain access to the skin which might already stimulate the immune system and influence the results. It is of course possible to treat this shaved skin with the P.L.E.A.S.E.<sup>®</sup> laser, too, as shown by published results but a high hair density is not essential anymore [242].

By changing to the ear as application site where mouse fur is less dense [173], we could even disclaim from the hair removal and diminish any influence from these preparation procedures. Mice could be treated directly on the first day of experiment. Another advantage of the application at the ear is the variety of available analysis techniques. The skin is rather thin, has a low hair density and can be easily harvested after cutting off the ear. The skin can then be pulled off the cartilage. Protocols for this simple preparation procedure are long known [243]. There are many ways published on how to separate and digest skin layers, to image the entire ear skin and the immune system is well characterized.

In our case, the only drawback was the limited area. Even after choosing a smaller adapter for the laser, it was not always possible to position the device in a way that the entire adapter area was in

contact with skin. In some cases, the effective area with micropores was therefore even smaller and some pores were lost.

### *Evaluation of Pore Density*

To get an estimation of the relevance of this problem, we can compare micropore number and hair follicle density. There was a linear relationship between pore density in the laser set up and number of created pores. In our pivotal study, I counted 16 pores for 1% density and 292 for the maximum 15% density (Figure 36). Transferring it to the settings for the mouse ear (8%), we create approximately 100 micropores per ear with a total area of pores of 1.8 mm<sup>2</sup>.

For a rough estimation of the area the hair follicles cover, we have to draw several assumptions to deal with the lack of published data. Bronaugh et al. reported a number of 658 hair follicles per cm<sup>2</sup> at the back of mice [170] and Ibrahim et al. published that hair follicle density is reduced at the ear about three fold compared to the back [173]. If we then combine the expected 219 hair follicles with published diameter of human hair follicles orifices at the human arm (75–80 μm), the follicles at the mouse ear cover in total an area of 0.97 mm<sup>2</sup> [55]. This area corresponds to a pore density around 3% and about 35 pores in an 8x8 mm square (55 in a 10x10 mm<sup>2</sup>).

The available area for nanoparticle application to the hair follicle is even smaller as there is still a hair in the center of these orifices. There is no data available on the size of orifices in mice. An advantage of the hair follicle might be the resident immune cells in the follicle while the P.L.E.A.S.E.<sup>®</sup> microporation first needs to attract cells to the pores. Nevertheless, we expect that the area of micropores that is about double as high as the natural hair follicles (1.8 vs 0.97 mm<sup>2</sup>, respectively) will more than compensate for the immune cells of the hair.

The number of pores after microporation will be about half of the hair density (100 vs 219, respectively), but every pore is much larger and has no hair in the center. The massage of formulation into the pore will be easier and the chance that enough cells get in contact with the nanoparticles raises.

For a potential treatment of human beings, the switch from mice to humans greatly influences this comparison with even more benefits for the laser-mediated application. The laser and the vaccine would probably be applied on the arm due to its good accessibility. There, reported hair follicle densities range from 17 to 32 follicles per cm<sup>2</sup> [55, 254] with an total available area of 0.08–0.14 mm<sup>2</sup>. The 100 micropores with the selected P.L.E.A.S.E.<sup>®</sup> settings would be 3–5 times more and the covered area would be at least 12 times higher than the hair follicles.

A higher hair density in human beings that is comparable to the one at the mouse ear is found only at the lateral forehead (300 hair follicles in human versus >650 in mice [55, 170]). But it is unrealistic that clinicians would be approved to apply the laser and the formulations there.

Using the P.L.E.A.S.E.<sup>®</sup> device instead of the transfollicular route increases the deliverable amounts and thus the chance to elicit a protective immune response. Furthermore, it allows the change of application site independent of hair density and emphasizes the benefits for the patients.

To summarize, we can claim that a suboptimal positioning of the laser on the ear and the consecutive loss of some pores is probably not a problem. The total area will still be far above the one of the natural hair follicles. Additionally, we do not destroy the hair follicles. They are still accessible for the formulation and might to a low percentage also contribute to the response.

### *Evaluation of Pore Depth to Optimize Immune Cell Reaction*

Besides the pore density, the P.L.E.A.S.E.<sup>®</sup> system allows the determination of depth of micropores. We wanted to investigate if superficial pores in the epidermis are enough or if the immune reaction is improved when pores hit the dermis as well. Literature research on skin layer thickness in mice resulted in only two publications reporting concrete numbers. Ibrahim et al. measured 90  $\mu\text{m}$  at the ear and 280  $\mu\text{m}$  at the back for the whole skin, while Bronaugh et al. published 840  $\mu\text{m}$  for the back [170, 173]. As these numbers differ a lot, we decided to rely more on the experience other scientists had with the P.L.E.A.S.E.<sup>®</sup> system on the mouse ear. Terhorst et al. administered protein-based vaccibodies successfully after P.L.E.A.S.E.<sup>®</sup>-mediated microporation at the mouse ear and measured potent antitumoral responses [67]. We used their parameters and compared it to a deeper set-up with 4 instead of only 2 pulses per pore.

We observed that the number of Langerhans cells in the epidermis decreased within 24 h after application of the P.L.E.A.S.E.<sup>®</sup> while activation markers increased. First changes were detectable already after 3 h (Figures Figure 39 and Figure 40). This fast reaction supports the hypothesis that the laser microporation generates a danger signal and activates the immune system. The Langerhans cells were stimulated and started their way through the dermis towards the draining lymph node. This is further supported by the shown upregulation of CD86 as a known response to danger signals. It is needed for the co-stimulation of T cells and thus a sign of dendritic cell maturation [244]. Such an unspecific immune stimulation after tissue manipulation is in concordance with available literature. For instance, tape stripping causes a comparable boost of CD86 activation markers on Langerhans cells [76]. The general activation of skin by sensitizing with FITC caused an increase of DC number in lymph nodes already after 6 h, with a maximum after 48 h [39]. A reduction of Langerhans cells in the epidermis after 24 h and the subsequent movement path was shown after transplantation of mouse ear skin to the back. In parallel, they proofed that the skin injury alone sufficiently stimulates the LCs in a similar way [243]. Machado et al. suggested such a wound healing like process happens after P.L.E.A.S.E.<sup>®</sup> treatment as indicated by cytokine and invading cells profiles [242]. We can conclude that the generation of a danger signal by the created microwounds with the P.L.E.A.S.E.<sup>®</sup> laser seems to be responsible for the immunostimulatory effect of the microporation.

Following the migration of Langerhans cells, we would expect an increase of LCs in the dermis, but we saw a decrease instead. This might be a problem in the calculation of percentages as invading monocytes and neutrophils increased the overall cell count of immune cells in the dermis. Thus, a constant or increased number of Langerhans cells would appear as a smaller percentage of this total immune cell population.

Monocytes and neutrophils are recruited from the blood stream and take the opposite way than the Langerhans cells. They first appear in the dermis with elevated activation marker levels and later, after 24 h in the epidermis which is supported by the presented data and in line with literature [40, 255]. The neutrophils as part of the acute reaction appeared already after 3 h in the dermis, while monocyte levels were mainly elevated after 24 h. This order fits well to the known function of the neutrophils. They react first, take up material like nanocarriers or cell debris, release their cytokines and thereby attract more immune cells like monocytes [256]. On the other side, there is the risk that uptake into neutrophils might result only in the destruction of cargo and carrier instead of transgene expression as their main function is phagocytosis and not the presentation of antigens on their surface [257, 258].

The spatial analysis with the CLSM confirmed that the MHCII positive cells like monocytes are attracted by the microporation (Figure 38). In the dermis, they assembled in a round shape around the hole while in epidermis we observed only an increase in general number and signal intensity after 24 h. We can speculate that immune cells would form a circle also in epidermis when having more

time. This is in line with the published findings, that skin disruption mobilizes skin resident dendritic cells [47, 259–261] and expression levels of MHCII are increased [243]. Wang et al. observed a maximum accumulation of MHCII positive cells 24 h after treatment of the skin with a different, non-ablative laser. The analyzed cytokine levels showed a similar profile like in our case with an onset after 6 h, the maximum after 24 h and resolution after 48 h [58]. Thus, our 24 h time point seemed suitable to show the maximum differences between laser settings.

### *Enhancement of Immune Stimulation after LPN Application*

This microscopic analysis proofed that the shallow pores, created with only 2 pulses per pore, end in the epidermis while deeper pores (4 pulses/pore) hit the dermis as well. This second type of micropores enhanced the effect onto immune cell migration and activation markers for LPNs and PBS controls.

Concentrating on the migration of immune cells first, mRNA-loaded LPN(70/30) stimulated as many cells as the PBS control when applied after deep microporation (Figure 41). After shallow pores, results of LPNs indicated a lower stimulation than after PBS. There were more Langerhans cells left and less invading neutrophils and monocytes than in the PBS control but still more than in the untreated control.

Comparing the effect of the two laser treatments in combination with the LPNs, especially in the epidermis, there were highly significant differences with benefits for deeper pores. In the dermis, differences were lower but still significant for monocytes.

It was surprising to see that the shallow pores ending in the epidermal skin layer also influenced cells in the dermis and elicited an effect almost as high as the deeper pores. This effect is probably due to the laser treatment itself as presence of LPNs did not further enhance the response above PBS control in most cases. In any case, this general stimulatory effect of the P.L.E.A.S.E.<sup>®</sup> differed clearly from the untreated control.

Despite comparable effects of LPNs and PBS onto cell movements when applied with deeper pores, the activation markers were about double as high when exposed to the nanocarriers compared to PBS (Figure 42). As discussed before, the P.L.E.A.S.E.<sup>®</sup> treatment leads to a general preconditioning of the skin via the secretion of inflammatory chemokines by skin resident cells that promote maturation and migration of antigen presenting cells [58, 242]. This proinflammatory milieu probably helps when skin cells are exposed to LPNs by generating an additional signal. The threshold for an adaptive immune reaction may be easier reached as such a potent reaction is only elicited if the signal intensity is strong enough and endures long enough. This additional second signal after LPN application is missing in the PBS control.

This higher stimulation of immune cells after LPN contact could be a sign for synergistic effects but it does not allow any conclusion about the translation status of the antigen encoded on the delivered mRNA. The presence of foreign mRNA in the cytosol could already stimulate defense mechanisms via pattern-recognition receptors. We chose a modified mRNA to reduce that immune stimulatory effect and to enable stable transfection, but its presence could still change the activation status of the cell. Both microporation settings resulted in similar levels of activation markers. This supports the theory that the microporation facilitates immune activation independent of pore depth and therefore may enhance the effect of skin vaccinations.

Summarizing the described observations, the shallow pores would be enough to increase the activation status of cells but deeper stimulated more cells to migrate. Destroying more cells with the deeper pores, potentially increased the intensity of the danger signal and the threshold towards a protective immune response is probably more easily reached with potential benefits for the success of the applied nanocarrier vaccine. An additional argument for the deeper pores is the added safety

effect. The thickness of skin layers is not always predictable and the basal plane is not straight but folded. Creating pores that are several micrometers deeper than the estimated border, reduces the risk of accidentally hitting only the epidermis. In any case, there were several signs that the laser treatment indeed has an influence on the immune system with the chance for synergistic effects when pores reach down to the dermis and are combined with mRNA-loaded LPNs.

### *T Cell Stimulation in Adoptive Transfer Mouse Model*

To answer the question if the delivered mRNA is also transcribed, we tested the LPNs in combination with the deeper pores in an adoptive transfer animal model. LPNs failed to stimulate antigen-specific T cells, both in the lymph nodes and in the spleen.

This might be a problem of the nanocarrier itself but also due to the low dose. In this experiment, we applied only 3.13 µg of mRNA per animal while it was 7.84 µg in the previous study with the laser optimization. Additionally, the LPNs were dispersed in 20 µl per ear instead of 10 µl which exceeded the liquid capacity of the ear. The effective dose might even be lower and thus simply lay beneath the stimulation threshold.

On the other side, the P.L.E.A.S.E.<sup>®</sup> laser worked well (Figure 43). When combined with protein instead of mRNA, we found CD4<sup>+</sup> T cells levels in the lymph node that are comparable (>85% of CD4<sup>+</sup> T cells) to the measured levels after subcutaneous injection of protein and adjuvant. The CD8<sup>+</sup> T cell levels were about 30% lower. The P.L.E.A.S.E.<sup>®</sup> laser enabled a stimulation of CD4<sup>+</sup> and CD8<sup>+</sup> T cells in the spleen about half and a third as high as injection, respectively.

This preference for CD4<sup>+</sup> T cells met the expectations as extracellular proteins are mainly recognized by immune cells and presented via MHCII that preferentially elicits a CD4<sup>+</sup> T cell response. For the subcutaneous control, the adjuvant CDA as nucleic acid derivative was added that is known to support in the CD8<sup>+</sup> direction resulting in a balanced immune reaction [262].

The trend with a CD4<sup>+</sup>-based stimulation after protein application was shown before in combination with the P.L.E.A.S.E.<sup>®</sup> device on mouse ears. Terhorst et al. reported percentages of 44% for CD8<sup>+</sup> and 86% for CD4<sup>+</sup> proliferating T cells in the draining lymph nodes. Their reduced activation of CD8<sup>+</sup> T cells might be caused by the application of a lower dose (3,3 µg OVA-protein instead of 5 µg in our case) or the selection of only 2 pulses per pore [67] as our experiments showed that the creation of deeper pores enhances the immune response.

Furthermore, the readout time point could simply be too early for the quantification of proliferating T cells in the spleen. At least for skin scarification with naked DNA, it was shown that CD4<sup>+</sup> T cell levels in the spleen are elevated after 15 days while proliferation in lymph node changes already after 3 days in a similar mouse model [247].

These results support our general approach and show that the minimally invasive vaccination is possible with the P.L.E.A.S.E.<sup>®</sup> system. A needle was not needed to overcome the skin barrier. The effect is comparable to the invasive subcutaneous injection in combination with a strong adjuvant representing the gold standard in this animal model. Differences in immune response would be even higher when protein without adjuvant is applied by subcutaneous injection even though we did not test that.

### *Transfer of laser parameters from Mouse to Human Skin*

These findings about optimized laser parameters needed to be transferred from the *in vivo* studies in mice to the human skin model. Because of the differences in layer thickness between mouse and human skin, the P.L.E.A.S.E.<sup>®</sup> parameters needed to be translated.

Expectedly, the exact same parameters of the mouse ear with 2 pulse per pore created pores that were too superficial and hardly detectable in the human skin (Figure 51). Applied nanoparticle would probably not stay in the pore but rather be wiped away during sample preparation. The deepest pores after 21 pulses caused burn marks at the upper edges of the pores which hindered re-epithelization. This prolonged disruption of skin barrier may later cause problems like bacterial infections or unwanted inflammation and pain.

Using 8 pulses per pore fulfilled our criteria to hit both skin layers without signs of burned tissues. Furthermore, these pores were re-epithelized after 24 h. We could even proof that applied nanocarriers – in this case fluorescent polystyrene nanoparticles – are enclosed under the newly built epidermis building a kind of depot and thus giving the cells more time for uptake. The concentration of the used FluoSpheres<sup>®</sup> was four times higher than the LPNs. The expected number of mRNA-loaded LPNs that end up in this cavity will be correspondingly smaller. We hypothesized that the higher viscosity of the LPN formulation after lyophilization helps to increase the time the LPNs stay in the pores until the APC like dendritic cells and macrophages appear but this needs to be proofed. The majority of nanoparticles anyways remained on the surface. Nevertheless, this set of laser parameters was used for the human skin model.

### *Versatility of Invasive Methods as Comparison for Laser Microporation*

The P.L.E.A.S.E.<sup>®</sup> laser worked in combination with proteins, but it was not clear if the lack of effect after mRNA application was a problem of the LPNs alone or of the combination with the laser. The *ex vivo* human skin model was implemented to investigate both options. Aiming for significant transfection levels in the skin first, the immune response could then be evaluated again in the mouse model. The general development process of the skin model has been discussed in 6.2 already. Here, the focus is on studying the potential benefits of the combined application with the P.L.E.A.S.E.<sup>®</sup> laser which raised the need for a second application method. The depot forming subcutaneous injection technique of the adoptive transfer mouse model could not be applied to the skin model as subcutaneous fat is removed prior to sample administration.

Due to the low hair follicle density in human abdominal skin and the low chance for successful transfection, the transfollicular route was not an option. *In vivo*, one could use intramuscular injection to compare the overall immune reaction and the needed mRNA amounts.

For the skin model, intra-epidermal application by tattooing or gene guns would be possible in theory, but this can be hardly realized and would add additional factors to the system. Having excluded all these options, only a direct injection into the skin remained. Intradermal injection needs some practice to guarantee the flat injection angle and applied volumes are limited especially with the 11 mm biopsies. As mouse studies showed that the P.L.E.A.S.E.<sup>®</sup> has the stronger effect when both epidermis and dermis are targeted, this injection technique seemed to be the fairest comparison and was therefore selected.

### *Reaction of the Skin Tissue after Different Application Routes of Nanocarriers*

Having all parameters adapted to the human abdominal skin, we compared this invasive intradermal injection, the laser-assisted application and the administration onto intact skin. First, I evaluated how many cells get in contact with the nanoparticles depending on the application route. When massaging the formulation into intact skin, the stratum corneum represented the predicted barrier to the LPNs. There were no nanoparticles detected in the viable skin layers. The P.L.E.A.S.E.<sup>®</sup>

treatment led to exposure of mainly epidermal cells with a few signals in the dermis. In contrast, after the injection we found almost all LPNs in the dermis and none in the epidermis. General exposure was much higher. In the previous chapter, we have already discussed the consequences of this exposure for the toxicity results but here I want to focus rather on the effects for immune reaction.

As mentioned before, the epidermis has a higher number of immune cells relative to the keratinocytes and bears the potential to compensate for the smaller number of cells that get in contact with the formulation. Ideally, specifically hitting mainly the immune cells of this epidermal layer is already enough to elicit an immune response while the rest of the skin is protected from any harmful influences. There are many published evidences that targeting the epidermis enhances the immune reaction. Seneschal et al. showed for example that the T cell response after skin scarification is stronger than injection into muscle, subcutaneous fat or even the dermis [27, 47]. The intradermal injection of naked DNA did not cause a luciferase signal above the background while tattooing raised it 10–20fold after 18 h [50]. Machado et al. confirmed this trend for the P.L.E.A.S.E.<sup>®</sup> system already. They found a 10fold weaker humoral and cellular response after intradermal injection of birch pollen compared to the laser, even though the exposure of tissue was about 50times higher when using the needle [242].

### *2.5 mol% PEG in LPN(70/30) with P.L.E.A.S.E.<sup>®</sup> as Most Promising Vaccine Candidate*

In line with these references, there were clear signs for transfected cells in the *ex vivo* human skin model only after the combination of the 2.5 mol% PEG in LPN(70/30) with the P.L.E.A.S.E.<sup>®</sup> system, but not after intradermal injection (Figure 63). In the supernatant, we found transfected cells for this sample as well which might be a sign for a reasonable immune reaction (Figure 62).

At the first time points, we found same numbers of transfected cells in the digested skin pieces after both application routes but after 4 days, when results became significant for the P.L.E.A.S.E.<sup>®</sup> sample, the number of live transfected cells was halved for injection samples. At the same time, the number of dying transfected cells increased allowing the conclusion that transfected cells died after the higher exposure following injection. As hypothesized before, the majority of transfected cells are probably keratinocytes that stay in place. The transfected immune cells leave the tissue toward the supernatant with a maximum after 48 h. We only measured for 24 h in the mouse and therefore might have missed the maximum effects but maybe a suboptimal cultivation in the skin model delayed the reaction as well. We can nevertheless assume that we observed the corresponding reaction in both models.

After the intradermal injection, there was no signal in the supernatant. The general exposure of the tissue was higher but probably hit only keratinocytes of the dermis. Without the attraction and non-specific activation of immune cells by the P.L.E.A.S.E.<sup>®</sup> microporation transfected keratinocytes are not able to elicit an immune reaction. This aspect is even more relevant *in vivo* as recruited blood cells invade the dermis first where they get in contact with the transfected cells for the first time. If the signal by keratinocytes is strong enough, they might then also stimulate a delayed immune response. Epidermal cells will probably not be involved as much. It needs to be tested *in vivo*, if and when this procedure really elicits an immune response and how strong it is compared to the P.L.E.A.S.E.<sup>®</sup> application. After 7 days of *ex vivo* cultivation, the translation of the proteins stopped in the skin model.

In summary, the results indicate a synergistic effect of the P.L.E.A.S.E.<sup>®</sup> microporation and the application of mRNA-loaded nanocarriers that outperformed intradermal injection. Findings should be solidified after optimization of the readouts in the *ex vivo* human skin model and followed by a comparison of elicited immune responses in a mouse model.

## 7 Conclusion and Outlook

Targeting the immune cells of the skin for vaccination purposes has the potential to improve the immunogenicity of applied vaccines with the chance to reduce needed doses and render adjuvants unnecessary. Safeguarding the integrity of the human body, the skin is an immune privileged tissue which is advantageous for vaccination but on the other side the high biological barrier to prevent pathogens and large molecules from penetration makes the application of vaccines difficult. As deliverable amounts of antigen are very low, it is a great opportunity for nucleic acids vaccines to show their benefits such as the feature of signal amplification by intracellular protein translation and the innate stimulation of immune receptors due to their presence in the cytosol. The aim of this work was to develop a vaccination platform combining mRNA-loaded nanocarriers for the first time with a minimally invasive application technique, namely the P.L.E.A.S.E.<sup>®</sup> laser, to transiently disrupt the outermost barrier and enable the contact of nanoparticles and immune cells of the skin.

Based on a published lipid-polymer hybrid nanoparticle (LPN), the influence of the lipid composition was investigated and tested with a model mimicking the challenging physiologic conditions of the skin. Studies revealed lack of colloidal stability and almost complete loss of transfection efficacy in the presence of medium supplements like serum for the original LPN, made of the cationic lipid DOTMA surrounding a polymeric PLGA core. Replacing the potentially toxic DOTMA stepwise with the zwitterionic phospholipid DOPE rendered the LPNs resistant to media components and generated good transfection rates in the dendritic cell line DC2.4 under this challenging conditions. For the best performing candidate composed of 70 mol% DOPE and 30 mol% DOTMA in the lipid layer (LPN(70/30)), performance in both medium conditions (with and without supplements) were comparable without a significant difference.

In parallel, the effect of medium components was specified by separately studying the influence of buffer, protein and RNase onto colloidal stability, mRNA binding and protection. While colloidal stability was the limiting factor for DOTMA-only LPN, it was the mRNA complexation for DOPE-only LPNs. RNase exposure experiment revealed that a loose attachment onto the nanoparticles' surface leading to a signal in gel electrophoresis is enough to protect the mRNA from degradation. This phenomenon was for instance found for LPN(70/30). The polymeric core showed its benefits for storage stability and robustness to lyophilization.

Raising the challenge further, this optimized LPN(70/30) was tested in primary bone-marrow derived dendritic cells and benefits of a higher DOPE content was again confirmed. mRNA delivery by this LPNs not only transfected these primary cells but even stimulated antigen-specific CD8<sup>+</sup> T cells indicating successful stimulation of presentation via MHC-I.

Despite these promising results, this LPN failed to elicit an immune response in an adoptive transfer mouse model and was therefore modified again by adding a pegylated lipid. Results in cell culture were comparable to the non-pegylated LPN(70/30) and underlined the need for more complex test systems for the nanocarrier optimization.

Facing the low correlation of *in vitro* and *in vivo* performance, an *ex vivo* human skin model was developed to test the nanocarriers already in human tissue and to enable an evaluation of the combined application with the minimally invasive P.L.E.A.S.E.<sup>®</sup> laser. Different cultivation and digestion protocols to generate a single-cell suspension were tested and further readouts like the collection of medium supernatants were implemented. The analyses of both cell populations focused on the viability and transfection status of cells. For supernatants, the total number of cells was considered, as well. Antigen contact in the skin leads to stimulation and activation of immune cells that then migrate to the draining lymph node to elicit a T cell-mediated, adaptive immune response. In case of the established human skin model, these cells end up in the supernatant.

## 7 Conclusion and Outlook

Next to the skin, the settings of the P.L.E.A.S.E.<sup>®</sup> laser were optimized to elicit the highest immune stimulatory effect. This was only possible in an animal study, as recruited leucocytes from the blood stream like monocytes and neutrophils represent one of the most important effects of the laser microporation. Micropores hitting only the epidermis were compared to deeper pores reaching down to the dermis. This second setup was more effective in stimulating Langerhans cells to evade, in attracting monocytes and neutrophils and in activating these immune cells. This effect was visualized by an antibody staining against MHC-II showing that the antigen presenting cells assemble in a round shape around the pore. Targeting the upper dermis with the deeper settings in an adoptive transfer mouse model, proofed the immune stimulatory potential of the laser microporation when combined with the protein instead of mRNA. Microporation stimulated CD4<sup>+</sup> and CD8<sup>+</sup> T cells almost as high as after subcutaneous injection with the strong adjuvant cyclic-di-AMP.

Having all optimized components in hand, the mRNA-loaded LPN(70/30) with and without pegylation was finally tested in the *ex vivo* human skin model. The laser-mediated application was always compared to invasive method of intradermal injection. Skin exposure after microporation was concentrated to the upper skin layers, especially the epidermis, while intradermal injection led to a generally much higher number of LPNs in the dermis and almost nothing in the epidermis. After application onto intact skin, no signal was detectable in the tissue.

In contrast to the high exposure of skin cells after intradermal injection, the most promising results were found after P.L.E.A.S.E.<sup>®</sup> microporation in combination with 2.5 mol% PEG in LPN(70/30). After 4 d of cultivation, live transfected cells differed significantly from the PBS control. The measured rates of transfected live cells were elevated the days before as well, but larger background signal and standard deviations rendered these findings insignificant. Nevertheless, detected live transfected cells in the supernatant, especially after 48 h, indicated the presence of antigen in the tissue. It can be hypothesized that the stable protein production rates in the skin biopsies are caused by transfected keratinocytes that stimulate immune cells by cross-presentation and cross-priming to migrate out of the tissue.

The presented studies emphasized the potential of laser-assisted, minimally invasive application of mRNA-loaded nanocarriers to the skin. Several indications for successful transfection and immune stimulation after administration of 2.5 mol% PEG in LPN(70/30) combined with dermis targeting micropores were found such as live transfected cells in the tissue and in the supernatant. Methodological limitations in the established *ex vivo* human skin model did not allow solid conclusions and leave room for optimization as has been already discussed. Though, using such a model adds many benefits to the nanoparticle development that cannot be shown in cell culture like the presented advantage of pegylation. Optimizing the skin model and reevaluation the performance of the mRNA-loaded LPNs will underline the potential of this developed nanocarrier. Results should then be confirmed in a mouse model with a dose of at least 8 µg mRNA per animal where the immune stimulatory effect of the P.L.E.A.S.E.<sup>®</sup> system can be fully unfolded. The next step would then be the challenge with the real pathogen to investigate the degree of protection. In that sense, the presented study paved the way for minimally invasive, mRNA-based skin vaccination by delivering the suitable test systems and a promising nanocarrier candidate.

## IV. References

1. Bianconi E, Piovesan A, Facchin F, Beraudi A, Casadei R, Frabetti F, Vitale L, Pelleri MC, Tassani S, Piva F, Perez-Amodio S, Strippoli P, Canaider S (2013) An estimation of the number of cells in the human body. *Ann Hum Biol* 40(6):463–471. doi:10.3109/03014460.2013.807878
2. Abbott A (2016) Scientists bust myth that our bodies have more bacteria than human cells. *Nature*. doi:10.1038/nature.2016.19136
3. Hu B, Guo H, Zhou P, Shi Z-L (2021) Characteristics of SARS-CoV-2 and COVID-19. *Nat Rev Microbiol* 19(3):141–154. doi:10.1038/s41579-020-00459-7
4. Anderson RM, May RM (1985) Vaccination and herd immunity to infectious diseases. *Nature* 318(6044):323–329. doi:10.1038/318323a0
5. Fine P, Eames K, Heymann DL (2011) "Herd immunity": a rough guide. *Clin Infect Dis* 52(7):911–916. doi:10.1093/cid/cir007
6. Shukla VV, Shah RC (2018) Vaccinations in Primary Care. *Indian J Pediatr* 85(12):1118–1127. doi:10.1007/s12098-017-2555-2
7. Bartsch SM, Wedlock PT, O'Shea KJ, Cox SN, Strych U, Nuzzo JB, Ferguson MC, Bottazzi ME, Siegmund SS, Hotez PJ, Lee BY (2021) Lives and Costs Saved by Expanding and Expediting Coronavirus Disease 2019 Vaccination. *J Infect Dis* 224(6):938–948. doi:10.1093/infdis/jiab233
8. Meyer H, Ehmann R, Smith GL (2020) Smallpox in the Post-Eradication Era. *Viruses* 12(2). doi:10.3390/v12020138
9. Dieu-Nosjean MC, Vicari A, Lebecque S, Caux C (1999) Regulation of dendritic cell trafficking: a process that involves the participation of selective chemokines. *J Leukoc Biol* 66(2):252–262. doi:10.1002/jlb.66.2.252
10. Steinman RM (1991) The dendritic cell system and its role in immunogenicity. *Annu Rev Immunol* 9:271–296. doi:10.1146/annurev.iy.09.040191.001415
11. Bhardwaj N, Young JW, Nisanian AJ, Baggers J, Steinman RM (1993) Small amounts of superantigen, when presented on dendritic cells, are sufficient to initiate T cell responses. *J Exp Med* 178(2):633–642. doi:10.1084/jem.178.2.633
12. Matsuo H, Yoshimoto N, Iijima M, Niimi T, Jung J, Jeong S-Y, Choi EK, Sewaki T, Arakawa T, Kuroda S (2012) Engineered hepatitis B virus surface antigen L protein particles for in vivo active targeting of splenic dendritic cells. *Int J Nanomedicine* 7:3341–3350. doi:10.2147/IJN.S32813
13. Cella M, Sallusto F, Lanzavecchia A (1997) Origin, maturation and antigen presenting function of dendritic cells. *Curr Opin Immunol* 9(1):10–16. doi:10.1016/s0952-7915(97)80153-7
14. Tarte K, Klein B (1999) Dendritic cell-based vaccine: a promising approach for cancer immunotherapy. *Leukemia* 13(5):653–663. doi:10.1038/sj.leu.2401394
15. Iwasaki A, Medzhitov R (2015) Control of adaptive immunity by the innate immune system. *Nat Immunol* 16(4):343–353. doi:10.1038/ni.3123
16. Adams NM, Grassmann S, Sun JC (2020) Clonal expansion of innate and adaptive lymphocytes. *Nat Rev Immunol* 20(11):694–707. doi:10.1038/s41577-020-0307-4
17. Condon C, Watkins SC, Celluzzi CM, Thompson K, Falo LD (1996) DNA-based immunization by in vivo transfection of dendritic cells. *Nat Med* 2(10):1122–1128. doi:10.1038/nm1096-1122
18. Klinman DM, Sechler JM, Conover J, Gu M, Rosenberg AS (1998) Contribution of cells at the site of DNA vaccination to the generation of antigen-specific immunity and memory. *J Immunol* 160(5):2388–2392
19. Dupuis M, Denis-Mize K, Woo C, Goldbeck C, Selby MJ, Chen M, Otten GR, Ulmer JB, Donnelly JJ, Ott G, McDonald DM (2000) Distribution of DNA vaccines determines their immunogenicity after intramuscular injection in mice. *J Immunol* 165(5):2850–2858. doi:10.4049/jimmunol.165.5.2850

#### IV References

20. Dubé E, Laberge C, Guay M, Bramadat P, Roy R, Bettinger J (2013) Vaccine hesitancy: an overview. *Hum Vaccin Immunother* 9(8):1763–1773. doi:10.4161/hv.24657
21. Taddio A, Ipp M, Thivakaran S, Jamal A, Parikh C, Smart S, Sovran J, Stephens D, Katz J (2012) Survey of the prevalence of immunization non-compliance due to needle fears in children and adults. *Vaccine* 30(32):4807–4812. doi:10.1016/j.vaccine.2012.05.011
22. Raz E, Carson DA, Parker SE, Parr TB, Abai AM, Aichinger G, Gromkowski SH, Singh M, Lew D, Yankauckas MA (1994) Intradermal gene immunization: the possible role of DNA uptake in the induction of cellular immunity to viruses. *Proc Natl Acad Sci U S A* 91(20):9519–9523. doi:10.1073/pnas.91.20.9519
23. Corr M, Lee DJ, Carson DA, Tighe H (1996) Gene vaccination with naked plasmid DNA: mechanism of CTL priming. *J Exp Med* 184(4):1555–1560. doi:10.1084/jem.184.4.1555
24. Wolff JA, Malone RW, Williams P, Chong W, Acsadi G, Jani A, Felgner PL (1990) Direct gene transfer into mouse muscle in vivo. *Science* 247(4949 Pt 1):1465–1468. doi:10.1126/science.1690918
25. Jelinek T, Kollaritsch H (2008) Vaccination with Dukoral against travelers' diarrhea (ETEC) and cholera. *Expert Rev Vaccines* 7(5):561–567. doi:10.1586/14760584.7.5.561
26. O'Ryan M, Linhares AC (2009) Update on Rotarix: an oral human rotavirus vaccine. *Expert Rev Vaccines* 8(12):1627–1641. doi:10.1586/erv.09.136
27. Liu L, Zhong Q, Tian T, Dubin K, Athale SK, Kupper TS (2010) Epidermal injury and infection during poxvirus immunization is crucial for the generation of highly protective T cell-mediated immunity. *Nat Med*:224–227. doi:10.1038/nm.2078
28. Gallo RL (2017) Human Skin Is the Largest Epithelial Surface for Interaction with Microbes. *J Invest Dermatol* 137(6):1213–1214. doi:10.1016/j.jid.2016.11.045
29. Streilein JW (1983) Skin-associated lymphoid tissues (SALT): origins and functions. *J Invest Dermatol* 80 Suppl:12s-16s. doi:10.1111/1523-1747.ep12536743
30. Kanitakis J (2002) Anatomy, histology and immunohistochemistry of normal human skin. *Eur J Dermatol* 12(4):390-9; quiz 400-1
31. Mathers AR, Larregina AT (2006) Professional antigen-presenting cells of the skin. *Immunol Res* 36(1-3):127–136. doi:10.1385/IR:36:1:127
32. Blakney AK, McKay PF, Ibarzo Yus B, Hunter JE, Dex EA, Shattock RJ (2019) The Skin You Are In: Design-of-Experiments Optimization of Lipid Nanoparticle Self-Amplifying RNA Formulations in Human Skin Explants. *ACS Nano*:5920–5930. doi:10.1021/acsnano.9b01774
33. Gelfant S (1982) "Of mice and men" the cell cycle in human epidermis in vivo. *J Invest Dermatol* 78(4):296–299. doi:10.1111/1523-1747.ep12507367
34. Helft J, Merad M (2010) Isolation of cutaneous dendritic cells. *Methods Mol Biol* 595:231–233. doi:10.1007/978-1-60761-421-0\_15
35. Bouloc A, Walker P, Grivel J-C, Vogel JC, Katz SI (1999) Immunization through dermal delivery of protein-encoding DNA: a role for migratory dendritic cells. *Eur. J. Immunol.* 29(2):446–454. doi:10.1002/(SICI)1521-4141(199902)29:02<446::AID-IMMU446>3.0.CO;2-A
36. Warfel AH, Thorbecke GJ, Belsito DV (1993) Langerhans cells as outposts of the dendritic cell system. *Adv Exp Med Biol* 329:469–480. doi:10.1007/978-1-4615-2930-9\_79
37. Nestle FO, Zheng XG, Thompson CB, Turka LA, Nickoloff BJ (1993) Characterization of dermal dendritic cells obtained from normal human skin reveals phenotypic and functionally distinctive subsets. *J Immunol* 151(11):6535–6545
38. Wamhoff E-C, Schulze J, Bellmann L, Rentzsch M, Bachem G, Fuchsberger FF, Rademacher J, Hermann M, Del Frari B, van Dalen R, Hartmann D, van Sorge NM, Seitz O, Stoitzner P, Rademacher C (2019) A Specific, Glycomimetic Langerin Ligand for Human Langerhans Cell Targeting. *ACS Cent Sci*:808–820. doi:10.1021/acscentsci.9b00093

#### IV References

39. Macatonia SE, Knight SC, Edwards AJ, Griffiths S, Fryer P (1987) Localization of antigen on lymph node dendritic cells after exposure to the contact sensitizer fluorescein isothiocyanate. Functional and morphological studies. *J Exp Med* 166(6):1654–1667. doi:10.1084/jem.166.6.1654
40. Allan RS, Smith CM, Belz GT, van Lint AL, Wakim LM, Heath WR, Carbone FR (2003) Epidermal viral immunity induced by CD8 $\alpha$ + dendritic cells but not by Langerhans cells. *Science* 301(5641):1925–1928. doi:10.1126/science.1087576
41. Gutowska-Owsiak D, Ogg GS (2012) The epidermis as an adjuvant. *J Invest Dermatol*:940–948. doi:10.1038/jid.2011.398
42. Bertolini M, McElwee K, Gilhar A, Bulfone-Paus S, Paus R (2020) Hair follicle immune privilege and its collapse in alopecia areata. *Exp Dermatol* 29(8):703–725. doi:10.1111/exd.14155
43. Giudice EL, Campbell JD (2006) Needle-free vaccine delivery. *Adv Drug Deliv Rev* 58(1):68–89. doi:10.1016/j.addr.2005.12.003
44. Ishii Y, Nakae T, Sakamoto F, Matsuo K, Matsuo K, Quan Y-S, Kamiyama F, Fujita T, Yamamoto A, Nakagawa S, Okada N (2008) A transcutaneous vaccination system using a hydrogel patch for viral and bacterial infection. *J Control Release*:113–120. doi:10.1016/j.jconrel.2008.07.025
45. Li N, Peng L-H, Chen X, Nakagawa S, Gao J-Q (2011) Transcutaneous vaccines: novel advances in technology and delivery for overcoming the barriers. *Vaccine* 29(37):6179–6190. doi:10.1016/j.vaccine.2011.06.086
46. Boyle JS, Silva A, Brady JL, Lew AM (1997) DNA immunization: induction of higher avidity antibody and effect of route on T cell cytotoxicity. *Proc Natl Acad Sci U S A* 94(26):14626–14631. doi:10.1073/pnas.94.26.14626
47. Seneschal J, Jiang X, Kupper TS (2014) Langerin+ dermal DC, but not Langerhans cells, are required for effective CD8-mediated immune responses after skin scarification with vaccinia virus. *J Invest Dermatol*:686–694. doi:10.1038/jid.2013.418
48. Denda M, Sokabe T, Fukumi-Tominaga T, Tominaga M (2007) Effects of skin surface temperature on epidermal permeability barrier homeostasis. *J Invest Dermatol* 127(3):654–659. doi:10.1038/sj.jid.5700590
49. Vogt A, Hadam S, Deckert I, Schmidt J, Stroux A, Afraz Z, Rancan F, Lademann J, Combadiere B, Blume-Peytavi U (2015) Hair follicle targeting, penetration enhancement and Langerhans cell activation make cyanoacrylate skin surface stripping a promising delivery technique for transcutaneous immunization with large molecules and particle-based vaccines. *Exp Dermatol* 24(1):73–75. doi:10.1111/exd.12589
50. van den Berg JH, Nuijen B, Beijnen JH, Vincent A, van Tinteren H, Kluge J, Woerdeman LAE, Hennink WE, Storm G, Schumacher TN, Haanen JBAG (2009) Optimization of intradermal vaccination by DNA tattooing in human skin. *Hum Gene Ther* 20(3):181–189. doi:10.1089/hum.2008.073
51. Verstrepen BE, Bins AD, Rollier CS, Mooij P, Koopman G, Sheppard NC, Sattentau Q, Wagner R, Wolf H, Schumacher TNM, Heeney JL, Haanen JBAG (2008) Improved HIV-1 specific T-cell responses by short-interval DNA tattooing as compared to intramuscular immunization in non-human primates. *Vaccine* 26(26):3346–3351. doi:10.1016/j.vaccine.2008.03.091
52. Fynan EF, Webster RG, Fuller DH, Haynes JR, Santoro JC, Robinson HL (1993) DNA vaccines: protective immunizations by parenteral, mucosal, and gene-gun inoculations. *Proc Natl Acad Sci U S A* 90(24):11478–11482. doi:10.1073/pnas.90.24.11478
53. Eisenbraun MD, Fuller DH, Haynes JR (1993) Examination of parameters affecting the elicitation of humoral immune responses by particle bombardment-mediated genetic immunization. *DNA Cell Biol* 12(9):791–797. doi:10.1089/dna.1993.12.791
54. Qiu P, Ziegelhoffer P, Sun J, Yang NS (1996) Gene gun delivery of mRNA in situ results in efficient transgene expression and genetic immunization. *Gene Ther* 3(3):262–268

#### IV References

55. Otberg N, Richter H, Schaefer H, Blume-Peytavi U, Sterry W, Lademann J (2004) Variations of hair follicle size and distribution in different body sites. *J Invest Dermatol* 122(1):14–19. doi:10.1046/j.0022-202X.2003.22110.x
56. Mittal A, Schulze K, Ebensen T, Weissmann S, Hansen S, Guzmán CA, Lehr C-M (2015) Inverse micellar sugar glass (IMSG) nanoparticles for transfollicular vaccination. *J Control Release* 206:140–152. doi:10.1016/j.jconrel.2015.03.017
57. Mittal A, Raber AS, Schaefer UF, Weissmann S, Ebensen T, Schulze K, Guzmán CA, Lehr C-M, Hansen S (2013) Non-invasive delivery of nanoparticles to hair follicles: a perspective for transcutaneous immunization. *Vaccine* 31(34):3442–3451. doi:10.1016/j.vaccine.2012.12.048
58. Wang J, Shah D, Chen X, Anderson RR, Wu MX (2014) A micro-sterile inflammation array as an adjuvant for influenza vaccines. *Nat Commun*:4447. doi:10.1038/ncomms5447
59. Hao Y, Li W, Zhou X, Yang F, Qian Z (2017) Microneedles-Based Transdermal Drug Delivery Systems: A Review. *J Biomed Nanotechnol* 13(12):1581–1597. doi:10.1166/jbn.2017.2474
60. Xu J, Xu D, Xuan X, He H (2021) Advances of Microneedles in Biomedical Applications. *Molecules* 26(19). doi:10.3390/molecules26195912
61. Levin Y, Kochba E, Hung I, Kenney R (2015) Intradermal vaccination using the novel microneedle device MicronJet600: Past, present, and future. *Hum Vaccin Immunother* 11(4):991–997. doi:10.1080/21645515.2015.1010871
62. Lee H-J, Choi H-J, Kim D-R, Lee H, Jin J-E, Kim Y-R, Lee M-S, Cho S-N, Kang YA (2016) Safety and efficacy of tuberculin skin testing with microneedle MicronJet600™ in healthy adults. *Int J Tuberc Lung Dis* 20(4):500–504. doi:10.5588/ijtld.15.0678
63. Hooper JW, Golden JW, Ferro AM, King AD (2007) Smallpox DNA vaccine delivered by novel skin electroporation device protects mice against intranasal poxvirus challenge. *Vaccine* 25(10):1814–1823. doi:10.1016/j.vaccine.2006.11.017
64. Scheiblhofer S, Strobl A, Hoepflinger V, Thalhamer T, Steiner M, Thalhamer J, Weiss R (2017) Skin vaccination via fractional infrared laser ablation - Optimization of laser-parameters and adjuvantation. *Vaccine* 35(14):1802–1809. doi:10.1016/j.vaccine.2016.11.105
65. Meesters AA, Nieboer MJ, Kezic S, Rie MA de, Wolkerstorfer A (2018) Parameters in fractional laser assisted delivery of topical anesthetics: Role of laser type and laser settings. *Lasers Surg Med*:813–818. doi:10.1002/lsm.22936
66. Scheiblhofer S, Drothler S, Braun W, Braun R, Boesch M, Weiss R (2021) Laser facilitated epicutaneous peptide immunization using dry patch technology. *Vaccine* 39(37):5259–5264. doi:10.1016/j.vaccine.2021.07.083
67. Terhorst D, Fossum E, Baranska A, Tamoutounour S, Malosse C, Garbani M, Braun R, Lechat E, Cramer R, Bogen B, Henri S, Malissen B (2015) Laser-assisted intradermal delivery of adjuvant-free vaccines targeting XCR1+ dendritic cells induces potent antitumoral responses. *J Immunol* 194(12):5895–5902. doi:10.4049/jimmunol.1500564
68. Lee W-R, Pan T-L, Wang P-W, Zhuo R-Z, Huang C-M, Fang J-Y (2008) Erbium:YAG laser enhances transdermal peptide delivery and skin vaccination. *J Control Release* 128(3):200–208. doi:10.1016/j.jconrel.2008.03.003
69. Engelke L, Winter G, Hook S, Engert J (2015) Recent insights into cutaneous immunization: How to vaccinate via the skin. *Vaccine* 33(37):4663–4674. doi:10.1016/j.vaccine.2015.05.012
70. Del Río-Sancho S, Lapteva M, Sonaje K, Böhler C, Ling V, Boehncke W-H, Kalia YN (2020) Targeted cutaneous delivery of etanercept using Er:YAG fractional laser ablation. *Int J Pharm* 580:119234. doi:10.1016/j.ijpharm.2020.119234
71. Rappuoli R (1994) Toxin inactivation and antigen stabilization: two different uses of formaldehyde. *Vaccine* 12(7):579–581. doi:10.1016/0264-410x(94)90259-3
72. Cottin P, Niedrig M, Domingo C (2013) Safety profile of the yellow fever vaccine Stamaril®: a 17-year review. *Expert Rev Vaccines* 12(11):1351–1368. doi:10.1586/14760584.2013.836320

## IV References

73. Groot AS de, Moise L, Terry F, Gutierrez AH, Hindocha P, Richard G, Hoft DF, Ross TM, Noe AR, Takahashi Y, Kotraiah V, Silk SE, Nielsen CM, Minassian AM, Ashfield R, Ardito M, Draper SJ, Martin WD (2020) Better Epitope Discovery, Precision Immune Engineering, and Accelerated Vaccine Design Using Immunoinformatics Tools. *Front Immunol* 11:442. doi:10.3389/fimmu.2020.00442
74. Tang DC, DeVit M, Johnston SA (1992) Genetic immunization is a simple method for eliciting an immune response. *Nature* 356(6365):152–154. doi:10.1038/356152a0
75. Löffler P (2021) Review: Vaccine Myth-Buster - Cleaning Up With Prejudices and Dangerous Misinformation. *Front Immunol* 12:663280. doi:10.3389/fimmu.2021.663280
76. Tajpara P, Schuster C, Schön E, Kienzl P, Vierhapper M, Mildner M, Elbe-Bürger A (2018) Epicutaneous administration of the pattern recognition receptor agonist polyinosinic-polycytidylic acid activates the MDA5/MAVS pathway in Langerhans cells. *FASEB J*:4132–4144. doi:10.1096/fj.201701090R
77. Pines E, Barrand M, Fabre P, Salomon H, Blondeau C, Wood SC, Hoffenbach A (1999) New acellular pertussis-containing paediatric combined vaccines. *Vaccine* 17(13-14):1650–1656. doi:10.1016/s0264-410x(98)00422-8
78. Mehanny M, Lehr C-M, Fuhrmann G (2021) Extracellular vesicles as antigen carriers for novel vaccination avenues. *Adv Drug Deliv Rev* 173:164–180. doi:10.1016/j.addr.2021.03.016
79. Weide B, Carralot J-P, Reese A, Scheel B, Eigentler TK, Hoerr I, Rammensee H-G, Garbe C, Pascolo S (2008) Results of the first phase I/II clinical vaccination trial with direct injection of mRNA. *J Immunother* 31(2):180–188. doi:10.1097/CJI.0b013e31815ce501
80. Schoenmaker L, Witzigmann D, Kulkarni JA, Verbeke R, Kersten G, Jiskoot W, Crommelin DJA (2021) mRNA-lipid nanoparticle COVID-19 vaccines: Structure and stability. *Int J Pharm* 601:120586. doi:10.1016/j.ijpharm.2021.120586
81. Kauffman KJ, Dorkin JR, Yang JH, Heartlein MW, DeRosa F, Mir FF, Fenton OS, Anderson DG (2015) Optimization of Lipid Nanoparticle Formulations for mRNA Delivery in Vivo with Fractional Factorial and Definitive Screening Designs. *Nano Lett* 15(11):7300–7306. doi:10.1021/acs.nanolett.5b02497
82. Kirschman JL, Bhosle S, Vanover D, Blanchard EL, Loomis KH, Zurla C, Murray K, Lam BC, Santangelo PJ (2017) Characterizing exogenous mRNA delivery, trafficking, cytoplasmic release and RNA-protein correlations at the level of single cells. *Nucleic Acids Res* 45(12):e113. doi:10.1093/nar/gkx290
83. Karikó K, Muramatsu H, Keller JM, Weissman D (2012) Increased erythropoiesis in mice injected with submicrogram quantities of pseudouridine-containing mRNA encoding erythropoietin. *Mol Ther* 20(5):948–953. doi:10.1038/mt.2012.7
84. Kormann MSD, Hasenpusch G, Aneja MK, Nica G, Flemmer AW, Herber-Jonat S, Huppmann M, Mays LE, Illenyi M, Schams A, Griese M, Bittmann I, Handgretinger R, Hartl D, Rosenecker J, Rudolph C (2011) Expression of therapeutic proteins after delivery of chemically modified mRNA in mice. *Nat Biotechnol* 29(2):154–157. doi:10.1038/nbt.1733
85. Thess A, Grund S, Mui BL, Hope MJ, Baumhof P, Fotin-Mleczek M, Schlake T (2015) Sequence-engineered mRNA Without Chemical Nucleoside Modifications Enables an Effective Protein Therapy in Large Animals. *Mol Ther* 23(9):1456–1464. doi:10.1038/mt.2015.103
86. Ulmer JB, Donnelly JJ, Parker SE, Rhodes GH, Felgner PL, Dwarki VJ, Gromkowski SH, Deck RR, DeWitt CM, Friedman A (1993) Heterologous protection against influenza by injection of DNA encoding a viral protein. *Science* 259(5102):1745–1749. doi:10.1126/science.8456302
87. Lauterbach H, Gruber A, Ried C, Cheminay C, Broucker T (2006) Insufficient APC capacities of dendritic cells in gene gun-mediated DNA vaccination. *J Immunol* 176(8):4600–4607. doi:10.4049/jimmunol.176.8.4600

#### IV References

88. Lew D, Parker SE, Latimer T, Abai AM, Kuwahara-Rundell A, Doh SG, Yang ZY, Laface D, Gromkowski SH, Nabel GJ (1995) Cancer gene therapy using plasmid DNA: pharmacokinetic study of DNA following injection in mice. *Hum Gene Ther* 6(5):553–564. doi:10.1089/hum.1995.6.5-553
89. Li J, Chen K, Dong X, Xu Y, Sun Q, Wang H, Chen Z, Liu C, Liu R, Yang Z, Mei X, Zhang R, Chang L, Tian Z, Chen J, Liang K, He C, Luo M (2022) YTHDF1 promotes mRNA degradation via YTHDF1-AGO2 interaction and phase separation. *Cell Prolif* 55(1):e13157. doi:10.1111/cpr.13157
90. Orlandini von Niessen AG, Poleganov MA, Rechner C, Plaschke A, Kranz LM, Fesser S, Diken M, Löwer M, Vallazza B, Beisert T, Bukur V, Kuhn AN, Türeci Ö, Sahin U (2019) Improving mRNA-Based Therapeutic Gene Delivery by Expression-Augmenting 3' UTRs Identified by Cellular Library Screening. *Mol Ther* 27(4):824–836. doi:10.1016/j.ymthe.2018.12.011
91. DeRosa F, Guild B, Karve S, Smith L, Love K, Dorkin JR, Kauffman KJ, Zhang J, Yahalom B, Anderson DG, Heartlein MW (2016) Therapeutic efficacy in a hemophilia B model using a biosynthetic mRNA liver depot system. *Gene Ther* 23(10):699–707. doi:10.1038/gt.2016.46
92. Donnelly JJ, Ulmer JB, Shiver JW, Liu MA (1997) DNA vaccines. *Annu Rev Immunol* 15:617–648. doi:10.1146/annurev.immunol.15.1.617
93. Martinon F, Krishnan S, Lenzen G, Magné R, Gomard E, Guillet JG, Lévy JP, Meulien P (1993) Induction of virus-specific cytotoxic T lymphocytes in vivo by liposome-entrapped mRNA. *Eur. J. Immunol.* 23(7):1719–1722. doi:10.1002/eji.1830230749
94. Lostalé-Seijo I, Montenegro J (2018) Synthetic materials at the forefront of gene delivery. *Nat Rev Chem* 2(10):258–277. doi:10.1038/s41570-018-0039-1
95. Fenton OS, Olafson KN, Pillai PS, Mitchell MJ, Langer R (2018) Advances in Biomaterials for Drug Delivery. *Adv Mater*:e1705328. doi:10.1002/adma.201705328
96. Tsui NBY, Ng EKO, Lo YMD (2002) Stability of endogenous and added RNA in blood specimens, serum, and plasma. *Clin Chem* 48(10):1647–1653
97. Zielińska A, Carreiró F, Oliveira AM, Neves A, Pires B, Venkatesh DN, Durazzo A, Lucarini M, Eder P, Silva AM, Santini A, Souto EB (2020) Polymeric Nanoparticles: Production, Characterization, Toxicology and Ecotoxicology. *Molecules* 25(16). doi:10.3390/molecules25163731
98. Hickey JW, Santos JL, Williford J-M, Mao H-Q (2015) Control of polymeric nanoparticle size to improve therapeutic delivery. *J Control Release* 219:536–547. doi:10.1016/j.jconrel.2015.10.006
99. Wheeler JJ, Palmer L, Ossanlou M, MacLachlan I, Graham RW, Zhang YP, Hope MJ, Scherrer P, Cullis PR (1999) Stabilized plasmid-lipid particles: construction and characterization. *Gene Ther* 6(2):271–281. doi:10.1038/sj.gt.3300821
100. Song LY, Ahkong QF, Rong Q, Wang Z, Ansell S, Hope MJ, Mui B (2002) Characterization of the inhibitory effect of PEG-lipid conjugates on the intracellular delivery of plasmid and antisense DNA mediated by cationic lipid liposomes. *Biochim Biophys Acta* 1558(1):1–13. doi:10.1016/s0005-2736(01)00399-6
101. Zhang S, Gao H, Bao G (2015) Physical Principles of Nanoparticle Cellular Endocytosis. *ACS Nano* 9(9):8655–8671. doi:10.1021/acsnano.5b03184
102. Sahay G, Querbes W, Alabi C, Eltoukhy A, Sarkar S, Zurenko C, Karagiannis E, Love K, Chen D, Zoncu R, Bugarim Y, Schroeder A, Langer R, Anderson DG (2013) Efficiency of siRNA delivery by lipid nanoparticles is limited by endocytic recycling. *Nat Biotechnol* 31(7):653–658. doi:10.1038/nbt.2614
103. Sonawane ND, Szoka FC, Verkman AS (2003) Chloride accumulation and swelling in endosomes enhances DNA transfer by polyamine-DNA polyplexes. *J Biol Chem* 278(45):44826–44831. doi:10.1074/jbc.M308643200
104. Juliano RL, Ming X, Nakagawa O (2012) Cellular uptake and intracellular trafficking of antisense and siRNA oligonucleotides. *Bioconjug Chem* 23(2):147–157. doi:10.1021/bc200377d

## IV References

105. Bally MB, Harvie P, Wong FM, Kong S, Wasan EK, Reimer DL (1999) Biological barriers to cellular delivery of lipid-based DNA carriers. *Adv Drug Deliv Rev* 38(3):291–315. doi:10.1016/s0169-409x(99)00034-4
106. Przybylski S, Gasch M, Marschner A, Ebert M, Ewe A, Helmig G, Hilger N, Fricke S, Rudzok S, Aigner A, Burkhardt J (2017) Influence of nanoparticle-mediated transfection on proliferation of primary immune cells in vitro and in vivo. *PLoS One* 12(5):e0176517. doi:10.1371/journal.pone.0176517
107. Pires P, Simões S, Nir S, Gaspar R, Düzgünes N, Pedroso de Lima MC (1999) Interaction of cationic liposomes and their DNA complexes with monocytic leukemia cells. *Biochim Biophys Acta* 1418(1):71–84. doi:10.1016/s0005-2736(99)00023-1
108. Dimitriadis GJ (1978) Entrapment of ribonucleic acids in liposomes. *FEBS Lett* 86(2):289–293. doi:10.1016/0014-5793(78)80582-1
109. Blakney AK, McKay PF, Yus BI, Aldon Y, Shattock RJ (2019) Inside out: optimization of lipid nanoparticle formulations for exterior complexation and in vivo delivery of saRNA. *Gene Ther* 26(9):363–372. doi:10.1038/s41434-019-0095-2
110. Wahane A, Waghmode A, Kappahn A, Dhuri K, Gupta A, Bahal R (2020) Role of Lipid-Based and Polymer-Based Non-Viral Vectors in Nucleic Acid Delivery for Next-Generation Gene Therapy. *Molecules* 25(12). doi:10.3390/molecules25122866
111. Zhou WZ, Hoon DS, Huang SK, Fujii S, Hashimoto K, Morishita R, Kaneda Y (1999) RNA melanoma vaccine: induction of antitumor immunity by human glycoprotein 100 mRNA immunization. *Hum Gene Ther* 10(16):2719–2724. doi:10.1089/10430349950016762
112. Blakney AK, Zhu Y, McKay PF, Bouton CR, Yeow J, Tang J, Hu K, Samnuan K, Grigsby CL, Shattock RJ, Stevens MM (2020) Big Is Beautiful: Enhanced saRNA Delivery and Immunogenicity by a Higher Molecular Weight, Bio-reducible, Cationic Polymer. *ACS Nano*:5711–5727. doi:10.1021/acsnano.0c00326
113. Blakney AK, Yilmaz G, McKay PF, Becer CR, Shattock RJ (2018) One Size Does Not Fit All: The Effect of Chain Length and Charge Density of Poly(ethylene imine) Based Copolymers on Delivery of pDNA, mRNA, and RepRNA Polyplexes. *Biomacromolecules*:2870–2879. doi:10.1021/acs.biomac.8b00429
114. Remaut K, Lucas B, Raemdonck K, Braeckmans K, Demeester J, Smedt SC de (2007) Protection of oligonucleotides against enzymatic degradation by pegylated and nonpegylated branched polyethyleneimine. *Biomacromolecules* 8(4):1333–1340. doi:10.1021/bm0611578
115. Hoerr I, Obst R, Rammensee HG, Jung G (2000) In vivo application of RNA leads to induction of specific cytotoxic T lymphocytes and antibodies. *Eur. J. Immunol.* 30(1):1–7. doi:10.1002/1521-4141(200001)30:1<1::AID-IMMU1>3.0.CO;2-#
116. Fotin-Mleczek M, Zanzinger K, Heidenreich R, Lorenz C, Thess A, Duchardt KM, Kallen K-J (2012) Highly potent mRNA based cancer vaccines represent an attractive platform for combination therapies supporting an improved therapeutic effect. *J Gene Med* 14(6):428–439. doi:10.1002/jgm.2605
117. Yasar, Hanzey Non-Invasive Vaccination by NP-based Messenger RNA (mRNA) delivery via the Transfollicular Route. Doktorarbeit, Thesis
118. Sharifnia Z, Bandehpour M, Hamishehkar H, Mosaffa N, Kazemi B, Zarghami N (2019) In-vitro Transcribed mRNA Delivery Using PLGA/PEI Nanoparticles into Human Monocyte-derived Dendritic Cells. *Iran J Pharm Res* 18(4):1659–1675. doi:10.22037/ijpr.2019.1100872
119. Kim H, Kirtane AR, Kim NY, Rajesh NU, Tang C, Ishida K, Hayward AM, Langer R, Traverso G (2023) Gastrointestinal Delivery of an mRNA Vaccine Using Immunostimulatory Polymeric Nanoparticles. *AAPS J* 25(5):81. doi:10.1208/s12248-023-00844-z
120. Baden LR, El Sahly HM, Essink B et al (2021) Efficacy and Safety of the mRNA-1273 SARS-CoV-2 Vaccine. *N Engl J Med* 384(5):403–416. doi:10.1056/NEJMoa2035389

## IV References

121. Gote V, Bolla PK, Kommineni N, Butreddy A, Nukala PK, Palakurthi SS, Khan W (2023) A Comprehensive Review of mRNA Vaccines. *Int J Mol Sci* 24(3). doi:10.3390/ijms24032700
122. Zhang R, El-Mayta R, Murdoch TJ, Warzecha CC, Billingsley MM, Shepherd SJ, Gong N, Wang L, Wilson JM, Lee D, Mitchell MJ (2021) Helper lipid structure influences protein adsorption and delivery of lipid nanoparticles to spleen and liver. *Biomater Sci* 9(4):1449–1463. doi:10.1039/d0bm01609h
123. Cheng X, Lee RJ (2016) The role of helper lipids in lipid nanoparticles (LNPs) designed for oligonucleotide delivery. *Adv Drug Deliv Rev* 99(Pt A):129–137. doi:10.1016/j.addr.2016.01.022
124. Granot Y, Peer D (2017) Delivering the right message: Challenges and opportunities in lipid nanoparticles-mediated modified mRNA therapeutics-An innate immune system standpoint. *Semin Immunol*:68–77. doi:10.1016/j.smim.2017.08.015
125. Mukalel AJ, Riley RS, Zhang R, Mitchell MJ (2019) Nanoparticles for nucleic acid delivery: Applications in cancer immunotherapy. *Cancer Lett* 458:102–112. doi:10.1016/j.canlet.2019.04.040
126. Cheng Q, Wei T, Farbiak L, Johnson LT, Dilliard SA, Siegwart DJ (2020) Selective organ targeting (SORT) nanoparticles for tissue-specific mRNA delivery and CRISPR-Cas gene editing. *Nat Nanotechnol* 15(4):313–320. doi:10.1038/s41565-020-0669-6
127. Semple SC, Akinc A, Chen J et al (2010) Rational design of cationic lipids for siRNA delivery. *Nat Biotechnol* 28(2):172–176. doi:10.1038/nbt.1602
128. Leung AKK, Hafez IM, Baoukina S, Belliveau NM, Zhigaltsev IV, Afshinmanesh E, Tieleman DP, Hansen CL, Hope MJ, Cullis PR (2012) Lipid Nanoparticles Containing siRNA Synthesized by Microfluidic Mixing Exhibit an Electron-Dense Nanostructured Core. *J Phys Chem C Nanomater Interfaces* 116(34):18440–18450. doi:10.1021/jp303267y
129. Billingsley MM, Singh N, Ravikumar P, Zhang R, June CH, Mitchell MJ (2020) Ionizable Lipid Nanoparticle-Mediated mRNA Delivery for Human CAR T Cell Engineering. *Nano Lett* 20(3):1578–1589. doi:10.1021/acs.nanolett.9b04246
130. Miao L, Lin J, Huang Y, Li L, Delcassian D, Ge Y, Shi Y, Anderson DG (2020) Synergistic lipid compositions for albumin receptor mediated delivery of mRNA to the liver. *Nat Commun* 11(1):2424. doi:10.1038/s41467-020-16248-y
131. Gustafson HH, Holt-Casper D, Grainger DW, Ghandehari H (2015) Nanoparticle Uptake: The Phagocyte Problem. *Nano Today* 10(4):487–510. doi:10.1016/j.nantod.2015.06.006
132. Patel S, Ashwanikumar N, Robinson E, Xia Y, Mihai C, Griffith JP, Hou S, Esposito AA, Ketova T, Welsher K, Joyal JL, Almarsson Ö, Sahay G (2020) Naturally-occurring cholesterol analogues in lipid nanoparticles induce polymorphic shape and enhance intracellular delivery of mRNA. *Nat Commun* 11(1):983. doi:10.1038/s41467-020-14527-2
133. LoPresti ST, Arral ML, Chaudhary N, Whitehead KA (2022) The replacement of helper lipids with charged alternatives in lipid nanoparticles facilitates targeted mRNA delivery to the spleen and lungs. *J Control Release* 345:819–831. doi:10.1016/j.jconrel.2022.03.046
134. Hong K, Zheng W, Baker A, Papahadjopoulos D (1997) Stabilization of cationic liposome-plasmid DNA complexes by polyamines and poly(ethylene glycol)-phospholipid conjugates for efficient in vivo gene delivery. *FEBS Lett* 400(2):233–237. doi:10.1016/s0014-5793(96)01397-x
135. Jayaraman M, Ansell SM, Mui BL, Tam YK, Chen J, Du X, Butler D, Eltepu L, Matsuda S, Narayanannair JK, Rajeev KG, Hafez IM, Akinc A, Maier MA, Tracy MA, Cullis PR, Madden TD, Manoharan M, Hope MJ (2012) Maximizing the potency of siRNA lipid nanoparticles for hepatic gene silencing in vivo. *Angew Chem Int Ed Engl* 51(34):8529–8533. doi:10.1002/anie.201203263
136. Tenchov R, Sasso JM, Zhou QA (2023) PEGylated Lipid Nanoparticle Formulations: Immunological Safety and Efficiency Perspective. *Bioconjug Chem* 34(6):941–960. doi:10.1021/acs.bioconjchem.3c00174

#### IV References

137. Harvie P, Wong FM, Bally MB (2000) Use of Poly(ethylene glycol)–Lipid Conjugates to Regulate the Surface Attributes and Transfection Activity of Lipid–DNA Particles. *J Pharm Sci* 89(5):652–663. doi:10.1002/(SICI)1520-6017(200005)89:5<652::AID-JPS11>3.0.CO;2-H
138. Chen D, Ganesh S, Wang W, Amiji M (2017) Plasma protein adsorption and biological identity of systemically administered nanoparticles. *Nanomedicine (Lond)* 12(17):2113–2135. doi:10.2217/nnm-2017-0178
139. Crook K, Stevenson BJ, Dubouchet M, Porteous DJ (1998) Inclusion of cholesterol in DOTAP transfection complexes increases the delivery of DNA to cells in vitro in the presence of serum. *Gene Ther* 5(1):137–143. doi:10.1038/sj.gt.3300554
140. Hatakeyama H, Akita H, Harashima H (2013) The polyethyleneglycol dilemma: advantage and disadvantage of PEGylation of liposomes for systemic genes and nucleic acids delivery to tumors. *Biol Pharm Bull* 36(6):892–899. doi:10.1248/bpb.b13-00059
141. Bradley AJ, Devine DV, Ansell SM, Janzen J, Brooks DE (1998) Inhibition of liposome-induced complement activation by incorporated poly(ethylene glycol)-lipids. *Arch Biochem Biophys* 357(2):185–194. doi:10.1006/abbi.1998.0798
142. Pozzi D, Colapicchioni V, Caracciolo G, Piovesana S, Capriotti AL, Palchetti S, Grossi S de, Riccioli A, Amenitsch H, Laganà A (2014) Effect of polyethyleneglycol (PEG) chain length on the bio-nano-interactions between PEGylated lipid nanoparticles and biological fluids: from nanostructure to uptake in cancer cells. *Nanoscale* 6(5):2782–2792. doi:10.1039/c3nr05559k
143. Mui BL, Tam YK, Jayaraman M, Ansell SM, Du X, Tam YYC, Lin PJ, Chen S, Narayanannair JK, Rajeev KG, Manoharan M, Akinc A, Maier MA, Cullis P, Madden TD, Hope MJ (2013) Influence of Polyethylene Glycol Lipid Desorption Rates on Pharmacokinetics and Pharmacodynamics of siRNA Lipid Nanoparticles. *Mol Ther Nucleic Acids* 2(12):e139. doi:10.1038/mtna.2013.66
144. Abrams MT, Koser ML, Seitzer J, Williams SC, DiPietro MA, Wang W, Shaw AW, Mao X, Jadhav V, Davide JP, Burke PA, Sachs AB, Stirdivant SM, Sepp-Lorenzino L (2010) Evaluation of efficacy, biodistribution, and inflammation for a potent siRNA nanoparticle: effect of dexamethasone co-treatment. *Mol Ther* 18(1):171–180. doi:10.1038/mt.2009.208
145. Su X, Fricke J, Kavanagh DG, Irvine DJ (2011) In vitro and in vivo mRNA delivery using lipid-enveloped pH-responsive polymer nanoparticles. *Mol Pharm*:774–787. doi:10.1021/mp100390w
146. Siewert CD, Haas H, Cornet V, Nogueira SS, Nawroth T, Uebbing L, Ziller A, Al-Gousous J, Radulescu A, Schroer MA, Blanchet CE, Svergun DI, Radsak MP, Sahin U, Langguth P (2020) Hybrid Biopolymer and Lipid Nanoparticles with Improved Transfection Efficacy for mRNA. *Cells*. doi:10.3390/cells9092034
147. Yasar H, Biehl A, Rossi C de, Koch M, Murgia X, Loretz B, Lehr C-M (2018) Kinetics of mRNA delivery and protein translation in dendritic cells using lipid-coated PLGA nanoparticles. *J Nanobiotechnology* 16(1):72. doi:10.1186/s12951-018-0401-y
148. Sharma A, Madhunapantula SV, Robertson GP (2012) Toxicological considerations when creating nanoparticle-based drugs and drug delivery systems. *Expert Opin Drug Metab Toxicol* 8(1):47–69. doi:10.1517/17425255.2012.637916
149. Terada T, Kulkarni JA, Huynh A, Tam YYC, Cullis P (2021) Protective Effect of Edaravone against Cationic Lipid-Mediated Oxidative Stress and Apoptosis. *Biol Pharm Bull* 44(1):144–149. doi:10.1248/bpb.b20-00679
150. Dehghani-Ghahnaviyeh S, Smith M, Xia Y, Dousis A, Grossfield A, Sur S (2023) Ionizable Amino Lipids Distribution and Effects on DSPC/Cholesterol Membranes: Implications for Lipid Nanoparticle Structure. *J Phys Chem B* 127(31):6928–6939. doi:10.1021/acs.jpcc.3c01296
151. Felgner JH, Kumar R, Sridhar CN, Wheeler CJ, Tsai YJ, Border R, Ramsey P, Martin M, Felgner PL (1994) Enhanced gene delivery and mechanism studies with a novel series of cationic lipid formulations. *J Biol Chem* 269(4):2550–2561

#### IV References

152. Zuhorn IS, Bakowsky U, Polushkin E, Visser WH, Stuart MCA, Engberts JBFN, Hoekstra D (2005) Nonbilayer phase of lipoplex-membrane mixture determines endosomal escape of genetic cargo and transfection efficiency. *Mol Ther* 11(5):801–810. doi:10.1016/j.ymthe.2004.12.018
153. Zhou X, Huang L (1994) DNA transfection mediated by cationic liposomes containing lipopolylysine: characterization and mechanism of action. *Biochimica et Biophysica Acta (BBA) - Biomembranes* 1189(2):195–203. doi:10.1016/0005-2736(94)90066-3
154. Felgner PL, Gadek TR, Holm M, Roman R, Chan HW, Wenz M, Northrop JP, Ringold GM, Danielsen M (1987) Lipofection: a highly efficient, lipid-mediated DNA-transfection procedure. *Proc Natl Acad Sci U S A* 84(21):7413–7417. doi:10.1073/pnas.84.21.7413
155. Pardi N, Tuyishime S, Muramatsu H, Kariko K, Mui BL, Tam YK, Madden TD, Hope MJ, Weissman D (2015) Expression kinetics of nucleoside-modified mRNA delivered in lipid nanoparticles to mice by various routes. *J Control Release*:345–351. doi:10.1016/j.jconrel.2015.08.007
156. Malone RW, Felgner PL, Verma IM (1989) Cationic liposome-mediated RNA transfection. *Proc Natl Acad Sci U S A* 86(16):6077–6081. doi:10.1073/pnas.86.16.6077
157. Kliesch L, Delandre S, Gabelmann A, Koch M, Schulze K, Guzmán CA, Loretz B, Lehr C-M (2022) Lipid-Polymer Hybrid Nanoparticles for mRNA Delivery to Dendritic Cells: Impact of Lipid Composition on Performance in Different Media. *Pharmaceutics* 14(12). doi:10.3390/pharmaceutics14122675
158. Weiss B, Schaefer UF, Zapp J, Lamprecht A, Stallmach A, Lehr C-M (2006) Nanoparticles made of fluorescence-labelled Poly(L-lactide-co-glycolide): preparation, stability, and biocompatibility. *J Nanosci Nanotechnol* 6(9-10):3048–3056. doi:10.1166/jnn.2006.424
159. Fogh-Andersen N, Altura BM, Altura BT, Siggaard-Andersen O (1995) Composition of interstitial fluid. *Clin Chem* 41(10):1522–1525. doi:10.1093/clinchem/41.10.1522
160. van Meerloo J, Kaspers GJL, Cloos J (2011) Cell sensitivity assays: the MTT assay. *Methods Mol Biol* 731:237–245. doi:10.1007/978-1-61779-080-5\_20
161. Kashem SW, Kaplan DH (2018) Isolation of Murine Skin Resident and Migratory Dendritic Cells via Enzymatic Digestion. *Curr Protoc Immunol* 121(1):e45. doi:10.1002/cpim.45
162. Lirussi D, Ebensen T, Schulze K, Reinhard E, Trittel S, Riese P, Prochnow B, Guzmán CA (2018) Rapid In Vivo Assessment of Adjuvant's Cytotoxic T Lymphocytes Generation Capabilities for Vaccine Development. *J Vis Exp* (136). doi:10.3791/57401
163. Lyons AB, Parish CR (1994) Determination of lymphocyte division by flow cytometry. *J Immunol Methods* 171(1):131–137. doi:10.1016/0022-1759(94)90236-4
164. Kim PY, Kim Y-S, Koo IG, Jung JC, Kim GJ, Choi MY, Yu Z, Collins GJ (2011) Bacterial inactivation of wound infection in a human skin model by liquid-phase discharge plasma. *PLoS One* 6(8):e24104. doi:10.1371/journal.pone.0024104
165. Kandárová H, Hayden P, Klausner M, Kubilus J, Sheasgreen J (2009) An in vitro skin irritation test (SIT) using the EpiDerm reconstructed human epidermal (RHE) model. *J Vis Exp* (29). doi:10.3791/1366
166. Watanabe T, Hasegawa T, Takahashi H, Ishibashi T, Itagaki H, Sugibayashi K (2002) Utility of MTT assay in three-dimensional cultured human skin model as an alternative for draize skin irritation test: approach using diffusion law of irritant in skin and toxicokinetics-toxicodynamics correlation. *Pharm Res* 19(5):669–675. doi:10.1023/a:1015366331634
167. (2012) Test No. 405: Acute Eye Irritation/Corrosion. OECD Guidelines for the Testing of Chemicals, Section 4. OECD Publishing, Paris
168. Xu Y, Szoka FC (1996) Mechanism of DNA release from cationic liposome/DNA complexes used in cell transfection. *Biochemistry* 35(18):5616–5623. doi:10.1021/bi9602019
169. Mittal A, Schulze K, Ebensen T, Weißmann S, Hansen S, Lehr CM, Guzmán CA (2015) Efficient nanoparticle-mediated needle-free transcutaneous vaccination via hair follicles requires adjuvantation. *Nanomedicine* 11(1):147–154. doi:10.1016/j.nano.2014.08.009

#### IV References

170. Bronaugh RL, Stewart RF, Congdon ER (1982) Methods for in vitro percutaneous absorption studies. II. Animal models for human skin. *Toxicol Appl Pharmacol* 62(3):481–488. doi:10.1016/0041-008x(82)90149-1
171. Khiao In M, Richardson KC, Loewa A, Hedtrich S, Kaessmeyer S, Plendl J (2019) Histological and functional comparisons of four anatomical regions of porcine skin with human abdominal skin. *Anatomia, histologia, embryologia* 48(3):207–217. doi:10.1111/ahe.12425
172. Scott RC, Corrigan MA, Smith F, Mason H (1991) The influence of skin structure on permeability: an intersite and interspecies comparison with hydrophilic penetrants. *J Invest Dermatol* 96(6):921–925. doi:10.1111/1523-1747.ep12475447
173. Ibrahim MM, Bond J, Bergeron A, Miller KJ, Ehanire T, Quiles C, Lorden ER, Medina MA, Fisher M, Klitzman B, Selim MA, Leong KW, Levinson H (2014) A novel immune competent murine hypertrophic scar contracture model: a tool to elucidate disease mechanism and develop new therapies. *Wound Repair Regen* 22(6):755–764. doi:10.1111/wrr.12238
174. Li JL, Goh CC, Keeble JL, Qin JS, Roediger B, Jain R, Wang Y, Chew WK, Weninger W, Ng LG (2012) Intravital multiphoton imaging of immune responses in the mouse ear skin. *Nat Protoc* 7(2):221–234. doi:10.1038/nprot.2011.438
175. Blakney AK, Abdouni Y, Yilmaz G, Liu R, McKay PF, Bouton CR, Shattock RJ, Becer CR (2020) Mannosylated Poly(ethylene imine) Copolymers Enhance saRNA Uptake and Expression in Human Skin Explants. *Biomacromolecules*:2482–2492. doi:10.1021/acs.biomac.0c00445
176. Brenner S, Jacob F, Meselson M (1961) An unstable intermediate carrying information from genes to ribosomes for protein synthesis. *Nature* 190:576–581. doi:10.1038/190576a0
177. Ostro MJ, Giacomoni D, Lavelle D, Paxton W, Dray S (1978) Evidence for translation of rabbit globin mRNA after liposome-mediated insertion into a human cell line. *Nature* 274(5674):921–923. doi:10.1038/274921a0
178. Dimitriadis GJ (1978) Translation of rabbit globin mRNA introduced by liposomes into mouse lymphocytes. *Nature* 274(5674):923–924. doi:10.1038/274923a0
179. Conry RM, LoBuglio AF, Wright M, Sumerel L, Pike MJ, Johanning F, Benjamin R, Lu D, Curiel DT (1995) Characterization of a messenger RNA polynucleotide vaccine vector. *Cancer Res* 55(7):1397–1400
180. Pardi N, Hogan MJ, Porter FW, Weissman D (2018) mRNA vaccines - a new era in vaccinology. *Nat Rev Drug Discov* 17(4):261–279. doi:10.1038/nrd.2017.243
181. Andries O, Mc Cafferty S, Smedt SC de, Weiss R, Sanders NN, Kitada T (2015) N(1)-methylpseudouridine-incorporated mRNA outperforms pseudouridine-incorporated mRNA by providing enhanced protein expression and reduced immunogenicity in mammalian cell lines and mice. *J Control Release* 217:337–344. doi:10.1016/j.jconrel.2015.08.051
182. Nelson J, Sorensen EW, Mintri S, Rabideau AE, Zheng W, Besin G, Khatwani N, Su SV, Miracco EJ, Issa WJ, Hoge S, Stanton MG, Joyal JL (2020) Impact of mRNA chemistry and manufacturing process on innate immune activation. *Sci Adv* 6(26):eaaz6893. doi:10.1126/sciadv.aaz6893
183. Karikó K, Muramatsu H, Ludwig J, Weissman D (2011) Generating the optimal mRNA for therapy: HPLC purification eliminates immune activation and improves translation of nucleoside-modified, protein-encoding mRNA. *Nucleic Acids Res* 39(21):e142. doi:10.1093/nar/gkr695
184. Bahl K, Senn JJ, Yuzhakov O, Bulychev A, Brito LA, Hassett KJ, Laska ME, Smith M, Almarsson Ö, Thompson J, Ribeiro AM, Watson M, Zaks T, Ciaramella G (2017) Preclinical and Clinical Demonstration of Immunogenicity by mRNA Vaccines against H10N8 and H7N9 Influenza Viruses. *Mol Ther* 25(6):1316–1327. doi:10.1016/j.ymthe.2017.03.035
185. Li M, Li Y, Li S, Jia L, Wang H, Li M, Deng J, Zhu A, Ma L, Li W, Yu P, Zhu T (2022) The nano delivery systems and applications of mRNA. *Eur J Med Chem* 227:113910. doi:10.1016/j.ejmech.2021.113910

#### IV References

186. Kim D, Lee J-Y, Yang J-S, Kim JW, Kim VN, Chang H (2020) The Architecture of SARS-CoV-2 Transcriptome. *Cell* 181(4):914-921. e10. doi:10.1016/j.cell.2020.04.011
187. Farhood H, Serbina N, Huang L (1995) The role of dioleoyl phosphatidylethanolamine in cationic liposome mediated gene transfer. *Biochimica et Biophysica Acta (BBA) - Biomembranes* 1235(2):289–295. doi:10.1016/0005-2736(95)80016-9
188. Weiss A-V, Koch M, Schneider M (2019) Combining cryo-TEM and energy-filtered TEM for imaging organic core-shell nanoparticles and defining the polymer distribution. *Int J Pharm* 570:118650. doi:10.1016/j.ijpharm.2019.118650
189. Templeton NS, Lasic DD, Frederik PM, Strey HH, Roberts DD, Pavlakis GN (1997) Improved DNA: liposome complexes for increased systemic delivery and gene expression. *Nat Biotechnol* 15(7):647–652. doi:10.1038/nbt0797-647
190. Litzinger DC, Huang L (1992) Phosphatidylethanolamine liposomes: drug delivery, gene transfer and immunodiagnostic applications. *Biochimica et Biophysica Acta (BBA) - Reviews on Biomembranes* 1113(2):201–227. doi:10.1016/0304-4157(92)90039-d
191. Mura S, Hillaireau H, Nicolas J, Le Droumaguet B, Gueutin C, Zanna S, Tsapis N, Fattal E (2011) Influence of surface charge on the potential toxicity of PLGA nanoparticles towards Calu-3 cells. *Int J Nanomedicine* 6:2591–2605. doi:10.2147/IJN.S24552
192. Hernández-Caselles T, Villalain J, Gómez-Fernández JC (1990) Stability of liposomes on long term storage. *J Pharm Pharmacol* 42(6):397–400. doi:10.1111/j.2042-7158.1990.tb06578.x
193. Shulkin PM, Seltzer SE, Davis MA, Adams DF (1984) Lyophilized liposomes: a new method for long-term vesicular storage. *J Microencapsul* 1(1):73–80. doi:10.3109/02652048409031539
194. Smith MC, Crist RM, Clogston JD, McNeil SE (2017) Zeta potential: a case study of cationic, anionic, and neutral liposomes. *Anal Bioanal Chem* 409(24):5779–5787. doi:10.1007/s00216-017-0527-z
195. Bukackova M, Rusnok P, Marsalek R (2018) Mathematical Methods in the Calculation of the Zeta Potential of BSA. *J Solution Chem* 47(12):1942–1952. doi:10.1007/s10953-018-0830-0
196. Walkey CD, Chan WCW (2012) Understanding and controlling the interaction of nanomaterials with proteins in a physiological environment. *Chem Soc Rev* 41(7):2780–2799. doi:10.1039/c1cs15233e
197. Ehrenberg MS, Friedman AE, Finkelstein JN, Oberdörster G, McGrath JL (2009) The influence of protein adsorption on nanoparticle association with cultured endothelial cells. *Biomaterials* 30(4):603–610. doi:10.1016/j.biomaterials.2008.09.050
198. Cedervall T, Lynch I, Lindman S, Berggård T, Thulin E, Nilsson H, Dawson KA, Linse S (2007) Understanding the nanoparticle-protein corona using methods to quantify exchange rates and affinities of proteins for nanoparticles. *Proc Natl Acad Sci U S A* 104(7):2050–2055. doi:10.1073/pnas.0608582104
199. Plank C, Mechtler K, Szoka FC, Wagner E (1996) Activation of the complement system by synthetic DNA complexes: a potential barrier for intravenous gene delivery. *Hum Gene Ther* 7(12):1437–1446. doi:10.1089/hum.1996.7.12-1437
200. Crook K, McLachlan G, Stevenson BJ, Porteous DJ (1996) Plasmid DNA molecules complexed with cationic liposomes are protected from degradation by nucleases and shearing by aerosolisation. *Gene Ther* 3(9):834–839
201. Zhou XH, Klibanov AL, Huang L (1991) Lipophilic polylysines mediate efficient DNA transfection in mammalian cells. *Biochim Biophys Acta* 1065(1):8–14. doi:10.1016/0005-2736(91)90003-q
202. Liu Y, Mounkes LC, Liggitt HD, Brown CS, Solodin I, Heath TD, Debs RJ (1997) Factors influencing the efficiency of cationic liposome-mediated intravenous gene delivery. *Nat Biotechnol* 15(2):167–173. doi:10.1038/nbt0297-167
203. Kranz LM, Diken M, Haas H, Kreiter S, Loquai C, Reuter KC, Meng M, Fritz D, Vascotto F, Hefesha H, Grunwitz C, Vormehr M, Hüseemann Y, Selmi A, Kuhn AN, Buck J, Derhovanessian E, Rae R,

#### IV References

- Attig S, Diekmann J, Jabulowsky RA, Heesch S, Hassel J, Langguth P, Grabbe S, Huber C, Türeci Ö, Sahin U (2016) Systemic RNA delivery to dendritic cells exploits antiviral defence for cancer immunotherapy. *Nature*:396–401. doi:10.1038/nature18300
204. Leventis R, Silvius JR (1990) Interactions of mammalian cells with lipid dispersions containing novel metabolizable cationic amphiphiles. *Biochim Biophys Acta* 1023(1):124–132. doi:10.1016/0005-2736(90)90017-i
205. Karikó K, Kuo A, Barnathan ES, Langer DJ (1998) Phosphate-enhanced transfection of cationic lipid-complexed mRNA and plasmid DNA. *Biochimica et Biophysica Acta (BBA) - Biomembranes* 1369(2):320–334. doi:10.1016/s0005-2736(97)00238-1
206. Yang JP, Huang L (1997) Overcoming the inhibitory effect of serum on lipofection by increasing the charge ratio of cationic liposome to DNA. *Gene Ther* 4(9):950–960. doi:10.1038/sj.gt.3300485
207. Uchida E, Mizuguchi H, Ishii-Watabe A, Hayakawa T (2002) Comparison of the efficiency and safety of non-viral vector-mediated gene transfer into a wide range of human cells. *Biol Pharm Bull* 25(7):891–897. doi:10.1248/bpb.25.891
208. Albanese A, Tang PS, Chan WCW (2012) The effect of nanoparticle size, shape, and surface chemistry on biological systems. *Annu Rev Biomed Eng* 14:1–16. doi:10.1146/annurev-bioeng-071811-150124
209. Nishino M, Matsuzaki I, Musangile FY, Takahashi Y, Iwahashi Y, Warigaya K, Kinoshita Y, Kojima F, Murata S (2020) Measurement and visualization of cell membrane surface charge in fixed cultured cells related with cell morphology. *PLoS One* 15(7):e0236373. doi:10.1371/journal.pone.0236373
210. Wang J, Byrne JD, Napier ME, DeSimone JM (2011) More effective nanomedicines through particle design. *Small* 7(14):1919–1931. doi:10.1002/sml.201100442
211. Dunglison GF, Kaye PL (1995) Endocytosis in mouse blastocysts: characterization and quantification of the fluid phase component. *Mol Reprod Dev* 41(2):225–231. doi:10.1002/mrd.1080410213
212. Fasbender A, Marshall J, Moninger TO, Grunst T, Cheng S, Welsh MJ (1997) Effect of co-lipids in enhancing cationic lipid-mediated gene transfer in vitro and in vivo. *Gene Ther* 4(7):716–725. doi:10.1038/sj.gt.3300459
213. Koshizaka T, Hayashi Y, Yagi K (1989) Novel liposomes for efficient transfection of .BETA.-galactosidase gene into COS-1 cells. *J. Clin. Biochem. Nutr.* 7(3):185–192. doi:10.3164/jcbn.7.185
214. Weickmann JL, Glitz DG (1982) Human ribonucleases. Quantitation of pancreatic-like enzymes in serum, urine, and organ preparations. *J Biol Chem* 257(15):8705–8710
215. Potenza N, Salvatore V, Migliozi A, Martone V, Nobile V, Russo A (2006) Hybridase activity of human ribonuclease-1 revealed by a real-time fluorometric assay. *Nucleic Acids Res* 34(10):2906–2913. doi:10.1093/nar/gkl368
216. Lu L, Li J, Moussaoui M, Boix E (2018) Immune Modulation by Human Secreted RNases at the Extracellular Space. *Front Immunol* 9:1012. doi:10.3389/fimmu.2018.01012
217. Landré JBP, Hewett PW, Olivot J-M, Friedl P, Ko Y, Sachinidis A, Moenner M (2002) Human endothelial cells selectively express large amounts of pancreatic-type ribonuclease (RNase 1). *J Cell Biochem* 86(3):540–552. doi:10.1002/jcb.10234
218. Deshpande RA, Shankar V (2002) Ribonucleases from T2 family. *Crit Rev Microbiol* 28(2):79–122. doi:10.1080/1040-840291046704
219. Zhang H, Rombouts K, Raes L, Xiong R, Smedt SC de, Braeckmans K, Remaut K (2020) Fluorescence-Based Quantification of Messenger RNA and Plasmid DNA Decay Kinetics in Extracellular Biological Fluids and Cell Extracts. *Adv Biosyst* 4(5):e2000057. doi:10.1002/adbi.202000057

#### IV References

220. Reiser A, Woschée D, Mehrotra N, Krzysztoń R, Strey HH, Rädler JO (2019) Correlation of mRNA delivery timing and protein expression in lipid-based transfection. *Integr Biol (Camb)* 11(9):362–371. doi:10.1093/intbio/zyz030
221. Pinnaduwa P, Schmitt L, Huang L (1989) Use of a quaternary ammonium detergent in liposome mediated DNA transfection of mouse L-cells. *Biochim Biophys Acta* 985(1):33–37. doi:10.1016/0005-2736(89)90099-0
222. Zhang YP, Sekirov L, Saravolac EG, Wheeler JJ, Tardi P, Clow K, Leng E, Sun R, Cullis PR, Scherrer P (1999) Stabilized plasmid-lipid particles for regional gene therapy: formulation and transfection properties. *Gene Ther* 6(8):1438–1447. doi:10.1038/sj.gt.3300965
223. Boczkowski D, Nair SK, Snyder D, Gilboa E (1996) Dendritic cells pulsed with RNA are potent antigen-presenting cells in vitro and in vivo. *J Exp Med* 184(2):465–472. doi:10.1084/jem.184.2.465
224. Harrison GS, Wang Y, Tomczak J, Hogan C, Shpall EJ, Curiel TJ, Felgner PL (1995) Optimization of gene transfer using cationic lipids in cell lines and primary human CD4+ and CD34+ hematopoietic cells. *Biotechniques* 19(5):816–823
225. Kenworthy AK, Hristova K, Needham D, McIntosh TJ (1995) Range and magnitude of the steric pressure between bilayers containing phospholipids with covalently attached poly(ethylene glycol). *Biophys J* 68(5):1921–1936. doi:10.1016/S0006-3495(95)80369-3
226. Godin B, Tuitou E (2007) Transdermal skin delivery: predictions for humans from in vivo, ex vivo and animal models. *Adv Drug Deliv Rev* 59(11):1152–1161. doi:10.1016/j.addr.2007.07.004
227. Whitehead KA, Matthews J, Chang PH, Niroui F, Dorkin JR, Severgnini M, Anderson DG (2012) In vitro-in vivo translation of lipid nanoparticles for hepatocellular siRNA delivery. *ACS Nano* 6(8):6922–6929. doi:10.1021/nn301922x
228. Blakney AK, McKay PF, Christensen D, Yus BI, Aldon Y, Follmann F, Shattock RJ (2019) 2019 JCR-D-19-00127R1 // Effects of cationic adjuvant formulation particle type, fluidity and immunomodulators on delivery and immunogenicity of saRNA. *J Control Release*:65–74. doi:10.1016/j.jconrel.2019.04.043
229. Pearton M, Kang S-M, Song J-M, Anstey AV, Ivory M, Compans RW, Birchall JC (2010) Changes in human Langerhans cells following intradermal injection of influenza virus-like particle vaccines. *PLoS One* 5(8):e12410. doi:10.1371/journal.pone.0012410
230. Bins AD, Jorritsma A, Wolkers MC, Hung C-F, Wu T-C, Schumacher TNM, Haanen JBAG (2005) A rapid and potent DNA vaccination strategy defined by in vivo monitoring of antigen expression. *Nat Med* 11(8):899–904. doi:10.1038/nm1264
231. Castagnoli C, Alotto D, Cambieri I, Casimiri R, Aluffi M, Stella M, Alasia ST, Magliacani G (2003) Evaluation of donor skin viability: fresh and cryopreserved skin using tetrazolium salt assay. *Burns* 29(8):759–767. doi:10.1016/j.burns.2003.01.001
232. Messenger S, Hann AC, Goddard PA, Dettmar PW, Maillard JY (2003) Assessment of skin viability: is it necessary to use different methodologies? *Skin Res Technol* 9(4):321–330. doi:10.1034/j.1600-0846.2003.00039.x
233. Blakney AK, Deletic P, McKay PF, Bouton CR, Ashford M, Shattock RJ, Sabirsh A (2020) Effect of complexing lipids on cellular uptake and expression of messenger RNA in human skin explants. *J Control Release*. doi:10.1016/j.jconrel.2020.11.033
234. Probst J, Weide B, Scheel B, Pichler BJ, Hoerr I, Rammensee H-G, Pascolo S (2007) Spontaneous cellular uptake of exogenous messenger RNA in vivo is nucleic acid-specific, saturable and ion dependent. *Gene Ther* 14(15):1175–1180. doi:10.1038/sj.gt.3302964
235. Barry ME, Pinto-González D, Orson FM, McKenzie GJ, Petry GR, Barry MA (1999) Role of endogenous endonucleases and tissue site in transfection and CpG-mediated immune activation after naked DNA injection. *Hum Gene Ther* 10(15):2461–2480. doi:10.1089/10430349950016816

#### IV References

236. Hermsmeier M, Jeong S, Yamamoto A, Chen X, Nagavarapu U, Evans CL, Chan KF (2018) Characterization of human cutaneous tissue autofluorescence: implications in topical drug delivery studies with fluorescence microscopy. *Biomed Opt Express* 9(11):5400–5418. doi:10.1364/BOE.9.005400
237. Laiho LH, Pelet S, Hancewicz TM, Kaplan PD, So PTC (2005) Two-photon 3-D mapping of ex vivo human skin endogenous fluorescence species based on fluorescence emission spectra. *J Biomed Opt* 10(2):24016. doi:10.1117/1.1891370
238. König K, Meyer H, Schneckenburger H, Rück A (1993) The study of endogenous porphyrins in human skin and their potential for photodynamic therapy by laser induced fluorescence spectroscopy. *Laser Med Sci* 8(2):127–132. doi:10.1007/BF02547809
239. Sanchez WY, Prow TW, Sanchez WH, Grice JE, Roberts MS (2010) Analysis of the metabolic deterioration of ex vivo skin from ischemic necrosis through the imaging of intracellular NAD(P)H by multiphoton tomography and fluorescence lifetime imaging microscopy. *J Biomed Opt* 15(4):46008. doi:10.1117/1.3466580
240. Casares S, Inaba K, Brumeanu TD, Steinman RM, Bona CA (1997) Antigen presentation by dendritic cells after immunization with DNA encoding a major histocompatibility complex class II-restricted viral epitope. *J Exp Med* 186(9):1481–1486. doi:10.1084/jem.186.9.1481
241. Tsien RY (1998) The green fluorescent protein. *Annu Rev Biochem* 67:509–544. doi:10.1146/annurev.biochem.67.1.509
242. Machado Y, Duinkerken S, Hoepflinger V, Mayr M, Korotchenko E, Kurtaj A, Pablos I, Steiner M, Stoecklinger A, Lübbers J, Schmid M, Ritter U, Scheibelhofer S, Ablinger M, Wally V, Hochmann S, Raninger AM, Strunk D, van Kooyk Y, Thalhamer J, Weiss R (2017) Synergistic effects of dendritic cell targeting and laser-microporation on enhancing epicutaneous skin vaccination efficacy. *J Control Release* 266:87–99. doi:10.1016/j.jconrel.2017.09.020
243. Larsen CP, Steinman RM, Witmer-Pack M, Hankins DF, Morris PJ, Austyn JM (1990) Migration and maturation of Langerhans cells in skin transplants and explants. *J Exp Med* 172(5):1483–1493. doi:10.1084/jem.172.5.1483
244. Rughetti A, Biffoni M, Sabbatucci M, Rahimi H, Pellicciotta I, Fattorossi A, Pierelli L, Scambia G, Lavitrano M, Frati L, Nuti M (2000) Transfected human dendritic cells to induce antitumor immunity. *Gene Ther* 7(17):1458–1466. doi:10.1038/sj.gt.3301266
245. Porgador A, Irvine KR, Iwasaki A, Barber BH, Restifo NP, Germain RN (1998) Predominant role for directly transfected dendritic cells in antigen presentation to CD8+ T cells after gene gun immunization. *J Exp Med* 188(6):1075–1082. doi:10.1084/jem.188.6.1075
246. Bins AD, Wolkers MC, van den Boom MD, Haanen JBAG, Schumacher TNM (2007) In vivo antigen stability affects DNA vaccine immunogenicity. *J Immunol* 179(4):2126–2133. doi:10.4049/jimmunol.179.4.2126
247. Akbari O, Panjwani N, Garcia S, Tascon R, Lowrie D, Stockinger B (1999) DNA vaccination: transfection and activation of dendritic cells as key events for immunity. *J Exp Med* 189(1):169–178. doi:10.1084/jem.189.1.169
248. Kupper TS (1990) The activated keratinocyte: a model for inducible cytokine production by non-bone marrow-derived cells in cutaneous inflammatory and immune responses. *J Invest Dermatol* 94(6 Suppl):146S-150S. doi:10.1111/1523-1747.ep12876130
249. Wang R, Doolan DL, Le TP, Hedstrom RC, Coonan KM, Charoenvit Y, Jones TR, Hobart P, Margalith M, Ng J, Weiss WR, Sedegah M, Taisne C de, Norman JA, Hoffman SL (1998) Induction of antigen-specific cytotoxic T lymphocytes in humans by a malaria DNA vaccine. *Science* 282(5388):476–480. doi:10.1126/science.282.5388.476
250. Fu TM, Ulmer JB, Caulfield MJ, Deck RR, Friedman A, Wang S, Liu X, Donnelly JJ, Liu MA (1997) Priming of cytotoxic T lymphocytes by DNA vaccines: requirement for professional antigen presenting cells and evidence for antigen transfer from myocytes. *Mol Med* 3(6):362–371

## IV References

251. Metlay JP, Puré E, Steinman RM (1989) Control of the immune response at the level of antigen-presenting cells: a comparison of the function of dendritic cells and B lymphocytes. *Adv Immunol* 47:45–116. doi:10.1016/s0065-2776(08)60662-8
252. Polack FP, Thomas SJ, Kitchin N, Absalon J, Gurtman A, Lockhart S, Perez JL, Pérez Marc G, Moreira ED, Zerbini C, Bailey R, Swanson KA, Roychoudhury S, Koury K, Li P, Kalina WV, Cooper D, Frenck RW, Hammitt LL, Türeci Ö, Nell H, Schaefer A, Ünal S, Tresnan DB, Mather S, Dormitzer PR, Şahin U, Jansen KU, Gruber WC (2020) Safety and Efficacy of the BNT162b2 mRNA Covid-19 Vaccine. *N Engl J Med* 383(27):2603–2615. doi:10.1056/NEJMoa2034577
253. Lademann J, Patzelt A, Richter H, Antoniou C, Sterry W, Knorr F (2009) Determination of the cuticula thickness of human and porcine hairs and their potential influence on the penetration of nanoparticles into the hair follicles. *J Biomed Opt* 14(2):21014. doi:10.1117/1.3078813
254. Seago SV, Ebling FJ (1985) The hair cycle on the human thigh and upper arm. *Br J Dermatol* 113(1):9–16. doi:10.1111/j.1365-2133.1985.tb02038.x
255. Gregorio J, Meller S, Conrad C, Di Nardo A, Homey B, Lauerma A, Arai N, Gallo RL, Digiovanni J, Gilliet M (2010) Plasmacytoid dendritic cells sense skin injury and promote wound healing through type I interferons. *J Exp Med*:2921–2930. doi:10.1084/jem.20101102
256. Bisso PW, Gaglione S, Guimarães PPG, Mitchell MJ, Langer R (2018) Nanomaterial Interactions with Human Neutrophils. *ACS Biomater Sci Eng* 4(12):4255–4265. doi:10.1021/acsbiomaterials.8b01062
257. Kambayashi T, Laufer TM (2014) Atypical MHC class II-expressing antigen-presenting cells: can anything replace a dendritic cell? *Nat Rev Immunol* 14(11):719–730. doi:10.1038/nri3754
258. Takashima A, Yao Y (2015) Neutrophil plasticity: acquisition of phenotype and functionality of antigen-presenting cell. *J Leukoc Biol* 98(4):489–496. doi:10.1189/jlb.1MR1014-502R
259. Romani N, Thurnher M, Idoyaga J, Steinman RM, Flacher V (2010) Targeting of antigens to skin dendritic cells: possibilities to enhance vaccine efficacy. *Immunol Cell Biol*:424–430. doi:10.1038/icb.2010.39
260. Steinman RM (2008) Dendritic cells in vivo: a key target for a new vaccine science. *Immunity* 29(3):319–324. doi:10.1016/j.immuni.2008.08.001
261. Sparber F, Tripp CH, Hermann M, Romani N, Stoitzner P (2010) Langerhans cells and dermal dendritic cells capture protein antigens in the skin: possible targets for vaccination through the skin. *Immunobiology*:770–779. doi:10.1016/j.imbio.2010.05.014
262. Volckmar J, Knop L, Stegemann-Koniszewski S, Schulze K, Ebensen T, Guzmán CA, Bruder D (2019) The STING activator c-di-AMP exerts superior adjuvant properties than the formulation poly(I:C)/CpG after subcutaneous vaccination with soluble protein antigen or DEC-205-mediated antigen targeting to dendritic cells. *Vaccine* 37(35):4963–4974. doi:10.1016/j.vaccine.2019.07.019

## V. Supplementary Figures

Table S 1: Hydrodynamic parameters of LPNs with and without fluorescent labels. Table has been modified from supplementary material of Kliesch et al. [157]

LPN	Marker	Size [nm]	PDI	Zeta potential [mV]	Batches tested
LPN(0/100)	-	194.43 ± 11.02	0.09 ± 0.02	21.67 ± 1.11	5
	FITC	200.30 ± 9.78	0.10 ± 0.03	24.79 ± 3.73	3
LPN(10/90)	-	200.49 ± 8.49	0.10 ± 0.02	22.49 ± 3.38	5
	DiD	198.60 ± 0.96	0.12 ± 0.03	29.7 ± 2.50	1
LPN(20/80)	FITC	197.09 ± 9.50	0.09 ± 0.02	25.87 ± 3.85	4
	-	208.73 ± 8.86	0.09 ± 0.02	26.33 ± 2.17	5
LPN(30/70)	FITC	225.06 ± 20.31	0.13 ± 0.07	28.73 ± 2.34	3
	-	215.69 ± 16.30	0.10 ± 0.02	29.71 ± 4.14	5
LPN(40/60)	FITC	209.87 ± 13.13	0.10 ± 0.02	28.66 ± 4.21	3
	-	219.84 ± 17.59	0.11 ± 0.03	30.28 ± 2.07	5
LPN(50/50)	FITC	237.69 ± 3.72	0.13 ± 0.06	32.41 ± 4.67	3
	-	229.15 ± 20.51	0.12 ± 0.03	32.90 ± 2.68	5
LPN(70/30)	FITC	243.22 ± 9.74	0.13 ± 0.02	34.74 ± 1.39	3
	-	219.77 ± 11.35	0.14 ± 0.02	38.26 ± 1.72	5
LPN(100/0)	DiD	218.85 ± 10.08	0.12 ± 0.04	28.56 ± 8.13	4
	FITC	243.93 ± 13.00	0.13 ± 0.03	34.00 ± 2.20	5
LPN(100/0)	-	205.86 ± 12.64	0.12 ± 0.02	-11.75 ± 0.69	5
	FITC	237.56 ± 26.28	0.14 ± 0.07	-9.77 ± 5.13	3

Table S 2: Hydrodynamic parameters of DiD labeled LPN(70/30).

LPN	PEG [mol%]	dye	mRNA	Size [nm]	PDI	Zeta potential [mV]	Batch size
LPN(70/30)	-	DiD	+	239.80 ± 3.06	0.18 ± 0.01	-18.7 ± 0.50	1
	2.5	DiD	+	260.67 ± 1.66	0.21 ± 0.01	-14.53 ± 0.65	1
	5	DiD	+	294.53 ± 3.77	0.26 ± 0.02	-16.43 ± 0.49	1

V Supplementary Figures

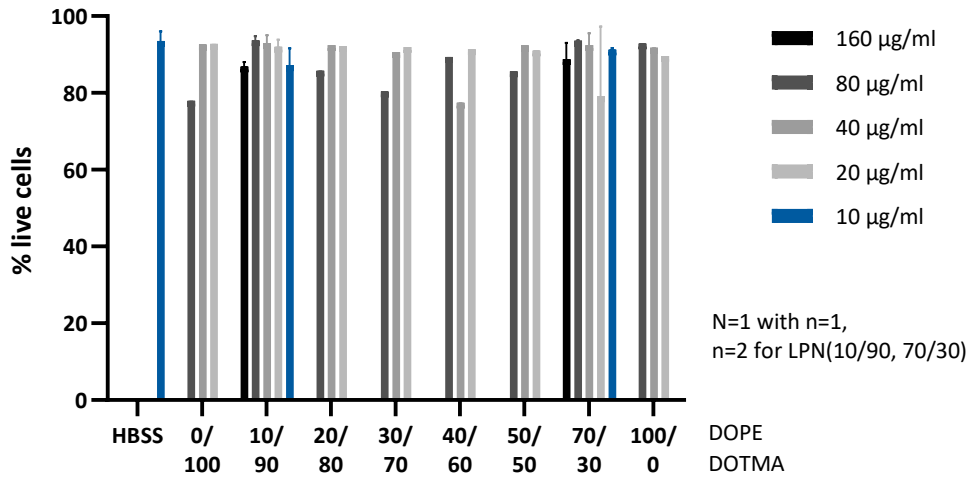
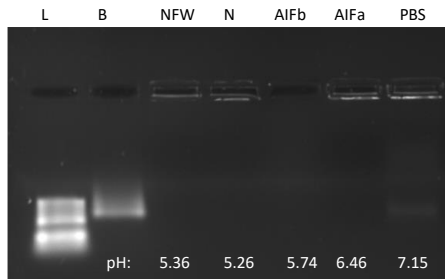


Figure S 1: Viability assessment of plain LPNs in DC2.4 cell line with different concentrations. Incubation time with LPNs dispersed in HBSS was 4 h. Dead cells were excluded by DAPI staining and flow cytometry analysis. All LPNs were well tolerated independent of the concentration as indicated by cell viabilities above 75%. Graph has been modified from supplementary material of Kliesch et al. [157]

A



B

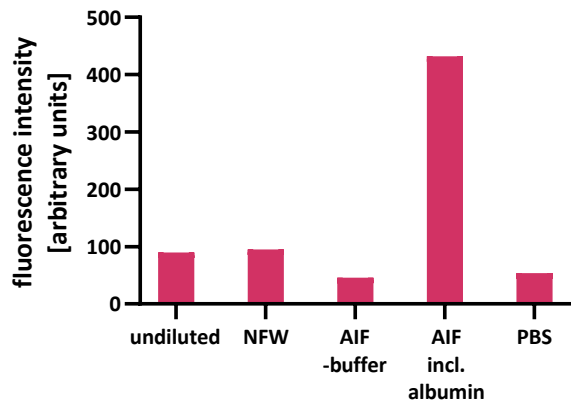


Figure S 2: Effect of salts and albumin on binding efficacy of LPN(10/90). (A): Gel electrophoresis. (B): Measured fluorescence intensities of RiboGreen® dye mixed with LPN(10/90). Nanoparticles were diluted in buffers or NFW prior to adding the mRNA for complexation. The strong interaction of LPN(10/90) with mRNA was independent of the buffer. Only the addition of albumin led to a faint band of naked mRNA. AIFb: artificial interstitial fluid – buffer only; AIFa: artificial interstitial fluid including albumin.

V Supplementary Figures

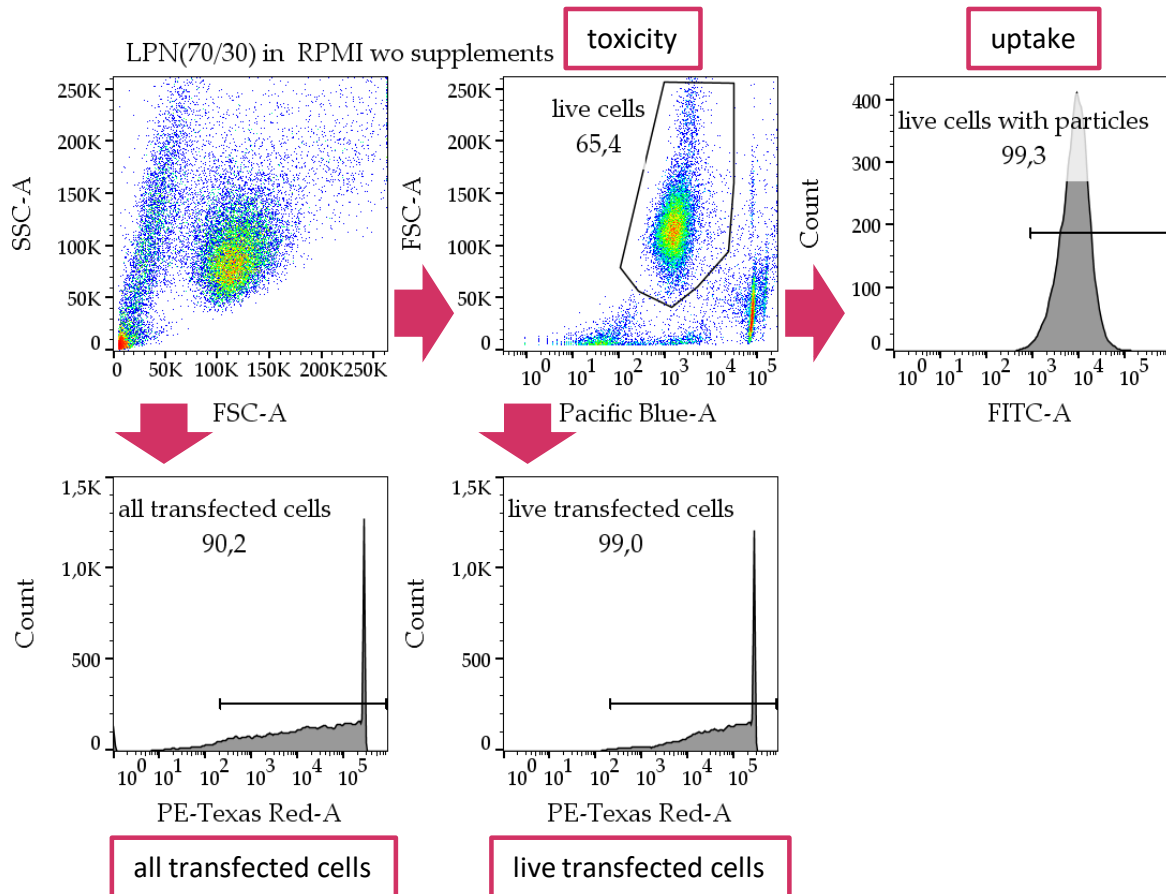


Figure S 3: Gating strategy for combined assay with quantification of cytotoxicity, uptake and transfection efficacy in parallel by flow cytometry. DAPI staining was used for dead cell exclusion. FITC-labeled LPNs for the uptake assessment and mRNA encoding for the fluorescent protein mCherry for the quantification of transfection efficacy. Graph has been modified from supplementary material of Kliesch et al. [157]

V Supplementary Figures

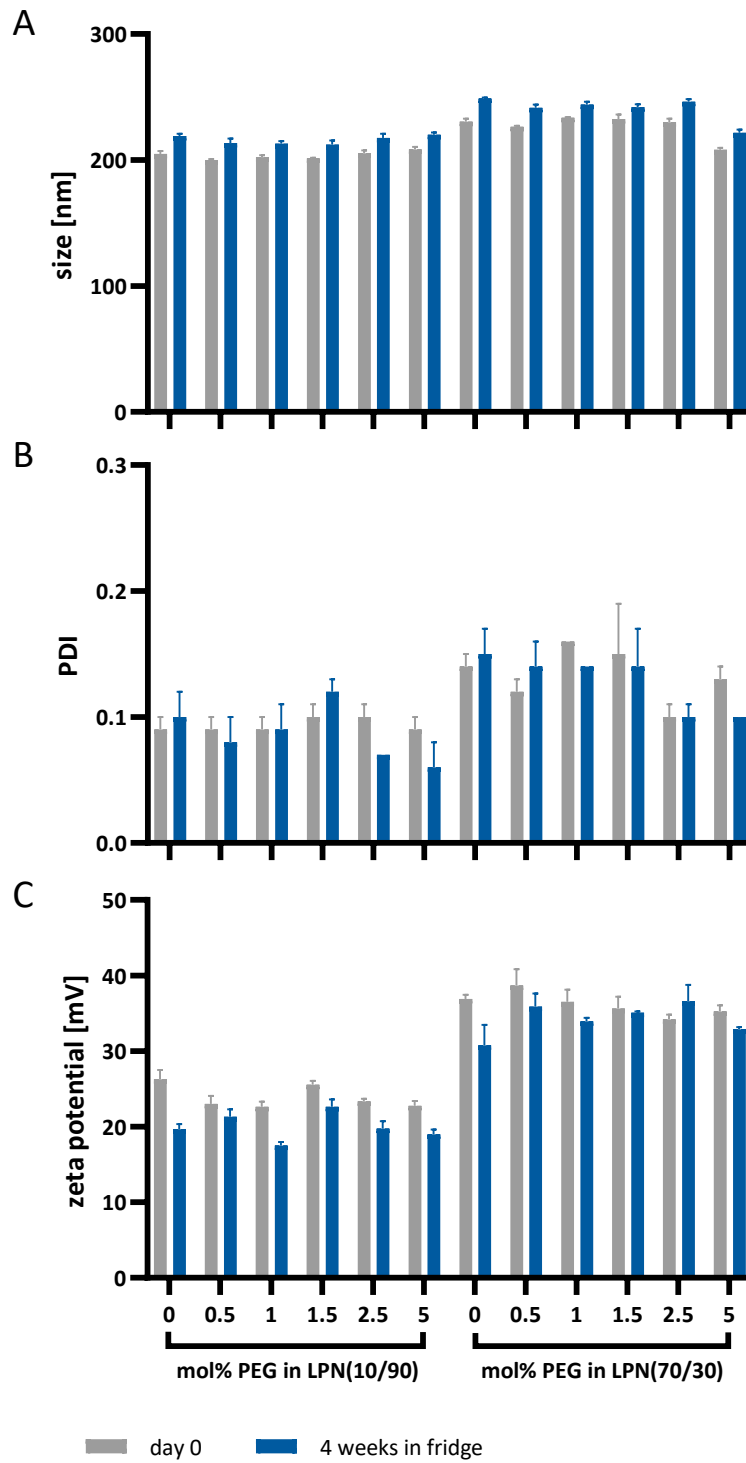


Figure S 4: Stability assessment of plain, pegylated LPNs over the course of 4 weeks. (A): Size (B): PDI (C): Zeta potential of LPN(10/90) and LPN(70/30). Pegylation did not affect stability of any of the tested parameters. Slight increase in size and reduction of surface potential were observed independent of pegylation.

## V Supplementary Figures

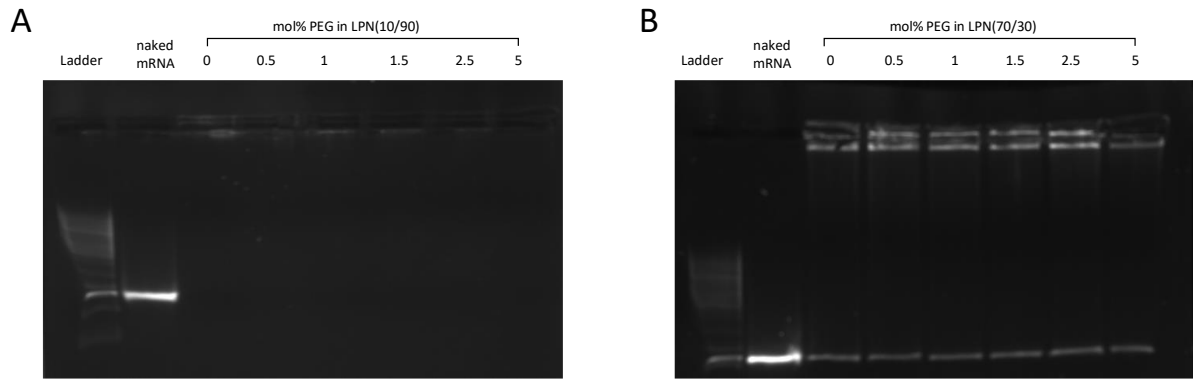


Figure S 5: Gel electrophoresis of pegylated LPNs. Pegylation did not show an influence on mRNA complexation properties.

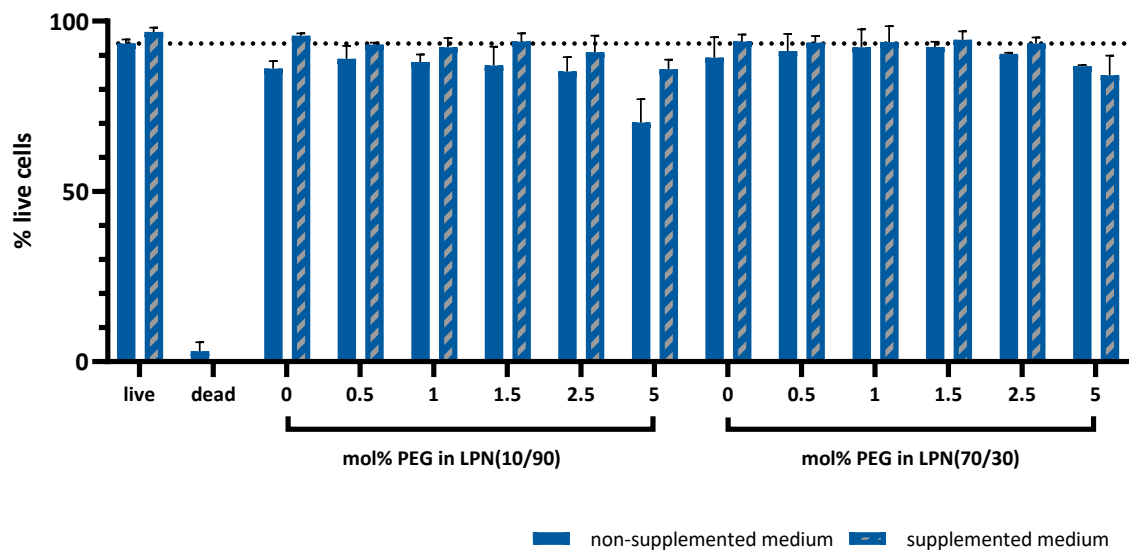
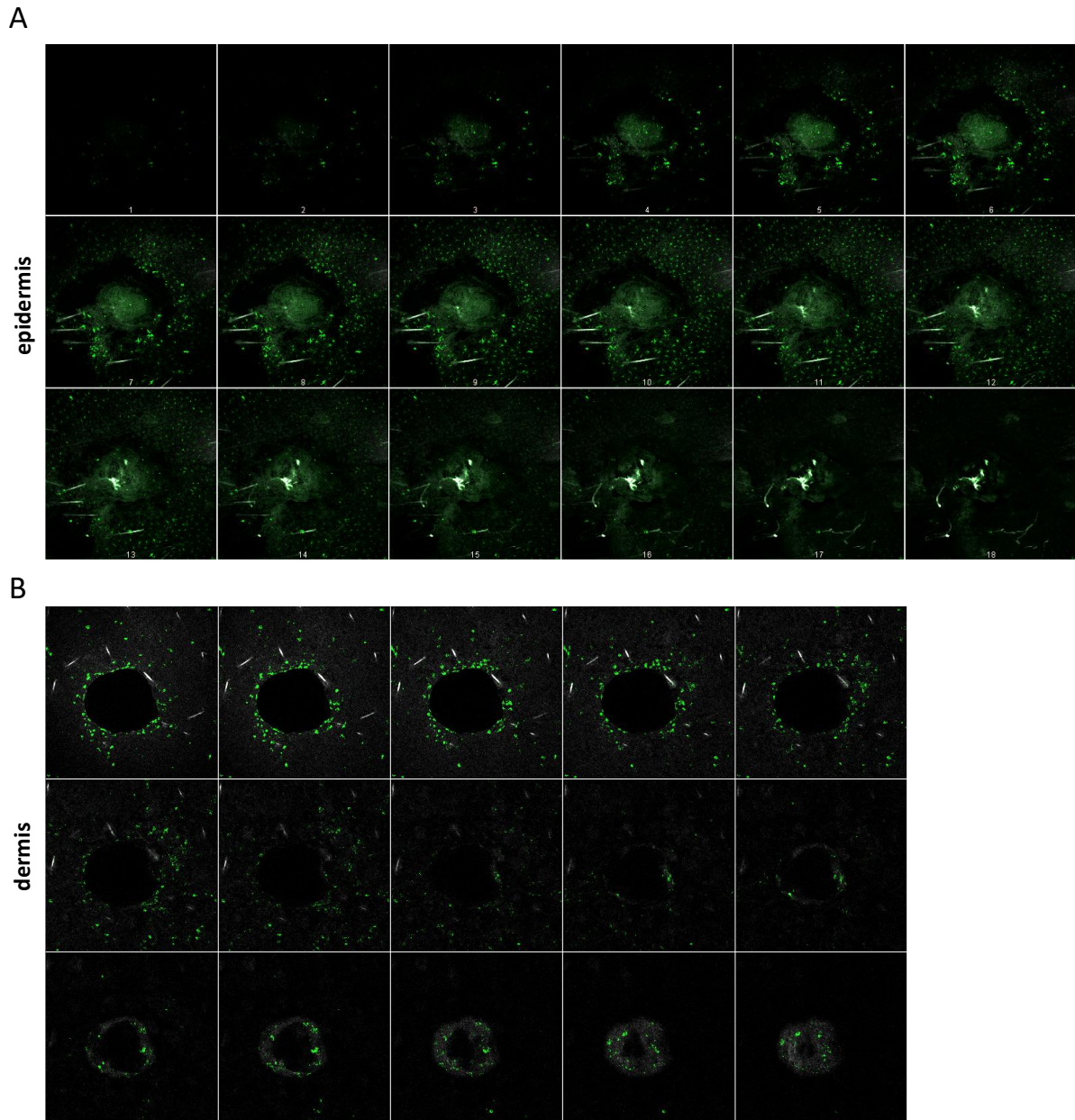


Figure S 6: Viability of DC2.4 cells after 24 h incubation with mCherry-mRNA-loaded, pegylated LPNs. Nanocarriers were either dispersed in non-supplemented RPMI medium or full growth medium with 10% FCS, HEPES-buffer (0.01M), non-essential amino acids (1X) and  $\beta$ -mercaptoethanol (0.0054X). Medium without nanoparticles was used as live, ethanol (5% in HBSS (v/v)) as dead control. Live cells were gated using FDA and DAPI staining. N=1 with total n= 2. All but 5 mol% PEG-LPNs in non-supplemented medium were well tolerated with viability values above 80%.



*Figure S 7: Microscopic cuts of microporated skin supplementing images of Figure 38 K and N. Laser settings: two pulses per pore and theoretical pore depth of 48  $\mu\text{m}$  (pulse length 75  $\mu\text{s}$ , repetition rate 200 Hz, pore density 8%, treatment area 8x8 mm). MHC-II staining using secondary antibody with BV421-linker displayed in green. Autofluorescence of mouse hair is shown in white. **(A)**: Epidermis of mouse ear 24 h after creation of deep pores. **(B)**: Dermis the same ear (24 h after deep pore microporation). Recruitment of MHC-II positive cells happens especially in the dermis where these cells assemble around the pore.*



## V Supplementary Figures

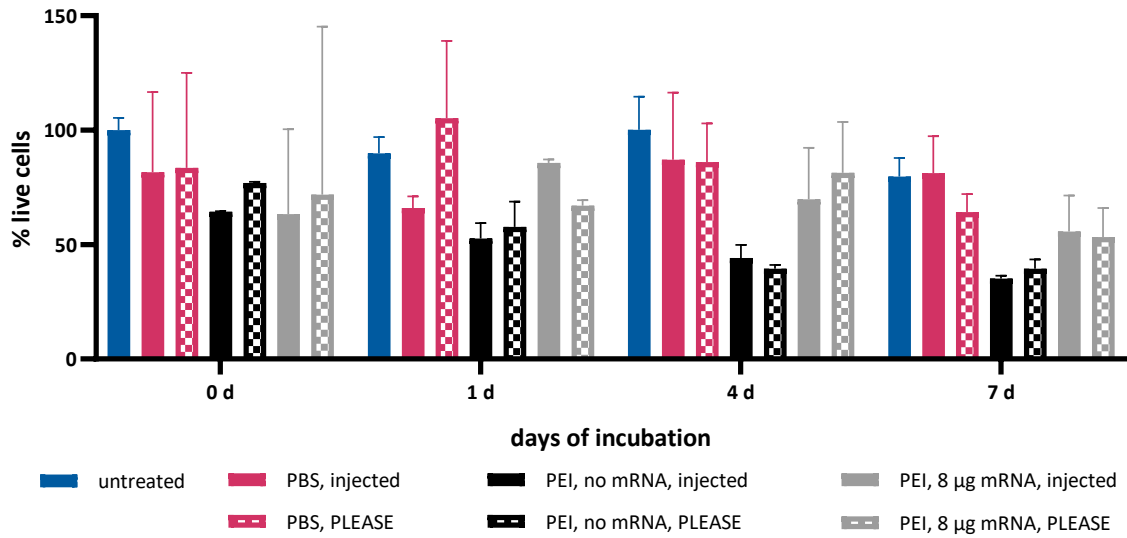


Figure S 9: MTT-mediated viability of skin biopsies after treatment with process controls either by intradermal injection (solid bars) or after P.L.E.A.S.E.® microporation (bars with pattern). Laser parameters: pulse length 75 µs, repetition rate 200 Hz, 8 pulses per pore, 8 x 8 mm treatment area. PBS was used as negative, PEI with mRNA as positive control (8 µg mRNA per biopsy). PEI without mRNA was added to assess toxic effects of polymer itself. Data acquired in five independent experiments with up to eight biopsies per treatment group in total (PEI without mRNA had only 1 data point per time point). Tissue viability was stable over the course of one week as demonstrated by comparable results for PBS samples. PEI complexed with mRNA seems less toxic compared to the blank polymer.

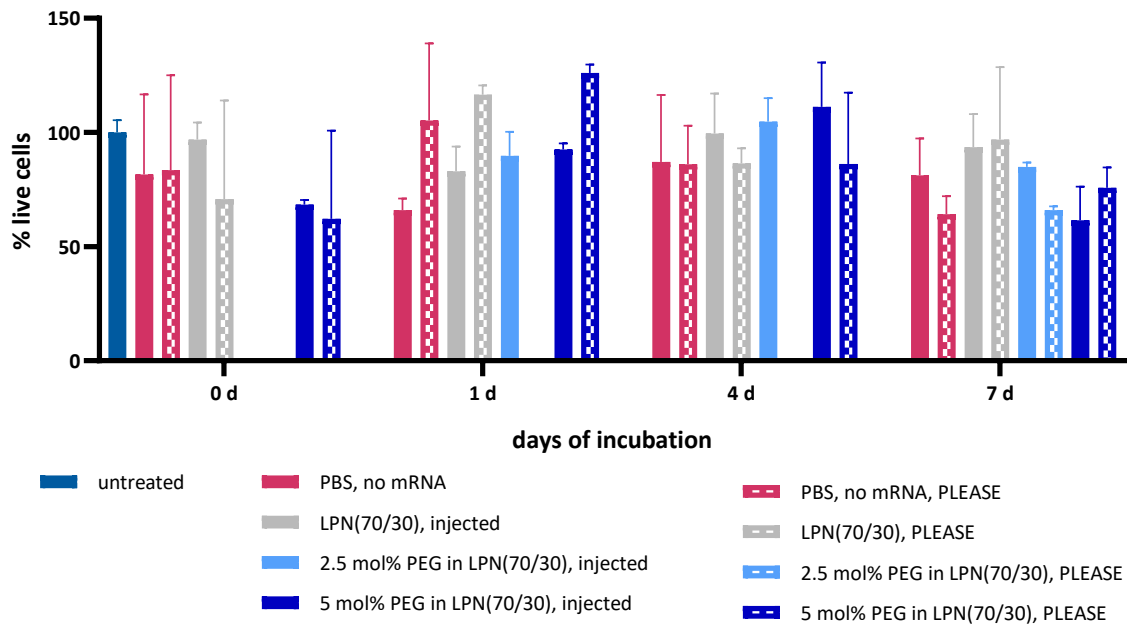


Figure S 10: MTT mediated viability of skin biopsies after application of mRNA-loaded LPNs either by intradermal injection (solid bars) or after P.L.E.A.S.E.® microporation (bars with pattern). Laser parameters: pulse length 75 µs, repetition rate 200 Hz, 8 pulses per pore, 8 x 8 mm treatment area. PBS was used as negative control; 8 µg mRNA per biopsy. Data acquired in five independent experiments with up to 6 biopsies per treatment group in total. LPNs were as well or even better tolerated than PBS.

## V Supplementary Figures

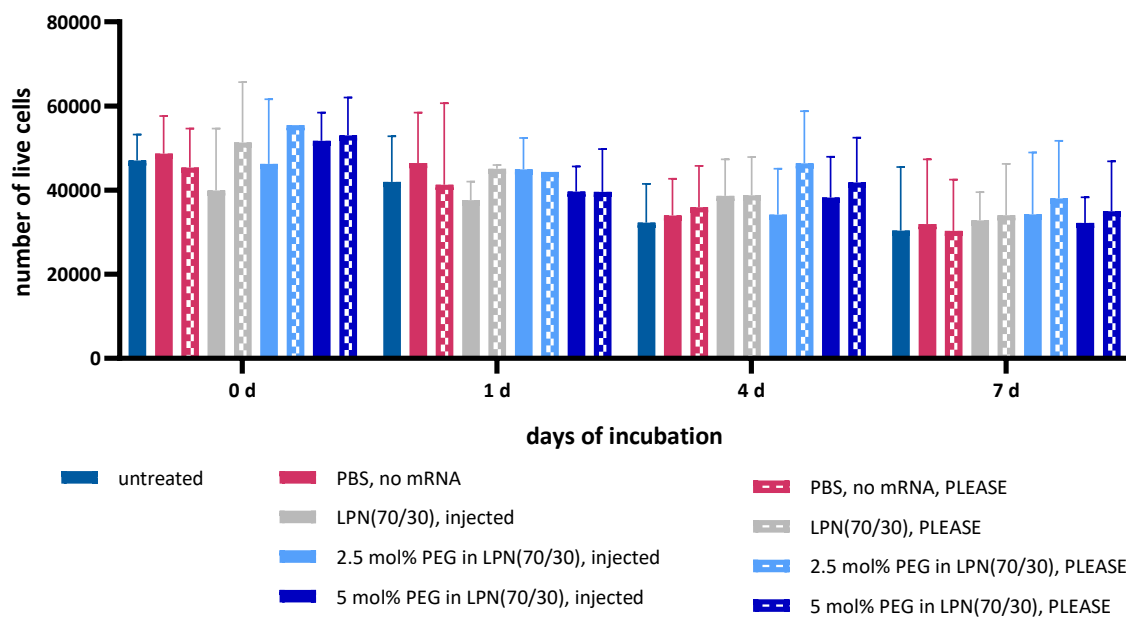


Figure S 11: Absolute viability of skin biopsies after application of mRNA-loaded LPNs either by intradermal injection (solid bars) or after P.L.E.A.S.E.<sup>®</sup> microporation (bars with pattern) (pulse length 75  $\mu$ s, repetition rate 200 Hz, 8 pulses per pore, 8 x 8 mm treatment area). PBS was used as negative control; 8  $\mu$ g mRNA per biopsy. DAPI and FDA addition enabled gating for live cells. 100,000 events counted in flow cytometer. Data acquired in five independent experiments with up to eight biopsies per treatment group in total. LPNs were as well tolerated as PBS and showed viability values comparable to the untreated control. Same data set as Figure 59 but presented differently.

## V Supplementary Figures

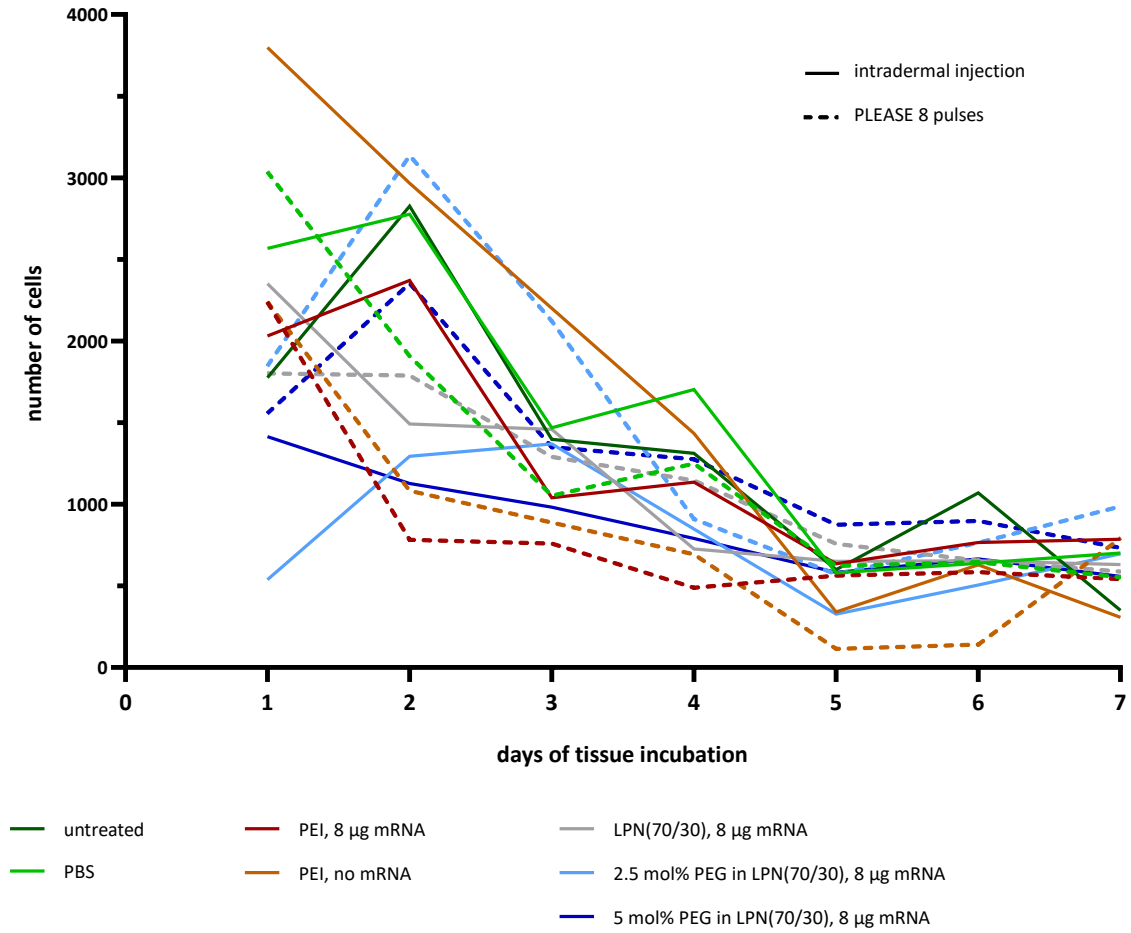


Figure S 12: Overview of number of all cells in the supernatant of cultivated skin biopsies over the course of one week. After daily collecting medium from the same biopsy, medium was replaced. Samples were analyzed by flow cytometry. DAPI and FDA were added to gate for live cells. Solid lines represent skin biopsies after intradermal injection, dotted line after P.L.E.A.S.E.® microporation (pulse length 75 µs, repetition rate 200 Hz, 8 pulses per pore, 8 x 8 mm treatment area). Most cells evaded the tissue within the first 48 h of cultivation. Samples without mRNA (untreated, PBS and blank PEI polymer) were among highest numbers, especially after 1 day. Only 2,5 mol% PEG in LPN(70/30) showed highest number after 2 days.

## VI. Scientific Output

### 7.1 Articles Published in Peer Reviewed Journals

Lena Kliesch, Simon Delandre, Aljoscha Gabelmann, Marcus Koch, Kai Schulze, Carlos A Guzmán, Brigitta Loretz, Claus-Michael Lehr (2022) Lipid-Polymer Hybrid Nanoparticles for mRNA Delivery to Dendritic Cells: Impact of Lipid Composition on Performance in Different Media. *Pharmaceutics* 14(12). doi:10.3390/pharmaceutics14122675

### 7.2 Oral Presentations

**“Lipid coated polymeric nanoparticles for mRNA delivery to cutaneous Dendritic Cells: Influence of Lipid composition”**, Galenus Workshop 2019, Frankfurt/Main, Germany

Flash Presentation for the Poster **“Effect of lipid composition on the mRNA delivery properties of polymer-lipid hybrid nanoparticles for Skin Vaccination”**, Annual meeting of Controlled Release Society (CRS) German chapter 2020, Munich, Germany

Flash Talk for the Poster **“Improving the in vitro - in vivo correlation to better predict the delivery of mRNA in vivo by selected in vitro assays”**, Annual meeting of CRS German chapter 2021, Virtual Meeting, Aachen, Germany

**“mRNA-based Skin Vaccination by Intradermal Application of Lipid coated Polymeric Nanoparticles”**, World Meeting on Pharmaceutics, Biopharmaceutics and Pharmaceutical Technology (PBP) 2021, Virtual Meeting, Vienna, Austria

**“Systematic evaluation of challenging factors to improve in vitro – in vivo correlation for mRNA delivery”**, Annual meeting of the international Controlled Release Society (CRS) 2021, Hybrid-Meeting, Montreal, Canada

Winner of video contest of CRS focus Group: Transdermal and Mucosal Delivery (TMD) with video presentation **“How can we improve in vitro – in vivo correlation for mRNA delivery by nanoparticles?”** in context of the annual meeting of the international Controlled Release Society (CRS) 2021, Montreal, Canada

### 7.3 Poster Presentations

**“Nanocarriers for Minimally Invasive Intradermal Vaccination”**, HIPS Symposium, 2019, Saarbrücken, Germany

**“Lipid-polymer hybrid nanoparticles for mRNA delivery in Dendritic cells: Impact of lipid composition”**, German Pharmaceutical society (DPhG) Annual Meeting 2019, Heidelberg, Germany

**“Lipid coated polymeric nanoparticles for mRNA delivery to Dendritic Cells: Influence of lipid composition on Transfection and Cytotoxicity”**, PhD Student Symposium (Doktorandentag) of Saarland University 2019, Saarbrücken, Germany

**“Effect of lipid composition on the mRNA delivery properties of polymer-lipid hybrid nanoparticles for Skin Vaccination”**, Controlled Release Society (CRS) German chapter meeting 2020, Munich, Germany

**“Systematic evaluation of challenging factors for mRNA delivery by lipid-polymer hybrid nanoparticles”**, International Conference on Biological Barriers 2021, Virtual Meeting, Saarbrücken, Germany

**“Advanced Vaccine Carriers – from biogenic extracellular vesicles to polymeric nucleic acid nanocarriers”**, HIPS Symposium 2021, Virtual Meeting, Saarbrücken, Germany

## VII. Acknowledgements

When I started to work with mRNA-based vaccination more than 5 years ago, the benefits of such a vaccine were more a theory than reality. This completely changed with the rise of the SARS Cov2 virus with tremendous effect onto everyone's life – private but also research wise. I am very thankful that completing this PhD was still possible despite this extraordinary situation. This was only possible with the help of many special people that I would like to acknowledge now.

First, I would like to thank Prof. Dr. Claus-Michael Lehr for giving me the chance to work on this very exciting project and entrusting in me. I profited a lot from his enthusiasm for science and the inspiring discussions we had. I am really grateful for all the conferences that he allowed me to visit to share my work.

I would like to express my gratitude for all the support I got from Brigitta Loretz in so many different ways. I knew that whatever problem I would have, I could ask her for advice and that she would always have an idea to open a new door. Finishing this thesis would have been very unlikely without her optimism and her endless patience. I am very grateful for the time she spent revising this thesis and all the other files and graphs I sent her during my PhD. I really appreciate how much more she did than I dared to expect. I hope every PhD student has someone like her in the team.

Furthermore, I would like to thank Prof. Alexandra Kiemer for being part of my thesis committee and revising this thesis. Her input helped a lot to save my analytical problems. Giving me the chance to use the equipment in her lab, enabled me to establish better protocols to prepare my samples.

For the outcome of this project, the collaboration with the colleagues from the HZI was very important. Prof. Carlos Guzmán and Kai Schulze always took the time to discuss new research hypothesis and strategies to investigate these ideas in the lab. I learned a lot from her immunological perspective onto my project and appreciated their helpful remarks. This is the right place to express my gratitude for the collaboration with Simon. I really enjoyed the hours we spent together in the lab. Despite the endless tasks we had, I learned a lot from him and really had fun working with him in the lab.

I would like to thank Sarah N for taking my hand at the beginning of my project and for introducing me to nucleic acid delivery. We shared experiments, our problems and many hours in the transport lab that passed by very quickly due to exciting conversations. I looked up to her broad knowledge and the ability to always develop new working hypothesis and experimental setups. I am confident that science is the right spot for her.

My time at the institute would have never been the same without all the other DDEL and BION team members. Next to the countless hours working on the same bench or in the transport lab, I really enjoyed our lunch breaks and the mensa walks. Meeting all of you was a great pleasure to me. Your passion for science and hearing how fruitful and exciting lab work can be, motivated me to continue my project overseeing all the drawbacks. I really enjoyed being part of the particle club and would like to express my gratitude to Benedikt, Kevin, Neha, Olga, Rebekka, Sangeun, Sarah, Yun and all the others for letting me participate in your success stories. A special thanks belongs to Samy. Sharing the office for most of my PhD time was absolutely great. I am impressed by his positivity, enthusiasm and energy and hope he will always maintain these characteristics. I profited a lot from his input even though our projects were very different. He always had an open ear and listened to all my concerns. I know he has everything he needs to realize his dreams. Mohamed and Aghiad joined us some time later and completed our nice office. I am very grateful for the time we had together discussing findings, results and everything beyond.

## VII Acknowledgements

I would like to thank Tobias for selecting my project for his Wahlpflichtpraktikum. His results are an important part of this thesis and supervising him made me realize how much I have already learned about the work in the lab. This feeling was further enhanced by introducing Aljoscha to all my protocols. Giving him a good start in his PhD work and knowing that someone profited from my hard-earned achievements, encouraged me that it was time for me to leave the lab and finish my research. I am more than grateful that he conducted my last experiments and I hope he enjoyed the short but intense lab time we had together as much as I did.

Last but not least, möchte ich dem Team von Technikern danken, die niemals müde wurden, gegen das Chaos und die Anarchie im Labor, dem Lager oder der Küche zu kämpfen. Bahnbrechende Forschung ist nicht möglich ohne Menschen wie Euch, die im Hintergrund die Streben zusammenhalten und uns Wissenschaftlern den Rücken freihalten. Danke, dass ihr immer alles versucht habt, Lösungen für meine Probleme zu finden und dabei immer ein gutes Wort auf den Lippen hattet. Dafür verdient Ihr meinen größten Respekt und Wertschätzung. Vielen Dank für alles – auch für die vielen schönen Mittagspausen.

Darüber hinaus möchte ich meiner Familie danken, die mich immer bei allem unterstützt. Ihr seid immer für mich da und habt den Abschluss dieser Doktorarbeit überhaupt erst möglich gemacht. Zuletzt möchte ich meinem fantastischen Mann Tobias danken, der sich mit mir auf das Experiment Promotion im Saarland eingelassen hat und mich immer aufgefangen hat, wenn im Labor mal wieder nichts zu klappen schien. Danke für die Freiheit, meine Träume zu verfolgen, die Geduld und das endlose Vertrauen in mich und meine Fähigkeiten.